TECHNICAL REPORT STANDARD TITLE PAGE

1. Report No.	2. Government Accession No.	3. Recipient's Catalog No.
FHWATX78-1981F		

4. Title and Subtitle	5. Report Date
CONTROL OF CRACKING ON THE SIDE FACES OF LARGE REINFORCED CONCRETE BEAMS	September 1978
	6. Performing Organization Code
7. Author(s)	8. Performing Organization Report No.
G. C. Frantz and J. E. Breen	Research Report 198-1F
9. Performing Organization Name and Address	10. Work Unit No.
Center for Highway Research The University of Texas at Austin Austin, Texas 78712	11. Contract or Grant No. Study No. 3-5-76-198
	13. Type of Report and Period Covered
12. Sponsoring Agency Name and Address Texas State Department of Highways and Public Transportation; Transportation Planning Division P. O. Box 5051 Austin, Texas 78763	Final
	14. Sponsoring Agency Code

15. Supplementary Notes

Study conducted in cooperation with the U. S. Department of Transportation, Federal Highway Administration

Research Study Title: "Crack Control on the Side Faces of Deep Concrete Beams"

16. Abstract

Several large reinforced concrete highway bent cap girders, designed according to ACI and AASHTO provisions, were found to have very wide cracks near middepth on the side faces. Although the crack width at the level of main reinforcement was acceptable, the side face cracks near middepth were up to three times as wide. This indicated potential durability problems. A 3/8 scale laboratory model using deformed bars and reduced maximum size aggregate accurately reproduced the crack pattern and crack widths of the full size bent caps. A simplified test specimen was developed to accurately simulate the behavior of a portion of a beam under constant moment loading. A series of 44 specimens investigated the variables affecting side face cracking: amount and distribution of side face reinforcement, cover, web width, and beam depth. A relatively simple two-dimensional finite element analysis generally confirmed the laboratory results. A new design procedure was developed to control side face crack widths and was simplified for code use. To verify the new design procedure, the original model bent cap with the serious side face cracking problem was redesigned and tested. The procedure worked very well. Although the new procedure requires substantially more side face reinforcement for large beams than present provisions do, it appears that the side face cracking problem can be controlled at little or no additional cost by considering the flexural strength contribution of the side face reinforcement.

17. Key Words	18. Distribution Statement
cracking, beams, concrete, reinforced, control, side faces, model, testing	No restrictions. This document is available to the public through the National Technical Information Service, Springfield, Virginia 22161.

19. Security Classif. (of this report)	20. Security Classif. (of this page)	21. No. of Pages	22. Price
Unclassified	Unclassified	262	

Form DOT F 1700.7 (8-69)

CONTROL OF CRACKING ON THE SIDE FACES OF LARGE REINFORCED CONCRETE BEAMS

by

G. C. Frantz and J. E. Breen

Research Report No. 198-1F

Research Project No. 3-5-76-198

"Crack Control on the Side Faces of Deep Concrete Beams"

Conducted for

Texas
State Department of Highways and Public Transportation

In Cooperation with the
U. S. Department of Transportation
Federal Highway Administration

by

CENTER FOR HIGHWAY RESEARCH
THE UNIVERSITY OF TEXAS AT AUSTIN

September 1978

The contents of this report reflect the views of the authors who are responsible for the facts and accuracy of the data presented herein. The contents do not necessarily reflect the views or policies of the Federal Highway Administration. This report does not constitute a standard, specification, or regulation.

There was no invention or discovery conceived or first actually reduced to practice in the course of or under this contract, including any art, method, process, machine, manufacture, design or composition of matter, or any new and useful improvement thereof, or any variety of plant which is or may be patentable under the patent laws of the United States of America or any foreign country.

P R E F A C E

This is the final report on Research Project 3-5-76-198, entitled "Crack Control on the Side Faces of Deep Concrete Beams." The studies described were conducted as a part of the overall research program at The University of Texas at Austin, Center for Highway Research. The work was sponsored jointly by the Texas Department of Highways and Public Transportation and the Federal Highway Administration.

The authors are very grateful to Dr. Stefan Soretz of TOR-ISTEG Steel Corporation, Luxembourg, and Dr. Gallus Rehm and Mr. B. Neubert of the University of Stuttgart, Germany, for generously providing information on their own research and the relevant research of others in Europe. Special thanks are due to Assistant Research Engineers Felisberto Martins Garrido Filho, who supervised the development of the reduced segment test specimen, and Thomas Herrin, who investigated the use of welded wire fabric mesh for side face crack control reinforcement.

Liaison with the Texas Department of Highways and Public Transportation was maintained through the contact representative Mr. Melvin G. Jackson. Mr. Jerry W. Bowman was the contact representative for the Federal Highway Administration.

S U M M A R Y

Several large reinforced concrete highway bent cap girders, designed according to ACI and AASHTO provisions, were found to have very wide cracks near middepth on the side faces. Although the crack width at the level of main reinforcement was acceptable, the side face cracks near middepth were up to three times as wide. This indicated potential durability problems. A 3/8 scale laboratory model using deformed bars and reduced maximum size aggregate accurately reproduced the crack pattern and crack widths of the full size bent caps. A simplified test specimen was developed to accurately simulate the behavior of a portion of a beam under constant moment loading. A series of 44 specimens investigated the variables affecting side face cracking: amount and distribution of side face reinforcement, cover, web width, and beam depth. A relatively simple two-dimensional finite element analysis generally confirmed the laboratory results. A new design procedure was developed to control side face crack widths and was simplified for code use. To verify the new design procedure, the original model bent cap with the serious side face cracking problem was redesigned and tested. The procedure worked very well. Although the new procedure requires substantially more side face reinforcement for large beams than present provisions do, it appears that the side face cracking problem can be controlled at little or no additional cost by considering the flexural strength contribution of the side face reinforcement.

I M P L E M E N T A T I O N

This report presents the details of a comprehensive laboratory investigation of large reinforced concrete girders which experienced very wide cracks near middepth on the side face. This type of cracking occurred in actual bridge structures and was undesirable from aesthetics, durability, and maintenance viewpoints.

The test program and an associated analytical study were used to develop new design recommendations for flexural reinforcement distribution to control this type of cracking. A relatively simple procedure was developed and specific provisions suitable for adoption as part of the AASHTO Bridge Specifications or the ACI Building Code are presented. Adoption of these recommendations would result in elimination of this problem in future bridges at little or no additional cost by considering the flexural strength contribution of the side face reinforcement. The large girders detailed in this fashion should also be more constructible, since some of the main reinforcement would be placed in the less congested side face regions.

C O N T E N T S

Chapter Page

T A B L E S

F I G U R E S

N O T A T I O N

a	shear span
A	average area of concrete per bar
A_c	$= (2c + D)(H_{sk})(2)$, edge area of concrete symmetrical with skin reinforcement
A_c	effective concrete tensile area
A_s	area of main flexural reinforcement
A_{sk}	area of skin reinforcement
b	width of compression flange
b_w	width of web
c	cover on reinforcement
C	compression force
CMR	$= w_w/w_s$, crack magnification ratio
d	effective depth
d_e	distance from centroid of main reinforcement to extreme tension face
d_t	tension depth, distance from neutral axis to centroid of main reinforcement
D	bar diameter
DL	dead load
E_c	modulus of elasticity of concrete
E_s	modulus of elasticity of reinforcement
f'_c	concrete cylinder compressive strength
f_s	reinforcement stress based on cracked section analysis
$f_{s,av}$	$= E_s \times \epsilon_{s,av}$; average reinforcement stress based on surface strain
f_{sp}	concrete split cylinder strength
f_t	concrete tensile strength
f_y	reinforcement yield strength
h	overall depth

h_1, h_2	distance from neutral axis to extreme tension face
H_{sk}	depth in which skin reinforcement is distributed
I	moment of inertia
kd	neutral axis depth
ℓ	span length
ℓ_{cr}	vertical distance from main reinforcement to location of maximum crack width in web
LL	live load
M	moment
n	$= E_s/E_c$, modular ratio
N	number of bars
NA	neutral axis
P	applied load
R	$= h_1/d_t$; h_2/d_t
R_{ak}	reinforcement yield stress
s	spacing of vertical shear reinforcement (Chapter 2); spacing of skin reinforcement (Chapter 6)
s_2	spacing of horizontal shear reinforcement
S_L	linear scale factor
t_b, t_s	distance from center of bar to concrete surface at bottom and side, respectively
T	tension force
T_1, T_2	force in skin reinforcement
v	shear
w	crack width
w_{av}	average crack width
w_b	maximum crack width on extreme tension face (Gergely-Lutz equation)
w_{max}	maximum crack width (Chapter 2); maximum allowable crack width (Chapter 7)
w_s	crack width at main reinforcement level; maximum crack width at main reinforcement level (Gergely-Lutz equation)
$w_{s,av}$	average crack width at main reinforcement level
$w_{s,max}$	maximum crack width at main reinforcement level
w_w	crack width in web

$w_{w,av}$	average crack width in web
$w_{w,max}$	maximum crack width in web
Δ	deflection
ϵ	surface strain
ϵ_c	concrete strain
ϵ_s	surface strain at main reinforcement level
ϵ_y	yield strain of reinforcement
ρ	ratio of main tension reinforcement
ρ_{bal}	ratio of main tension reinforcement producing balanced strain condition
ρ_e	effective ratio of reinforcement
ρ_{sk}	ratio of skin reinforcement

CHAPTER 1

INTRODUCTION

1.1 Crack Control in Concrete Structures

The past two decades have witnessed a major change in reinforced concrete design philosophy. Strength design procedures, which proportion members on the basis of their capacity at factored or ultimate loads have largely replaced working stress design procedures, which proportioned members on the basis of allowable material stresses at service loads. In addition, there has been an increased use of high strength reinforcement ($f_y > 40$ ksi). These changes have resulted in structures with considerably higher service load stresses than those of the 1950's and early 1960's.

Substantial savings can result from the use of high strength reinforcement. However, some designers are reluctant to use it because they fear the possibility of very wide cracks developing at the higher service load stresses. Some type of design for serviceability (i.e., crack control and deflection limitation) must accompany the strength design to assure satisfactory performance.

Control of cracking is necessary for aesthetic reasons and for the protection of the structure from corrosion damage. The point at which cracks become unsightly is a subjective decision and depends on the type of structure, location, surface texture of the concrete, and lighting. Even if they do not actually affect the strength of the structure, wide cracks may suggest a false sense of danger or distress to the layperson.

Most concrete bridge damage results from deterioration of the concrete following corrosion of the reinforcement. As reinforcement corrodes it expands in volume, causing internal stresses that can be

large enough to spall the concrete cover. Maintenance costs for concrete bridges have been increasing steadily. In 1971, about $40 million was spent on concrete bridge repairs in the United States.[1] In 1973, the cost was estimated to be about $70 million annually.[2]

In uncracked concrete the highly alkaline cement paste reacts with the reinforcement to form a stable layer of oxide that inhibits further reaction and protects the metal from corrosion. This protection can be decreased if moisture containing salt penetrates the concrete. Concrete quality, thickness of cover, and the aggressiveness of the environment greatly affect the penetration of moisture.[3,4] Researchers disagree about the significance of cracking on corrosion[4] (specifically, whether cracking is more or less important than the previous three factors). However, cracks must increase the penetration of corrosive solutions and thus influence the possibility and rate of corrosion.[3,4] Husain and Ferguson[5] have shown that cracks are narrower at the reinforcement surface than at the exterior concrete surface. The crack width at the reinforcement may be more important for corrosion than the surface crack width. Most researchers, however, consider the crack width at the concrete surface an important indicator of corrosion susceptibility due to cracking, probably because crack width data at the concrete surface are easier to obtain than at the reinforcement surface.

The AASHTO Specifications[6] and the ACI Building Code[7] indirectly set the maximum crack widths considered acceptable for exterior exposure at 0.012 and 0.013 in., respectively. According to the Commentary to the ACI Code, their value was chosen "primarily to give reasonable reinforcing details in terms of practical experiences with existing structures." ACI Committee 224[8] has suggested a smaller maximum crack width of about 0.007 in. for exterior exposure in the vicinity of seawater or deicing chemicals. The CEB-FIP Recommendations[9] specify an allowable crack width of about 0.008 in. for exterior exposure.

One of the apparent reasons for the large difference in allowable crack widths specified by the United States AASHTO and ACI provisions and the European CEB-FIP provision is the importance each one associates with the reinforcement cover on the possibility of corrosion. The AASHTO and ACI provisions require a minimum clear cover on the reinforcement of 2 in. and 1.5 or 2 in., respectively, for concrete exposed to weather, with the additional requirement that for corrosive environments the cover be increased above these values. The European provisions permit much smaller covers: 2 cm (0.79 in.) or 2 bar diameters for exterior exposure without water present, 3 cm (1.18 in.) or 1.25 bar diameters for severe exposure, and if over 5 cm (1.97 in.) additional mesh reinforcement must be used. The AASHTO and ACI provisions try to move the reinforcement farther away from the point of entry of corrosive substances while the CEB provision tries to control the crack width at the surface. At the present time there is a lack of clear evidence to judge which of these two methods is most effective in controlling corrosion of reinforcement.

Using the smaller cover of the CEB Code, it is easier to keep the surface crack widths smaller than when using the AASHTO and ACI required covers. A clear cover of 2 in. or a cover of about 2.5 in. on the main reinforcement can lead to impractical main reinforcement distribution requirements, if crack widths much smaller than 0.012 or 0.013 in. are specified. Using the current AASHTO Specifications or the ACI Building Code, crack widths on the extreme tension face and at the main reinforcement level can be kept to acceptable values of 0.012 or 0.013 in. (see Fig. 1.1).

1.2 Observations of the Side Face Cracking Problem

Several cases have been reported where wide cracks have developed on the side faces of large (about 3 ft or larger) concrete beams in the region between the neutral axis and the main tension reinforcement (Fig. 1.2). Present specifications[6,7] do provide some guidance in the design of auxiliary side face crack control reinforcement. However,

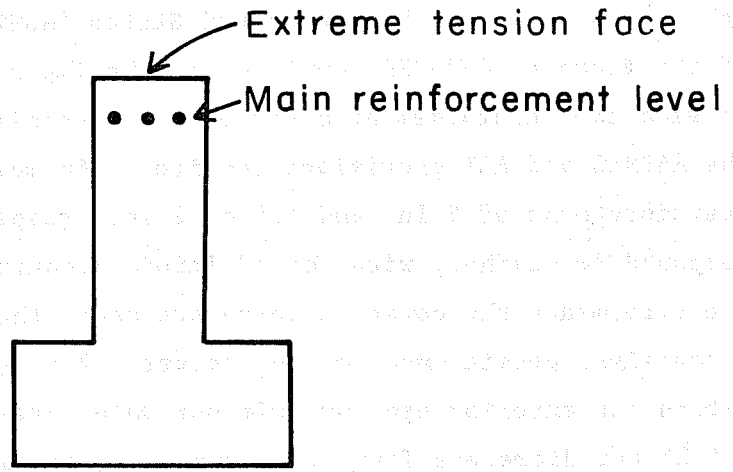

Fig. 1.1 Regions of crack control near main reinforcement

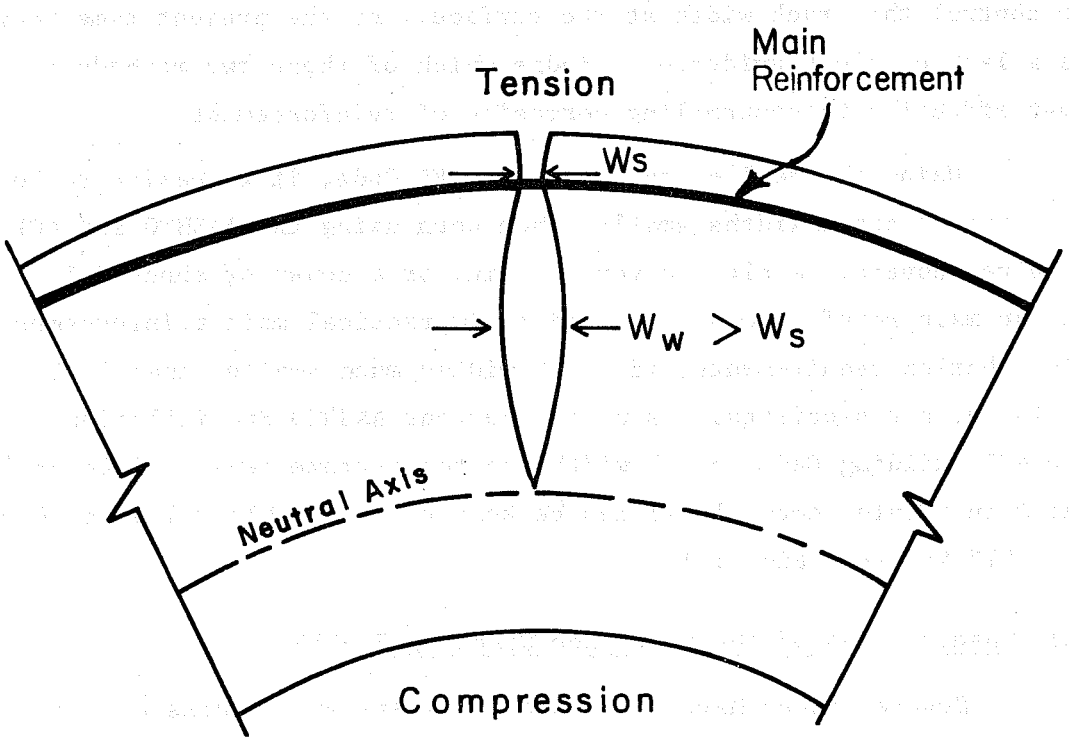

Fig. 1.2 Side face cracking in large beam

results of laboratory tests[10,11,12] and observations of actual structures designed according to the latest specifications have questioned the effectiveness of these provisions.

Observations of undesirable side face cracking in a recent project of the Texas Department of Highways and Public Transportation led to the initiation of this research study. The project had approximately 80 inverted T-beam bent caps that showed serious side face cracking problems in the regions near the column face, see Figs. 1.3 and 1.4. These bent caps are generally supported by a single central column. Precast, prestressed concrete girders rest on the flanges. A cast-in-situ deck slab acts compositely with the prestressed beams.

Crack widths of 0.010 to 0.015 in. were measured on the side faces of most of the bent caps when the structures were subjected to only dead load. In two of the bent caps an error had been made in determination of loads, with the result that the bent caps under dead load only had steel stresses typical of bent caps under one dead plus one live load (about 35 ksi). Figure 1.5 shows the crack patterns on the side faces of these two bent caps at a steel stress of 35 ksi. Also shown are crack widths measured at various locations in the webs. Crack patterns and crack widths were similar on the other sides of these bent caps. The maximum crack width was 0.015 in. near the main tension reinforcement and 0.037 in. near middepth. These cracks are wide enough to be easily visible from the ground.

These bent caps were otherwise designed according to the latest AASHTO Specifications.[6] They had the required amount of supplementary reinforcement distributed along the side faces, which was supposed to control this type of wide web cracking. Considering that crack width data can have a scatter of up to ±50 percent in tests of identical specimens,[14] the crack widths observed near the main reinforcement are close to those values suggested by AASHTO and ACI provisions. However, the crack widths in the web of the two bent caps which had actual dead load stresses as high as design service dead plus live load stresses

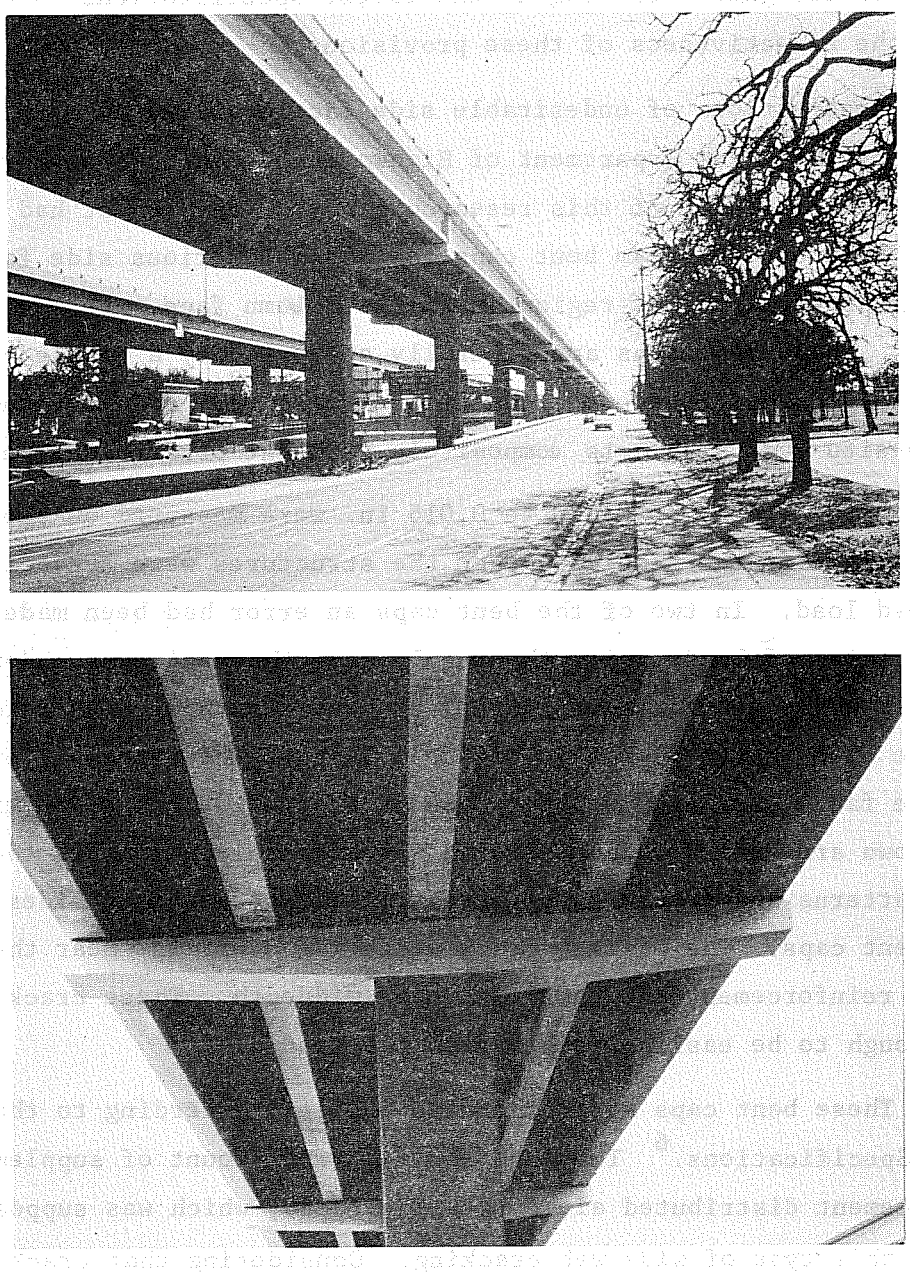

Fig. 1.3 Photographs of the bridge structure

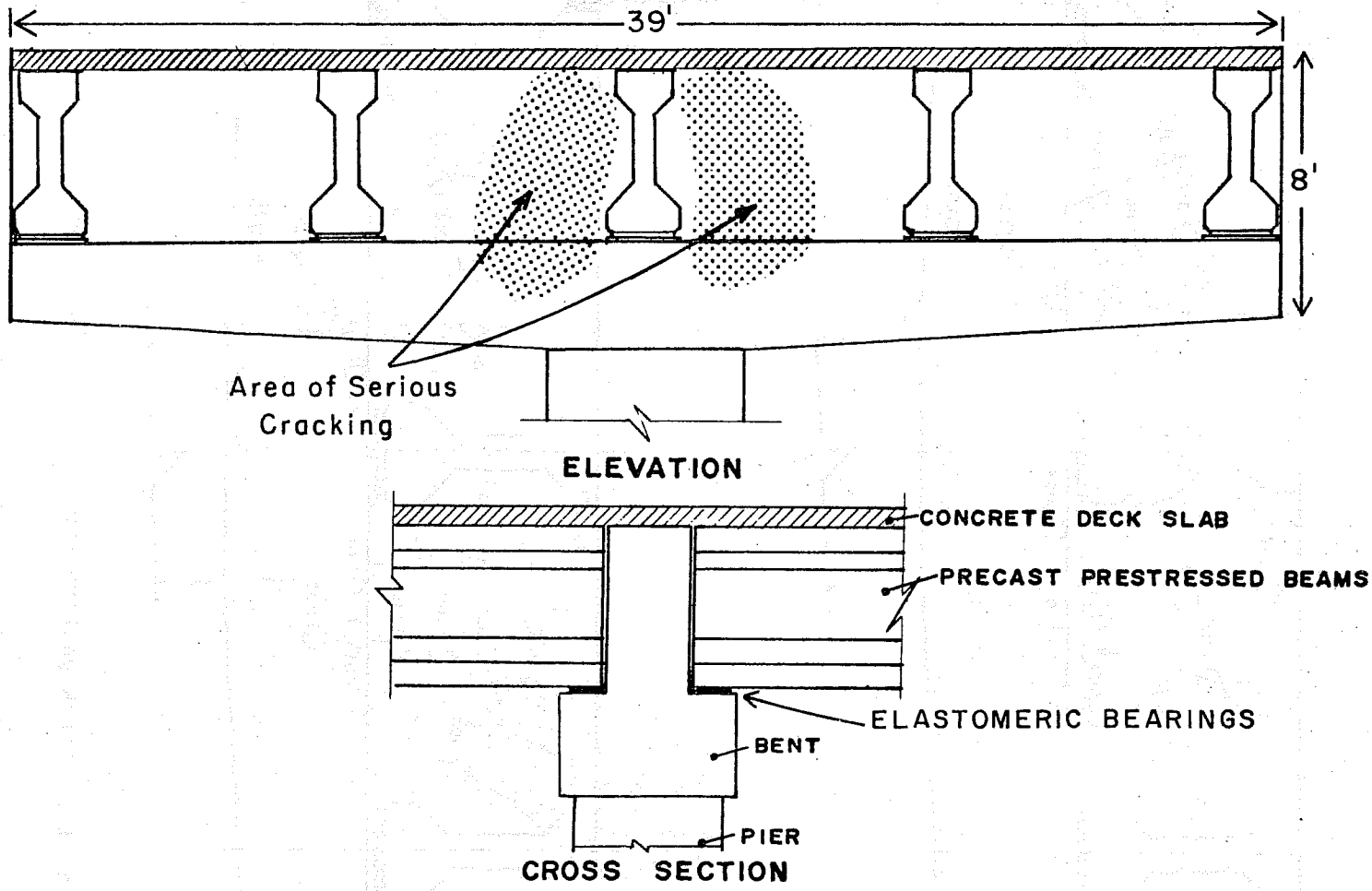

Fig. 1.4 Sketches of the bridge structure

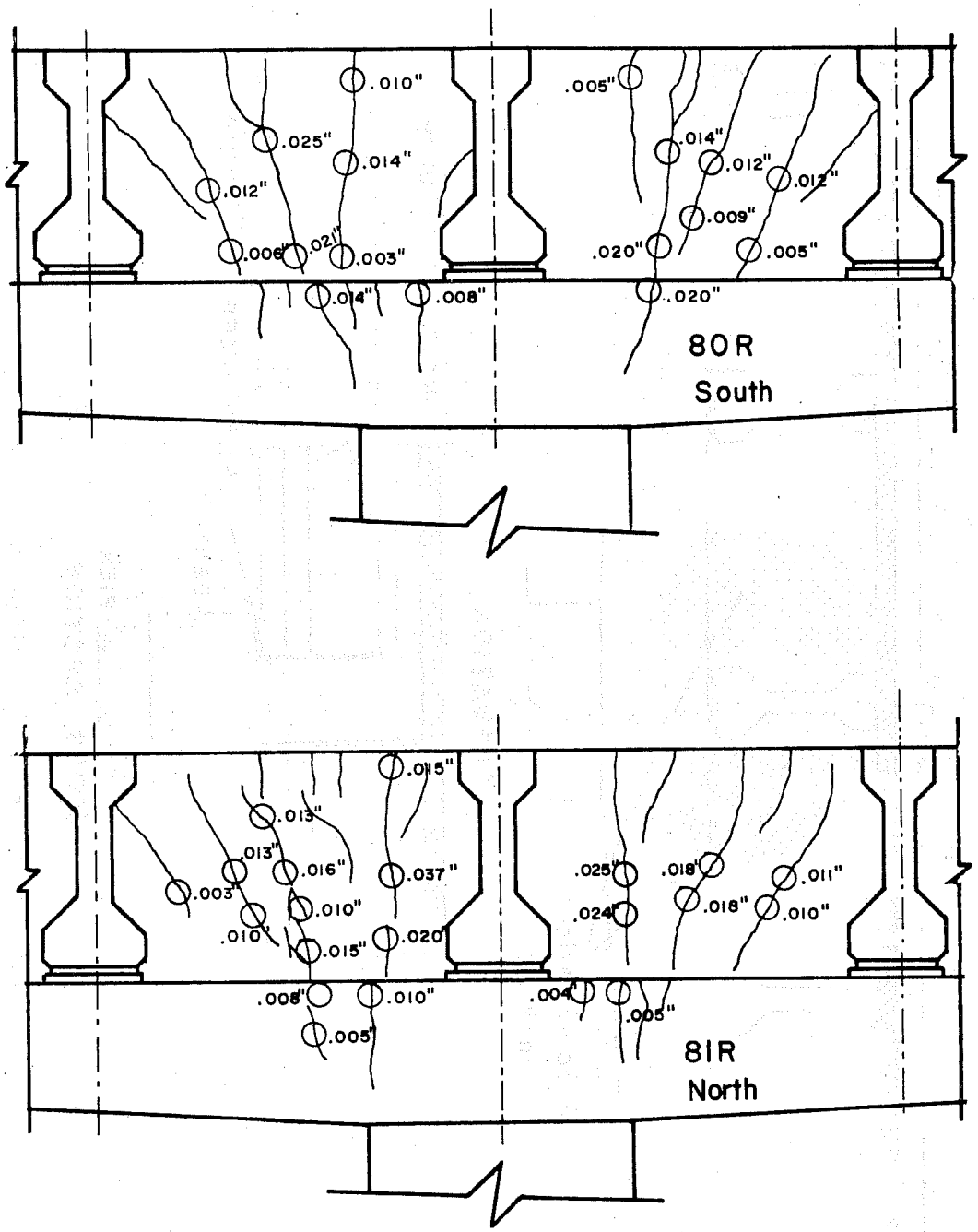

Fig. 1.5 Crack patterns and crack widths in the bent caps

were as large as 0.037 in. These are about three times the maximum value recommended by AASHTO. This is too large a difference to be attributed to only typical crack data scatter. Even though these two bent caps had design flaws, these cracks are typical of what would be found in the other bent caps under application of design live load. Such large cracks are undesirable because the bent caps are heavily reinforced with vertical stirrups that would be endangered by possible corrosion.

Although these bent caps are fairly short and stocky, they would not be classified as deep beams according to the ACI Code. The Code (Section 10.7) specifies that a member shall be designed as a deep flexural member taking into account nonlinear distribution of strain if the depth to clear span ratio exceeds 0.8 for simple spans. These bent caps had a ratio of about 0.48. The Code (Section 11.8) also specifies that for a member with a clear span to depth ratio less than 5 and loaded at the top or compression face, the design for shear should be based on deep beam concepts. The bent caps have a clear span to depth ratio of 2.1; however, they are loaded through the bottom flanges. They cannot develop the truss action that deep beams can when loaded on the opposite side from the reaction (see Fig. 2.7), and, therefore, they cannot develop the extra shear capacity this provision tries to utilize. According to the Code provisions, the main reinforcement should be designed using simple beam theory, and the shear reinforcement should be designed using the shear provisions for ordinary beams.

Other instances of wide side face cracking have been reported. For instance, engineers in Dallas, Texas, have reported wide side face cracking in highly visible members in a prominent downtown building. Personnel from this project inspected the structure and observed that cracks at the main reinforcement level were barely noticeable but were very wide near middepth.

1.3 Overview of Project

1.3.1 Objectives. Since several structures designed according to the AASHTO Specifications and ACI Building Code have developed serious side face cracking problems, it was felt necessary to reevaluate the design process concerning side face crack control reinforcement. The objectives of this research were as follows:

(1) To document the side face cracking solution.

(2) To show it feasible to use laboratory size specimens to study a problem associated with large beams.

(3) To explain the occurrence of this cracking.

(4) To investigate various methods to control this cracking (try various amounts and distributions of deformed bars and also welded wire fabric mesh).

(5) To develop an effective but simple design method that would reduce the side face crack widths to acceptable values.

The use of high strength reinforcement can result in substantial savings if excessive cracking can be controlled at the higher service load stresses. This research was directed at providing a basis for modification of the AASHTO and ACI provisions for side face crack control reinforcement.

1.3.2 Scope. The chapter divisions of this report reflect the major work divisions of the project:

Chapter 2 summarizes the results of an extensive literature search of work done in the general area of cracking and specifically in the area of side face cracking.

Chapter 3 reports on the construction and testing of a 3/8 scale model of the inverted T-beam bent cap discussed in Sec. 1.2. A simplified test method was then developed and verified, and these results are presented.

Chapter 4 gives the details of a laboratory experimental program that examined the important parameters that influence side face cracking.

Chapter 5 presents a semi-analytical study of the side face cracking problem using a two-dimensional finite element model.

Chapter 6 is a discussion of the data obtained in both the laboratory and finite element studies.

Chapter 7 presents the development of a revised design procedure to control side face cracking. Results of tests performed to verify this new procedure are discussed.

Chapter 8 gives the final conclusions of this study.

CHAPTER 2

LITERATURE REVIEW

2.1 Introduction

An extensive literature search was performed to study the state of the art on cracking on the side faces of concrete beams. Reports on general theories of cracking near the main tension reinforcement were also examined. This chapter summarizes the finding of the literature search. Further detail is included in Ref. 54.

2.2 Previous Research in Crack Control in Beams

2.2.1 In the Vicinity of the Main Tension Reinforcement.

Many of the studies of reinforced concrete cracking begin with a single, axially loaded tensile specimen for which equations for crack spacing and crack width are derived. Cracks will form at some irregular spacing at weak points in the concrete, see Fig. 2.1. Additional cracks can develop in between the initial cracks if there is enough distance between them to transfer sufficient force by bond from the bar to the concrete to reach the fracture stress of the concrete. This suggests there is some limiting value (L_{min}) to which the spacing can be reduced. If the initial cracks B and C are spaced at a distance of $2L_{min}$ or greater, then a crack can form at A. If, however, the original distance is less than $2L_{min}$, then no additional cracks can form within that interval. Thus, the crack spacing can vary from L_{min} to $2L_{min}$ with an average of $1.5L_{min}$. Because of this randomness in crack spacing, there is an inherent ±33 percent scatter in crack spacing data. Hognestad[14] has stated that variation in material properties can raise this scatter to ±50 percent in tests of identical specimens. The essential difference between most of the simple, axial tension theories is the assumed distribution of bond stress between

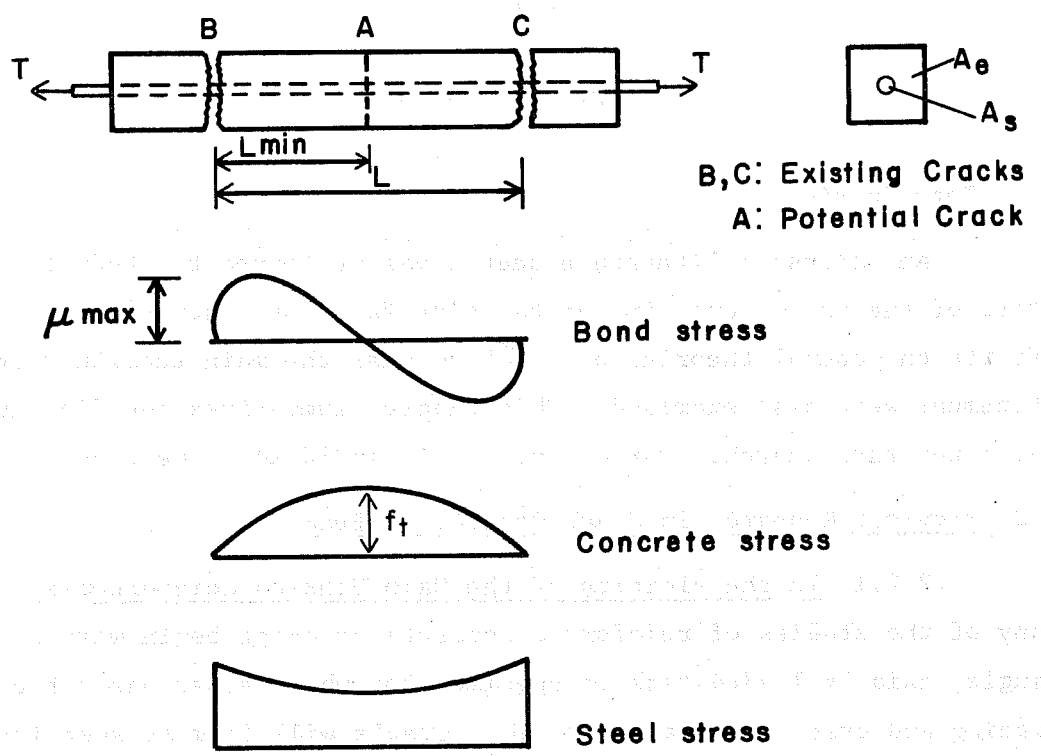

Fig. 2.1 Crack spacing in axial tension specimen

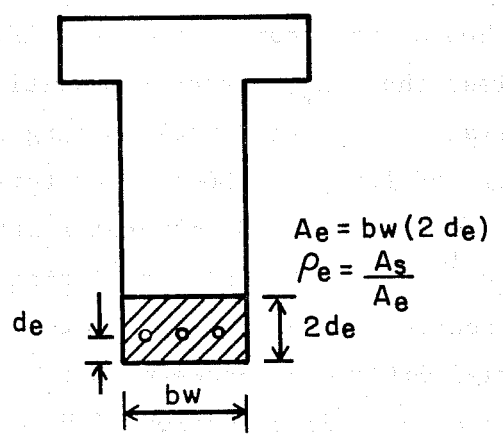

Fig. 2.2 Effective concrete tensile area in flexural specimen

cracks. The tensile specimen theories are modified to apply to flexural members by suitable definition of the effective concrete tensile area, A_e. Typically an effective area of concrete is taken to be that area of concrete symmetrical about the tension reinforcement (Fig. 2.2).

In the early 1960's the Portland Cement Association conducted an extensive investigation in the control of flexural cracking. From these tests Hognestad[14] concluded that in the vicinity of the main reinforcement the crack width (1) is proportional to the steel stress (or strain), (2) is not proportional to the bar diameter, (3) is not affected by the concrete strength, (4) is proportional to the concrete cover, (5) is not proportional to the crack spacing, and (6) is not as strongly dependent on $p_e = A_s/A_e$ as the CEB theory[17] indicates. After further tests, Kaar and Mattock[10] concluded that there is a strong correlation between the crack width and average area of concrete surrounding each reinforcing bar, indicating many small bars control cracking better than a few large bars. Their suggested equation for maximum crack widths at the main reinforcement level was

$$w_s = 0.115 \sqrt[4]{A}\, f_s \times 10^{-3} \text{ in.}$$

where A is the average concrete area per bar [A_e (Fig. 2.2) divided by N, the number of bars].

Gergely and Lutz[19] did a statistical analysis of crack width data from six other investigations. They found that the most important variables were (1) steel stress or strain, (2) concrete cover, (3) concrete area per bar, and (4) the strain gradient. The bar diameter was not a significant variable. Referring to Fig. 2.3, their equations for the maximum crack widths (x 0.001 in.) were for cracks on the tension face,

$$w_b = 0.091 \sqrt[3]{t_b A}\, R(f_s - 5)$$

and for cracks at the level of main reinforcement,

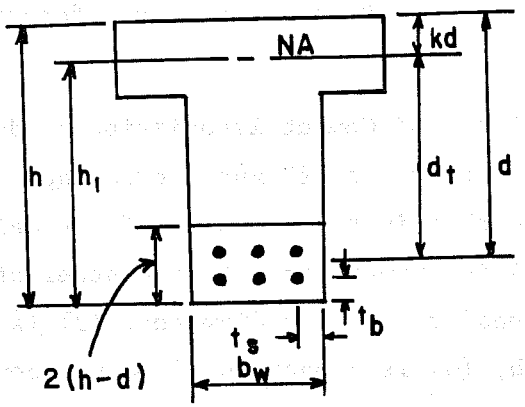

$$A_e = 2(h-d)(b_w)$$

$$A = \frac{A_e}{N}$$

N = no. of bars

$$R = \frac{h_1}{d_t}$$

Fig. 2.3 Notation for Gergely-Lutz equations

$$w_s = \frac{0.091 \sqrt[3]{t_s A}}{1 + t_s/d_t} (f_s - 5)$$

where $A = A_e/N$

t_s, t_b = distance from the center of bar to concrete surface at side and bottom, respectively

h = overall depth

d = effective depth

kd = neutral axis depth

$d_t = d - kd$

$h_1 = h - kd$

$R = h_1/d_t$

Ferry-Borges,[21] the CEB[9] Recommendations of 1970, and Albandar and Mills[22] all subsequently recommended equations for crack width at the main reinforcement level. Although each of these equations uses different combinations of variables, they all indicate the importance of steel stress. Most show the strong influence of cover, and the majority use the average concrete area per bar. It appears that within the

expected accuracy of crack width data (±33 percent to ±50 percent) each of these equations (except for the simple axial tensile theory) predicts crack widths in the vicinity of the main tension reinforcement reasonably well.

2.2.2 In the Web. By proper detailing of the main reinforcement according to the equations presented in Sec. 2.2.1, crack widths in the vicinity of the main tension reinforcement can be controlled to values intended by the AASHTO or ACI provisions (Sec. 1.2). However, as discussed in Chapter 1, members with a depth exceeding about 3 ft can develop cracks near middepth that are several times as wide as cracks near the main reinforcement (Fig. 2.4). Several cracks that begin at the tension face may join together to become a single crack that extends into the web (Fig. 2.5), forming a tree branch crack pattern.

This problem was discussed at a meeting of the CEB committee on cracking in 1966.[23] Several current methods of controlling this type of cracking were discussed. They were (1) distributing the principal tension reinforcement throughout the entire tension zone, or (2) placing auxiliary small diameter bars along the lateral faces. The first method is similar to design methods that have been suggested for deep flexural members.[24] Ferry-Borges noted there was a lack of sufficient theoretical and experimental justification for the design of auxiliary crack control reinforcement.

Ros[25] and Lazard[26,27] tested beams about 3 ft deep and showed that including auxiliary side face or skin reinforcement significantly modified the cracking behavior of the beams. The crack pattern was changed from a tree branch pattern to one where many more cracks extended into the web. The width of cracks in the web was reduced considerably.

At the Portland Cement Association, Gaston and Hognestad[28] tested two 0.38 scale model T-beams, 18 in. deep with a 2.6 in. web and 0.57 in. of cover on the main reinforcement. They were models of

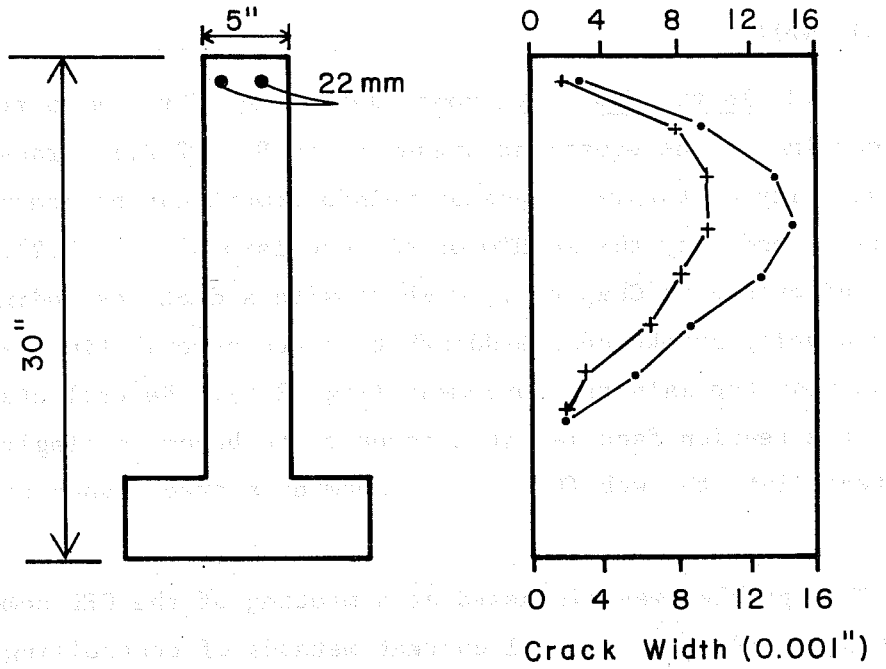

Fig. 2.4 Variation in width of cracks on side face (Ref. 11, Fig. 11)

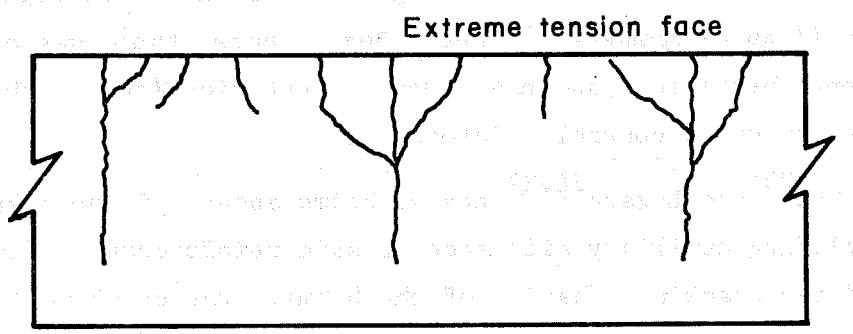

Fig. 2.5 Typical tree branch crack pattern in large beams without side face crack control reinforcement

4 ft deep T-beams that were to be built later. To control side face cracking, one model had three #2 bars placed along each side face. The skin reinforcement was 0.30 sq. in. or about 19 percent of the main tension reinforcement area. The specimen with skin reinforcement had more cracks in the web and smaller crack widths than the one without any crack control bars. A full size T-beam spanning about 58 ft, with a 4 ft depth, a 7 in. web width, and six #4 side face bars, was built and tested.[29] The results supported the earlier model test results; crack widths in the web were smaller than at the main reinforcement level. In this case, the skin reinforcement area was 1.2 sq. in., 15 percent of the main reinforcement area. In addition, the main reinforcement was well distributed on the side faces of the lower quarter of the web.

Further tests in this PCA series were reported by Kaar and Mattock.[10] They tested a series of half scale highway bridge girders spanning 24 ft with a 26 in. depth and cast with a composite slab. The girders were I, T, and rectangular shapes with web thicknesses of 3.5, 4, and 8 in., respectively. To study side face crack control, each beam had three #2 face bars with 1 in. cover placed along each side face for half the span length. This reinforcement had an area of 0.30 sq. in., 12 percent of the main reinforcement area. Without face reinforcement the crack magnification ratios (ratios of the crack widths in the web to crack widths at the main reinforcement level) for flexural cracks in the constant moment region in the I, T, and rectangular beams were about 2.5, 2.3, and 1.7, respectively. With face bars the ratios were reduced to about 1.5, 1.5, and 1.1, respectively. They noted that the face reinforcement was not as effective in reducing diagonal crack widths. These tests seem to have been the basis for development of current ACI and AASHTO side face reinforcement requirements.

In the late 1960's and early 1970's an extensive study of cracking in reinforced concrete was carried out at the Cement and Concrete Association. Beeby derived semi-empirical general cracking equations to predict crack spacing and crack widths in slabs,[30] rectangular

beams,[20] pure tension members,[31] and on the side faces of beams.[11] These equations are given in Appendix C of Ref. 54. Using these equations, he was able to predict the crack widths on the side faces of beams without any side face reinforcement and show analytically the increase in crack width down the side face. Beeby,[11] in 1971, reported on tests of a series of 30 in. deep T-beams spanning 15 ft with a 5 in. thick web and 1 in. cover. Side face reinforcement was uniformly distributed along the side face and was either two 6 mm (0.088 sq. in.), four 6 mm (0.076 sq. in.), or four 10 mm (0.49 sq. in.) bars, which was 7.5, 15, or 41 percent of the main reinforcement area, respectively. His test region was in a constant moment zone. He reported that the cracks were widest near middepth and were about 4.5 times as wide as cracks at the main reinforcement level when no skin reinforcement was used. The skin reinforcement did not noticeably affect the crack patterns of the beam. The skin reinforcement consisting of two or four 6 mm bars had no effect on the web crack widths, while the four 10 mm bars had only a slight effect.

In 1972, Soretz and Colanna-Ceccaldi[12] reported on a significant series of tests that examined the effects of the amount and distribution of skin reinforcement on the side face cracking problem. The beams were 11.8 in. wide x 39 in. deep rectangular beams spanning 33 ft with 1.26 in. clear cover on the main reinforcement, two 1.57 in. bars (3.9 sq. in.). Twelve different arrangements of skin reinforcement were tried, varying from 0 to 1.87 sq. in. (48 percent of the main reinforcement area). Crack widths were measured in the constant moment zone and in the shear spans of the beams. Without any side face reinforcement the web cracks were about 2.5 times as wide as the cracks at the main reinforcement level. Their results are summarized as follows:

(1) Changing the main reinforcement distribution from two bars to ten bars, but maintaining the same total area significantly reduced

crack widths at the main reinforcement level. There was no conclusive evidence of its effect on the web crack widths.

(2) Provision of skin reinforcement increased the number of long cracks that penetrated into the web.

(3) Provision of skin reinforcement slightly reduced crack widths at the main reinforcement level.

(4) With proper stirrups and skin reinforcement, diagonal crack widths were reduced as effectively as flexural crack widths.

(5) To reduce web cracks to the same width as cracks at the main reinforcement level, a total area of horizontal skin reinforcement should be provided equal to 0.5 percent of the web area between the main tension reinforcement and the neutral axis (1.24 sq. in., or 32 percent of the main reinforcement area for these specimens). This reinforcement should be distributed with one-half of this amount near each side face in the tension zone.

(6) Because of experimental scatter, it was not possible to determine any effect from various distributions of the skin reinforcement. They recommend concentrating the skin reinforcement in two bars, located at one-third of the distance between the main reinforcement and the neutral axis.

Although not dealing specifically with beams of large depths, some work done at the University of Stuttgart[32] is relevant to this side face cracking problem. These tests studied the use of wire mesh skin reinforcement to improve the cracking performance of beams reinforced with large diameter (2 in.) bars. Wire mesh was placed close to the beam surface throughout the tension zone, and very significantly increased the number of cracks and reduced the crack widths both at the extreme tension face and on the side faces. A suggested limit of 4 in. was proposed for the maximum spacing of skin reinforcement.

2.3 Present Code Provisions

2.3.1 Side Face Reinforcement for Large Beams. The ACI 318-77 Code[7] contains a provision for crack control on the side faces of large concrete beams. It appears that the PCA tests[10,28,29] served as the basis of this provision. Section 10.6.7 reads as follows:

> 10.6.7 - If the depth of a web exceeds 3 ft, longitudinal reinforcement having a total area equal to at least 10 percent of the area of the flexural tension reinforcement shall be placed near the side faces of the web and distributed in the zone of flexural tension with a spacing not more than the web width, nor 12 in. Such reinforcement may be included in strength computations only if a strain compatibility analysis is made to determine stresses in the individual bars or wires.

A similar provision in the 1976 AASHTO Specifications,[6] Section 1.5.8(b) reads as follows:

> 1.5.8(b) - If the depth of the side face of a member exceeds 2 ft. longitudinal reinforcement having a total area at least equal to 10 percent of the principal tension reinforcement shall be placed near the side faces of the member and distributed in the zone of flexural tension. The spacing of such reinforcement shall not exceed 12 in. or the width of the web, whichever is less. Such reinforcement may be included in computing the flexural capacity only if a stress and strain compatibility analysis is made to determine stresses in the individual bars.

The CEB-FIP 1970 Code[9] has a provision for side face crack control reinforcement as follows:

> R53.413 Longitudinal Distribution Reinforcement
>
> When the depth of the web of a member in bending (expressed in metres) exceeds $1 - 10^{-5} R_{ak}$, where R_{ak} is expressed in N/cm^2, the engineer should provide longitudinal distribution reinforcement on each side of the two faces of the web. This longitudinal distribution reinforcement, known as surface reinforcement, should be of the same quality as the longitudinal tensile reinforcement. Its geometric proportion, with respect to the section of the web excluding the cover to the main tensile reinforcement, should be at least 0.05 percent in each of the two faces.
>
> Moreover, the spacing of individual bars in this reinforcement should not exceed 20 cm.

> Bars forming the main tensile reinforcement may be spread over a considerable portion of the lower part of the beam, as long as their exact positions are taken into account in calculating the strength.

In customary units this critical depth limit (in.) is $39.4 - 0.272f_y$, where f_y is expressed in ksi (29 in. for 40 ksi and 23 in. for 60 ksi). The spacing limit is 8 in.

2.3.2 Deep Beam and Wall Reinforcement. Design criteria for deep beams may be applicable to the side face cracking problem of large beams. Deep beams differ from shallow beams in two respects. First, deep beams perform differently than shallow beams under shear loading. Figure 2.6[33] shows that as the shear span to depth (a/d) decreases there is a change in mode of failure from flexure to shear. Figure 2.7 illustrates the behavior of a deep beam (with $a/d \leq 1$) with loads and reactions applied on the top and bottom of the beam. Such a beam usually shows a considerable increase in load capacity after diagonal cracking, even without any shear reinforcement being used. This is because after cracking the load transfer mechanism changes from beam action to something similar to tied arch action. The concrete provides the compression struts and the main reinforcement supplies the lower tension tie. The high compression stresses at the load point prevent the diagonal crack from running to the top and failing the beam. If the loads and reactions were all applied to the bottom of the beam or if the loads were applied to the lateral sides through shear, the beam could not develop this arch action. Unless shear reinforcement was provided, the beam would fail after initial diagonal cracking. The ACI Code (Sec. 11.8) requires that special shear strength equations be used for beams with a clear span to depth ratio of less than 5 and loaded on the top or compression face. The Code requires that the minimum area of vertical shear reinforcement be $0.0015b_w s$, where b_w is the web width and s is the bar spacing, and the minimum area of horizontal shear reinforcement be $0.0025b_w s_2$, where s_2 is the bar spacing.

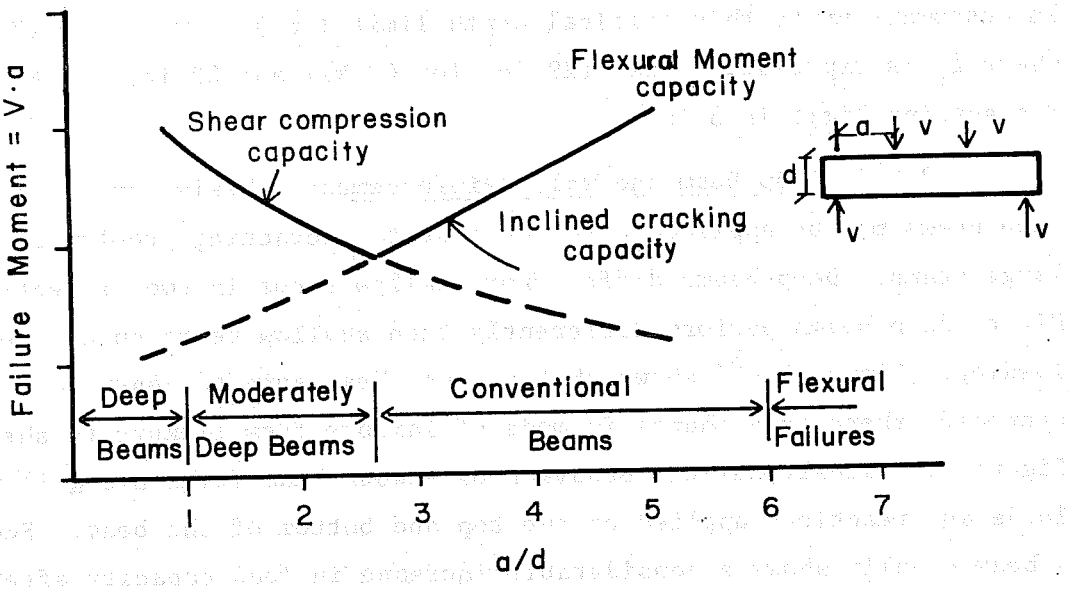

Fig. 2.6 Variation in shear capacity with a/d for rectangular beams (Ref. 33)

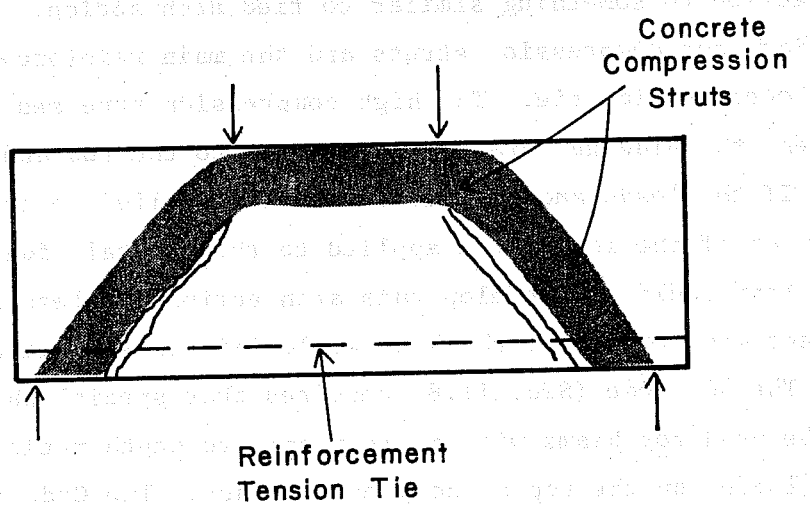

Fig. 2.7 Tied arch behavior of deep beams (a/d < 1)

The second difference between deep and shallow beams is that for beams with span-to-depth ratios less than 1.25 for simple spans and 2.5 for continuous spans the assumption that plane sections before bending remain plane after bending is not valid. The normal stresses induced by loads and reactions significantly influence the longitudinal stress distribution. The ACI Code (Sec. 10.7) requires that for deep flexural members (according to the above definition of "deep") this nonlinearity must be accounted for in the design process (Refs. 24 and 34 outline such design processes). The minimum vertical reinforcement should be the greater of that required by Sec. 11.8 (shear provision) $0.0015\ b_w s$ or by Sec. 14.2 (wall provisions) 0.0012 times the gross section area. The minimum horizontal reinforcement should be the greater of that required by Sec. 11.8, $0.0025\ b_w s_2$, or by Sec. 14.2, 0.0020 times the gross section area.

2.3.3 Adequacy of Existing Provisions

2.3.3.1 Reinforcement for Large Beams. The ACI and AASHTO provisions define the required area of skin reinforcement as 10 percent of the main tension reinforcement area. The test results of Beeby[11] and Soretz[12] show that in the beams which they tested a skin reinforcement area of only 10 percent of the main reinforcement had little effect on the side face crack widths.

In addition, the present provisions seem illogical. Consider the case of a designer who must provide a certain moment capacity in a beam. As he increases the depth of the member, he increases the moment lever arm. Therefore, the amount of main tension reinforcement needed for flexure decreases. Thus, the amount of skin reinforcement required (10 percent of the main tension reinforcement) decreases as the depth increases. Intuition suggests that as the depth increases, the web cracking problem becomes more serious, requiring an increase in the skin reinforcement rather than a decrease.

The CEB provision defines the total area of skin reinforcement as 0.10 percent of the web area. In the beams of Soretz[12] this

requires a skin reinforcement area of 0.44 sq. in., whereas he recommended that 1.24 sq. in. be used. If the CEB recommended value of 0.44 sq. in. was used, it appears that the crack width in the web would be about 1.6 to 1.9 times the crack width at the main reinforcement level.

As a means of comparing the ACI and CEB recommendations, note that for a rectangular beam with a main tension reinforcement percentage of 1 percent, the required skin reinforcement area by the ACI provision is 10 percent $A_s = 0.1\ (0.01bd) = 0.001bd = 0.10$ percent bd, the same as required by the CEB provision.

2.3.3.2 Reinforcement for Deep Beams. These provisions do not appear to address adequately the side face cracking problem. As discussed in Chapter 1, the bent caps that had the serious cracking problem are not classified as deep beams by the ACI provisions (flexure or shear). The beams tested by Beeby,[11] and Soretz,[12] and Kaar and Mattock[10] had span-to-depth ratios of 6, 10, and 11, none in the range of deep beams. They all reported significant crack width increases near middepth in the constant moment region.

Based on these reported tests and also the observation of actual structures, the existing Code provisions for side face crack control reinforcement are inadequate. Tests were required to document the effect of the beam depth and width on the side face cracking problem. Additional tests were required to identify the amount and distribution of skin reinforcement needed to reduce the side face crack width to an acceptable value.

CHAPTER 3

DEVELOPMENT OF TESTING METHOD

3.1 Introduction

Although the side face cracking problem was initially observed and documented in a series of actual bridge support structures, a complete investigation required a study under laboratory conditions. Since a test program of forty to fifty specimens was envisioned to fully explore the variables, it was impractical to use full size test members because of handling and testing problems. The initial part of the project was directed at verifying the similitude of cracking behavior between the inverted T-beams observed in the field (Figs. 1.2, 1.3, and 1.4) and a 3/8-scale model constructed in the laboratory. Different investigators have reached different conclusions as to whether crack patterns and crack widths can be successfully modeled.

3.2 3/8-Scale Model Bent Cap Test

3.2.1 General. Under service load conditions, the prototype structure is subjected to ten concentrated loads, each equal to approximately 70 kips. At design ultimate these loads are 125 kips each. Considering the size (8 ft deep and 38 ft long) and the weight (140 kips) of the prototype structure as well as the applied loads, it would have been difficult to test a full size structure in the laboratory. Therefore, a very accurate model of the prototype was constructed.

Direct models are routinely used in structural engineering for reinforced concrete structures. In direct concrete models, the specimens are constructed with microconcrete, a reduced size aggregate mix, designed to keep the material properties essentially identical to those of the prototype mix. Various investigators have studied the accuracy

of modeling the cracking behavior of reinforced concrete members. One of the biggest problems in such studies is the large amount of scatter typically found in cracking test results. Hognestad[14] stated that a scatter of 50 percent is common in crack data and is due to the randomness of the cracking phenomenon. Also, as the model scale decreases, cracks become smaller and harder to locate and measure. This leads to some of the differences of opinion on cracking similitude.

Borges and Lima[36] used all deformed bars and scaled the maximum aggregate size and found that both flexural crack width and crack spacing scaled satisfactorily in 1/4 and 1/2.5-scale models when compared to full size 40 in. deep beams. Janney[37] used rusted wire reinforcement and microconcrete for his models and found very good agreement between the flexural cracking patterns of 1/8 scale and full size 8 x 16 in. beams. However, he reported significantly less agreement in 1/16-scale models. Alami[38] tested 1/4, 1/3, 1/2, 2/3, and full size models ranging in depth from 3 to 15.6 in. made with deformed bars and reduced maximum size aggregate, and found reasonable similtude in crack spacing, but observed that differences were greatest for the smaller models. Swamy[39] tested 1/3 and 1/2-scale models of 9 in. deep T-beams and found good cracking similitude in models where the maximum aggregate size was also scaled. If the maximum aggregate was not scaled, he reported that crack spacing and width increased as the model scale decreased. Beeby[30] tested one-way slabs 4.5 to 15 in. deep and concluded that the crack spacing did not scale but crack widths did scale if bond, aggregate interlock, and internal cracking also scaled. A dimensional analysis of the Gergely-Lutz equations and Beeby's general cracking equation shows that each predicts crack widths to be directly proportional to the scale factor.

In cracking of T-beam flanges in 1/4, 1/2, and full size 40 in. deep beams, Kaar[40] noted that cracking patterns were similar in various size models, but the number of cracks decreased in smaller models.

Kaar used deformed bars and the same concrete mix for all specimens. He found that crack widths were proportional to the square root of the scale factor. Clark[41] tested 1/3.7-scale microconcrete and deformed bar models of the slabs used by Beeby[30] and found that both cracking patterns and crack widths depended on the absolute size of the model and were not related to the scale factor.

Considering all the different opinions on cracking similitude, it appears that the best results are obtained using large models, both large in scale and in absolute size. To minimize differences in bond characteristics between the model and the prototype, deformed bars should be used in the models. The maximum size of the aggregate used in the concrete should be scaled.

3.2.2 Design of Specimen

3.2.2.1 Type of Specimen Chosen. The main objective of the first large model test was to determine if satisfactory cracking similitude existed between the prototype and model structures. However, the specimen was also designed to provide data for the development and validation of the compact test specimen (see Sec. 3.3). The smallest deformed bar available for these model bent caps was a Swedish 6 mm bar, while the smallest bar used in the prototype was a #5 bar (used as a face bar). The 6 mm bar was used to model the #5 bar with the resulting scale factor equal to 0.378 or about 3/8. The model structure is shown in Fig. 3.1. It was modified to include a constant moment region between the two cantilever ends (compare with Fig. 1.3). Loads were applied symmetrically on each cantilever. The column stub had a pinned connection, while a specially constructed roller assembly was used at the other support. The specimen length was determined by (1) a constant moment centerspan length that would yield a well-developed crack pattern, and (2) the location of tie-down points in the laboratory test slab.

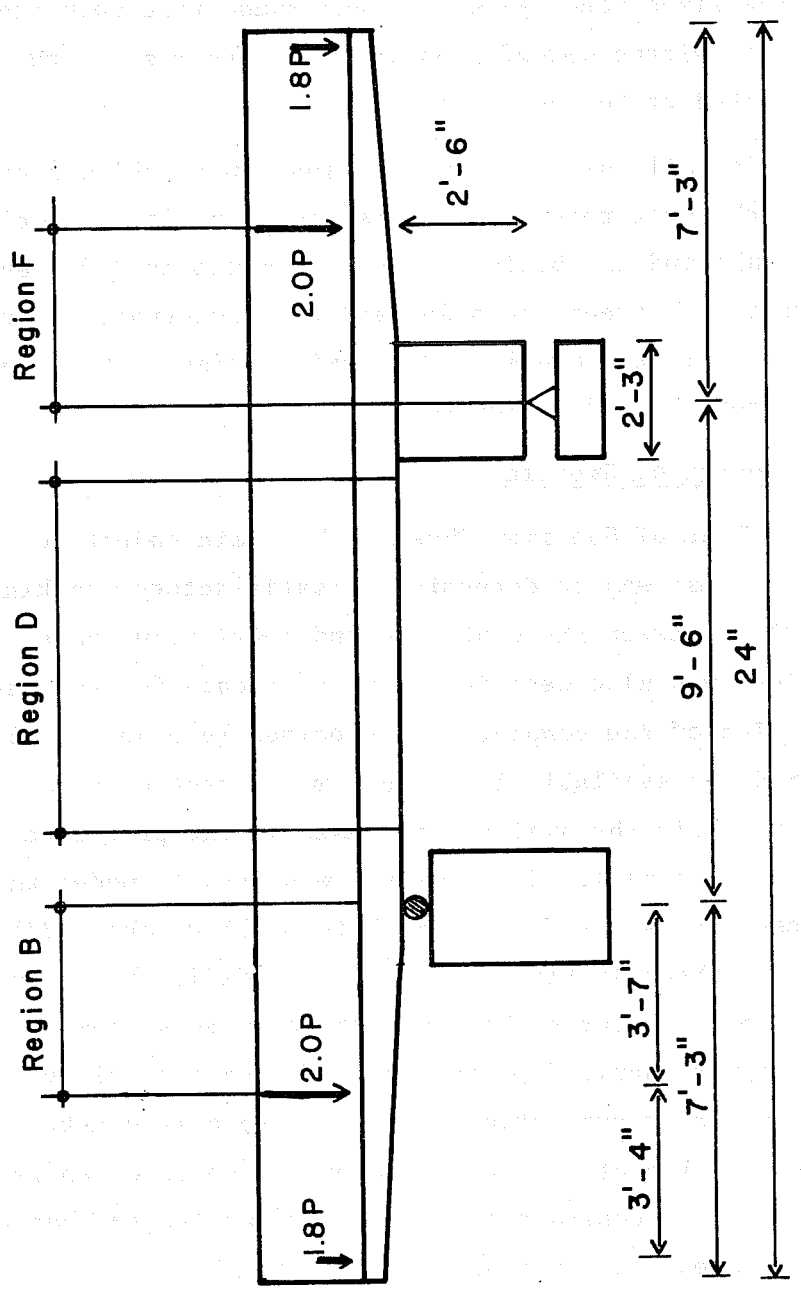

Fig. 3.1 3/8-scale model bent cap (Ref. 13)

For test purposes, the model was divided into different regions. Regions F and B, located in the cantilever sections, provided information on cracking similitude with the prototype. Region D, located in a constant moment region, provided data for a statistical analysis of the crack width profile in the web. Comparison of F, B, and D indicated if shear influenced the crack width profile significantly.

3.2.2.2 Specimen Details and Materials. A 3/8-scale model closely corresponding to the prototype bent cap was constructed. Figure 3.2 gives the reinforcing details of the beam and column stub. Except for the #2 bars, which were smooth bars and were used for some of the stirrups, all the reinforcement utilized deformed bars. To allow a more accurate comparison between Regions F and D, reinforcement in Region D was identical to that used at the column face. Table 3.1 lists the reinforcement material properties. Some of the reinforcement in the flange and the column stub of the model was of a higher grade steel than in the prototype, but this is not important, since overstrength in these areas would not affect the flexural behavior of the bent cap. The model face reinforcement also was of a higher grade steel, but again this is not significant for the crack investigation portion of this test, since it was expected that the face steel would reach its yield strength only near ultimate flexural capacity of the structure.

The concrete used in the two prototype bents had a 28-day design compressive strength of 3600 psi using Type I cement. However, the measured 7-day compressive strengths were about 5500 psi, indicating a 28-day strength of 7000 psi or more. These strengths were considered to be unrepresentative (too high) of typical concrete strengths found in such structures. Therefore, an average compressive strength of 5000 psi at 28 days was chosen for the model. Investigations[14,20] have shown that concrete strength has a minor secondary effect on cracking behavior (beyond first cracking). Table 3.1 presents the concrete material properties. The maximum aggregate size was scaled

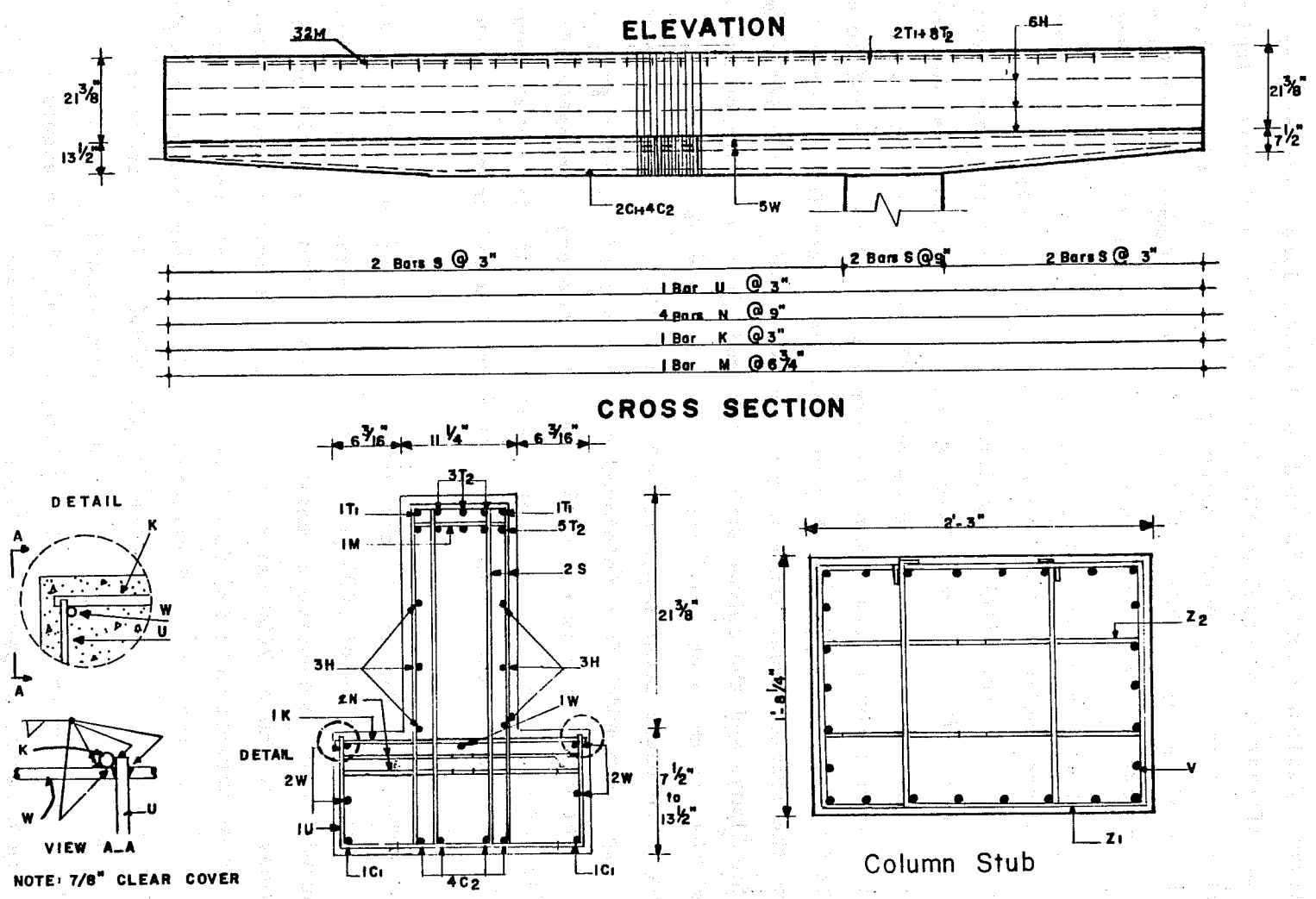

Fig. 3.2 3/8-scale model bent cap details

TABLE 3.1 MATERIAL PROPERTIES FOR PROTOTYPE AND MODEL BENT CAPS

Reinforcement

Use	Bar ID	Prototype Size	Prototype Grade	Model Size	Model Grade
Main Tension	T1,T2	#11	60	#5,#4	60
Compression	C1,C2	#9	60	#4,#3	60
Face Bars	H	#5	60	6 mm	77
Stirrups	S	#5	60	6 mm	77
Flange Steel	W	#9	40	#3	40
Flange Steel	N	#5	60	6 mm	77
Flange Steel	K	#9	60	#4	60
Flange Steel	U	#5	40	6 mm	77
Column Stub	V	#11	40	#5	60
	Z1,Z2	#5	40	#2	40

Concrete

Mix Design (1 cu. yd.)

	Cement (lb) Type I	Aggregate (lb.) Coarse	Aggregate (lb.) Fine	Water Gal.
Prototype	564	2031 (1.5" max)	1053	28.2
3/8 Model	541	1813 (5/8" max)	1483	28.7

Strength (psi)

	Compression	Tension (Split Cylinder)
Prototype	5500	Not reported
3/8 Model	5400 (flange), 4100* (web)	490 (flange)

*Estimated using concrete impact hammer.

approximately from 1.5 in. to 5/8 in. The flange of the model bent cap was cast with a 3.25 in. slump, and the web with a 6 in. slump (see Sec. 3.2.2.3). Concrete test cylinders were made using only the flange concrete and indicated a flange concrete strength of 5400 psi. The compressive strength of the web concrete was estimated as 4100 psi, using a calibrated concrete impact test hammer.

3.2.2.3 Fabrication. The wooden forms were lightly oiled prior to concrete placement. The column stub was cast first as in the prototype construction. The bent cap was then formed with the steel cage tied in place. Figure 3.3 shows the completed reinforcing cage.

Ready-mixed concrete with a 3 in. slump was placed in two lifts; one lift for the flange and one for the web. Internal vibrators were used for consolidation. Because of delays in casting the flange, congestion of main reinforcement, and the concrete's low slump, substantial difficulty was expected in placing the web concrete. To overcome this problem additional water was added to the remaining mix until the slump was increased to 6 in. The web was then cast. Test cylinders were made with flange concrete only, and the web concrete strength was estimated using a concrete impact hammer.

3.2.3 Testing Method

3.2.3.1 Loading System. Under symmetrical vertical loading, the specimen must move horizontally to prevent bending in the column. Therefore, the loading system must not restrict such motion. Figure 3.4 shows a general view of the test setup. Figure 3.5 shows the loading system.

At the locations corresponding to where a bridge girder bears on the prototype flange, a 2-7/8 in. diameter high-strength steel bar (A) was passed through a hole in the web and rested on steel bearing plates on each side of the web. Two 1-1/2 in. steel bars (B) attached this loading bar to a load distribution beam (C). Resting on this

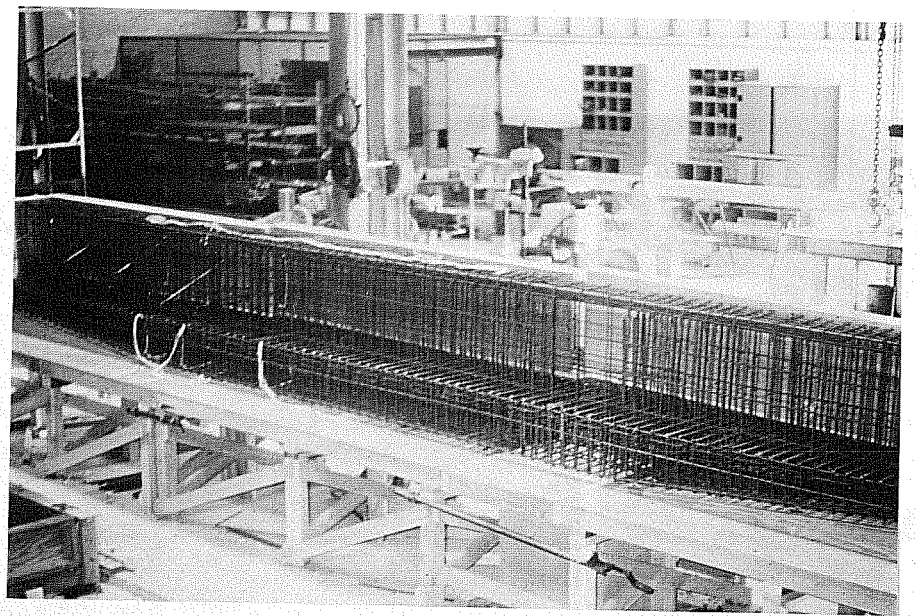

Fig. 3.3 Reinforcing cage for model bent cap

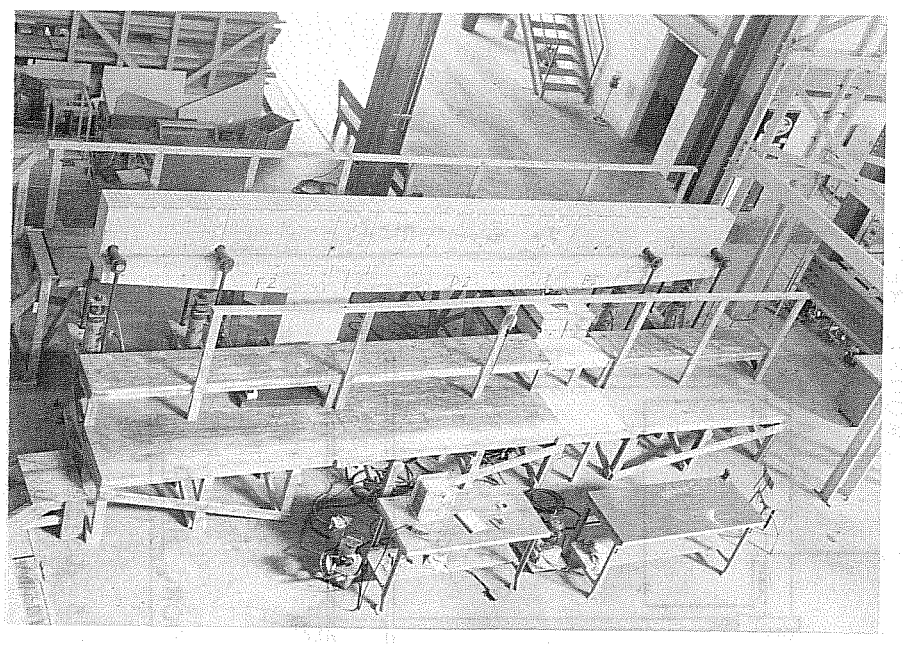

Fig. 3.4 General view of model bent cap test setup

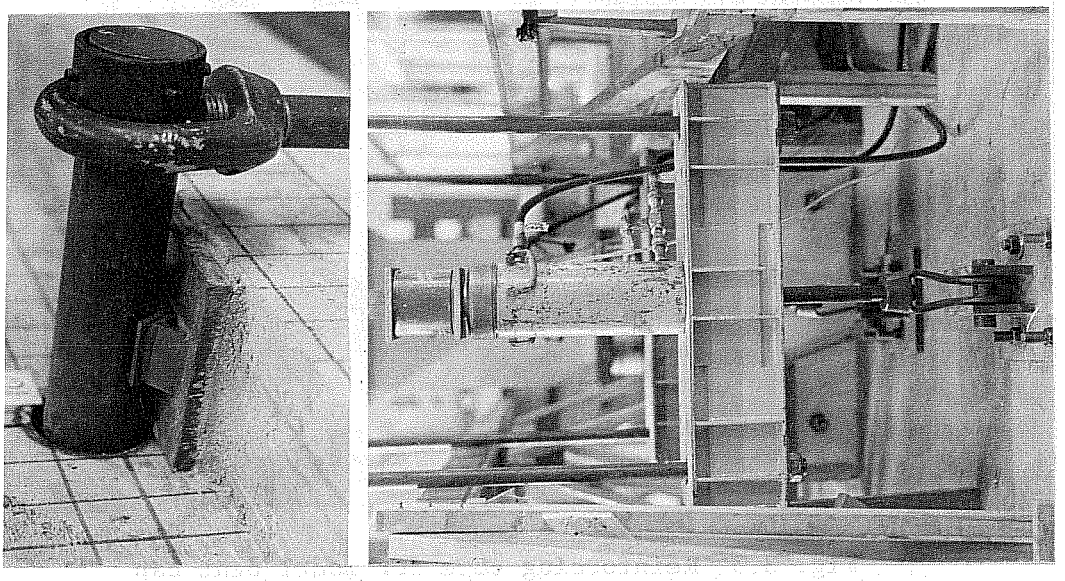

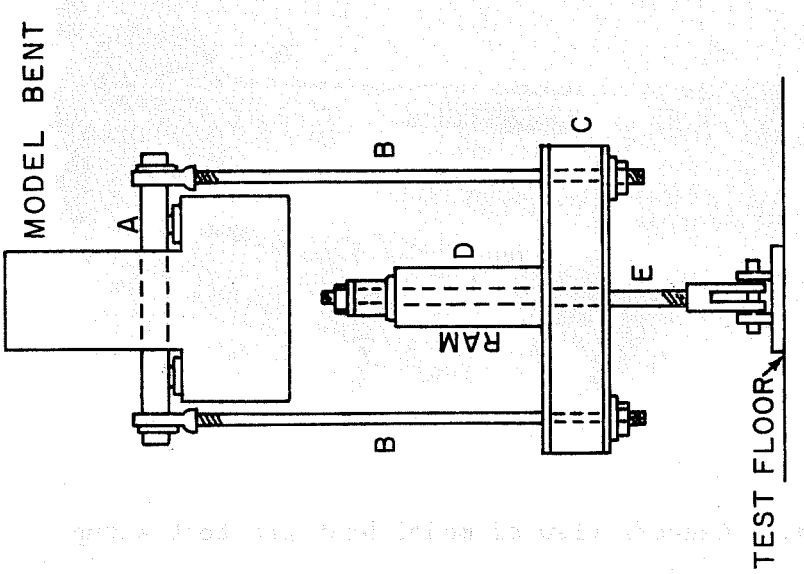

Fig. 3.5 Loading system for model bent cap

beam were a 100-ton ram (D) and load cell, through which passed a 1-1/2 in. bar (E) which was anchored on the top and was attached on the bottom to a clevis-pin device anchored to the test floor. This system loaded both sides of the flanges simultaneously. The flexibility of the system easily accommodated the horizontal movement of the beam (less than 1 in.). To fit the floor tie-down pattern, the actual load application points were changed slightly from those in the prototype. However, load was controlled to apply the correct moment at the column centerline. As in the prototype structure, the exterior loads were 90 percent the value of the interior loads.

Load was applied symmetrically with the two exterior points controlled by one hydraulic system and the two interior points controlled by a second system. Within each set the loads were approximately the same, since the rams were identical and were supplied the same pressure. However, loads were checked by load cells at each ram.

3.2.3.2 Testing Procedure. Ram loads were applied incrementally in a static loading pattern. At each load stage, valves in the hydraulic system at each ram were closed to minimize fluid loss. Then, load cell and hydraulic pressure readings were taken. Deflection readings were taken on dial gages located at the cantilever tip, in the centerspan, and at the roller support (for horizontal movement).

Surface strains were measured at four levels down the side of the beam using Demec points epoxied at 8 in. spacings at each level in the center 6 ft of the beam. An extensometer with a 16 in. gage length provided overlapping deformation measurements from which the average surface strain could be calculated.

At each load stage the structure was checked and cracking marked. Using 60^{X} microscopes graduated to 0.001 in., all cracks in each region were measured wherever a crack intersected horizontal lines drawn on about a 3 in. grid.

Three load stages were used to reach the first cracking load. Load was increased through fifteen additional load stages until the ultimate flexural capacity of the structure had been reached. Several of these load stages corresponded to special loading conditions of the prototype bent cap; for example, dead load moment at the column face, dead plus live load moment at the column face, and dead plus live load moment at centerspan. Testing was stopped when a plot of cantilever tip deflection vs applied load became approximately horizontal (indicating yielding of the main tension reinforcement). At this time a tip deflection of over 3 in. was measured.

3.2.4 Test Results and Comparison with Prototype. The model crack pattern development is shown in Fig. 3.6. At initial cracking in the centerspan, a fairly regular series of long, vertical cracks developed and extended well into the web. With further loading, shorter cracks formed with some curving towards and sometimes joining the nearest long crack. This tree-branch pattern has been discussed by Kani[42] and Beeby[11] (see Sec. 6.2.2). The same pattern developed in the cantilever spans with the exception that some of the cracks inclined towards the support because of shear.

Figure 3.7 shows a comparison between the crack patterns of the two prototype structures and the model structure in the cantilever span at the column. The patterns look quite similar, both in number of cracks and general appearance.

Figure 3.8 shows the distribution of crack widths on the side face of the model in the constant moment region. The average values correspond to the average crack width of all cracks at that level in Region D. The maximum value is the maximum of any crack at that level in Region D. The effect of steel stress on the crack width is shown in Fig. 3.9. Notice that the average and maximum width curves both at the main steel level and in the web are fairly linear with steel stress. Throughout the entire stress range, the crack width in the web was 2 to 2.5 times as large as the crack width at the main

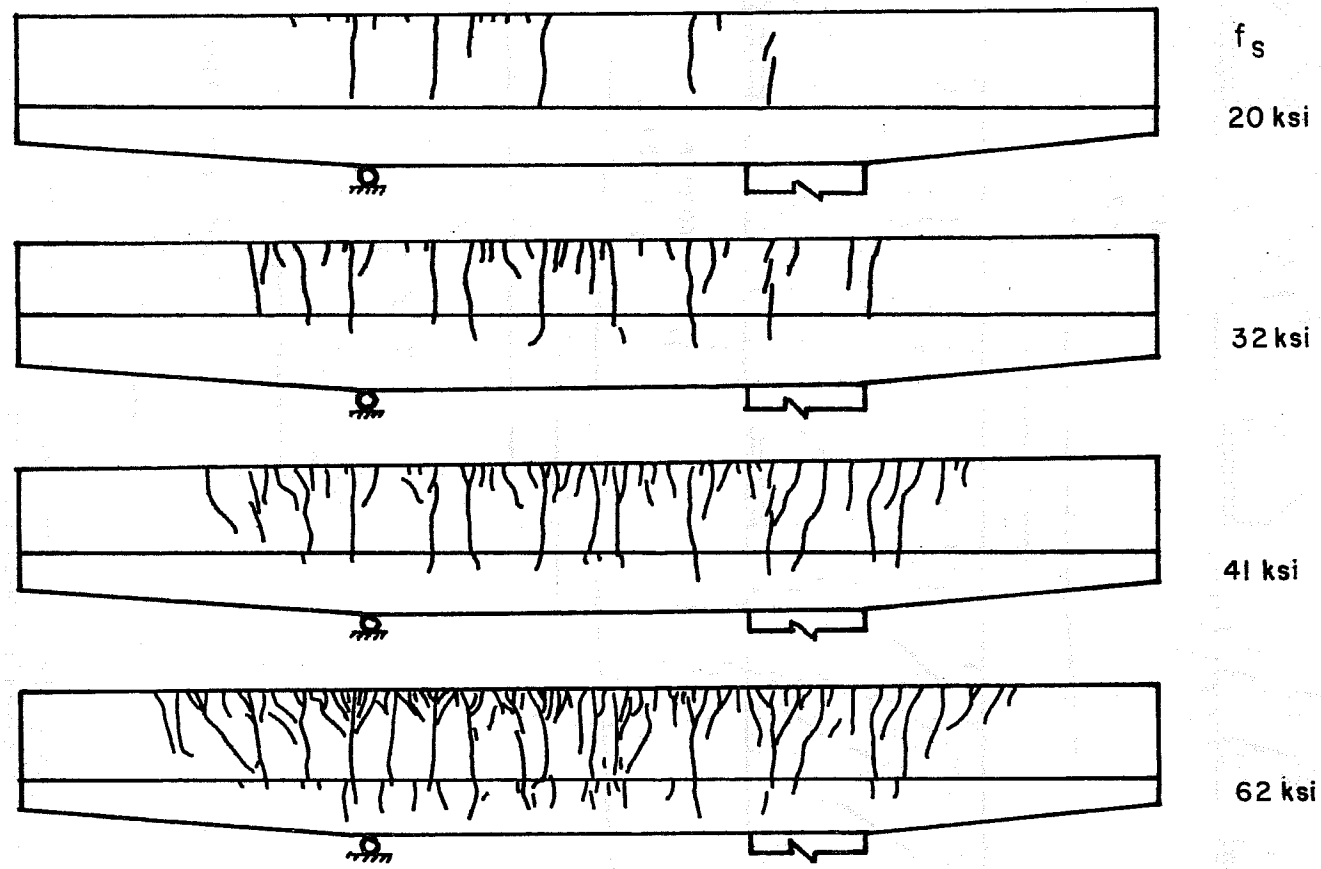

Fig. 3.6 Crack pattern development in 3/8-model bent cap (Ref. 13)

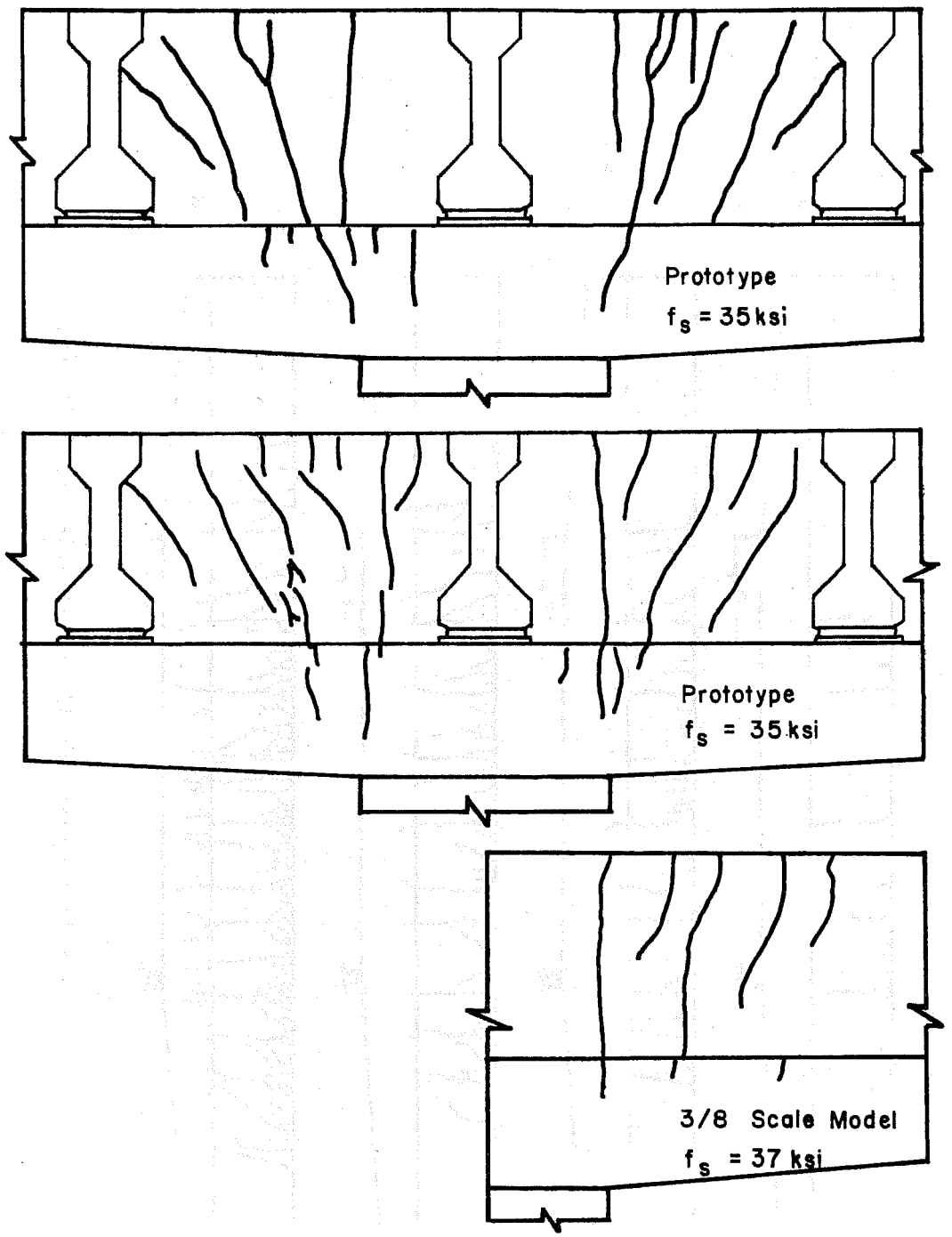

Fig. 3.7 Comparison of crack patterns in prototype and 3/8-scale model bent caps (Ref. 13)

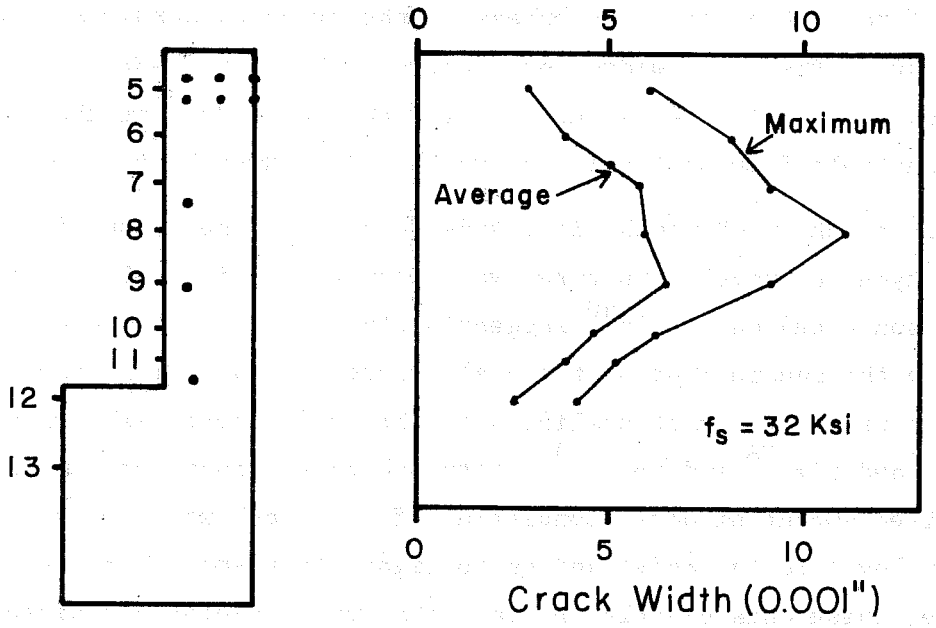

Fig. 3.8 Typical crack profile on side face on model bent cap

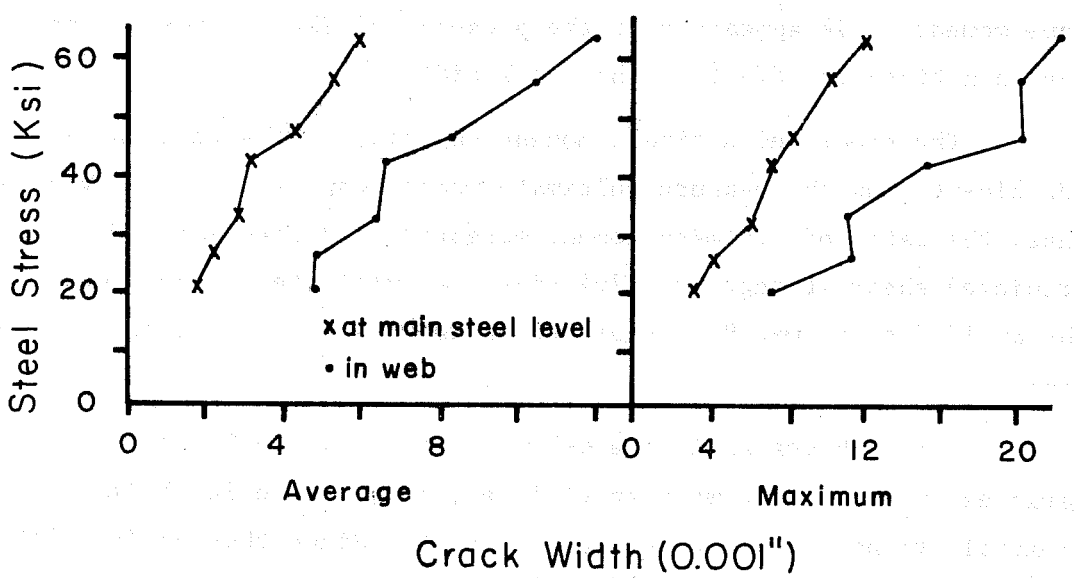

Fig. 3.9 Variation of average and maximum crack widths with steel stress in model bent cap

reinforcement level, even though the bent cap had crack control side face reinforcement slightly in excess of the existing AASHTO and ACI requirements. The crack widths near the main reinforcement were just at the maximum acceptable value. The large crack widths in the web are unacceptable from aesthetic, corrosion, and durability standpoints.

To check crack width similitude, cracks at the column face of the prototype and model structures were compared. Figure 3.10 shows a comparison based on Kaar's[40] suggestion that crack widths are related by the square root of the scale factor. Figure 3.11 shows a comparison based on direct scaling with the scale factor as suggested by Borges and Lima[36] and Beeby.[30] Although this comparison is based on a limited amount of data, consisting of two crack width measurements per level in the model and up to eight measurements in the prototype, these data clearly indicate that crack widths are directly proportional to the scale factor.

Figure 3.12 compares crack widths in the shear span with crack widths in the constant moment region. Cracks at the column face of the prototype and model (subjected to shear and moment) are compared to a long crack in the centerspan of the model (no shear but same moment). It appears that the presence of shear force did not have a noticeable effect on the crack widths.

The predicted ultimate moment capacity of the bent cap was 432 kip-ft, and the measured ultimate moment capacity was 472 kip-ft. Thus, the ratio of ultimate moment measured/predicted was 1.095. The predicted shear strength was 204 kips. At ultimate flexural moment, the applied shear was 91.7 kips; the specimen was well below its shear capacity.

Although cracks in the web were about 2.0 to 2.5 times as large as cracks at the main steel level, no decrease in ultimate flexural strength was noticed in this test. Since the applied shear was significantly less than the specimen's predicted capacity, no

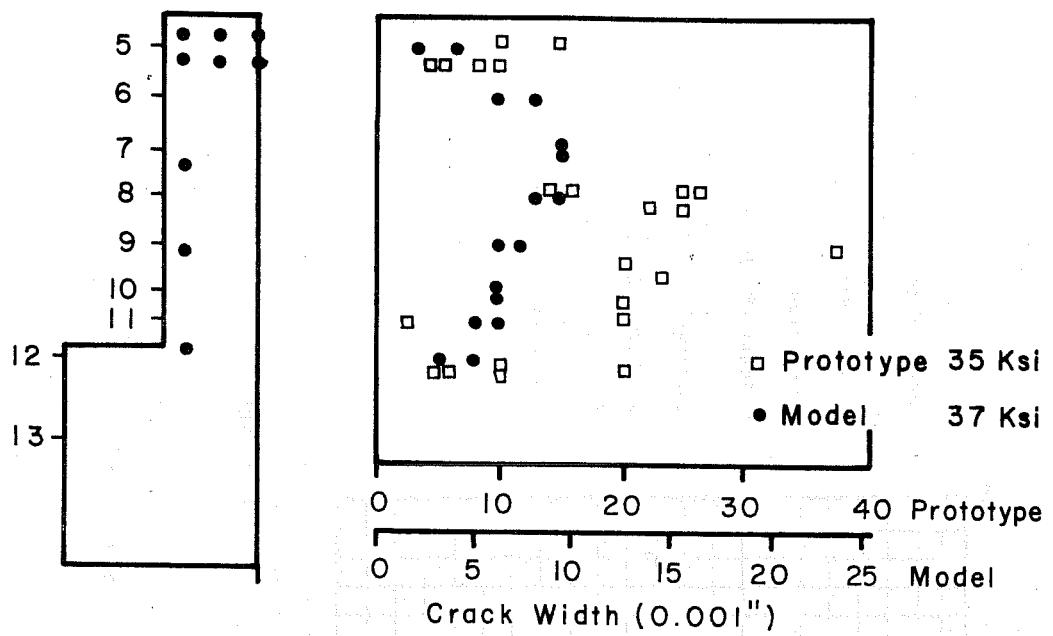

Fig. 3.10 Comparison of crack widths in prototype and model bent caps, scaled to $\sqrt{S_L}$ (Ref. 13)

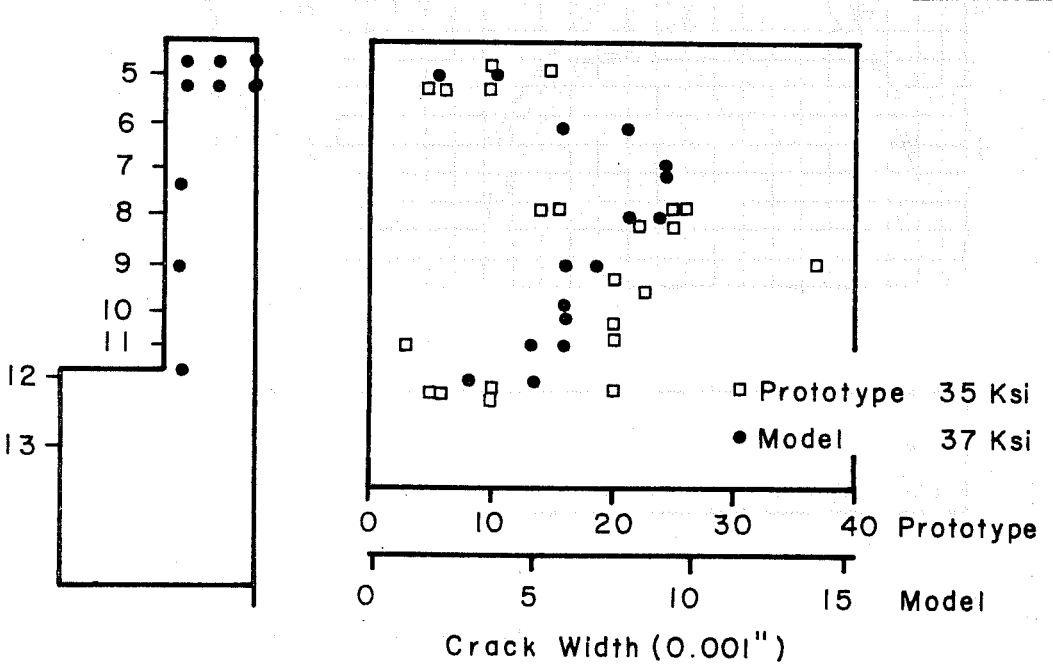

Fig. 3.11 Comparison of crack widths in prototype and model bent caps, scaled to S_L (Ref. 13)

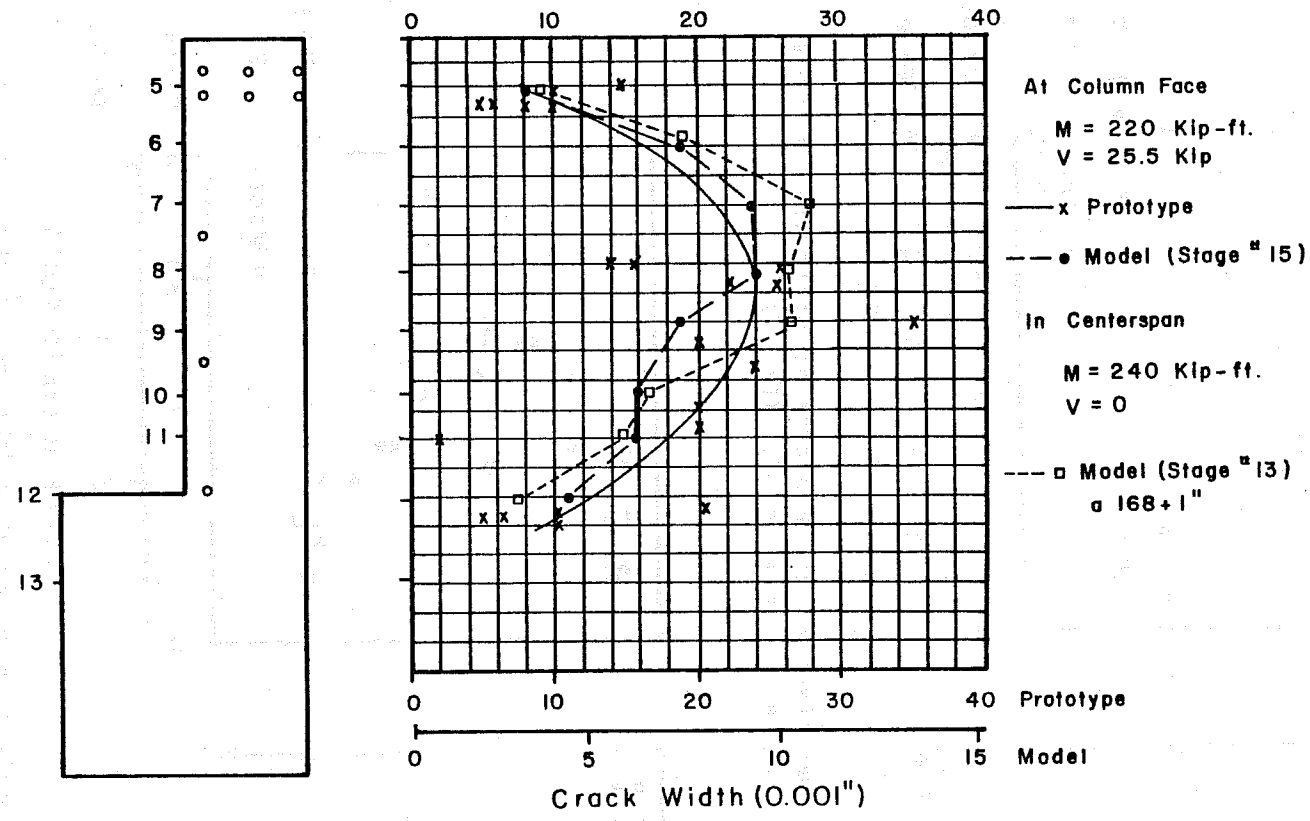

Fig. 3.12 Effect of shear force on crack profile

conclusive statement can be made regarding the effect of the wide side face cracks on the shear capacity at the beam.

3.2.5 Conclusions of Model Test. The results of the 3/8 scale model test support the following conclusions:

(1) Satisfactory crack similitude (pattern and width) was obtained using the direct modeling technique at 3/8 scale with a reduced maximum size aggregate and deformed bars.

(2) The existing ACI and AASHTO code requirements for side face crack control reinforcement are not adequate.

(3) The side face cracking problem exists under conditions of pure moment as well as with shear present.

(4) In this test, cracks in the shear span were not significantly larger than cracks in the constant moment region.

(5) The wide cracks in the web may be objectionable because of corrosion and appearance problems, but they do not seem to affect the ultimate flexural strength of the member.

3.3 Reduced Segment Specimens

3.3.1 Choice of Specimen. Since the overall test program was envisioned to consist of 40 to 50 tests, it would be more economical, more efficient, and more convenient to use a test specimen simpler than the model bent. The model bent test showed that the side face cracking problem is not a result of high shear distress but is also present in regions of constant moment. Therefore, a number of simplified test specimens were studied, all of which permitted testing a region of constant moment. After detailed study, the simplified bent cap specimen shown in Fig. 3.13 was chosen. This specimen may be thought of as representing a segment of a beam under pure moment, with the ends of the specimen approximating long flexural cracks. Tension forces are applied to the main reinforcement, and compression

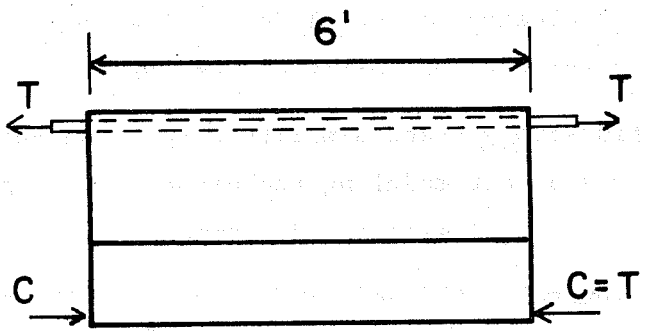

Fig. 3.13 Simplified simulated flexure specimen

forces are applied and located as required by a cracked, transformed area analysis of the section, thus inducing moment in the specimen.

3.3.2 Test Setup. A general view of the test setup is shown in Figs. 3.14 and 3.15. The specimen (A) was supported by rollers on two concrete blocks (B) to raise it to a convenient testing height. Hydraulic rams (C) applied the required tension force directly to the main reinforcement that was extended from each end of the specimen. Rams (D) applied the compression force. A steel frame (E) surrounded the specimen and provided reactions for the rams.

Figure 3.16 shows a detailed view of the tension loading system. Load was transmitted from the ram to the specimen through a series of high strength (150 ksi yield) 1-1/2 in. diameter steel bars and two sets of load distribution channels. Each set of distribution channels was made of two channels, separated by steel pipe spacers to allow passage of the loading bars and the reinforcing bars and then bolted together. A similar load distribution device had been used at West Virginia University[43] in studies of reinforcing bar development lengths. The reinforcing steel was extended through holes drilled in a 1 in. x 6 in. x 12 in. steel plate and was fillet

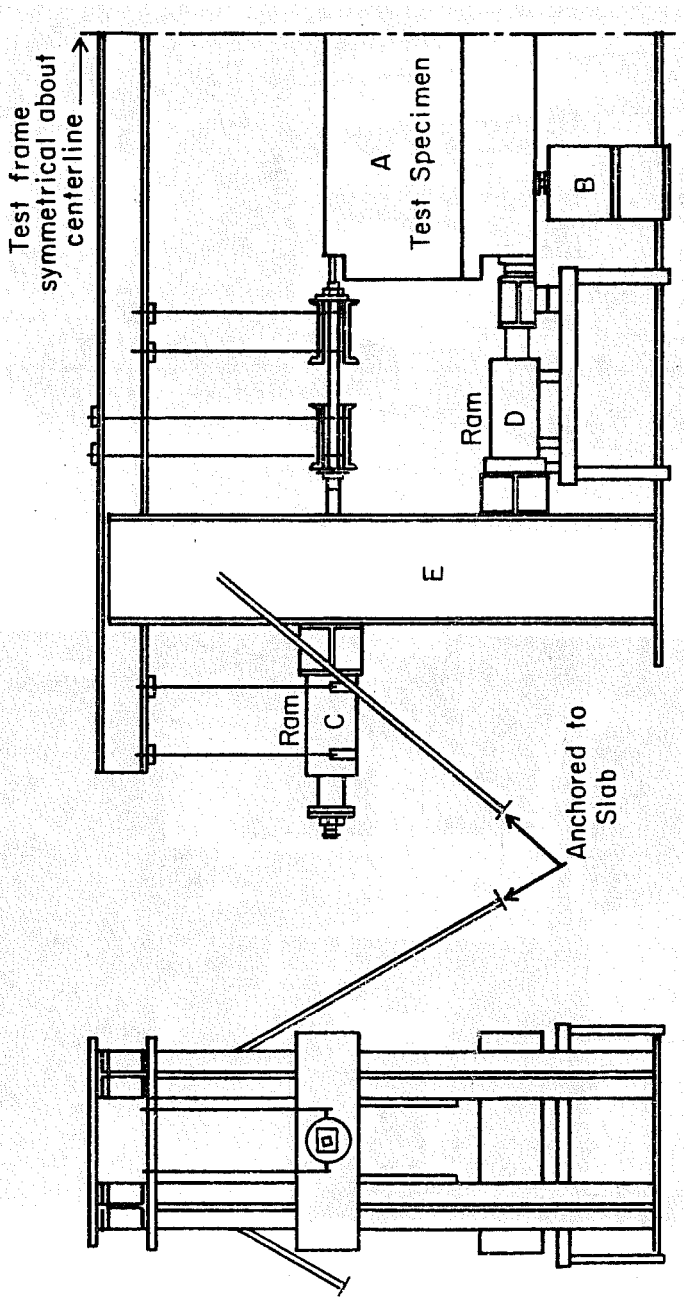

Fig. 3.14 Reduced segment test setup (Ref. 45)

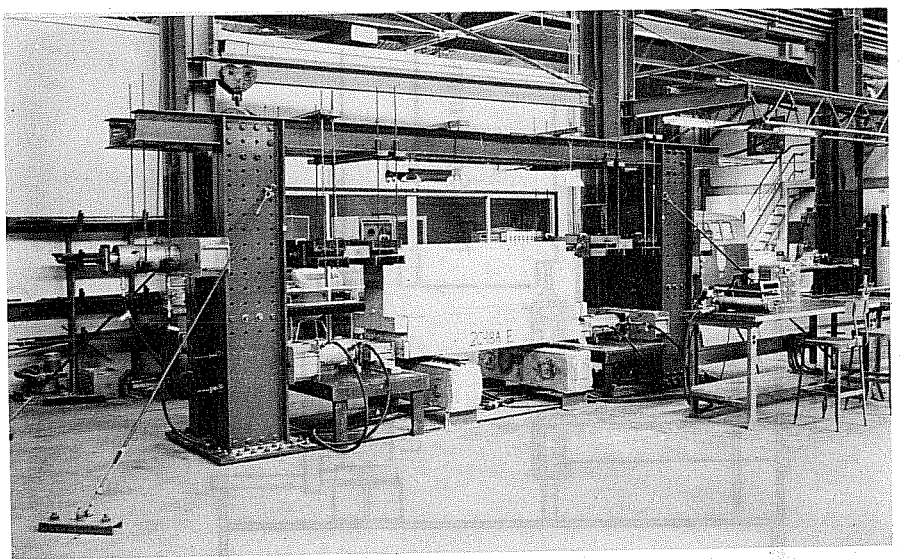

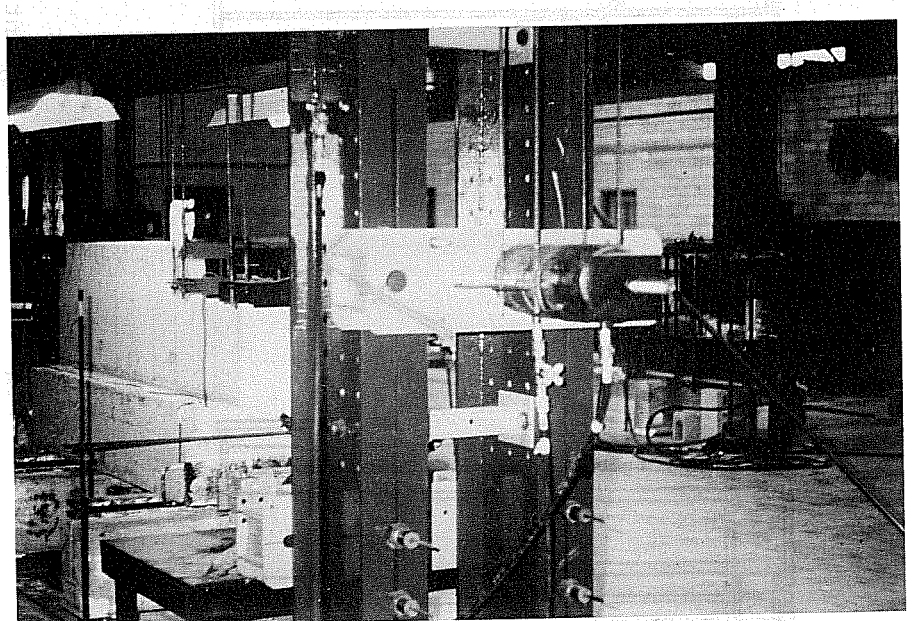

Fig. 3.15 General view of reduced segment test setup

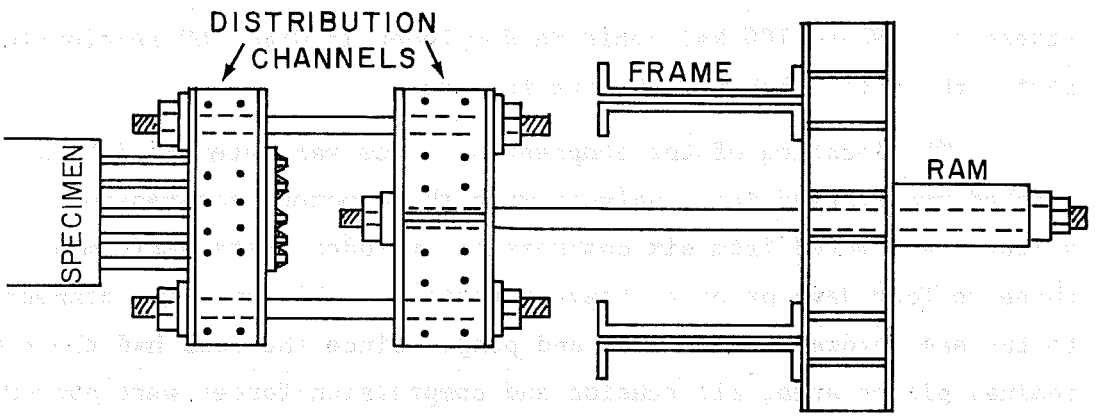

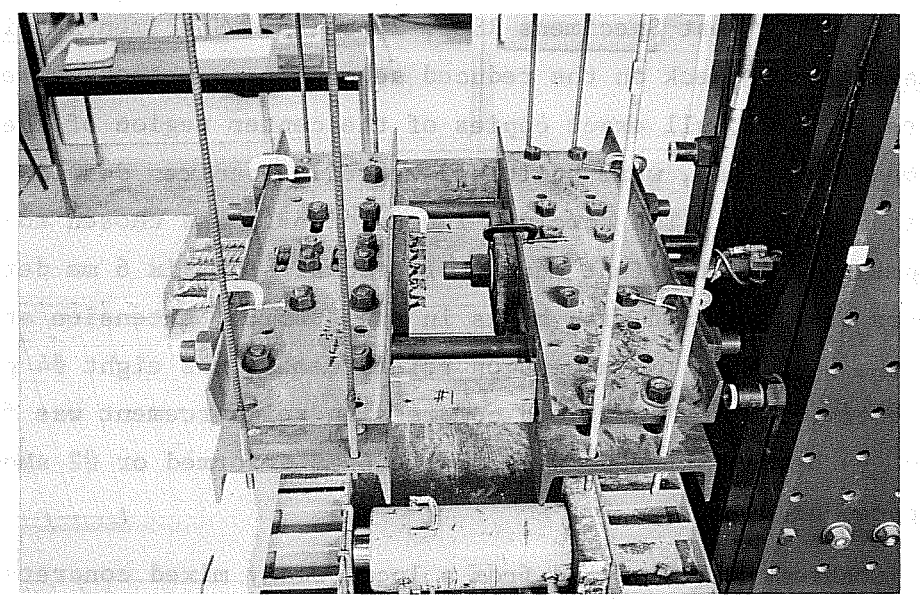

Fig. 3.16 Reduced segment tension loading system

welded to the plate. This plate provided bearing against the load distribution channels. Initial tests on this detail showed that bar stresses of 90 to 100 ksi could be developed in Grade 60 reinforcing bars with ductile behavior before failure.

The location of the compression force was determined by a cracked transformed area analysis with the concrete compression strength estimated from six compression cylinder tests performed three to four days prior to segment testing. All rams were connected to the same hydraulic manifold and pump. Since the rams had the same nominal piston area, all tension and compression forces were approximately equal. Load was controlled by monitoring the strain in the main loading bars in the tension system, which had been calibrated prior to segment testing.

3.3.3 Verification of Test Method

3.3.3.1 Test Specimens RS-1, 2, and 3. Specimen Details and Materials. As a check on the reduced segment test method, a series of three segments, all exact copies of the center region of the 3/8 scale model bent cap, were built and tested. Specimen details are shown in Fig. 3.17. The specimen length of 6 ft was chosen to allow development of a sufficient number of cracks. The six 6 mm deformed face bars were anchored with hooks in the 4.25 in. extension at each end of the specimen. Main tension reinforcement was eight #4 plus two #5 bars (2.22 sq. in.), and compression reinforcement was four #3 plus two #4 bars. Stirrups were double 6 mm deformed or #2 smooth bars spaced at 3 in.

Concrete was obtained from a local ready mixed concrete plant and was 5/7 in. maximum size aggregate, sand, and Type I cement. Specimens RS-1 and RS-2 were cast with a slump of about 8 in., while RS-3 had a slump of 5 in. Table 3.2 gives a summary of all material properties.

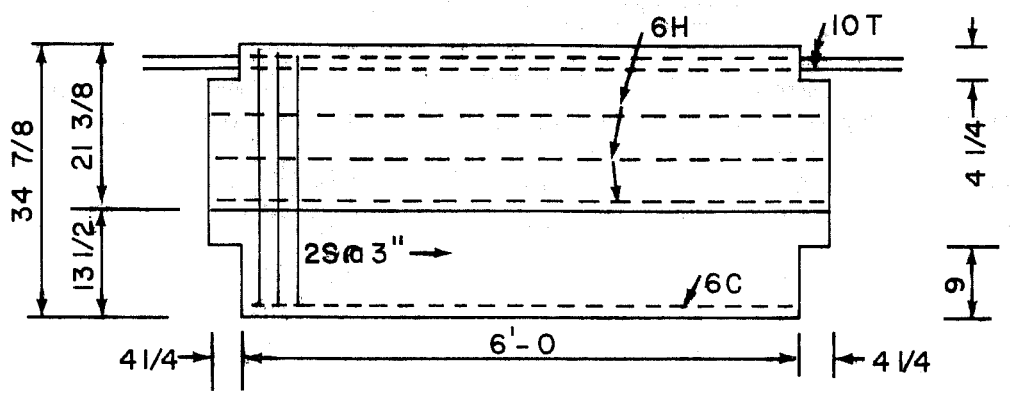

Fig. 3.17 Details of Specimens RS-1, 2, and 3 (see Fig. 3.2 for more complete details)

Fabrication. Specimens were cast with tension reinforcement on top. Cages were tied and placed in the forms, which were the same as used for the 3/8 model bent. The cages were held accurately in position with bottom chairs to provide bottom cover and lateral tie bars to provide side cover. The specimens were cast in two lifts, one for the flange and one for the web.

Instrumentation. For strain measurements, Demec points were attached to the specimen with epoxy prior to testing at locations shown in Fig. 3.18. Within the center 4 ft of the specimen, Demec points were spaced at 8 in. Using a 16 in. gage length extensometer to measure between every other point, there was an overlap of 8 in. in every reading. To determine any strain correction due to temperature variation, reference gages were attached to a second unstressed beam.

A grid was drawn with felt tip pens on the side and tension face of the specimen. The grid, shown in Fig. 3.19, was used to identify crack locations. Each grid point was identified by a

TABLE 3.2 MATERIAL PROPERTIES OF RS-1, 2, AND 3

Concrete Mix (1 cu. yd.)

Specimen	Cement Type I (lb)	Aggregate (lb) Coarse (5/8")	Sand	Water (Gal)	Slump (in)
RS-1	541	1813	1483	35	8
RS-2	541	1813	1483	35	8
RS-3	541	1813	1483	30	5

Concrete Strength (psi)

Specimen	f'_c	f_{sp}
RS-1	2944	—
RS-2	3183	—
RS-3	4920	410

Reinforcement

Bars		Stress (ksi) Yield	Ultimate
Main Tension (T)	#5	71.8	104.4
	#4	62.3	91.8
Face Bars (H)	6 mm	77.0	—
Compression (C)	#4	62.3	91.8
	#3	65.6	91.5

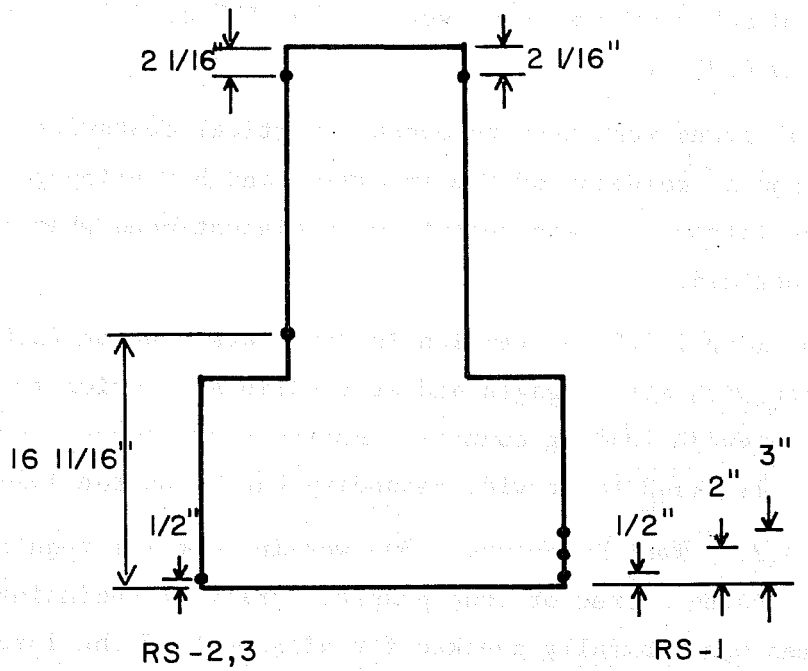

Fig. 3.18 Demec layout for strain measurements

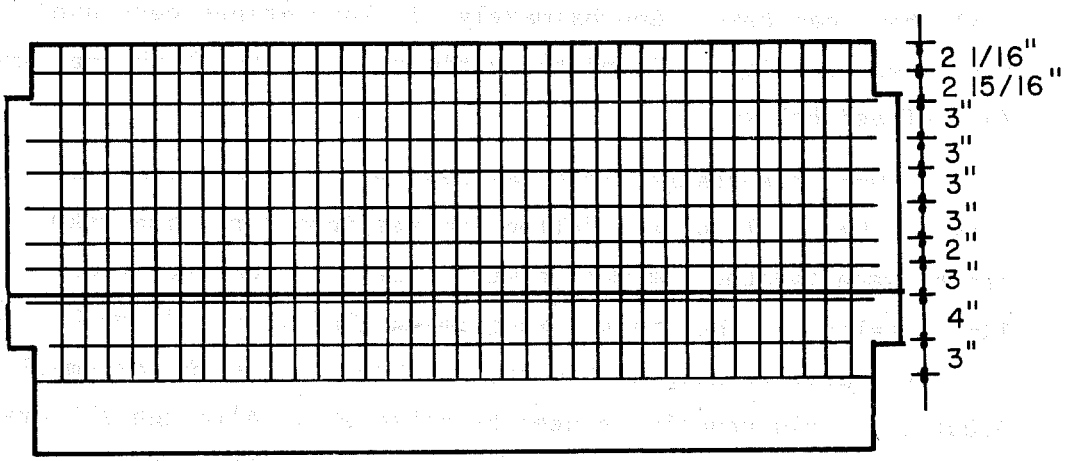

Fig. 3.19 Grid layout for crack measurements

horizontal level line and a distance measured from the end of the specimen. Crack widths were measured using 50^{x} or 60^{x} microscopes graduated to 0.001 in.

Dial gages were used to measure vertical centerline deflection, horizontal movement of the specimen, and bar slippage at the welds. The latter two measurements were discontinued when no problems were noticed.

The main 1-1/2 in. tension loading bars, one on each end, were instrumented with strain gages and were calibrated prior to specimen testing to provide loading control. Pressure transducers and pressure gages were also used to provide secondary checks on the load.

3.3.3.2 Test Procedure. One working day was required to test a specimen, using a crew of four people. Prior to beginning the test, the specimen was carefully checked for alignment of the loading system. Initial readings were recorded for the Demec points, loading bars, pressure gages, and dial gages. Two load stages were used to reach the estimated first cracking load. At these stages, Demec readings and loading measurements were taken. The first cracking load was carefully noted. After cracking, load was applied such that the main steel stress in the segment was the same as the stress in the 3/8 scale bent cap test. Approximately six load stages were used between the first cracking load and the ultimate capacity of the specimen (as defined below).

Once the desired load was reached, the valves at each ram were closed. Demec, load, and deflection readings were then taken. All cracks were located and marked with a felt tip marker by drawing a line parallel to the crack. Magnifying glasses and "trouble lights" were available to help locate cracks; however, cracks as small as 0.001 in. could usually be seen by naked eye. Although all cracks were marked, only those cracks in the center 4 ft of the specimen were measured, omitting 1 ft at each end because of possible localized

effects due to the loading method. Crack width measurements were taken where a crack crossed a horizontal grid line. A pencil mark was placed at the location of measurement so that at subsequent load stages the same location would be measured. Sometimes a crack would divide itself into two or three closely spaced smaller cracks for a short distance. In these instances the crack was considered to be a single crack of width equal to the sum of the smaller cracks. However, close parallel cracks that were clearly separate cracks were considered individually. Cracks were not separated as primary and secondary cracks. Crack patterns were drawn and photographed at each load stage. Before opening the valves, second readings were taken on the loading bars.

The final load stage occurred at yielding of the main reinforcement that extended out each end of the specimen. The loading channels were closely watched for any twisting, which indicated yielding of the reinforcement. If twisting occurred, the test was stopped to avoid any damage to the loading system. At the conclusion of the test, reference readings were taken on the loading bars, pressure gages, and dial gages.

3.3.3.3 Test Results. The general cracking performance of RS-1, 2, and 3 was quite similar. Initial cracking was easily detected by a sharp popping noise. Cracking developed with the formation of several long cracks that sometimes extended to the flange. With further loading, these cracks extended, and shorter cracks also formed. Several of these shorter cracks extended vertically towards the flange, while some cracks curved inwards towards the nearest long crack. The crack pattern development of RS-1, 2, and 3 is shown in Fig. 3.20. Beyond a main steel stress to 30 - 35 ksi, very few new cracks formed, and older cracks extended slightly.

Each specimen had crack widths in the web that were more than double the crack widths at the main steel level (see Fig. 3.24).

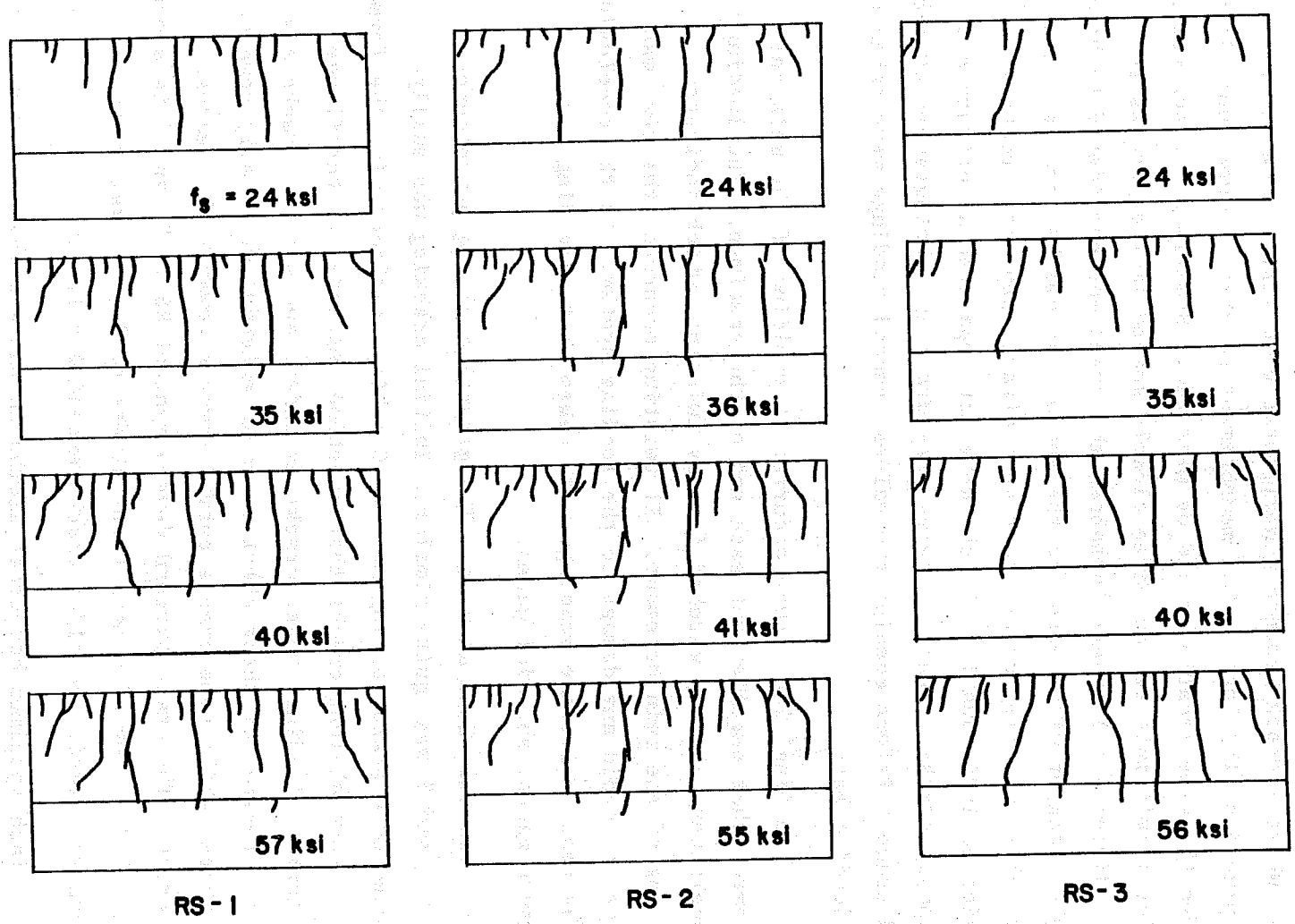

Fig. 3.20 Crack pattern development for RS-1, 2, and 3

Figure 3.21 presents the variation of the average and maximum crack widths with steel stress for the three specimens.

3.3.3.4 Comparison of Segment and Beam Test Results. Segment Specimens RS-1, 2, and 3 were compared with the 3/8 scale model bent cap to check the segment test method. Three test results were compared: moment-curvature relationships, crack patterns, and crack width profiles.

The moment-curvature relationships for the bent cap and RS-3 are shown in Fig. 3.22. Average curvatures were determined from the Demec surface strain measurements with a least squares analysis used to describe the different levels of Demec points. Moments in the bent cap correspond to moments at the column centerline, while moments in the segment are calculated from the measured applied load and the lever arm between the tension and compression forces. Both curves are very similar and can be represented well by two straight lines, an initial steeper segment corresponding to an uncracked specimen and a flatter section where cracking occurred. The difference between the results prior to first cracking is not significant, because in this region strains are quite small and small errors in strain measurements greatly affect the calculated curvature. The results show that the reduced segments deformed similar to a beam under constant moment loading.

Crack patterns are compared in Fig. 3.23. The center 6 ft of the bent cap is shown. Although the steel stresses vary from 41 to 48 ksi, the patterns are all very similar. Approximately the same number of cracks formed in each specimen.

The variation of crack widths down the side faces of the specimens at different steel stresses is shown in Fig. 3.24. The reduced segments and the bent cap all have very similar crack width profiles, both in shape and size of crack widths. Figure 3.25 shows the

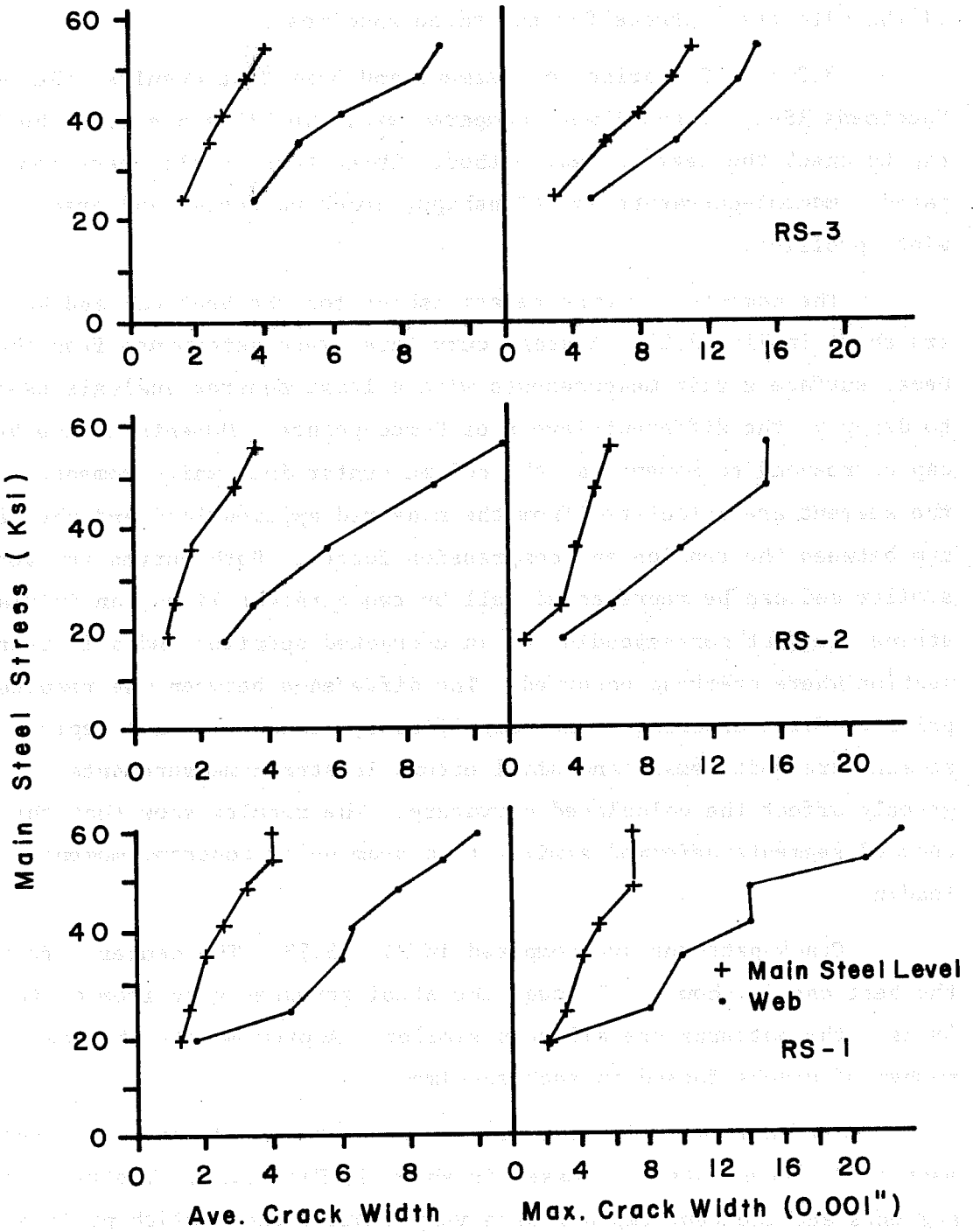

Fig. 3.21 Variation of average and maximum crack widths with steel stress for RS-1, 2, and 3

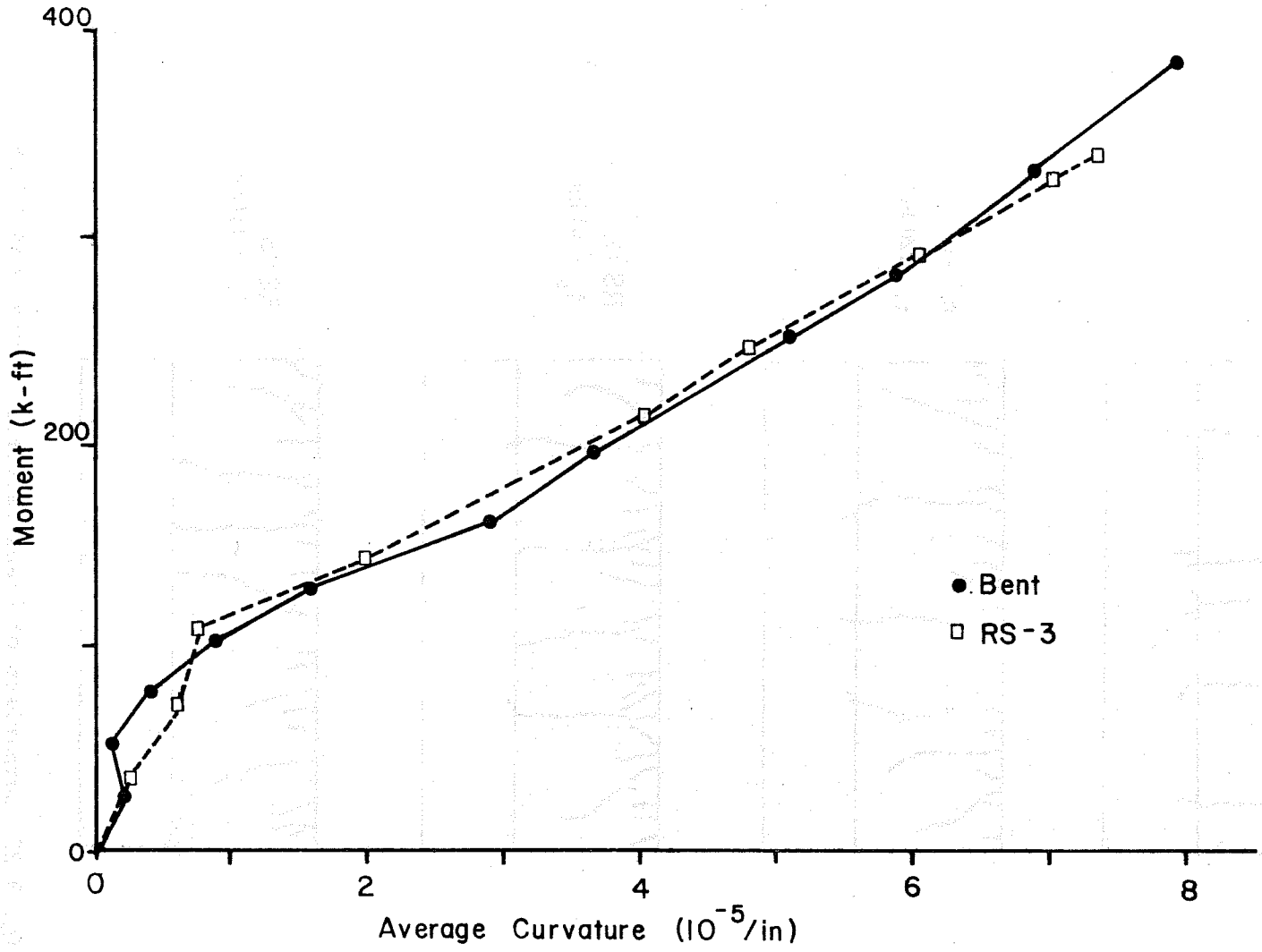

Fig. 3.22 Moment-curvature relationships for model bent and Specimen RS-3 (Ref. 13)

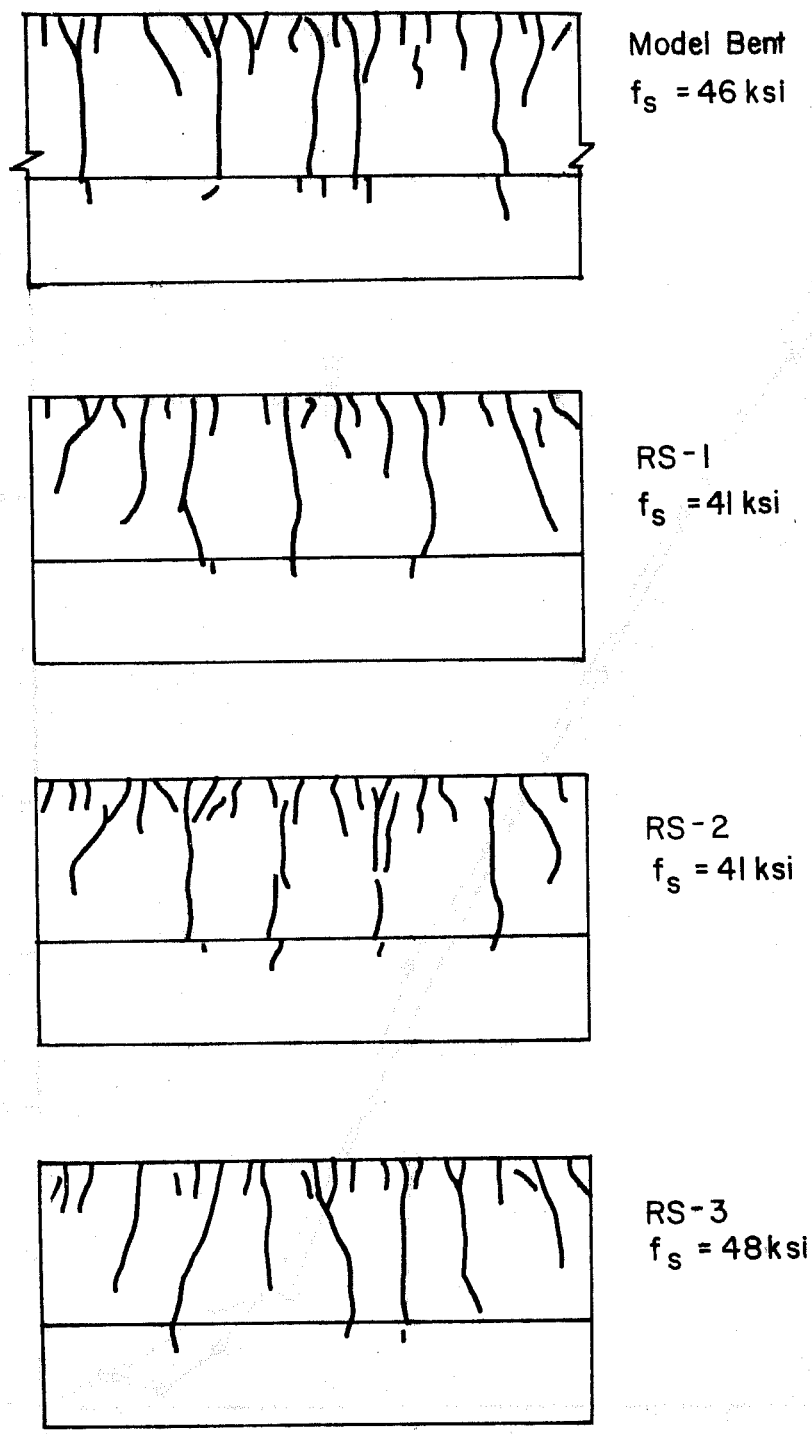

Fig. 3.23 Comparison of crack patterns between model bent and reduced specimens (Ref. 13)

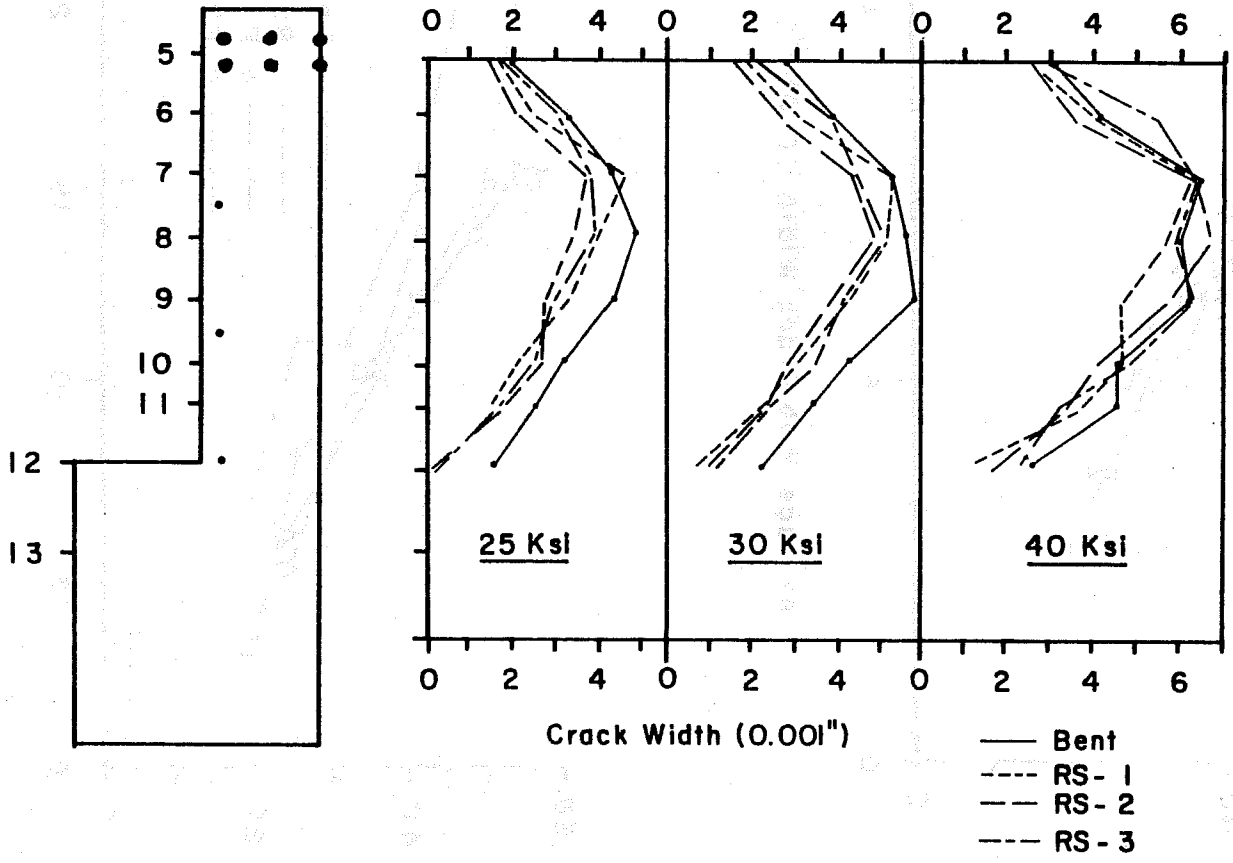

Fig. 3.24 Comparison of average crack width profiles for bent and reduced specimens

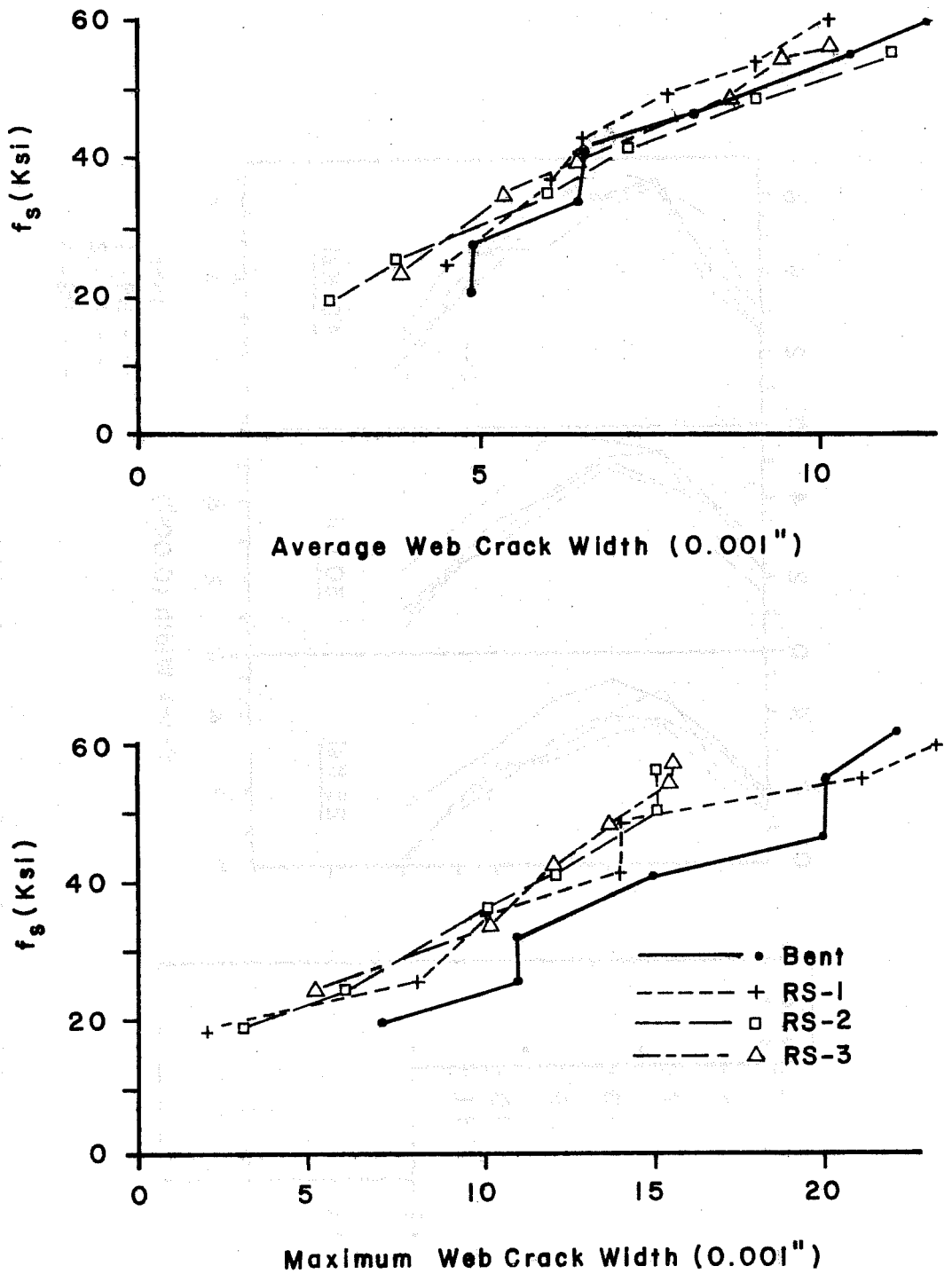

Fig. 3.25 Variation of average and maximum web crack widths in model bent, RS-1, 2, and 3

variation of average and maximum web crack widths with steel stress for all specimens. Again, there is good agreement between the reduced segments and the bent cap.

3.3.4 Conclusions of Reduced Segment Tests. The reduced segment test results support the following conclusions:

(1) The reduced segment specimen accurately simulates the crack patterns, crack profiles, and deformation of a section of a full length beam under constant moment loading.

(2) The side face cracking problem exists under conditions of pure moment.

(3) The three reduced segments had similar test results, indicating good reproducibility of results.

(4) If a large number of specimens must be tested, a reduced segment specimen would probably be more economical and efficient than a full length beam specimen.

On the basis of the very good results from the reduced segment tests, the reduced segment specimen was chosen as the test specimen for the parameter study that followed. A redesigned full length model bent cap and its companion reduced segment were built and tested as the final two specimens in this project. These tests will be discussed in Chapter 7; however, their results also supported the validity of the reduced segment test method.

CHAPTER 4

EXPERIMENTAL PARAMETER STUDY

4.1 Objectives

Since little previous work had been done on side face crack control, a flexible test program was designed, research objectives were formulated, and tentative specimen series were planned. However, specimen designs were finalized throughout the entire course of the project as further information was obtained. The testing program required two years of laboratory work with most of the reduced segment testing being done at the rate of three or four tests per month.

A total of 44 specimens was constructed and tested in the experimental program, including four specimens used in the test method development (Chapter 3) and two specimens constructed to verify a new design procedure (Chapter 7). The experimental program examined the effects of the following variables on the web crack width:

(1) Amount and location of skin reinforcement

(2) Cover on skin reinforcement

(3) Type of skin reinforcement--deformed bars or welded wire fabric mesh

(4) Beam depth

(5) Beam width

In addition, the secondary effects of concrete strength and main tension reinforcement distribution were also studied.

4.2 Specimen Details

Forty-two specimens were constructed using the reduced segment specimen developed in Chapter 3. Two full-length model bent

cap specimens, one exact copy of the prototype bent cap and one redesigned bent cap were also built. Table 4.1 and Fig. 4.1 give all specimen details. Figs. 3.17 and 3.2 show typical side views of the reduced segment and bent cap specimens, respectively. Each specimen is identified by a label, X-N. where X is a letter indicating the test series and N is an integer. Any specimen identified as X-N-0 has no skin reinforcement. In specimens without shear reinforcement, the skin steel was positioned with three stirrups, one at the center and one at each end of the specimen.

Segments RS-1, 2, and 3 were exact copies of the centerspan region of the model bent cap BC-1 described in Chapter 3. They were used to verify the reduced segment test method. RS-4-0 was similar to RS-1, 3, and 3, but had only main tension and compression reinforcement; thus it had no stirrups, skin, or flange reinforcement. Segment A-15 and bent cap specimen BC-2 were proof tests of a new design procedure, as discussed in Chapter 7. In all these specimens the main tension reinforcement was placed as ten bars.

The effect of amount and location of skin reinforcement was examined in Series A. The cross section was similar to Series RS, but the main tension reinforcement was changed from eight #4 plus two #5 bars to five #6 bars to simplify construction.

The effect of cover on the skin reinforcement was studied in Series C. All specimens had identical amounts and distribution of skin reinforcement, but with covers on the skin reinforcement of 3/4 in., 1-1/2 in., 2 in., and 3 in.

The effect of beam depth by varying the specimen depth from 22.8 in. to 32.8 in. (Specimen A-2-0) to 47.1 in. was examined in Series D. Specimen D-4-0 was approximately a 2/3 scale model of D-2-0 and was used to check the results of the 47 in. deep section.

Four different welded wire fabric meshes were used for skin reinforcement in Series M. Sheets of mesh were bent into a U-shape

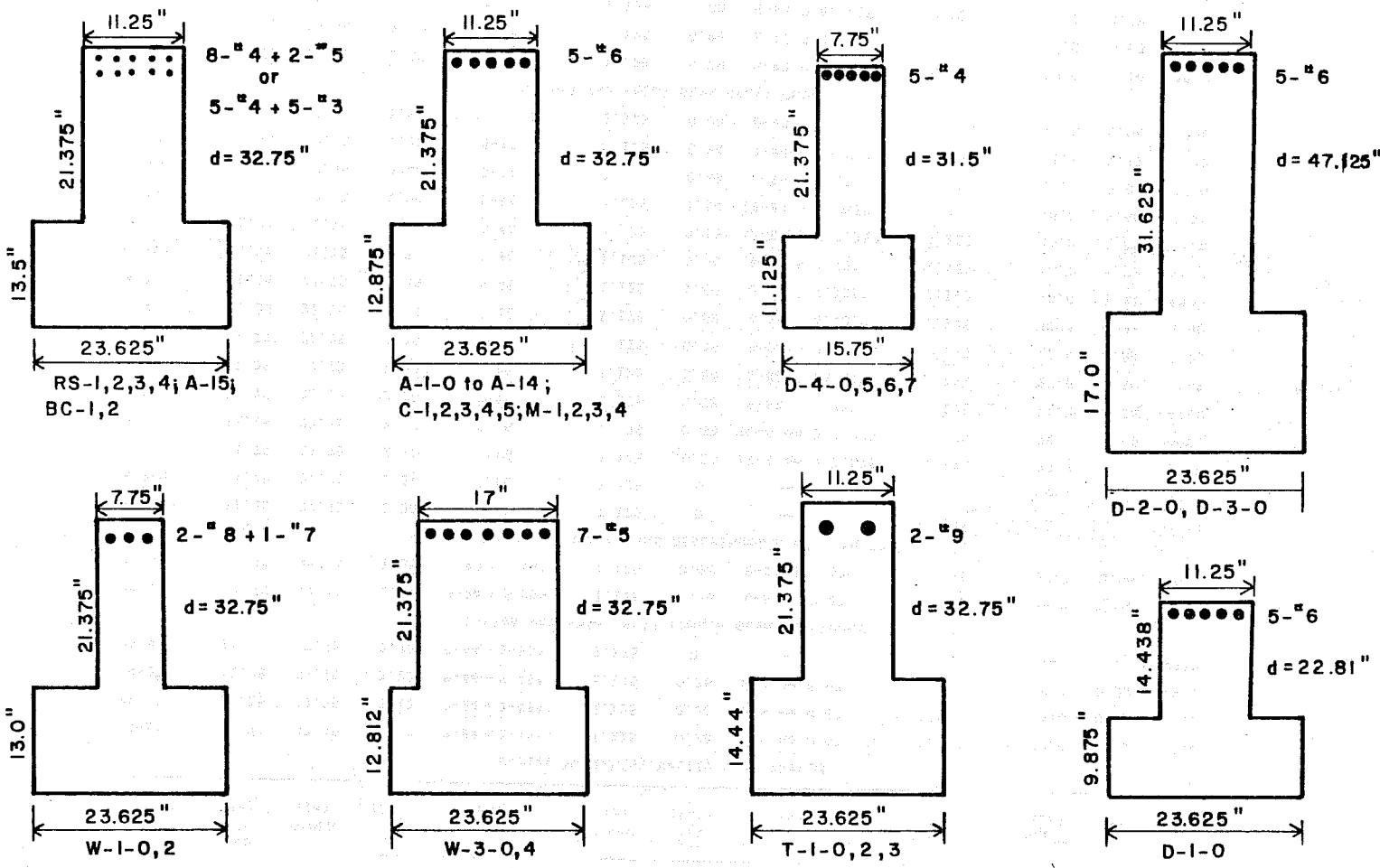

Fig. 4.1 Specimen cross section details (see Table 4.1 for skin reinforcement location and reinforcement cover)

TABLE 4.1 SPECIMEN DETAILS

Spec ID	Web Width (in)	Depth (in)	Main Reinforcement A_s (in^2)	Main Reinforcement Bars	Main Reinforcement Cover (in)	Skin Reinforcement A_{sk} (in^2)	Skin Reinforcement Bars	Skin Reinforcement Cover (in)	H_{sk}** (in)	ρ_{sk}† (%)	f'c (psi)
Series Variable: Verify Test Method											
RS-1§	11.25	32.75	2.22	8-#4 + 2-#5*	1.125	0.26	6-6 mm @ 6"	1.125	24.0	0.22	2944
RS-2§	11.25	32.75	2.22	8-#4 + 2-#5*	1.125	0.26	6-6 mm @ 6"	1.125	24.0	0.22	3183
RS-3§	11.25	32.75	2.22	8-#4 + 2-#5*	1.125	0.26	6-6 mm @ 6"	1.125	24.0	0.22	4920
RS-4-0	11.25	32.75	2.22	8-#4 + 2-#5*	1.125	0	—	—	—	0	4890
Series Variable: Full Length Beam Specimens											
BC-1§	11.25	32.75	2.22	8-#4 + 2-#5*	1.125	0.26	6-6 mm @ 6"	1.125	24.0	0.22	5739
BC-2§	11.25	32.75	1.55	5-#3 + 5-#4*	1.125	0.88	8-#4 @ 3.5"	1.125	17.5	0.96	4613
Series Variable: Amount and Distribution of Skin Steel											
A-1-0	11.25	32.75	2.20	5-#6	1.125	0	—	—	—	0	4913
A-2-0	11.25	32.75	2.20	5-#6	1.125	0	—	—	—	0	4975
A-3	11.25	32.75	2.20	5-#6	1.125	0.53	12-6 mm @ 3.875"	1.125	27.1	0.39	5320
A-4	11.25	32.75	2.20	5-#6	1.125	0.88	20-6 mm @ 2.375"	1.125	26.1	0.68	6062
A-5	11.25	32.75	2.20	5-#6	1.125	0.88	8-#3 @ 5.25"	1.125	26.2	0.64	6310
A-6	11.25	32.75	2.20	5-#6	1.125	0.88	2-#6 @ 13.375"	1.125	26.8	0.56	4669
A-7	11.25	32.75	2.20	5-#6	1.125	0.35	8-6 mm @ 4.125"	1.125	20.6	0.34	5521
A-8	11.25	32.75	2.20	5-#6	1.125	0.88	8-#3 @ 4.125"	1.125	20.6	0.81	4580
A-9	11.25	32.75	2.20	5-#6	1.125	1.60	8-#4 @ 4.125"	1.125	20.6	1.41	5231
A-10	11.25	32.75	2.20	5-#6	1.125	0.80	4-#4 @ 6.75"	1.125	20.2	0.72	5438
A-11	11.25	32.75	2.20	5-#6	1.125	0.53	12-6 mm @ 2.25"	1.125	15.8	0.67	5416
A-12	11.25	32.75	2.20	5-#6	1.125	1.54	14-#3 @ 2.063"	1.125	16.5	1.80	5320
A-13	11.25	32.75	2.20	5-#6	1.125	0.88	2-#6 @ 8.5"	1.125	17.0	0.86	4810
A-14	11.25	32.75	2.20	5-#6	1.125	0.84	2-#4+4-#3 @ 2.875"	1.125	11.5	1.37	4810
A-15§	11.25	32.75	1.55	5-#3 + 5-#4*	1.125	0.88	8-#3 @ 3.5"	1.125	17.5	0.96	4636
Series Variable: Skin Steel Cover											
C-1	11.25	32.75	2.20	5-#6	1.125	0.88	8-#3 @ 4.125"	0.75	20.6	1.14	4878
C-2	11.25	32.75	2.20	5-#6	1.125	0.88	8-#3 @ 4.125"	1.50	20.6	0.63	5290
C-3	11.25	32.75	2.20	5-#6	1.125	0.88	8-#3 @ 4.125"	2.00	20.6	0.49	4783
C-4	11.25	32.75	2.20	5-#6	1.125	0.88	8-#3 @ 4.125"	3.00	20.6	0.38	4768
C-5	11.25	32.75	2.20	5-#6	1.125	0.88	8-#3 @ 4.125"	3.00	20.6	0.38	4386

Series Variable: Beam Depth											
D-1-0	11.25	22.81	2.20	5-#6	1.125	0	—	—	—	—	3876
D-2-0	11.25	47.125	2.20	5-#6	1.125	0	—	—	—	—	3979
D-3-0	11.25	47.125	2.20	5-#6	1.125	0	—	—	—	—	5330
D-4-0	7.75	31.5	1.00	5-#4	0.75	0	—	—	—	—	5000
D-5	7.75	31.5	1.00	5-#4	0.75	0.44	10-6 mm @ 2.75"	0.75	16.5	0.76	3339
D-6	7.75	31.5	1.00	5-#4	0.75	0.88	8-#3 @ 3.375"	0.75	16.9	1.39	4969
D-7	7.75	31.5	1.00	5-#4	0.75	1.54	14-#3 @ 2.063"	0.75	16.5	2.52	3410
Series Variable: Welded Wire Fabric Mesh as Skin Steel											
M-1	11.25	32.75	2.20	5-#6	1.125	0.17	12.5 Gage†† @ 2"×4"	1.125	26.8	0.15	4780
M-2	11.25	32.75	2.20	5-#6	1.125	0.50	5 Gage†† @ 4"×3"	1.125	26.8	0.42	5960
M-3	11.25	32.75	2.20	5-#6	1.125	0.70	5 Gage†† @ 3"×4"	1.125	26.8	0.58	6085
M-4	11.25	32.75	2.20	5-#6	1.125	1.10	5 Gage†† @ 2"×1.5"	1.125	26.8	0.91	4740
Series Variable: Full Size Beam											
T-1-0	11.25	32.75	2.00	2-#9	2.50	0	—	—	—	0	4693
T-2	11.25	32.75	2.00	2-#9	2.50	0.35	8-6 mm @ 4.125"	1.125	20.6	0.34	5009
T-3	11.25	32.75	2.00	2-#9	2.50	0.88	8-#3 @ 4.125"	1.125	20.6	0.81	4269
Series Variable: Web Width											
W-1-0	7.75	32.75	2.18	2-#8 + 1-#7	1.125	0	—	—	—	0	4025
W-2	7.75	32.75	2.18	2-#8 + 1-#7	1.125	0.88	8-#3 @ 4.125"	1.125	20.6	0.81	3418
W-3-0	17.0	32.75	2.17	7-#5	1.125	0	—	—	—	0	4480
W-4	17.0	32.75	2.17	7-#5	1.125	0.88	8-#3 @ 4.125"	1.125	20.6	0.81	3433

flange width = 23.625" except for D-4-0, 5, 6, and 7, where it is 15.75"

*A_s bars in two layers with 1" clear spacing

**H_{sk} = depth of web in which A_{sk} is distributed (see Fig. 6.42)

†ρ_{sk} = percentage of skin reinforcement (see Fig. 6.42)

§Double 6 mm stirrups at 3"

††12.5 Gage = 0.098" diameter

5.0 Gage = 0.252" diameter

grid spacing is horizontal bar spacing by vertical bar spacing

so that longitudinal bars were uniformly distributed along the top tension face and throughout the depth. The mesh had a grid of identical longitudinal and transverse bars, and no transverse bars were removed.

Series T had the same cross section as Series A, but was detailed so that it would represent a "full size" exterior structure of that same depth. Main tension reinforcement was two #9 bars with a cover of 2-1/2 in. and a predicted crack width of 0.012 in. at the main reinforcement level.

The effect of beam width was isolated in Series W (and with A-2-0 and A-8). The web width was varied from 7-3/4 in. to 11-1/4 in. to 17 in. in specimens both without any skin reinforcement or with identical amounts and distributions of skin reinforcement. All specimens had approximately the same amount of main tension reinforcement and were designed so that the crack width at the main reinforcement level was the same in each specimen.

The maximum force that could be applied to the tension loading system corresponded to a reinforcement stress of about 60 ksi (yield stress) in the main reinforcement which extended from the ends of the specimen. If skin reinforcement was used, the primary reinforcement stress inside the specimen was lower than the stress applied to the main reinforcement extending outside the specimen because the face bars helped carry the total tension force. Because the amount of skin reinforcement used in D-6 and D-7 was high compared to the main tension reinforcement area, the tension loading system was modified for these specimens. Two of the #4 main reinforcement bars were spliced to two short pieces of #6 bars in the 1 ft ends of the specimen, with hooks and confining stirrups used to develop these bars. Figure 4.2 shows this detail. Thus, the main reinforcement inside the crack measurement zone was five #4 bars, as required, while the loading bars were three #4 bars plus two #6 bars, allowing a main reinforcement stress of 50 ksi and 40 ksi in D-6 and D-7, respectively.

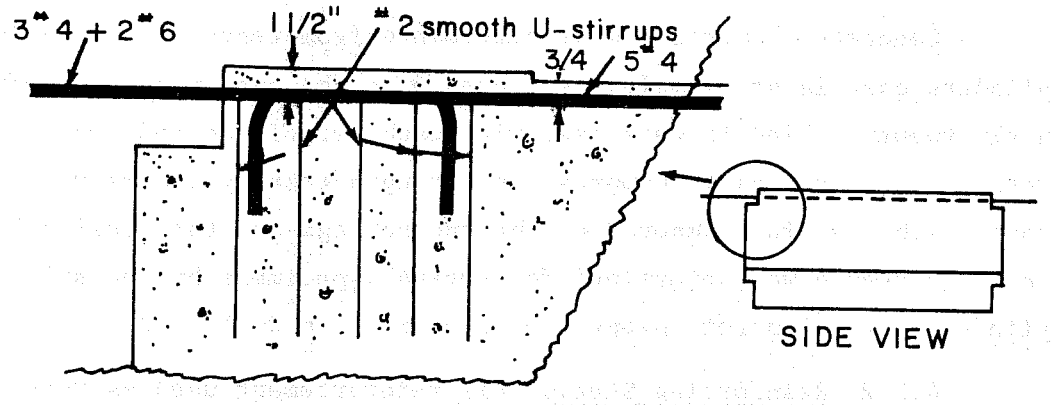

Fig. 4.2 Splice detail in Specimens D-6 and D-7

Compression reinforcement consisting of four #3 plus two #4 bars was used in RS-1, 2, 3, 4-0, A-15, BC-1, and BC-2. All other specimens had two #4 bars, except Series M which had no compression reinforcement.

4.3 Material Properties

4.3.1 Concrete. The concrete used in the inverted T-beam bent caps discussed in Sec. 1.2 was Class C concrete which has a minimum allowable compressive strength of 3600 psi. However, the concrete compressive strength of these bent caps was actually about 7000 psi. Therefore, for this study a concrete compressive strength of 5000 psi was chosen to be fairly typical of the strength of concrete actually placed for such structures.

The concrete mix (for 1 cu. yd.) was 470 - 564 lb (5 - 6 sacks) Type I cement, 1813 lb 5/8 in. maximum coarse aggregate, 1483 lb river sand, 30-1/4 oz water-reducing and set-retarding admixture, and 32 - 34 gal. of water as needed to reach a slump of 4 - 6 in. Because of changes in weather conditions, the cement content was varied during the program to keep the compressive strength at about 5000 psi. About 75 percent of all specimens used 517 lb cement per cu. yd.

Concrete properties were determined from tests of 6 x 12 in. cylinders cast in steel molds and cured with the specimens. Approximately twenty cylinders were cast with each set of two reduced segments or each bent cap. Compression strength test cylinders were capped with a sulfur compound on the end not against the steel mold. Tensile strength was determined for several specimens by the split cylinder test. Concrete properties are given in Table 4.2.

4.3.2 Reinforcing Steel. All reinforcement used as main tension, compression, or skin reinforcement was deformed Grade 60 bars. Swedish deformed 6 mm bars, Grade 77, were also used as skin reinforcement and stirrups. Plain #2 bars, Grade 40, were used for some stirrups. Welded wire fabric, composed of plain wire welded at intersection points, was also used as skin reinforcement. In tensile tests of the mesh reinforcement a sample piece was tested with the intersection welds not broken. Additional reinforcement required in the flange of BC-1, BC-2, RS-1, 2, 3, and A-15 was Grade 40 or Grade 60. Material properties for all steel used as main tension, compression, or skin reinforcements are given in Table 4.3. The values shown are the averages of three or more tests.

4.4 Specimen Fabrication

Specimen RS-1, 2, 3, 4-0, A-1-0, BC-1, and BC-2 were cast with the tension reinforcement on top. Fabrication details for these specimens are given in Chapter 3. Specimens A-1-0 and BC-2 were cast with all forms in place since their main tension reinforcement was not as congested as in the RS Series. Specimens A-1-0 and A-2-0 were identical except for casting position. Test results from these two specimens indicated that casting position did not affect the side face cracking significantly. Therefore, for ease in fabrication, the remaining specimens were cast with the main tension reinforcement on bottom and all forms in place. Formwork was similar to that described in Chapter 3. Two specimens were usually cast at the same time

TABLE 4.2 CONCRETE PROPERTIES

Spec ID	f'_c (psi) Average	f'_c (psi) Standard Deviation	f_{sp} (psi) Average	f_{sp} (psi) Standard Deviation
RS-1	2944	176		
RS-2	3183	285		
RS-3	4920	302	410	20
RS-4-0	4890	390	592	25
BC-1	5739	463	492	31
BC-2	4613	231	522	64
A-1-0	4913	323		
A-2-0	4975	212		
A-3	5320	540		
A-4	6062	422		
A-5	6310	303		
A-6	4669	370		
A-7	5521	189		
A-8	4580	264		
A-9	5231	252		
A-10	5438	250		
A-11	5416	322		
A-12	5320	433		
A-13	4810	366		
A-14	4810	366		
A-15	4636	171		
W-1-0	4025	345		
W-2	3418	177		
W-3-0	4480	260		
W-4	3433	179		
C-1	4878	312		
C-2	5290	161		
C-3	4783	167	563	77
C-4	4768	327		
C-5	4386	90		
D-1-0	3876	331		
D-2-0	3979	451		
D-3-0	5330	148	531	99
D-4-0	5000	370		
D-5	3339	174		
D-6	4969	355	529	52
D-7	3410	208		
M-1	4780	412	615	46
M-2	5960	392	632	95
M-3	6085	509		
M-4	4740	372		
T-1-0	4693	192		
T-2	5009	281		
T-3	4269	297		

For all specimens: Average f'_c = 4775 psi

Standard Deviation = 818 psi

TABLE 4.3 REINFORCING STEEL PROPERTIES

Bar ID	Used in Specimens	Stress (ksi) Yield	Ultimate
12.5 Gage	M-2, 3, 4	—	76.0
W-5	M-1	—	96.3
6 mm -1	BC-1; RS-1, 2, 3	77.0	—
-2	A-3, 4, 7, 11; D-5; T-2	73.3	99.5
#3-1	BC-1; RS-1, 2, 3, 4	65.6	91.5
-2	A-5, 8, 12, 14; W-2, 4; C-1, 2, 3, 4	65.8	97.5
-3	D-6, 7; C-5; T-3; A-15	68.5	110.0
-4	BC-2	70.9	107.1
#4-1	BC-1; RS-1, 2, 3, 4; A-1-0, 2-0, 3; D-1-0; W-1-0, 3-0	62.3	91.8
-2	all others using #4	62.7	95.8
-3	A-15; BC-2	68.5	104.8
#5-1	BC-1; RS-1, 2, 3, 4; W-3-0	71.8	104.4
-2	W-4	63.1	97.5
#6-1	A-1-0, 2-0; D-1-0, 2-0	63.6	93.2
-2	A-3, 4, 5, 7, 8, 9, 10, 11, 12, 13, 14; D-3-0; C-1, 2, 3, 4; M-1, 2, 3, 4	61.7	100.7
-3	C-5; D-6, 7; A-6	55.4	90.0
#7-1	W-1-0, 2	63.8	—
#8-1	W-1-0, 2	63.4	106.3
#9-1	T-1, 2, 3	63.8	—

along with test cylinders. Concrete was obtained from a local batch plant and, using an overhead crane and bucket, was placed in two lifts, one for the web and one for the flange. About one hour after trowelling the tops, the specimens and cylinders were covered with plastic sheets and allowed to cure in the laboratory for seven days before stripping the form.

4.5 Instrumentation

4.5.1 Reinforcement Strain Gages. To check the load distribution from the tension loading system to the main tension reinforcement, Specimen A-1-0 had electrical resistance SR-4 strain gages epoxied to the main reinforcement bars approximately 6 in. outside the concrete section. Strain gages were applied to several main tension and skin reinforcement bars of A-4 and A-7 to determine if the wide web crack widths caused bar stresses higher than would be predicted by a cracked cross section analysis. These gages were located where a crack was expected to form, but no "crack former" was used to artificially initiate a crack. All gages were applied according to the manufacturer's instructions and were waterproofed. Almost all gages performed satisfactorily.

4.5.2 Demec Gages. Surface strains were measured with Demec gages and a mechanical extensometer. Three rows of Demec gages were typically used, one at the centroid of the main tension reinforcement, one at about specimen middepth, and one 1/2 in. from the compression face (see Sec. 3.3.3 for other details).

4.5.3 Crack Width Readings. The location of horizontal grid lines varied between specimens, depending on the depth of the specimen and the main reinforcement distribution. The grid shown in Fig. 3.19 is typical.

4.5.4 Load Cells. Load was controlled in the reduced segment tests by monitoring the calibrated main loading bars and in the bent

cap tests by monitoring load cells at each pull-down point. In addition, pressure gages and transducers were used to measure the hydraulic fluid pressure in the loading system.

4.6 Test Method and Test Procedure

Details of the bent cap test method and procedure are given in Sec. 3.2.3 and details of the reduced segment test method and procedure are given in Secs. 3.3.2 and 3.3.3.2. Approximately one-third of the way through the test program several segments failed prematurely due to fracturing of the main tension reinforcement at the bar anchorage plate weld at stress levels below yield (about 55 ksi). These specimens used a newly delivered shipment of #6 reinforcing bars, and the fractures appeared to be due to an incompatibility between the bar's chemical properties and the welding process. Further tests of the welding process showed that satisfactory welds, i.e., high strength and ductile behavior, could be achieved using a preheat of 500° F applied to the bars and anchorage plate. The welding process was so modified in all remaining specimens.

Most specimens were loaded in seven to eight stages up to yielding of the main reinforcement extending from the specimen ends. Some tests were stopped prior to yielding of these bars because of bar fracturing or time limitations.

4.7 Test Results

4.7.1 General. Surface strain measurements and crack width measurements were reduced using a Fortran computer program. At each load stage, surface strains were measured along several horizontal rows of Demec points. A least squares regression analysis of these data yielded a best fit equation that would predict the surface strain at any level in the specimen. The average steel stress ($f_{s,av}$) was calculated as the product of the average surface strain at the steel centroid level and the modulus of elasticity of steel.

The steel stress at a cracked section (f_s) was based on a cracked, transformed area analysis. Unless identified by the term "average," all steel stresses used here will be based on an elastic cracked section analysis.

At each load stage all visible cracks were marked. With good lighting, cracks as small as 0.001 in. could be seen with the unaided eye. However, it is possible that some very small cracks were not noticed, especially in regions with rough surfaces. Missing such a small crack would affect the average crack width only slightly and would not affect the maximum crack width at all. Only cracks in the center 4 ft of the specimen were measured. Sometimes under magnification a crack was observed to be actually two or three closely spaced smaller cracks over a short distance. In these instances the crack width was recorded as the sum of the smaller cracks. For each load stage the computer program tabulated for every horizontal grid line the maximum crack width, the average crack width, the standard deviation, and the total number of cracks measured at that level. Crack widths were measured to an accuracy of ±0.0005 in., and an attempt was made to measure each crack at the same location at every load stage.

4.7.2 Crack Pattern Development. In all specimens first cracking was easily detected by sharp, popping noises accompanying the near simultaneous formation of several long cracks. Generally, the first cracks extended well into the web and sometimes reached the flange. After initial cracking, the crack pattern development was influenced by the presence of any skin reinforcement.

The crack pattern development of Specimen A-2-0 (no skin reinforcement) is presented in detail and is typical of specimens with very little or no side face reinforcement. Figure 4.3 shows the crack patterns on the east side of this specimen. The west side was was very similar. Almost all cracks could be traced from one side

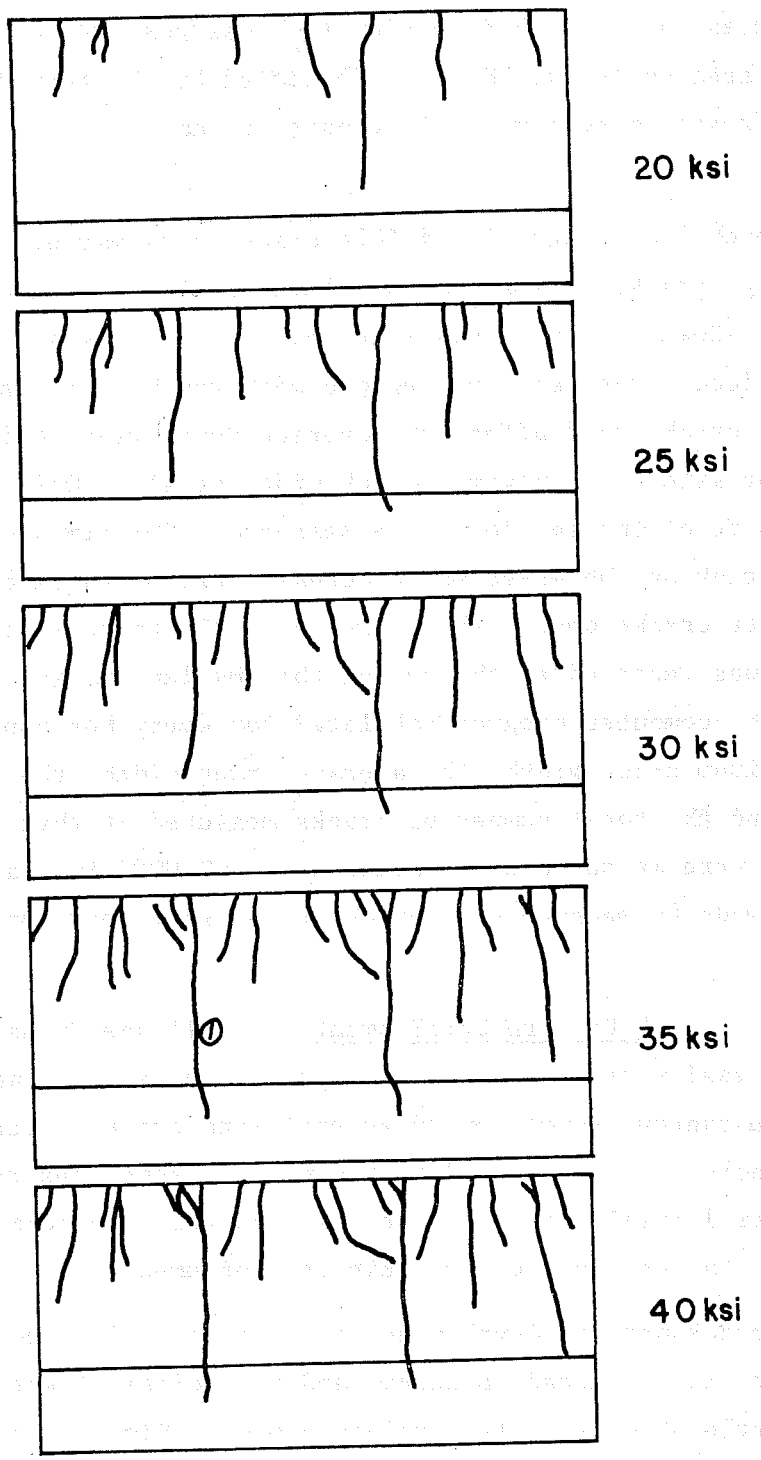

Fig. 4.3 Crack pattern development of A-2-0 (no skin reinforcement)

across the top tension face to the other side. The first flexural cracks occurred just prior to reaching a main steel stress of 20 ksi. With further loading these cracks extended, and shorter cracks formed. The shorter cracks tended to curve towards and sometimes joined the nearest long crack resulting in the tree branch pattern typical of specimens with very little or no side face reinforcement. Very few new cracks formed beyond a steel stress of 35 ksi, as most cracks extended slightly and became wider with increasing load.

Specimen A-5 is presented as a typical specimen with a significant amount of skin reinforcement (four #3 bars along each side face). Again, initial cracking began with the formation of several long cracks. See Fig. 4.4. However, as loading continued, the shorter cracks formed and tended to remain vertical and extended down into the web. The tree-branch pattern of Specimen A-2-0 was not as apparent in this specimen. The crack pattern was essentially fully developed at a steel stress of 35 to 40 ksi.

Appendix A contains the crack patterns of the east side of all specimens at a main reinforcement stress of 35 ksi. Above a steel stress of 40 to 45 ksi, short cracks sometimes developed in the vicinity of the main reinforcement. Often these cracks did not extend to the extreme tension face.

4.7.3 Number of Cracks. From the previous section it is apparent that the presence of side face reinforcement affects the crack pattern of the specimen by increasing the number of long cracks that extend into the web. Figure 4.5 shows how the number of cracks at several horizontal levels in the web varied with steel stress in A-2-0 and A-5. Data for all specimens are given in Appendix A. The number of cracks at the main reinforcement level and at approximately middepth of the web are listed for steel stress levels of 25, 30, 35, and 40 ksi. Note that in the full length bent cap specimens the test zone was 6 ft, 9 in. long, while in the reduced segment specimens it was 4 ft, 0 in.

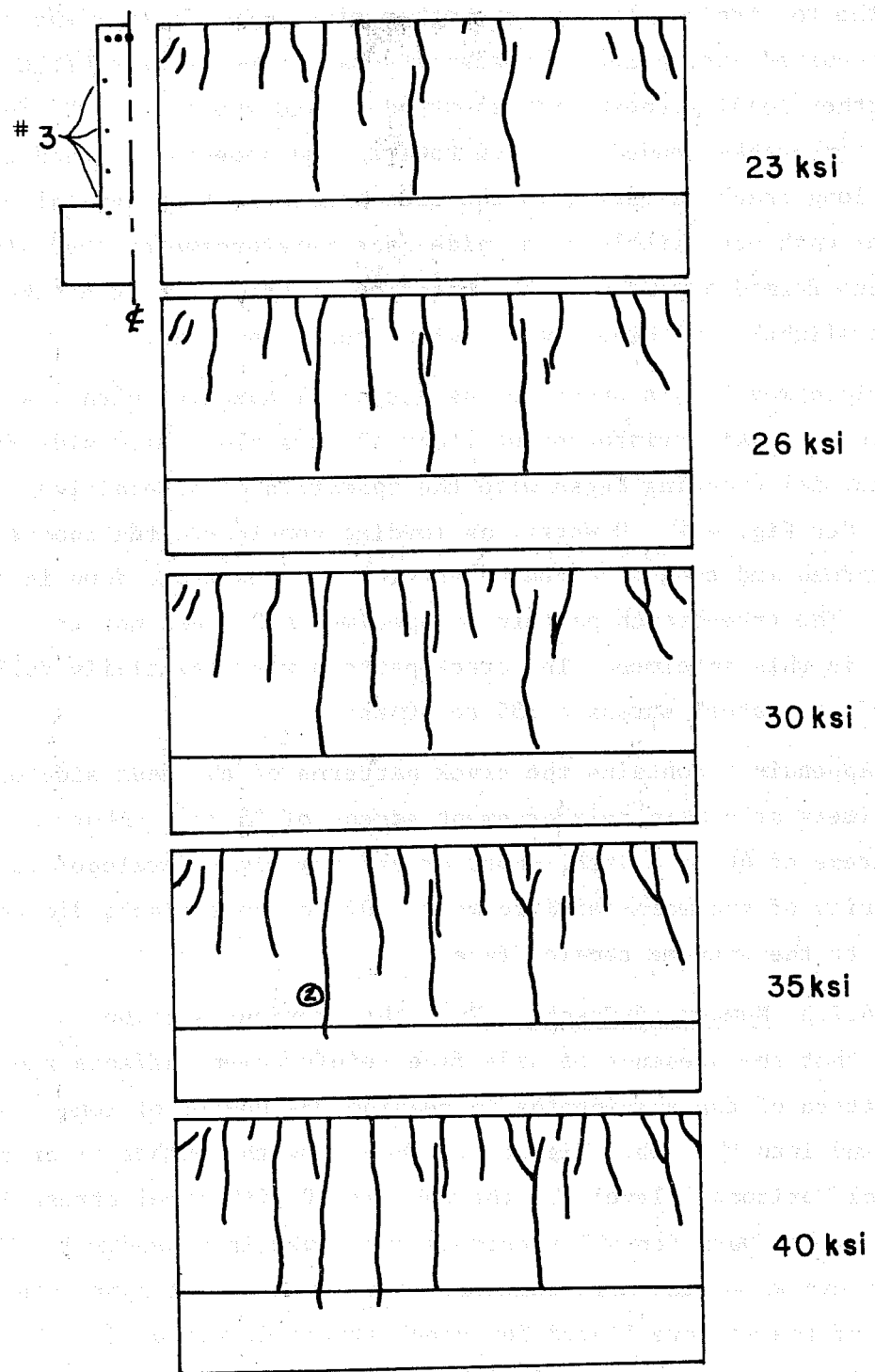

Fig. 4.4 Crack pattern development of A-5 (skin reinforcement = eight #3 bars)

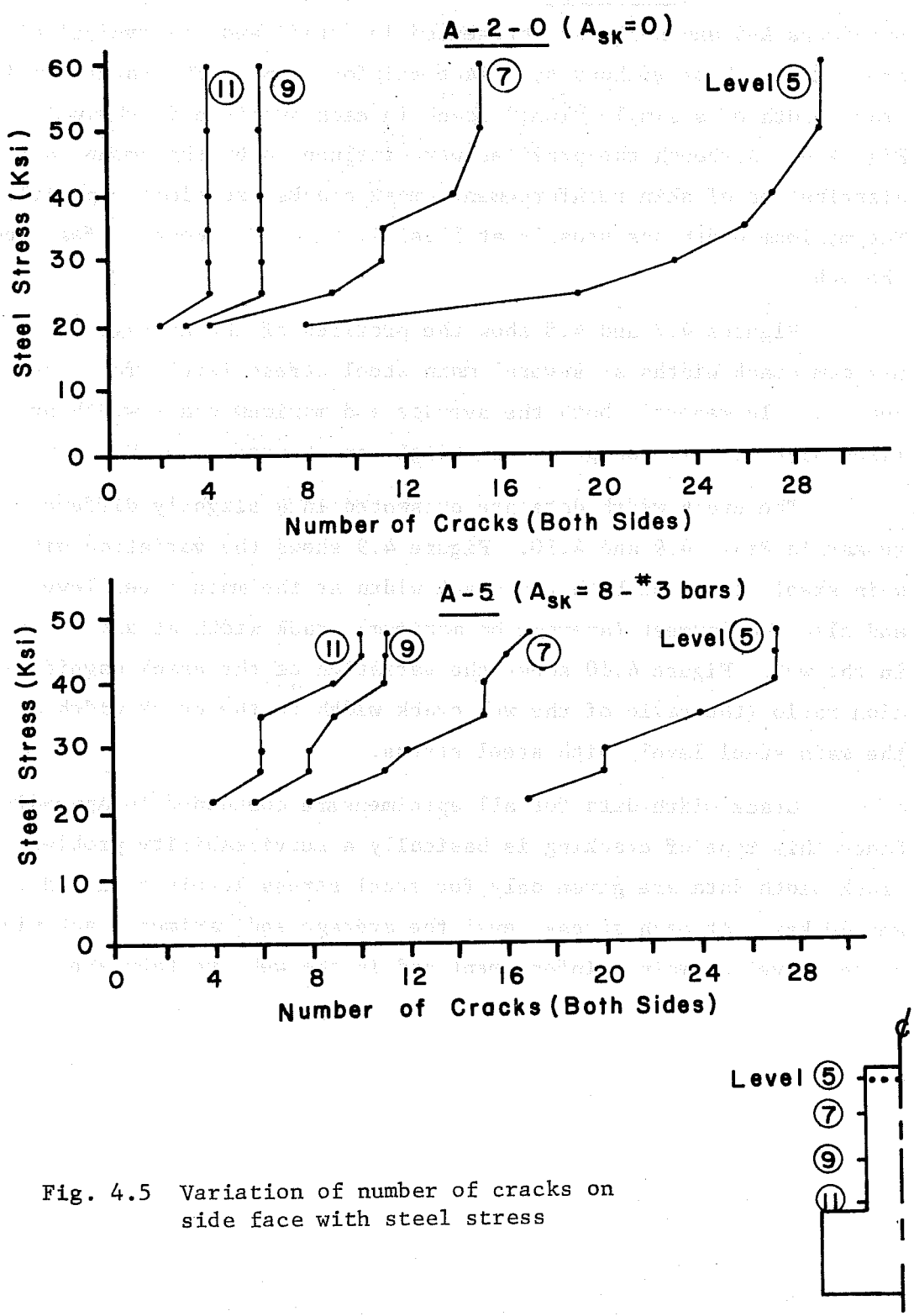

Fig. 4.5 Variation of number of cracks on side face with steel stress

4.7.4 Crack Widths. The crack width measurements of Specimens A-5 and A-2-0 are presented in detail and are typical of specimens with or without side face reinforcement. The variation in crack width of a single "long" crack in each specimen is shown in Fig. 4.6. Although the profiles were influenced by the amount and distribution of skin reinforcement, most cracks had similar profiles. The maximum width was usually at level 7, 8, or 9, about halfway down the web.

Figures 4.7 and 4.8 show the profiles of the average and maximum crack widths at several main steel stress levels for A-2-0 and A-5. In general, both the average and maximum crack width profiles have the same shape as the single crack profile of Fig. 4.6.

The crack width data are presented in a slightly different format in Figs. 4.9 and 4.10. Figure 4.9 shows the variation with main steel stress of both the crack width at the main steel level and also the largest (average or maximum) crack width at any level in the web. Figure 4.10 shows the variation of the crack magnification ratio (the ratio of the web crack width to the crack width at the main steel level) with steel stress.

Crack width data for all specimens are contained in Appendix A. Since this type of cracking is basically a serviceability problem, crack width data are given only for steel stress levels of 25, 30, 35, and 40 ksi. At each stress level the average and maximum crack widths at the level of main reinforcement and in the web are tabulated.

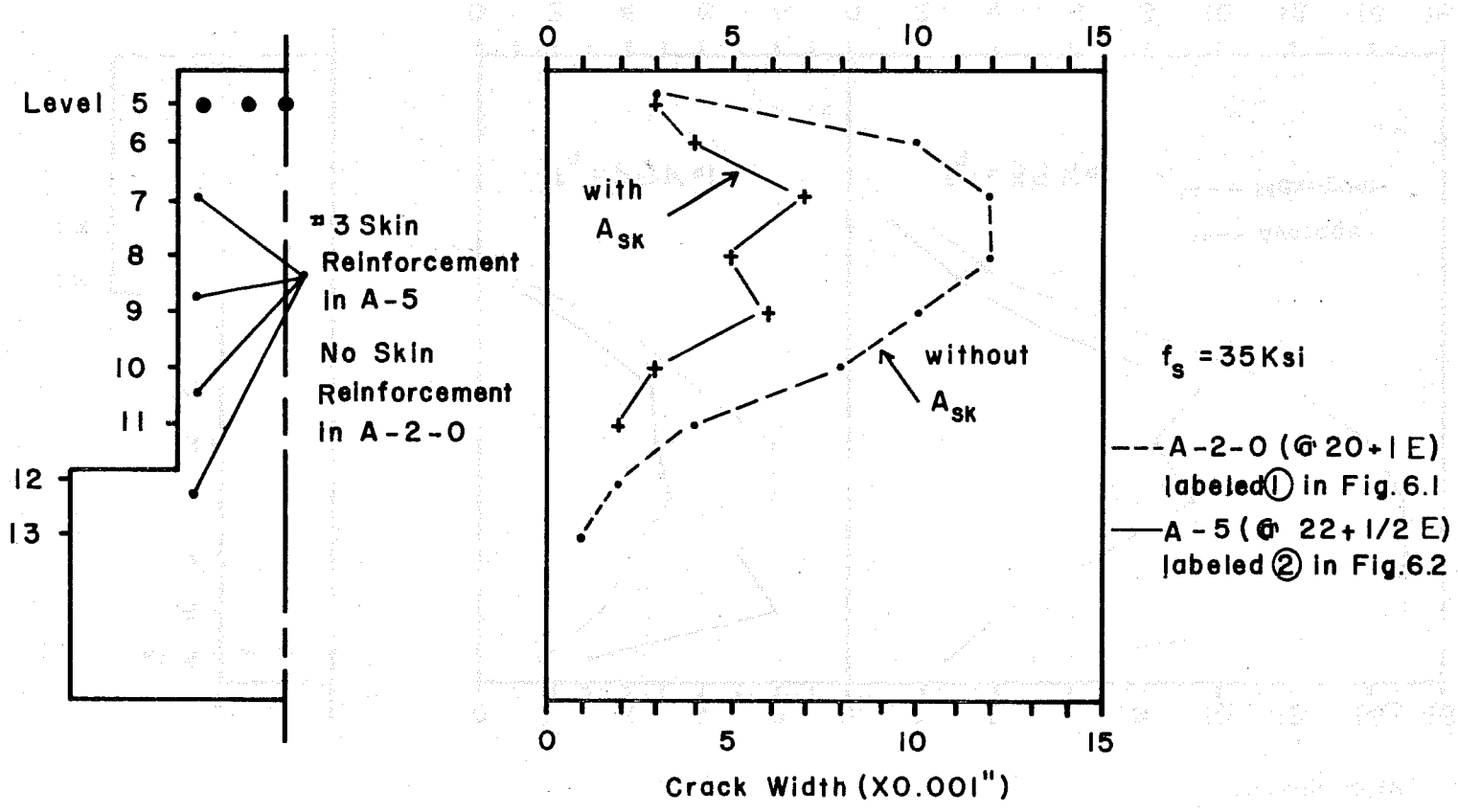

Fig. 4.6 Crack profile of a single crack in A-2-0 and A-5

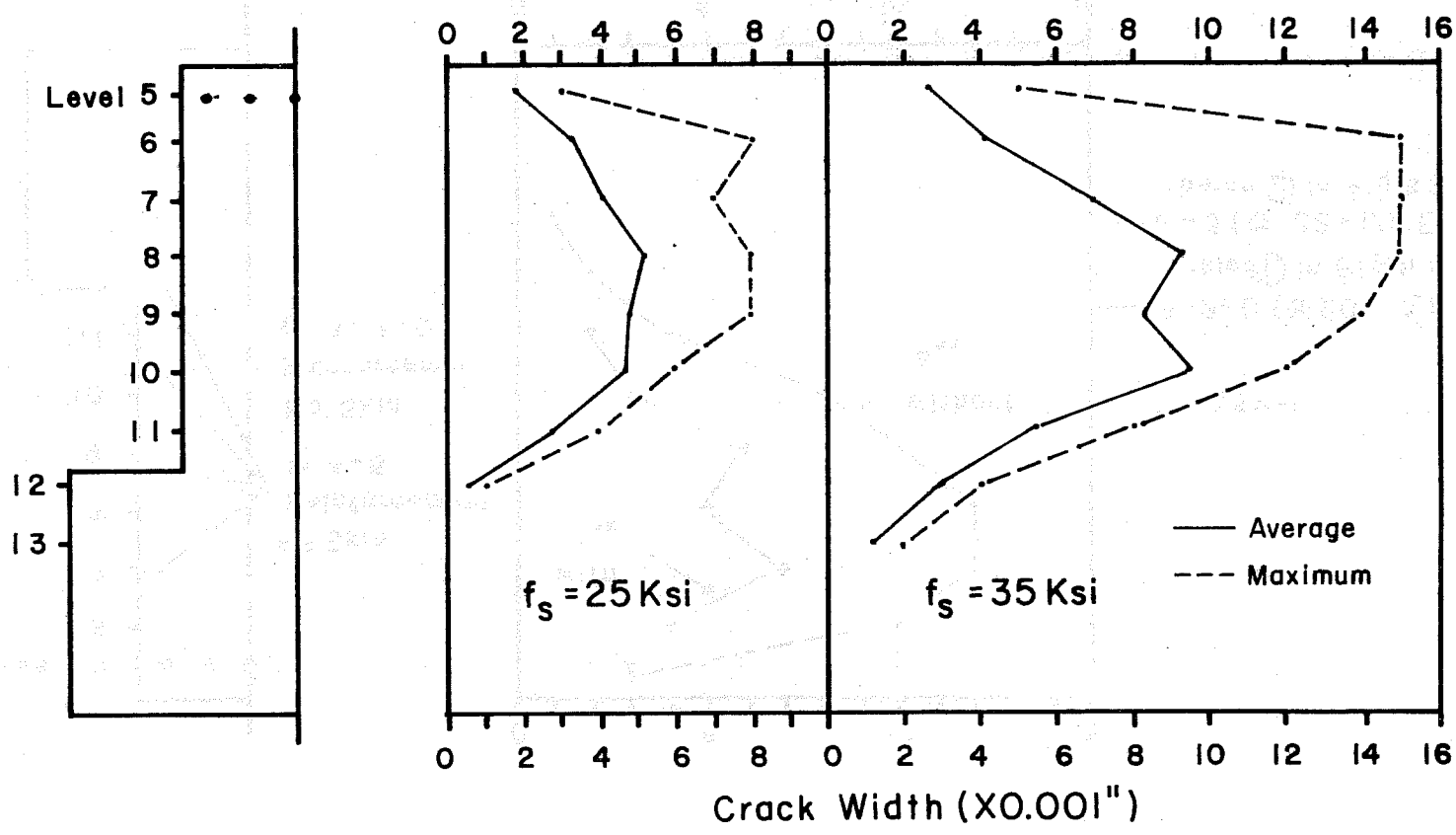

Fig. 4.7 Profile of average and maximum crack widths for A-2-0 (no skin reinforcement)

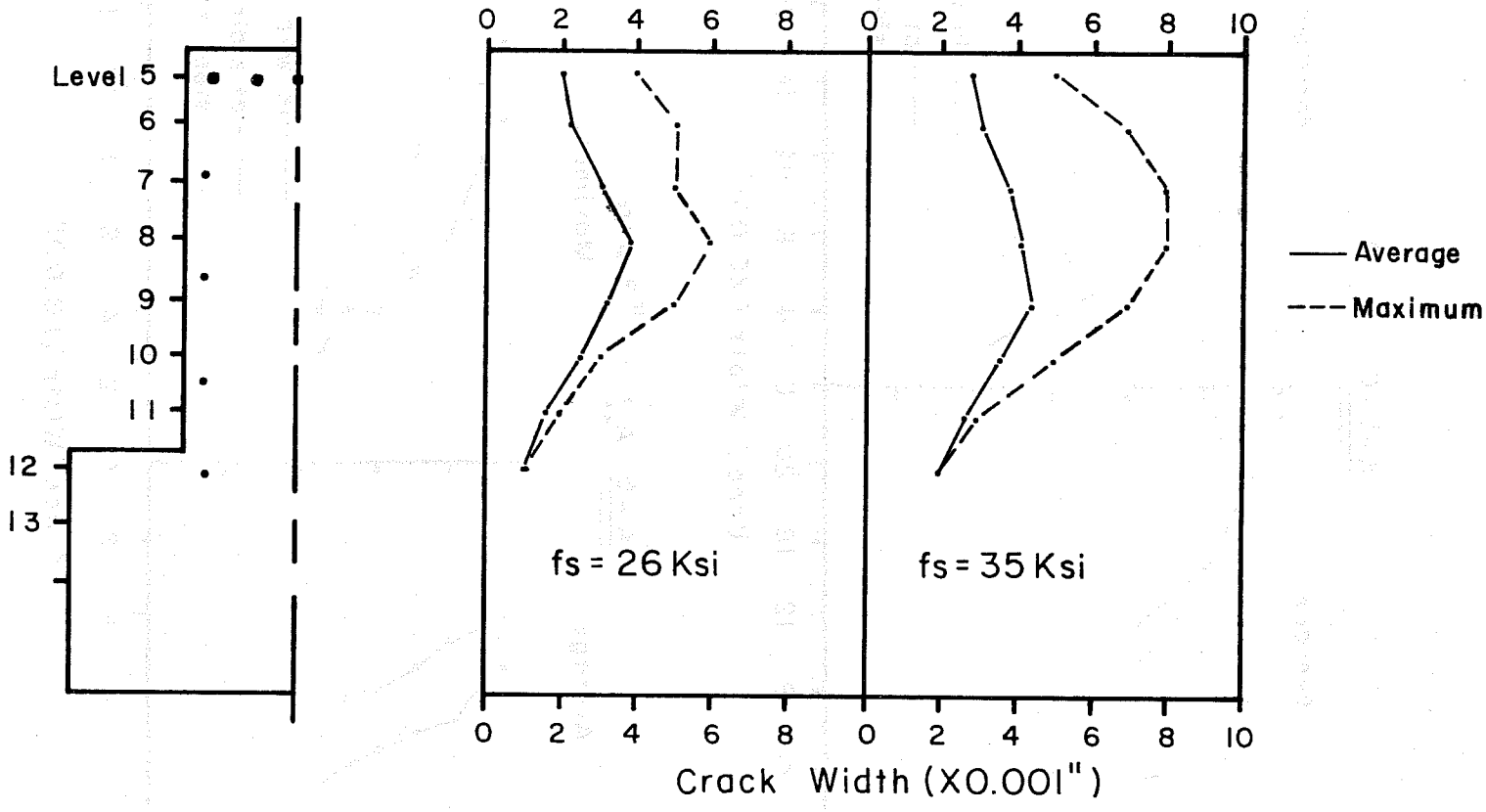

Fig. 4.8 Profile of average and maximum crack widths for A-5 (with skin reinforcement)

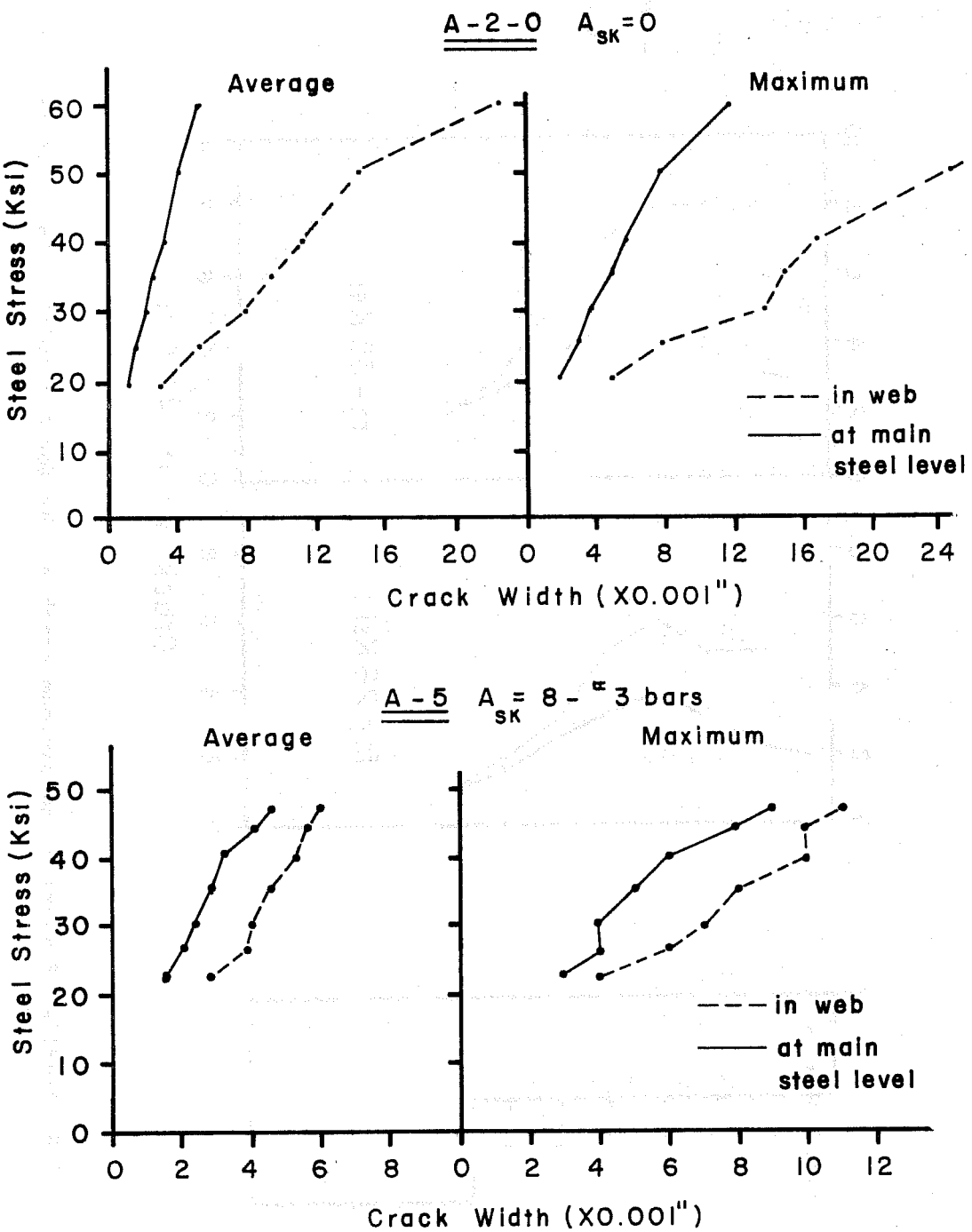

Fig. 4.9 Variation of average and maximum crack widths with steel stress - A-2-0 and A-5

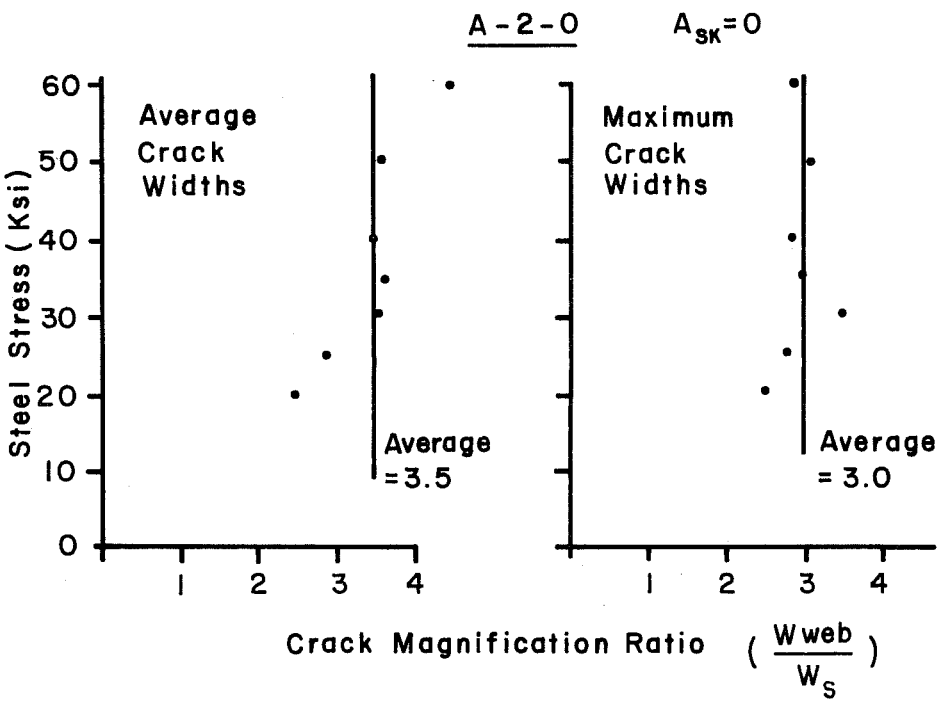

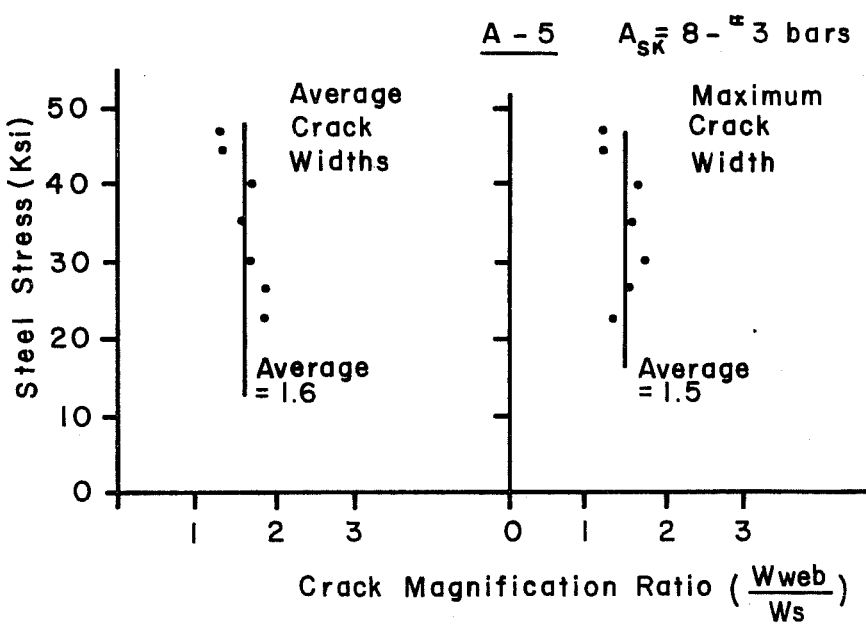

Fig. 4.10 Variation of crack magnification ratio with steel stress - A-2-0 and A-5

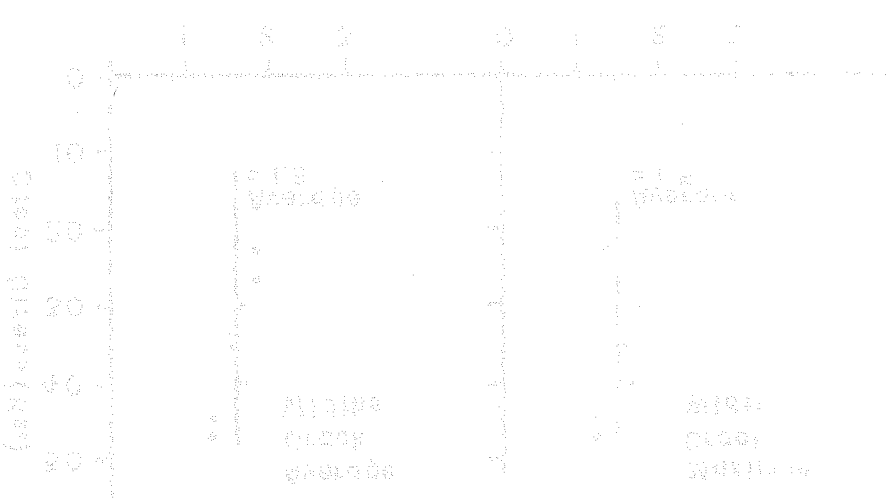

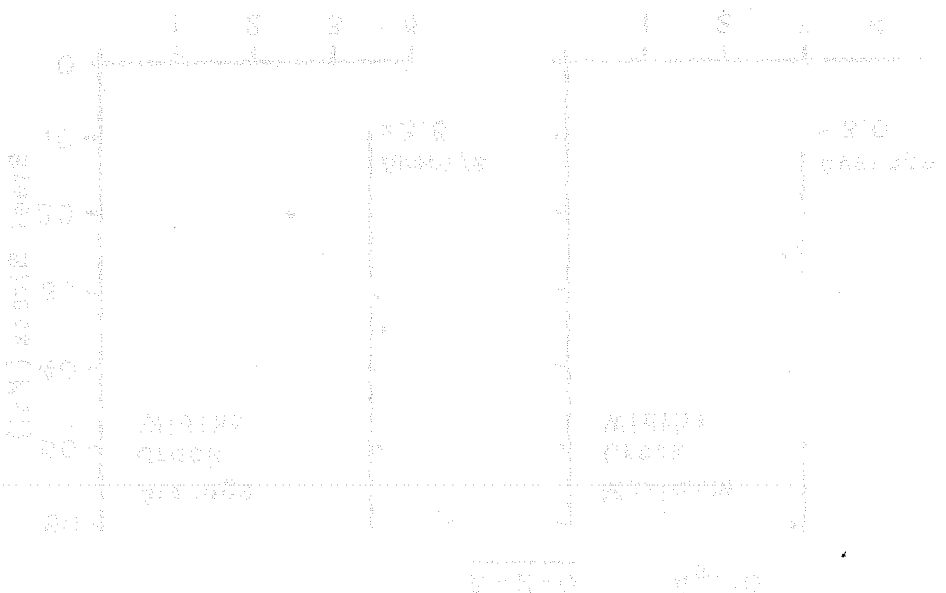

CHAPTER 5

ANALYTICAL STUDY

5.1 Introduction

This chapter discusses the development and use of a finite element model to study the side face cracking problem. Since very little other work on side face crack control has been reported, it was felt that an analytical model would provide valuable information on the important variables affecting side face cracking. The results of the analytical model would be very useful in checking the results from the laboratory tests. The model is semi-empirical, since information obtained in the experimental study (Chapters 3 and 4) was used in defining the value of the bond-slip relationship which is a critical factor in the method and in defining crack length and spacing.

The finite element method has been previously applied to reinforced concrete and can account for nonlinear material properties and can approximate the bond between the reinforcing bar and the concrete.[45,46,47] Cracking is usually studied by loading the model in small increments, examining the calculated element stresses, and modifying the finite element mesh in regions where high tensile stresses indicate a crack would form. In modeling cracking of reinforced concrete, the finite element method is handicapped by an incomplete theory of bond and the inherent randomness of crack development in actual concrete structures.

5.2 Parameter Study

5.2.1 Development of the Finite Element Model. For a beam without any skin reinforcement, the web crack width depends on the depth of the member and on the crack width at the main reinforcement

level, which in turn is a function of the amount, distribution, and cover of the main reinforcement. In addition to these variables, the web crack width in a beam with skin reinforcement also depends on the amount, distribution, and cover of the skin reinforcement. From the laboratory tests, it was evident that skin reinforcement affected the side face cracking in two distinct ways. First, skin reinforcement increased the number of long cracks that penetrated into the web. Second, any crack that crossed a side face bar was restrained from further opening by the closing force exerted by the bar. The problem requires a three-dimensional model to accurately examine all variables. However, for this study it was felt sufficiently adequate to approximate the specimen with a much simpler two-dimensional finite element model and to study the effect of skin reinforcement restraining force on the width of a "long" crack. With such a model, it was felt major effects of skin reinforcement on crack control would be indicated.

Figure 5.1 shows the development of the finite element model. In Fig. 5.1a a beam under constant moment loading with a crack pattern of a uniform series of long cracks was chosen for study. A section of the beam was removed by cutting along lines of symmetry halfway between adjacent long cracks (Fig. 5.1b). Rostam and Byskov[48] used a similar model in studies of crack lengths. The specimen was supported by rollers along the left edge (Fig. 5.1c). A moment was applied to the right edge by one force at the top and one force at the bottom of a very stiff loading arm (stiff enough to remain straight under loading). The specimen cross section was similar to those used in the experimental study and was reduced to a one-dimensional strip, as indicated in Fig. 5.1d. The main reinforcement was smeared across the web width. The skin reinforcement was smeared across the tributary edge strip affected by the skin reinforcement (see Sec. 6.4). The web width was approximately twice as wide as this tributary edge strip.

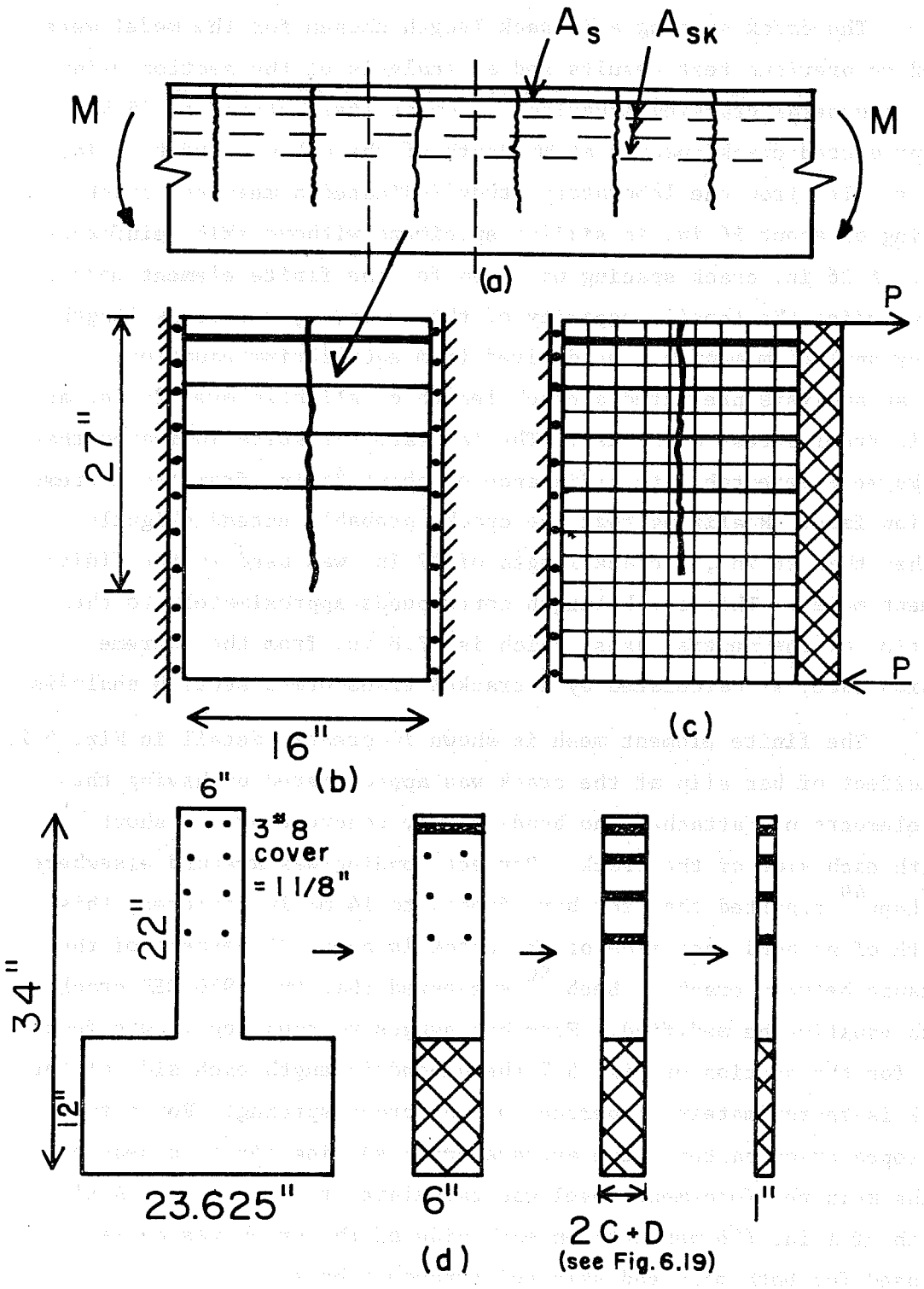

Fig. 5.1 Development of finite element model

The crack spacing and crack length chosen for the model were based on previous test results and an analysis of the section using Beeby's general cracking equation.[11] For a steel stress of 35 ksi, the predicted crack spacing at middepth of the web was about 14 in. Test results from the laboratory study indicated a measured crack spacing of about 16 in. in similar specimens without skin reinforcement. A 16 in. crack spacing was used for the finite element model. By including the tensile capacity of the concrete, the crack length at any applied moment can be derived from equilibrium equations. Such an analysis predicted a crack length of slightly over 24 in. at a main steel stress of 35 ksi. The laboratory results indicated that cracks were detectable to a distance of about 26 in. from the extreme tension face. Realizing that the cracks probably extend slightly further than 26 in., a crack length of 27 in. was used in the finite element model. This crack length corresponds approximately to the location of the neutral axis, which is 27.8 in. from the extreme tension face, as calculated by a cracked transformed section analysis.

The finite element mesh is shown in greater detail in Fig. 5.2. The effect of bar slip at the crack was approximated by having the bar elements not attached (no bond) to the concrete over a short length each side of the crack. Perfect bonding was assumed elsewhere. Faulkner[49] reported that for bars from 4 to 14 mm in diameter, this length of no bond each side of the crack is about 27 percent of the distance between cracks. Beeby[50] suggested that the 1970 CEB crack width equation be modified. From his suggested equation it was found that for the section of Fig. 5.1 the unbonded length each side of the crack is approximately 23 percent of the crack spacing. For a fully developed crack pattern, the average crack spacing for this section at the main reinforcement level was calculated to be 3.9 in. A slip length of 1 in. (26 percent) on each side of the crack was chosen and was used for both main and skin reinforcement bars.

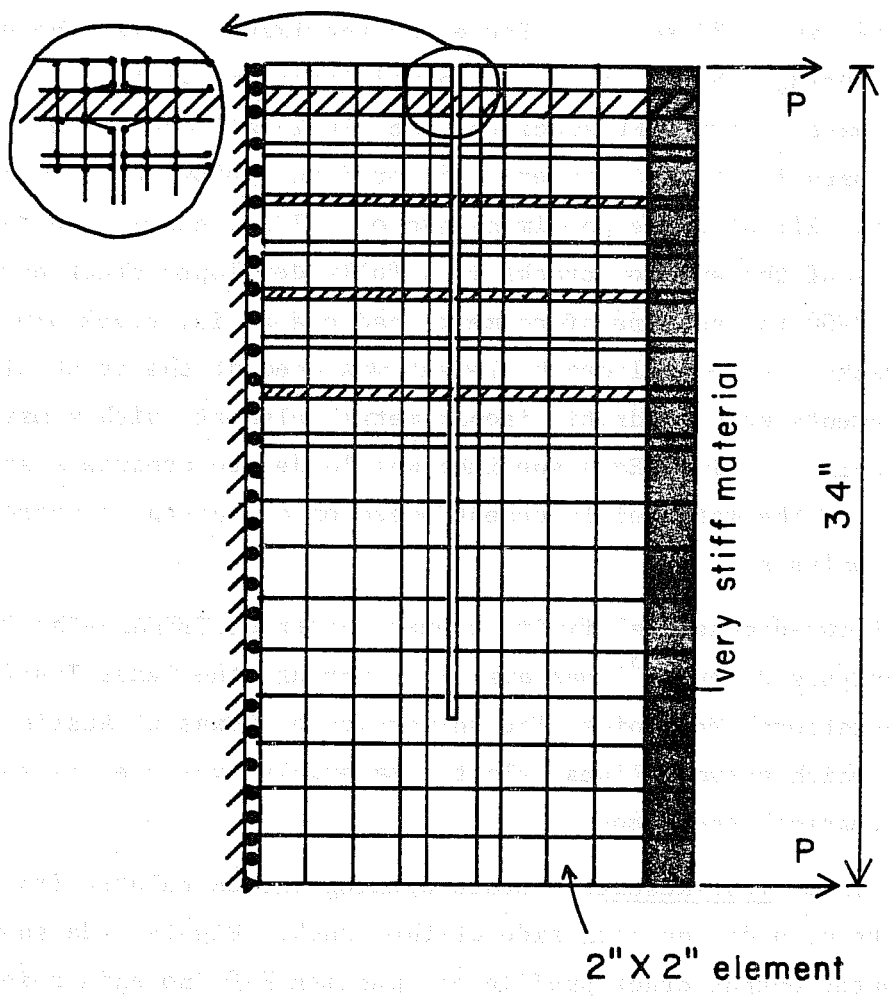

Fig. 5.2 Finite element mesh

5.2.2 Test Specimens. In the parameter study, nine specimens were analyzed (see Table 5.1). In a later portion of the study, several additional very deep models were examined to determine size effects. In the basic parameter study, Specimen F-0, the control specimen, had no skin reinforcement. Series FA specimens (and FD-6) all had six bars for skin reinforcement with a total area of steel of 0.44, 0.88, and 1.32 sq. in. Series FD specimens studied the effect of distributing 0.88 sq. in. of skin reinforcement in two, six, or fourteen bars. Series FL specimens (and FD-2) all had two 0.75 in. diameter bars located at either 4, 6, or 8 in. below the main reinforcement. All of these specimens had one 27 in. crack. To determine the effect of the shorter cracks in a fully developed crack pattern, Specimen F-00 (no skin reinforcement) had one 27 in. crack plus two 8 in. cracks. A special crack element was used at the crack tip. Other elements were quadratic isoparametric elements with a maximum size of 2 in. x 2 in. Each specimen was loaded to produce a stress of 35 ksi in the main reinforcement based on a cracked, transformed section analysis.

A two-dimensional finite element program, TEXGAP--The Texas Grain Analysis Program,[51] was available through the Texas Institute for Computational Mechanics, The University of Texas at Austin. This program, which assumes linear elastic materials, was used to analyze the mathematical specimens.

5.2.3 Test Results. Crack opening was calculated from displacements of nodes on each side of the crack. Figure 5.3a shows the computer output crack profile of Specimen F-0 (no skin reinforcement). Figure 5.3b includes profiles of several similar specimens with no skin reinforcement tested in the laboratory. The computer results are in generally good agreement with the laboratory results. Figure 5.4a shows the computer output crack profile for F-00 (no skin reinforcement, two additional cracks). Also shown is the profile of F-00 after being increased by the ratio of crack widths at the main

TABLE 5.1 SPECIMEN DETAILS--FINITE ELEMENT ANALYSIS

Spec ID	Series Variable	Skin Reinforcement A_{sk} (in^2)	Skin Reinforcement Bars
F-0	Control	0	—
FD-2	Distribution of A_{sk}	0.88	2-0.750" dia. @ 8"
FD-6		0.88	6-0.432" dia. @ 4"
FD-14		0.88	14-0.283" dia. @ 2"
FA-6A	Amount of A_{sk}	0.44	6-0.306" dia. @ 4"
FA-6B		1.32	6-0.529" dia. @ 4"
FL-2A	Location of A_{sk}	0.88	2-0.750" dia. @ 4"
FL-2B		0.88	2-0.750" dia. @ 6"
F-00†	Short Cracks	0	—

†has 2 additional 8" cracks

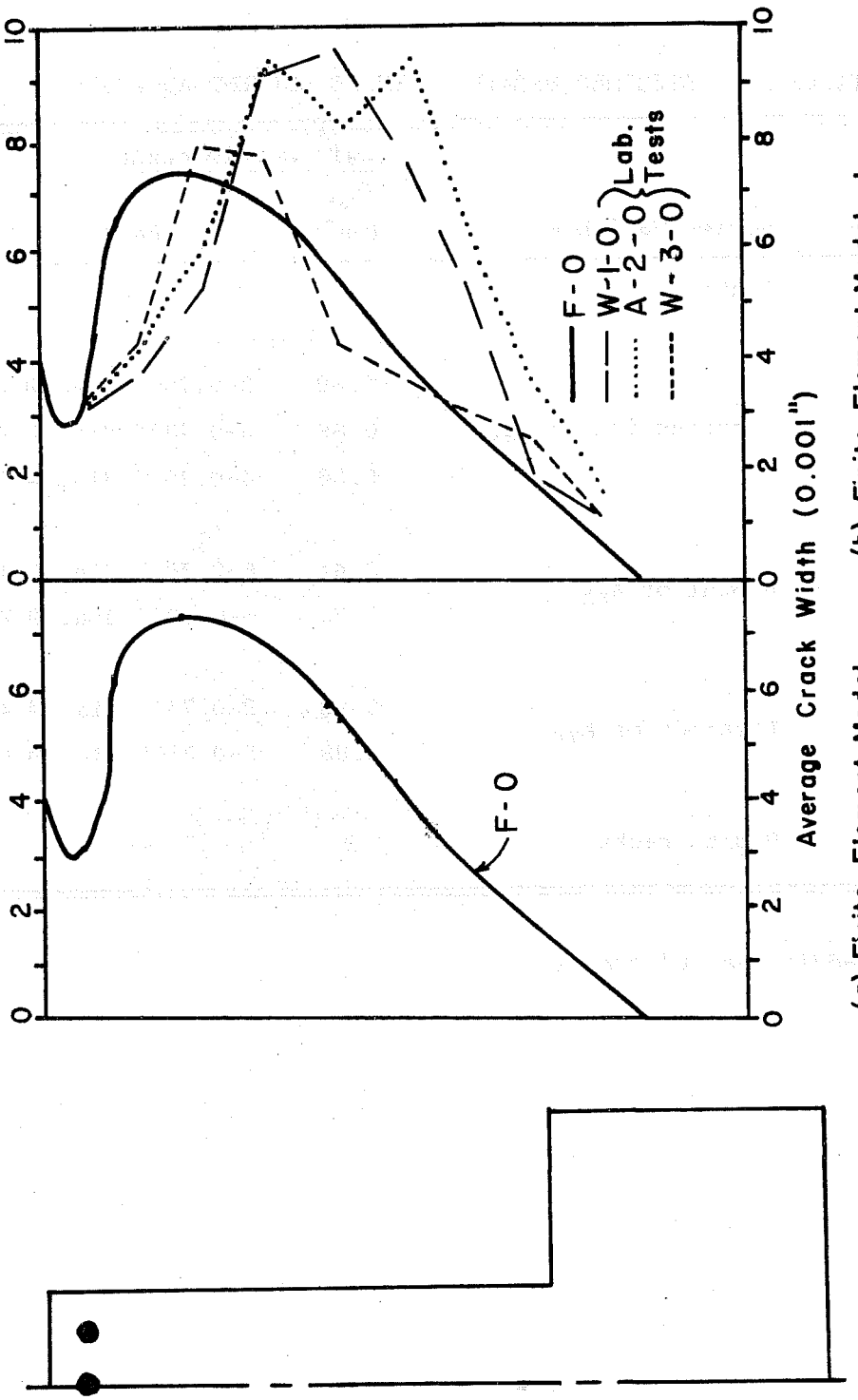

Fig. 5.3 Crack profile - control specimen, no skin reinforcement

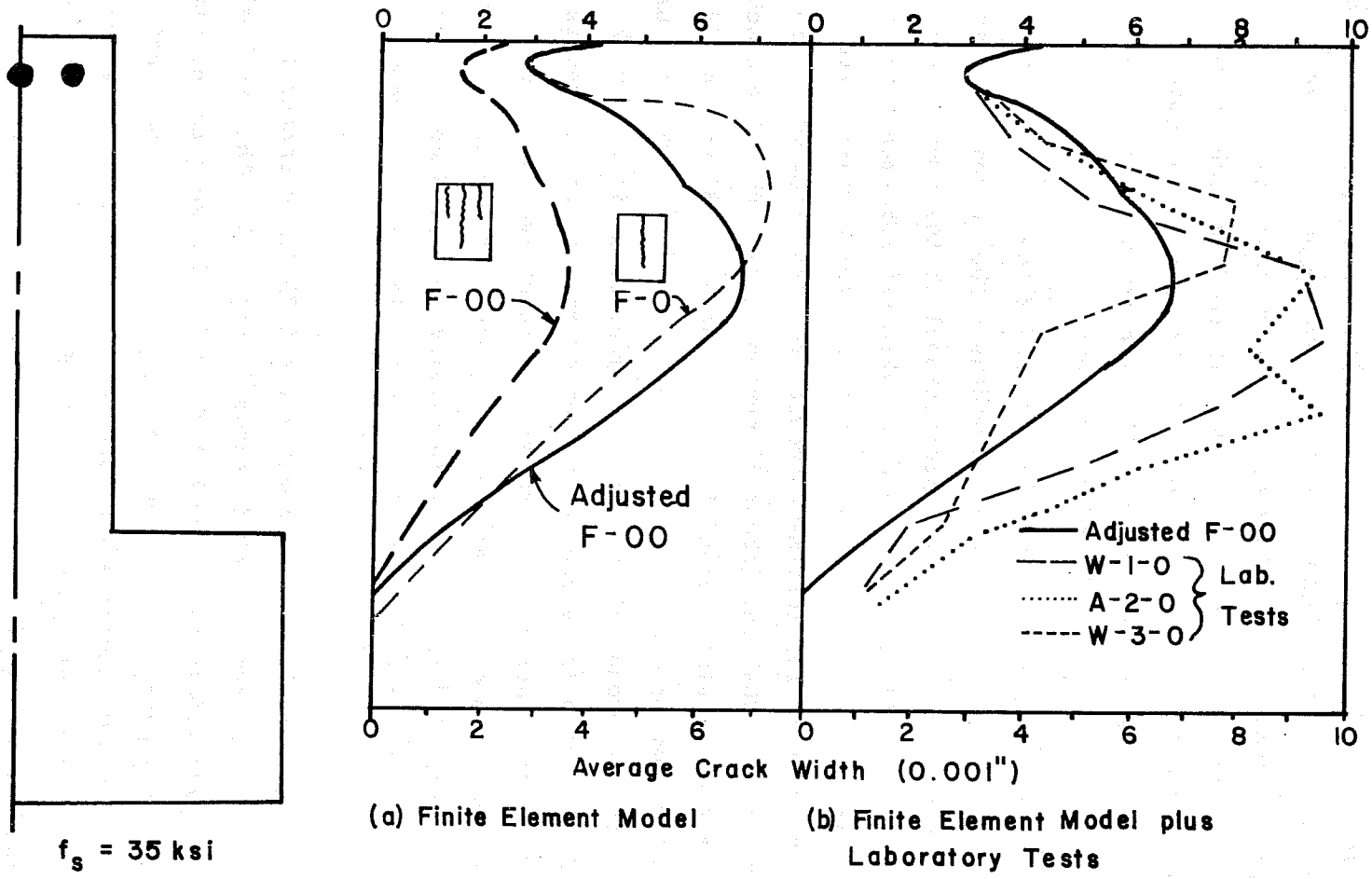

Fig. 5.4 Crack profile - specimen with additional short cracks

reinforcement level of F-0/F-00. The additional 8 in. cracks changed the profile of the long crack by reducing the crack width and by shifting the location of maximum width further down the web. Figure 5.4b compares the adjusted F-00 with the same laboratory specimens. Specimen F-00 agrees with the laboratory specimens better than F-0 does because, like the physical specimens, it also had shorter cracks which act like stress relievers.

Figures 5.5 and 5.6 show the effect of the amount of skin reinforcement on the side face crack widths. The decrease in maximum web crack width was not directly proportional to the area of skin reinforcement provided. As the area of skin reinforcement increased, the side face crack width decreased, but at a lesser rate. About 0.6 sq. in. of skin reinforcement reduced the web crack width from 0.0075 to about 0.0045 in. (about 55 percent larger than the crack width at the main reinforcement level). However, 1.32 sq. in. of skin reinforcement reduced it only slightly more to 0.0040 in. Large increases in the amount of skin reinforcement occur if the crack magnification ratio is reduced below approximately 1.5. A realistic reduction of side face crack width must be specified to avoid excessive and uneconomical amounts of skin reinforcement. Providing 0.44, 0.88, and 1.32 sq. in. of skin reinforcement reduced the crack width at the main reinforcement level by 13, 16, and 18 percent, respectively.

The effect of the placement of two 0.75 in. diameter face bars (0.88 sq. in. total area) is shown in Fig. 5.7. The crack width in the immediate vicinity of the bar was reduced almost to the same width as at the main reinforcement level, but it increased considerably at points some distance from the bar. Specimen FL-2B, which had the skin reinforcement approximately one-fourth of the way between the main reinforcement level and the neutral axis, had the smallest side face crack widths of the three specimens.

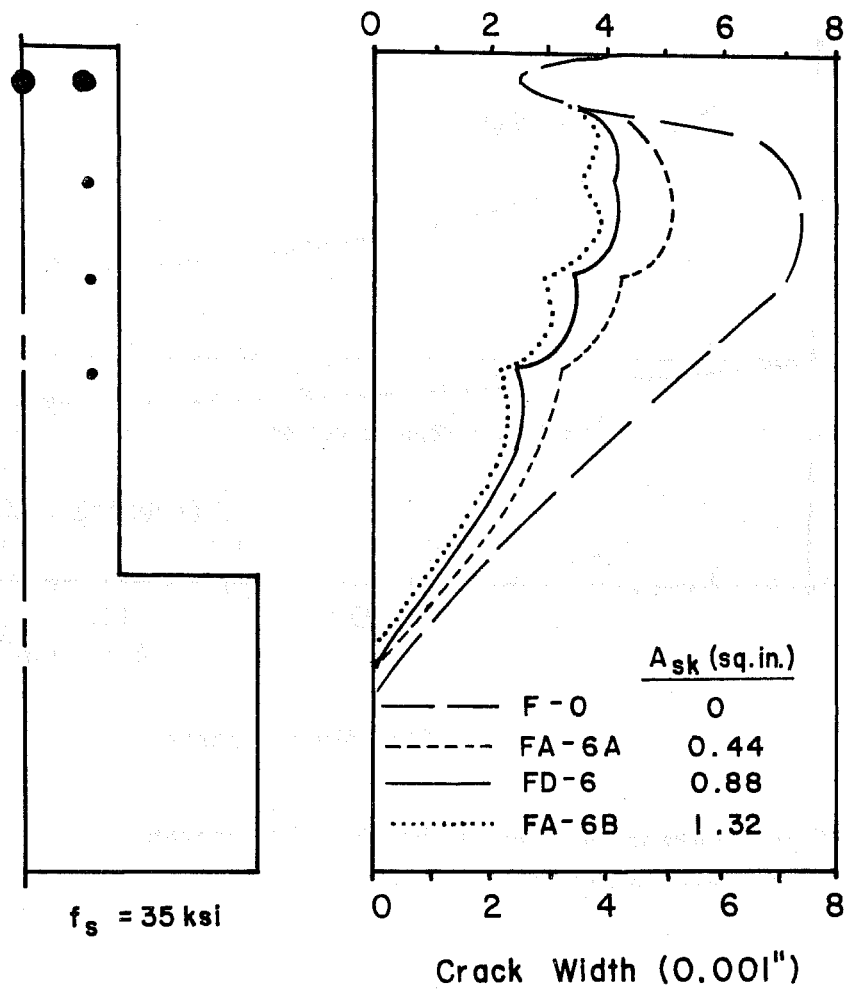

Fig. 5.5 Effect of amount of skin reinforcement on crack profile

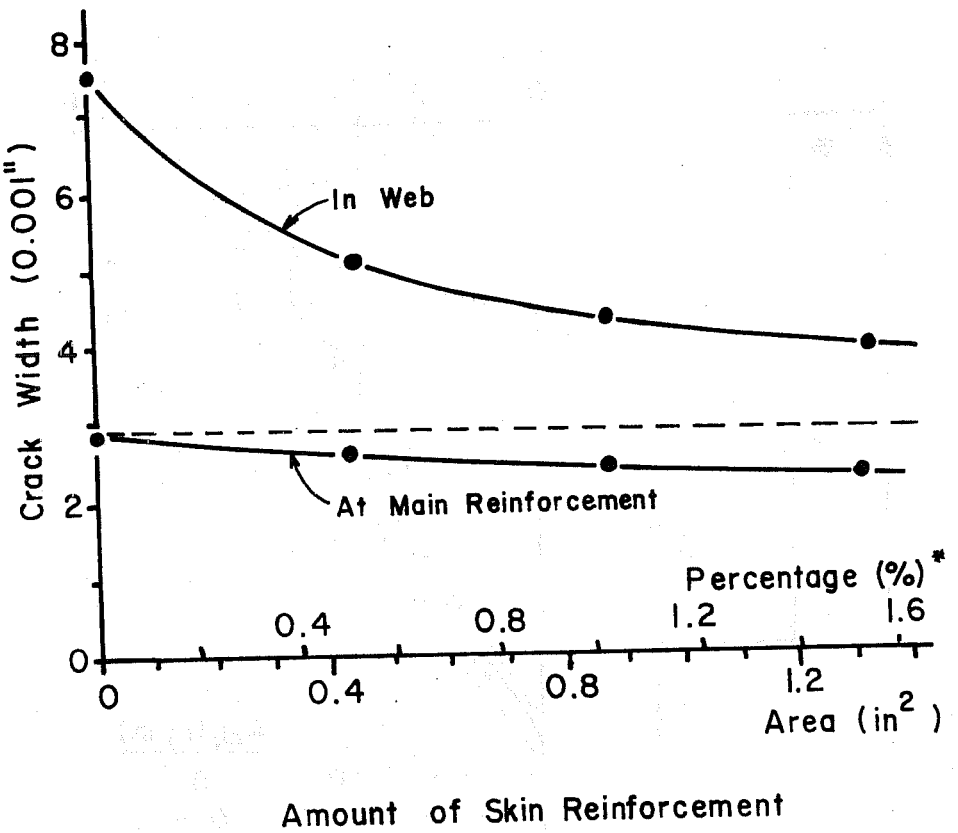

*See Section 6.9 for definition of percentage of Skin Reinforcement

Fig. 5.6 Effect of amount of skin reinforcement on crack widths

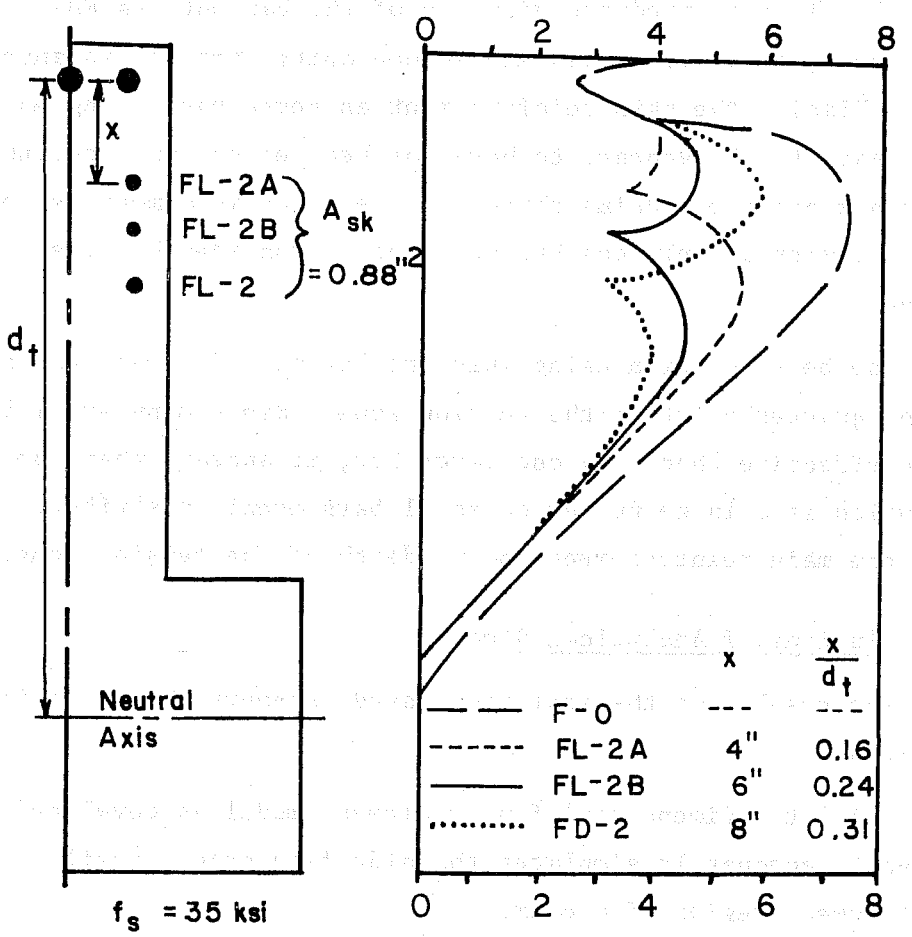

x = distance from main reinforcement to face bar

d_t = " " " " " neutral axis

Fig. 5.7 Effect of location of skin reinforcement

Figure 5.8 presents a comparison of the crack profiles for for F-0, FD-2, FD-6, and FD-14. A face bar reduces the crack width considerably in the immediate vicinity of the bar but, as FD-2 clearly shows, the crack width may become quite large a distance from the bar. Placing the skin reinforcement as seven bars along each side face (14 bars total) appears to have the best effect on reducing the entire crack profile. Using three bars per face is almost as good as seven bars, whereas only one bar per face is considerably less effective.

The best location using only one bar per side face was at about the quarter point of the tension zone. Since many small bars are more effective than only one large bar, it appears that the best distribution is a large number of small bars evenly distributed between the main reinforcement and middepth of the tension zone.

5.3 Conclusions of Analytical Study

The results of the analytical study support the following conclusions:

(1) A two-dimensional finite element model as developed in this chapter adequately simulates the side face crack profile in the constant moment region of a beam.

(2) The reduction in web crack width is not directly proportional to the provided area of skin reinforcement. As the area provided increases, the web crack width decreases, but at a decreasing rate.

(3) Skin reinforcement has a slight effect on reducing the crack width at the main tension reinforcement level.

(4) Given an amount of skin reinforcement, the wide side face cracking is best controlled by using a large number of small bars rather than a few large bars.

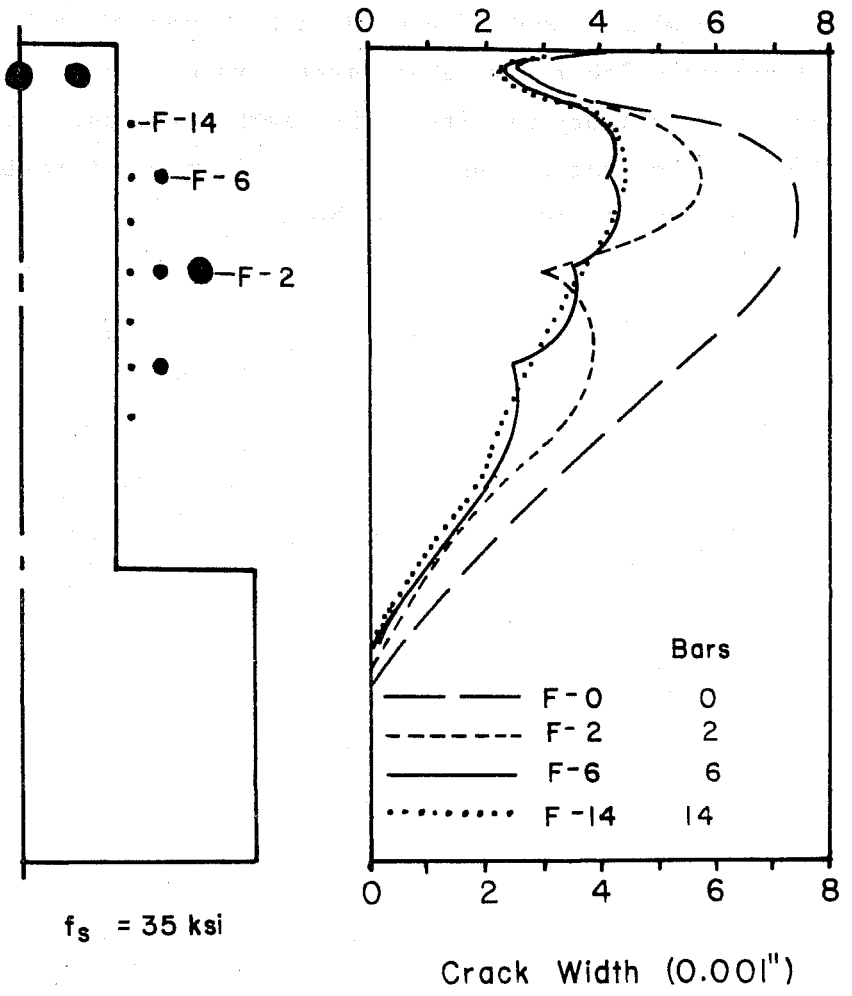

Fig. 5.8 Effect of skin reinforcement distribution with constant A_{sk} (0.88 sq. in.)

(5) The skin reinforcement should be evenly distributed along the side faces between the main reinforcement and middepth of the tension zone.

The finite element method proved to be a very useful tool for both interpreting laboratory experimental results and for extending the range of laboratory results. This method was used in Sec. 7.3 to extrapolate the laboratory results for development of design provisions which would apply to very large beams.

CHAPTER 6

DISCUSSION OF RESULTS

6.1 Introduction

6.1.1 General. This chapter discusses the results from the laboratory and computer studies. The effect of the following variables on the side face cracking is discussed:

(1) Amount and distribution of skin reinforcement
(2) Cover over skin reinforcement
(3) Type of skin reinforcement
(4) Beam depth
(5) Beam web width
(6) Concrete strength
(7) Crack width at the main reinforcement level

6.1.2 Methods of Comparing Test Results. There are several ways to compare cracking test results. The first is to compare crack patterns in different beams at the same level of stress. There is necessarily some subjectivity in this comparison; however, the crack patterns should give a good qualitative indication of how effectively the skin reinforcement is modifying the web cracking behavior. A second method is to compare the complete crack profiles. This gives a numerical indication of the skin reinforcement's effectiveness in controlling the entire crack profile. A third method is to compare the crack magnification ratios (CMR), the ratio of the crack width in the web to the crack width as the main reinforcement level.

Figure 6.1 shows how the crack magnification ratio varies with reinforcement stress for two typical specimens, A-5 with eight #3 bars for skin reinforcement, and A-2-0 without any skin reinforcement.

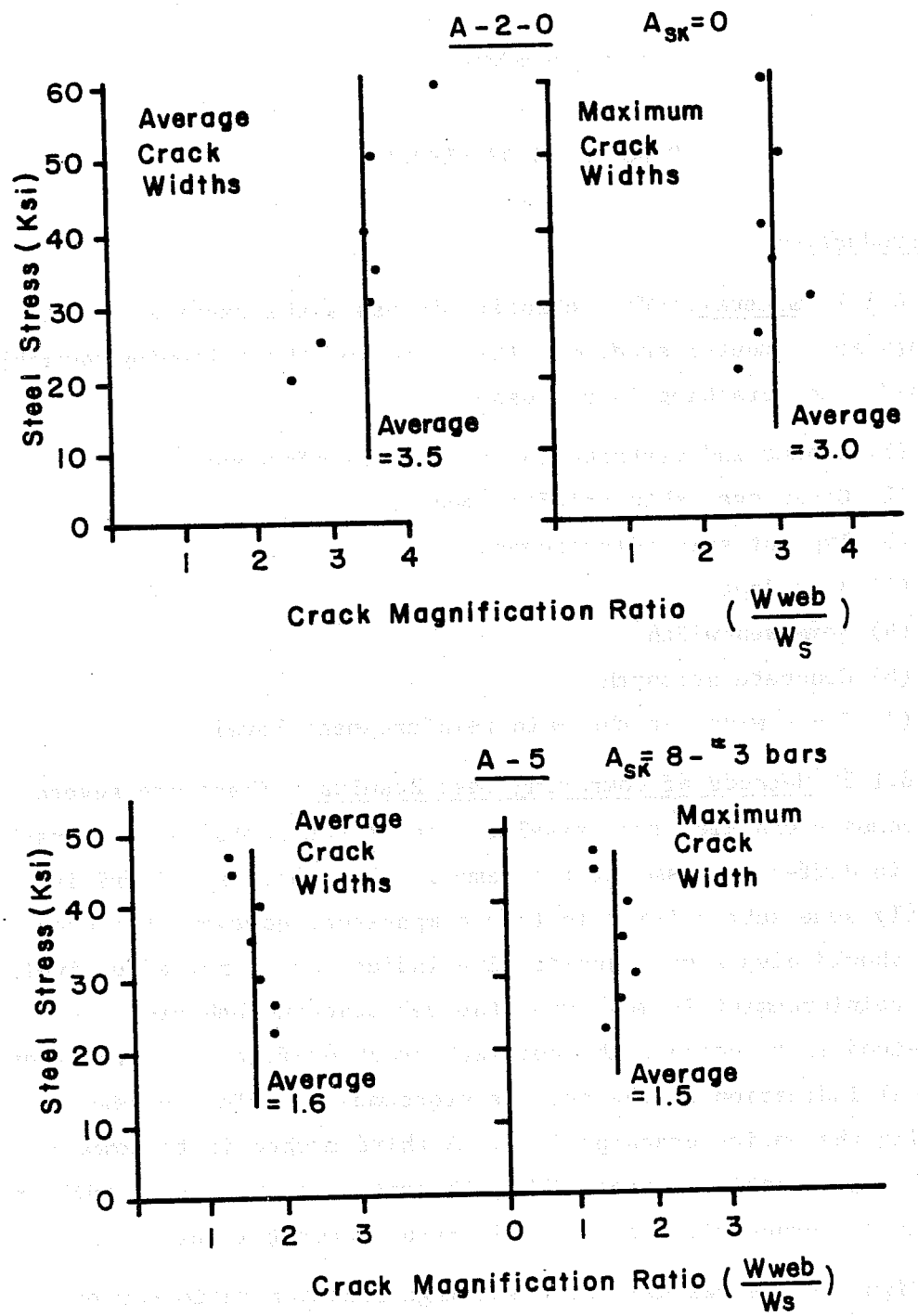

Fig. 6.1 Variation of crack magnification ratio with steel stress - A-2-0 and A-5

In general, once the specimen reaches a stabilized or fully developed crack pattern at a stress of about 30 to 35 ksi, the crack magnification ratio remains fairly constant. This trend was observed for both average and maximum crack widths and was shown, in general, by all specimens. Beeby's[11] equations for cracking, included in Ref. 54, are derived on the basis that w/ϵ at any level in the beam remains constant. Although there is some variation, an average crack magnification ratio determined when the main reinforcement tensile stress is in the range of 30 to 40 ksi is a good indicator of the skin reinforcement's effectiveness. Section 6.9 provides more discussion on the suitability of using the average CMR. In most cases, several or all methods were used to judge the effectiveness of the various types or patterns of skin reinforcement.

6.1.3 Scatter in Data. Over 24,000 crack width measurements were taken in this study. The random nature of crack spacing can lead to an expected scatter of up to ±50 percent in crack width or crack spacing data in tests of identical specimens.[14] Figure 6.2 shows a frequency diagram of crack width data at the main reinforcement level for Specimens A-1-0 and A-2-0, identical specimens with no skin reinforcement. The parameter w/ϵ (the crack width/surface strain) permits data from all load stages to be considered together. Also shown is the normal distribution curve. The data are slightly skewed but are quite close to the normal distribution curve. The coefficient of variation (V) was 50 percent.

Coefficients of variation were calculated for all Series A specimens. At the level of main reinforcement, V varied between 28 and 51 percent. For crack widths in the web, V varied between 23 and 77 percent. In twelve out of fifteen specimens the coefficient of variation was about the same in the web and at the main reinforcement level. It appears that there was a little less scatter in the data than what might be expected.

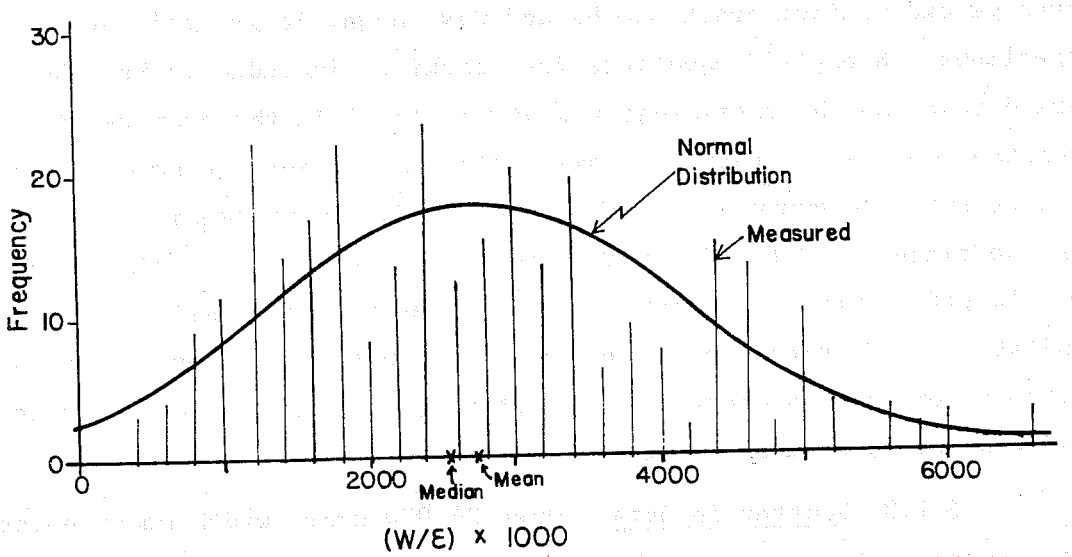

Fig. 6.2 Frequency distribution for crack widths at main reinforcement for A-1-0 and A-2-0

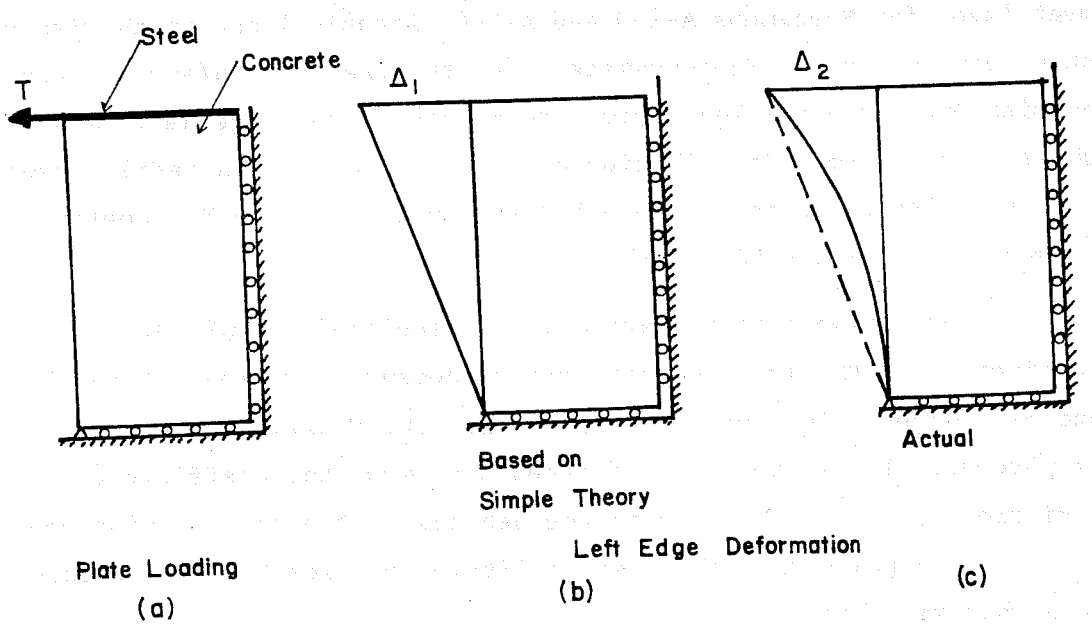

Fig. 6.3 Shear lag concept

It was observed that, in general, the crack magnification ratio for a specimen (with or without skin reinforcement) was about the same for both the average and maximum crack widths (see Fig. 6.1). This indicates that the skin reinforcement affects both the maximum and average crack widths equally. Therefore, in most of the following discussion the average rather than the maximum crack widths are analyzed.

6.2 General Concepts of Side Face Cracking

6.2.1 Why Cracks Are Not Wedge-shaped. It seems logical that cracks on the extreme tension face should be wider than at the main reinforcement level, because Navier's hypothesis of plane sections indicates that the strain is higher on the extreme face, and it is commonly accepted that crack widths are proportional to strain. However, some engineers would probably be surprised to hear of instances where flexural cracks were wider near middepth than at the main reinforcement level.

Figure 6.3a shows a plate supported along two edges and loaded with a single force at the upper left corner. If the plate is analyzed using elementary strength of materials (that is, $\sigma = My/I$) the deformation of the left edge would be a straight line, with maximum deformation at the top and zero deformation at the bottom (see Fig. 6.3b). However, this deformation is incorrect. The effect of the force, T, is strongly felt in the upper part of the plate and only gradually diffuses down into the lower part. The actual stresses and deformations lag behind the simple theory predictions. The actual deformation is maximum at the top but it decreases rapidly away from the load (see Fig. 6.3c). This phenomenon is called diffusion or shear lag.[52]

The same concept applies to a crack in a reinforced concrete beam (Fig. 6.4). A section containing a crack in a constant moment

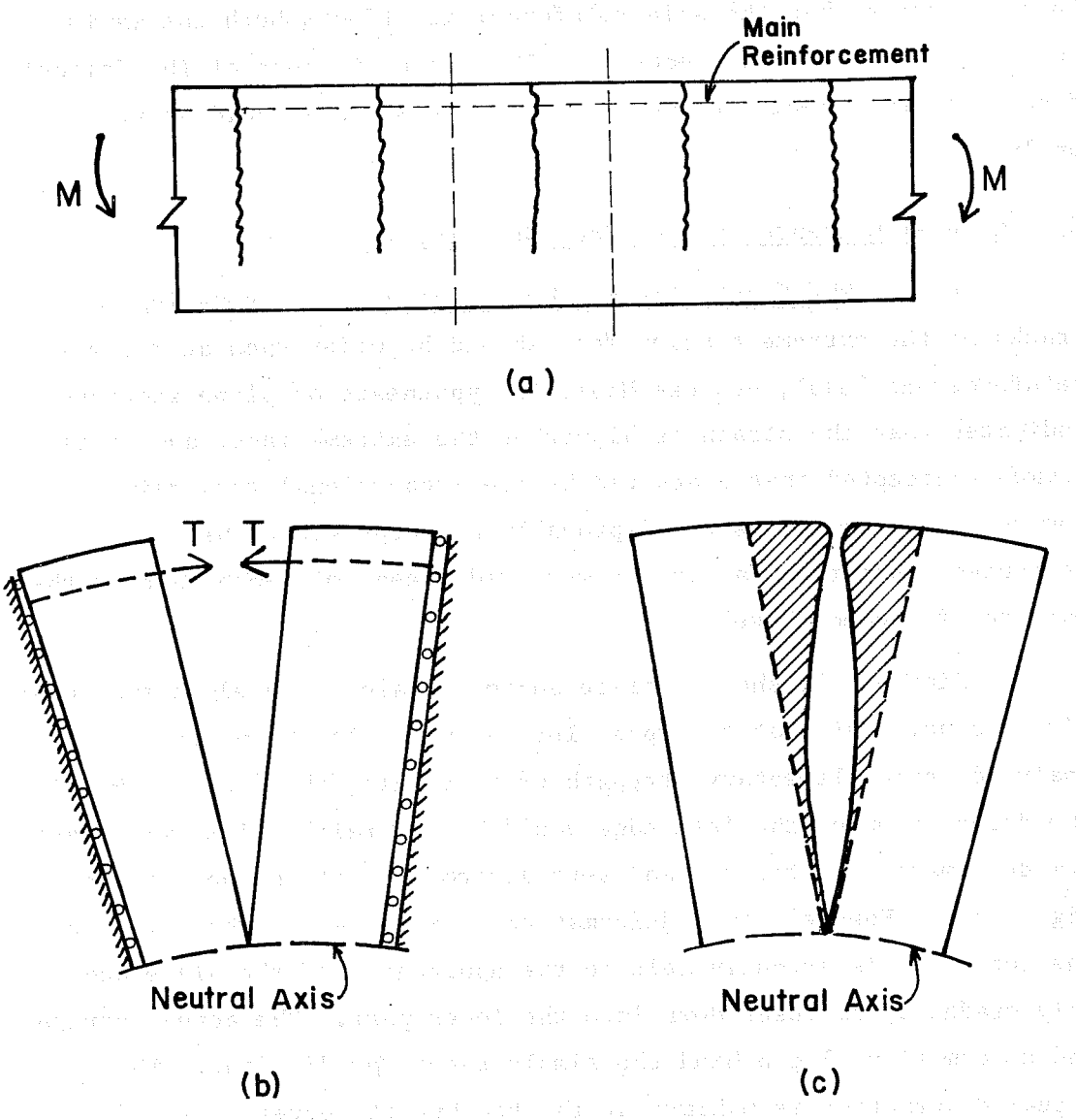

Fig. 6.4 Why side face crack is not wedge-shaped

region of a beam is removed in Fig. 6.4a. The cutting planes are along lines of symmetry assumed halfway between cracks. In Fig. 6.4b, the main tension reinforcement provides restraining forces, T, which try to close the crack. Using the same concept presented in Fig. 6.3, the effects of these forces tend to remain concentrated in the upper regions of the section. The resulting deformation of the edges is shown as the hatched areas in Fig. 6.4c. The remaining crack opening is seen on the side face. As shown here, the crack is definitely not wedge-shaped. This shape agrees with the general crack shape noted in many of the test specimens.

6.2.2 How Skin Reinforcement Affects Side Face Cracking. Skin reinforcement has a very pronounced effect on the crack pattern. As the amount of skin reinforcement increased, the crack pattern gradually changed from a tree branch crack pattern (in specimens without skin reinforcement) to one where more cracks remained vertical and extended into the web. Figure 6.5 shows this effect in typical specimens with and without skin reinforcement.

The mechanics of side face crack development are shown in Fig. 6.6. In Fig. 6.6a, a short crack is developing next to a long crack in a specimen without skin reinforcement. At a crack the tension force in the main reinforcement depends on the length of the crack. The force is highest at the longest crack and lower at the shorter cracks because at the shorter cracks there is more uncracked concrete between the crack and the neutral axis to help carry the total tension force. Therefore, there is a net force, ΔT, acting on the tooth. Loaded as a short cantilever, the tooth tends to crack following the dashed line, curving towards and perhaps joining the long crack. Fig. 6.6b shows a similar situation in a specimen with skin reinforcement. As in Fig. 6.6a, there is some force ΔT (not necessarily the same magnitude) acting on the tooth. At the long crack are also forces T_1 and T_2 from the skin reinforcement. As a skin bar extends into the concrete, it transfers some force to the concrete, creating a zone of tensile stresses (hatched areas) that tend to crack

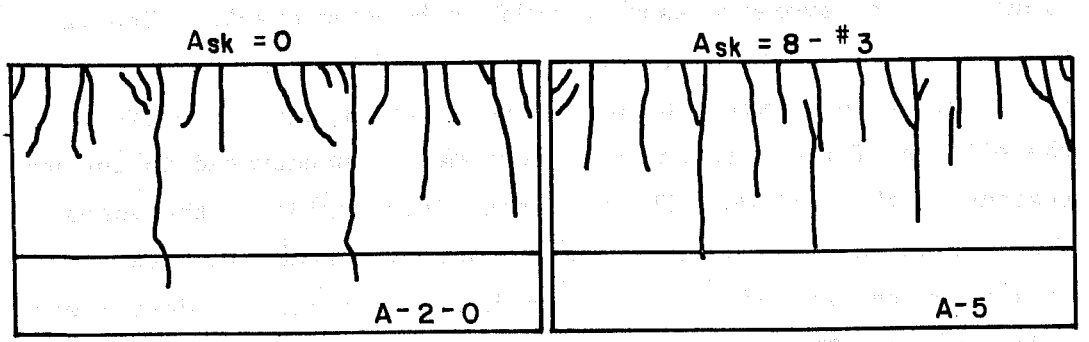

(a) Crack patterns @ f_s = 35 ksi

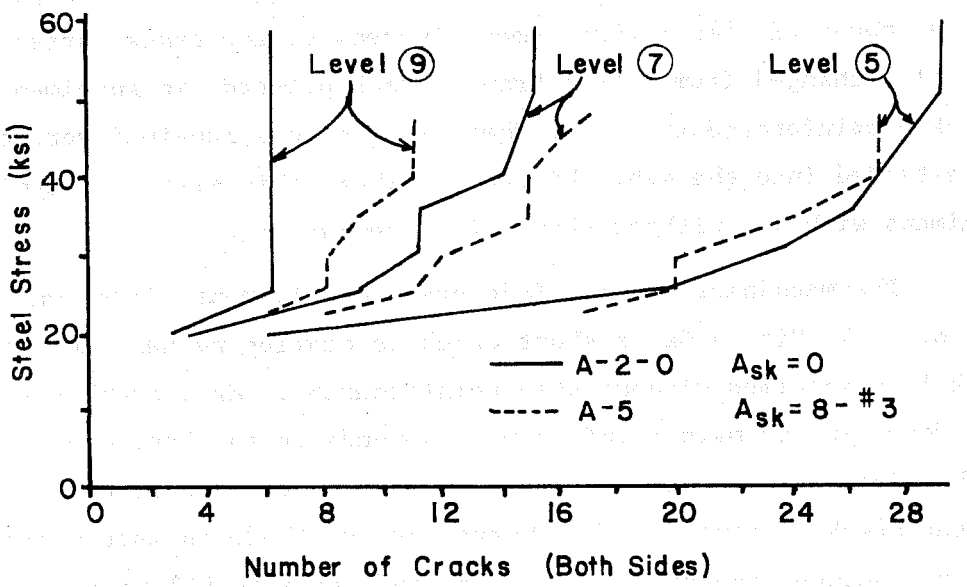

(b) Cracks on side faces

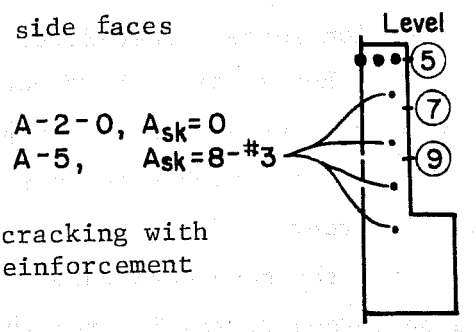

Fig. 6.5 Typical side face cracking with and without skin reinforcement

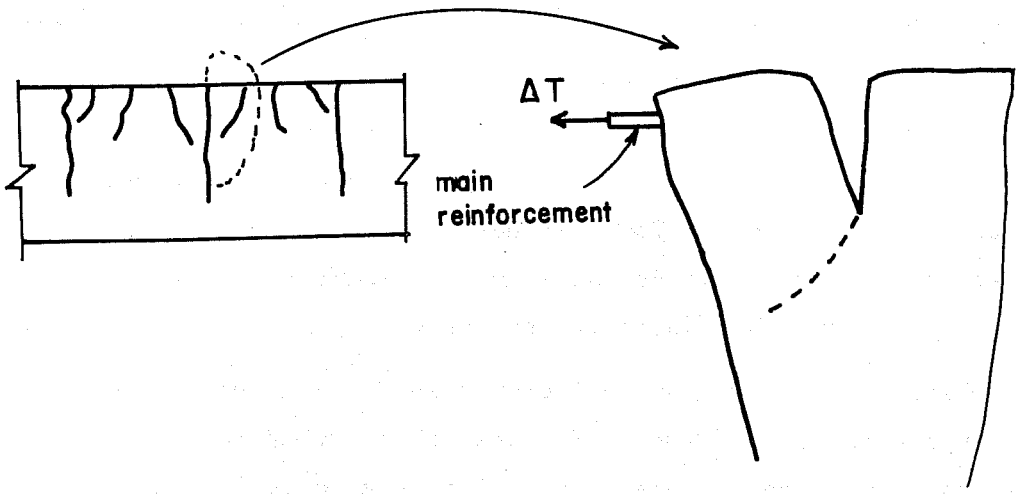

(a) Without skin reinforcement

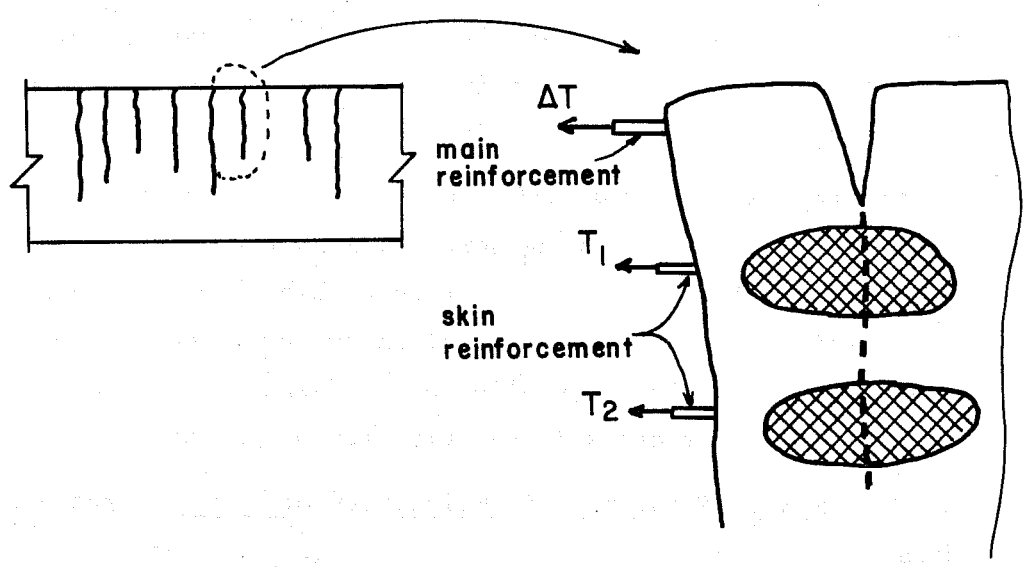

(b) With skin reinforcement

Fig. 6.6 Mechanics of side face crack development

the concrete perpendicular to the bar's axis, as in an axial tension specimen. If a sufficient amount of skin reinforcement is provided, these stresses overshadow the tendency of the ΔT force to crack the tooth as a cantilever, and the crack extends vertically. If the skin reinforcement is located too far away from this crack development zone, the shorter crack would be affected predominantly by the ΔT force and would curve towards the long crack before it could be affected by the face bar anchorage stresses.

Figure 6.7 shows how an increase in the area of skin reinforcement increases the number of cracks that extend to web middepth for Series A specimens. Soretz and Colanna-Ceccaldi[12] reported the same effect in their tests. Increasing the number of cracks that penetrate the web is an important benefit of using skin reinforcement. With a given amount of curvature, there is a certain elongation that must occur at every level in the tensile zone. An increase in the number of cracks at any level means a smaller width per crack at that level. This seems to be a prime contribution of skin reinforcement.

Another way skin reinforcement influences the side face cracking is by providing restraining forces across the cracks. Just as the force in the main reinforcement tries to close (or restrain from further opening) the crack in the vicinity of the main reinforcement (Fig. 6.4), the force supplied by the skin reinforcement will also try to close the crack in the vicinity of the bar.

6.2.3 How Web Width and Skin Reinforcement Cover Affect Side Face Cracking. Investigations by Gergely and Lutz[19] and others[10,14,20,21] on crack control in the vicinity of the main reinforcement have indicated that the exterior crack width increases as the reinforcement cover or the area of concrete concentric with the reinforcement increases. Husain and Ferguson[5] injected epoxy into the cracks in the vicinity of the main reinforcement and then sawed the beams into sections and measured internal crack widths. Their results showed that cracks were relatively narrow at the surface of the reinforcement and increased in width towards the exterior concrete surface. Beeby has

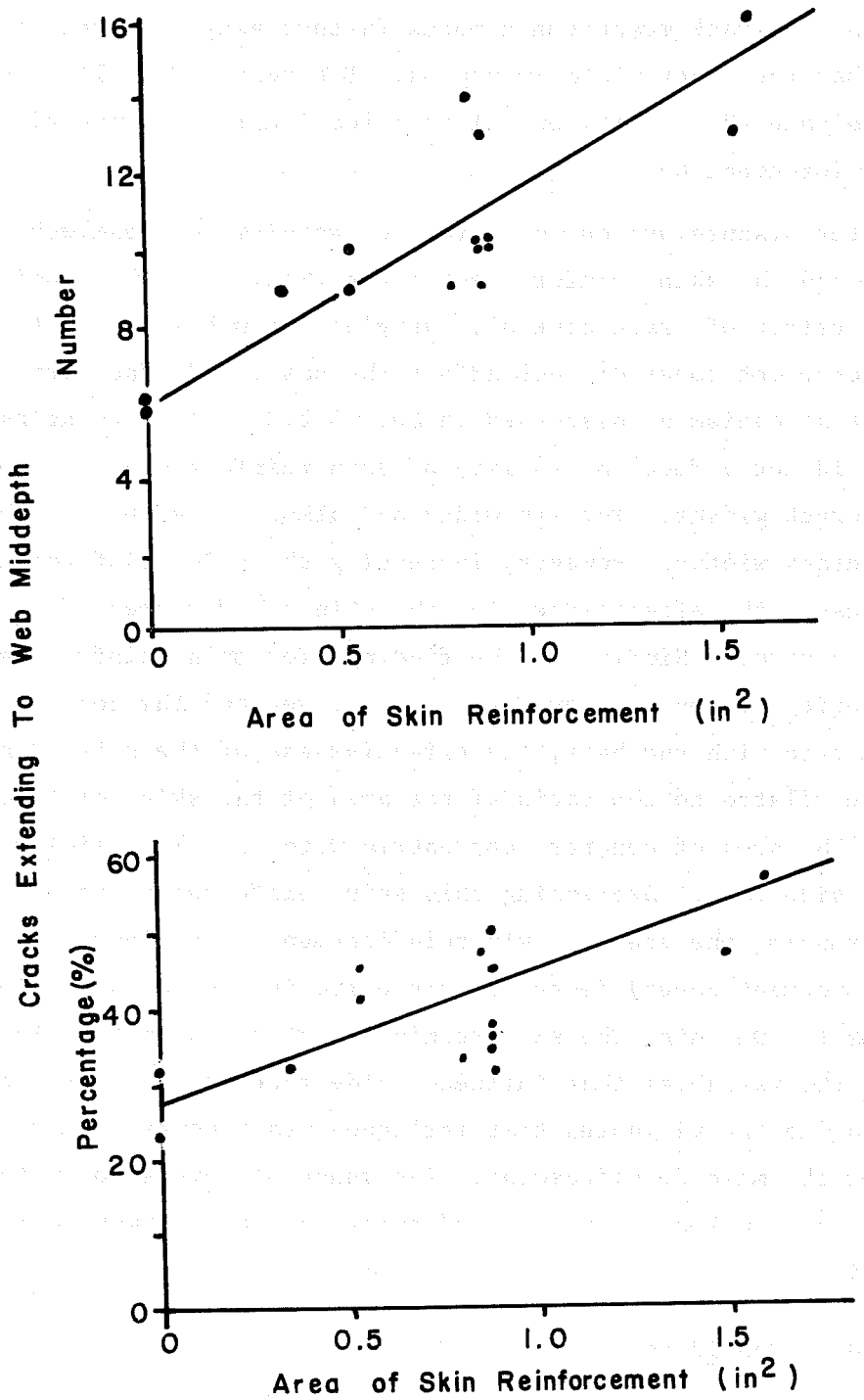

Fig. 6.7 Effect of area of skin reinforcement on number of cracks extending to web middepth

also shown in tests of slabs,[30] tension members,[31] and beams[11] that as the point of crack measurement moves farther away from the reinforcement bar the crack width increases. The results of all these studies indicate that crack control is a local effect in the vicinity of the reinforcement bar.

Later discussions on the effect of varying the beam web width (Sec. 6.4) and the skin reinforcement cover (Sec. 6.5) also indicate this local effect of crack control. Varying the web width or the skin reinforcement cover did not affect the basic side face crack development mechanism as discussed in Sec. 6.2.2. Also, changing the web width did not affect the ability of skin reinforcement to control side face crack widths. The web width had almost no effect on the side face crack widths. However, increasing the skin reinforcement cover decreased the effectiveness of the skin reinforcement for side face crack control. Similar to the findings for main reinforcement, where the effectiveness is governed by the cover and the concrete area concentric with the bars, the effectiveness of the skin reinforcement can be related to the ratio of the area of the skin reinforcement divided by the area of concrete concentric with the skin reinforcement along each side face. Decreasing this skin reinforcement ratio (by either decreasing the area of skin reinforcement or by increasing the skin reinforcement cover) decreases the effectiveness of the skin reinforcement. Defining the skin reinforcement ratio in this manner shows that the variables that influence side face crack control are very similar to the variables that influence crack control in the vicinity of the main reinforcement. The range of covers for which this was proven applicable is the ordinary range of minimum covers specified in codes.

6.3 Secondary Considerations

6.3.1 Effect of Concrete Strength on Cracking. Specimens RS-1, 2, and 3 were identical except for concrete compressive strength

(2944, 3183, and 4290 psi, respectively). Although the range of concrete strengths is not that large, some tentative conclusions can be drawn on the effect of concrete strength on the side face cracking. When comparing the average crack width profiles (Fig. 3.24) and the variation of crack widths with steel stress (Fig. 3.25), it is impossible to detect any influence from variation in concrete strength; all results are very similar. The same conclusion is reached when comparing crack patterns (Fig. 3.20 and Fig. 3.23). This conclusion is not surprising because other investigators[14,20] have reported that concrete strength does not affect cracking behavior beyond first cracking.

6.3.2 Effect of Crack Width at Main Reinforcement Level on Side Face Cracking. Soretz and Colanna-Ceccaldi[12] reported that when they changed the main reinforcement in their specimens from two large bars to ten smaller bars of the same total area there was a significant reduction in the crack widths in the vicinity of the main reinforcement. However, they also said that the accompanying reduction in maximum side face crack widths was within the scatter of their test data. Therefore, they could not say conclusively how the reduction in crack width at the main reinforcement level affected the side face crack width.

Using the equations of Beeby,[11] it is possible to predict how a variation in the crack width at the main reinforcement level affects the crack width on the side face of a beam without skin reinforcement (see Fig. 6.8), as given in Appendix C of Ref. 54.

The relationship between the side face crack width and the crack width at the main reinforcement level is shown in Fig. 6.9. At a d_t of 60 in., reducing the maximum crack width at the main reinforcement level from 0.012 to 0.006 in. (50 percent reduction) reduces the maximum web crack width from 0.040 to 0.025 in. (38 percent reduction). This figure can be used to determine the tension depth above which

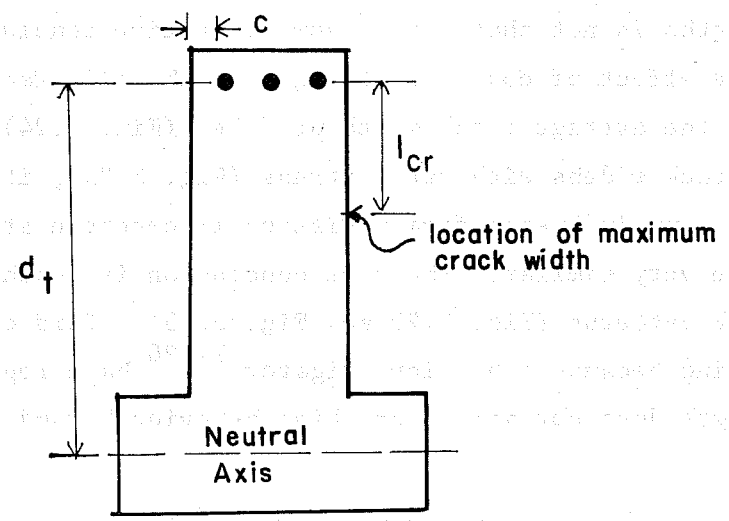

Fig. 6.8 Notation for side face cracking equation

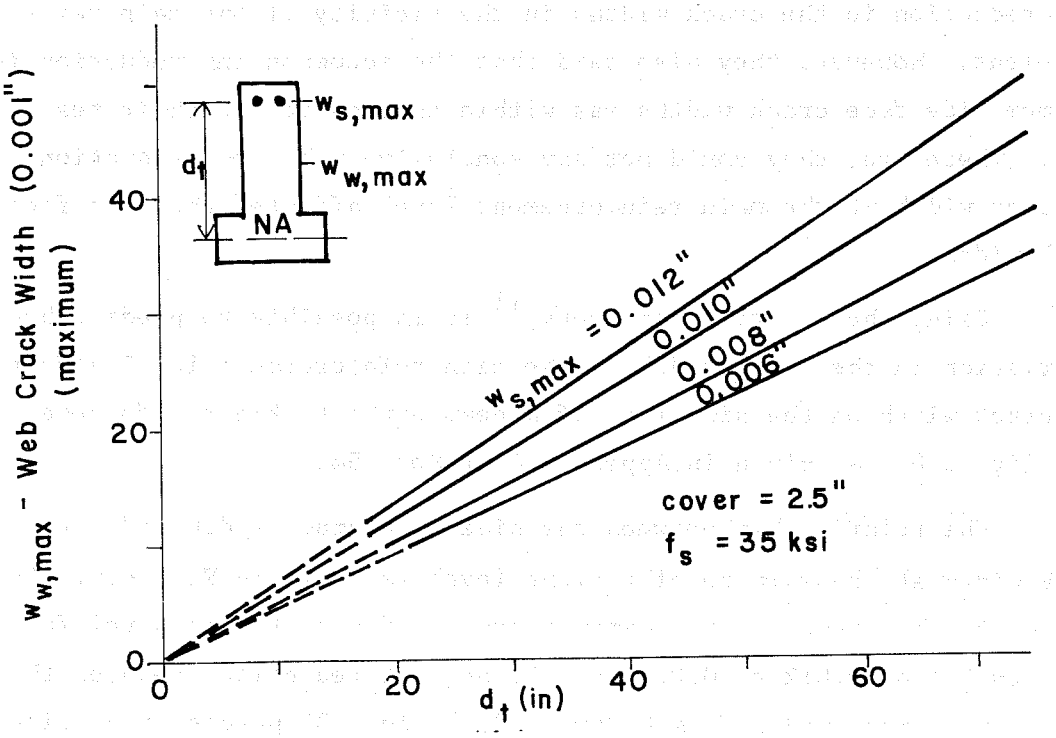

Fig. 6.9 Effect of crack width at main reinforcement level on web crack width

skin reinforcement is required to limit the web crack width to a prescribed value. For example, to limit the web crack width to 0.016 in., the maximum allowable d_t is about 23 in. if the crack width at the main reinforcement level is 0.012 in. Above a d_t of 23 in., skin reinforcement is required to control the side face cracking. If the crack width at the main reinforcement level is reduced to 0.006 in., then the critical d_t can be increased to about 34 in. for the same web crack width of 0.016 in.

Specimen T-1-0 was designed as a typical full size member with a depth, d, of 32.8 in. and a tension zone depth, d_t, of 27 in. Main reinforcement was two #9 bars with a cover of 2-1/2 in. The maximum crack width at the level of main reinforcement was calculated by the Gergely-Lutz equation to be 0.0116 in. According to Fig. 6.9, the predicted maximum web crack width for this specimen is about 0.018 in. The maximum measured crack width in the web was 0.013 in. Although the measured crack width is within 33 percent of the predicted value (a typical scatter for cracking data), this result indicates that these curves may be predicting crack widths that are slightly too large. However, without further tests, a definite conclusion cannot be reached.

These equations predict that decreasing the crack width at the main reinforcement level will also decrease the side face crack width but at a lesser rate. However, with a typical cover of 2 to 3 in., reducing the main reinforcement crack width from 0.012 to, say, 0.007 in. may require a very large increase in the number of main reinforcement bars (Fig. 6.10). Such a change would significantly increase construction costs and increase congestion in the region of the main reinforcement. Additional side face crack control reinforcement would probably still be required to reduce the web crack width to an acceptable level. Therefore, reducing the crack width at the main reinforcement level is neither a practical nor effective way of controlling the side face cracking problem.

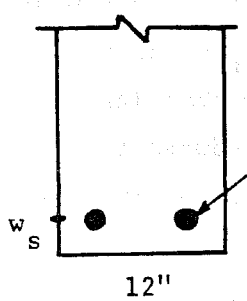

typical detail

2 - #9 Bars

cover = 2½"

by Gergely-Lutz equation (see 2.2.1)

$$w_s = \frac{0.091\sqrt[3]{t_s A}}{1 + t_s/h_1} (f_s - 5)$$

using h_1 = 27 inches

and f_s = 35 ksi

$w_s = 12.0 \times 10^{-3}$ inches

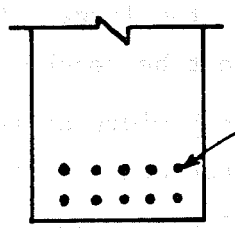

revised detail to reduce w_s approximately 40%

10 - #4 Bars

cover = 2½"

by Gergely-Lutz equation

$w_s = 7.1 \times 10^{-3}$ inches

Fig. 6.10 Required change in main reinforcement placement to substantially reduce crack width at main reinforcement level

6.3.3 Stress in Reinforcement

6.3.3.1 Outside the Specimen. Speciman A-1-0 had main reinforcement consisting of five #6 bars in one layer. Ideally, the loading system should induce the same stress in each bar. If the stresses are unequal (say much higher in the outer bars), then the cracking of the specimen may be seriously affected. Electrical resistance SR-4 strain gages were applied to each main reinforcement bar of A-1-0 approximately 6 in. outside the concrete section. The gages were monitored throughout the entire test. Figure 6.11 presents some of the stress data obtained. The measured stress in each bar is plotted against the "applied" uniform stress (measured applied force/ main reinforcement area). Except for two points, all measured stresses lie within or very close to ±5 percent of the average applied stress. The results are very good and indicate an even load transfer from the loading system to the main reinforcement.

6.3.3.2 Inside the Specimen. The large crack widths on the side face may induce high stresses in the skin reinforcement. To check this possibility, Specimens A-7 and A-4 had strain gages applied to the skin reinforcement. Gages were placed at locations where a crack was expected to form, based on previous test results. Although the bar stresses at a crack were desired, the specimens were not forced to crack at the gage locations because it was felt unwise to try to alter the natural crack development. Nevertheless, in most cases a long crack formed within 1 or 2 in. from the gage locations.

Figures 6.12 and 6.13 show the measured skin reinforcement stresses at a predicted main reinforcement stress of 35 ksi. The predicted stress distribution is a straight line distribution based on a cracked transformed area analysis with a main reinforcement stress of 35 ksi. The gages are shown on a sketch of the specimen's crack patterns. One column of gages in A-7 indicates stresses well above the predicted values by up to 38 percent. A similar pattern is

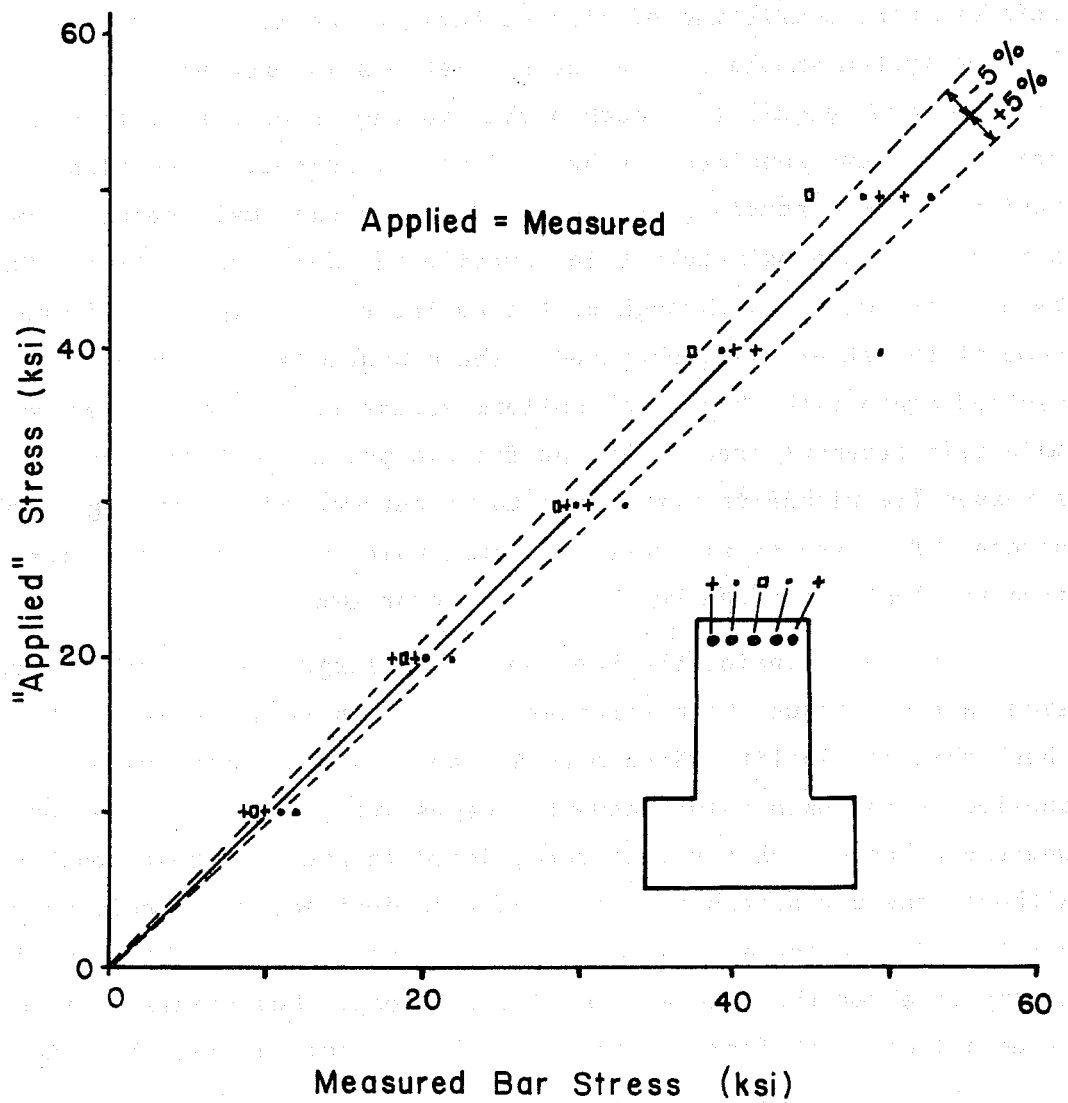

Fig. 6.11 Stresses in main reinforcement outside specimen

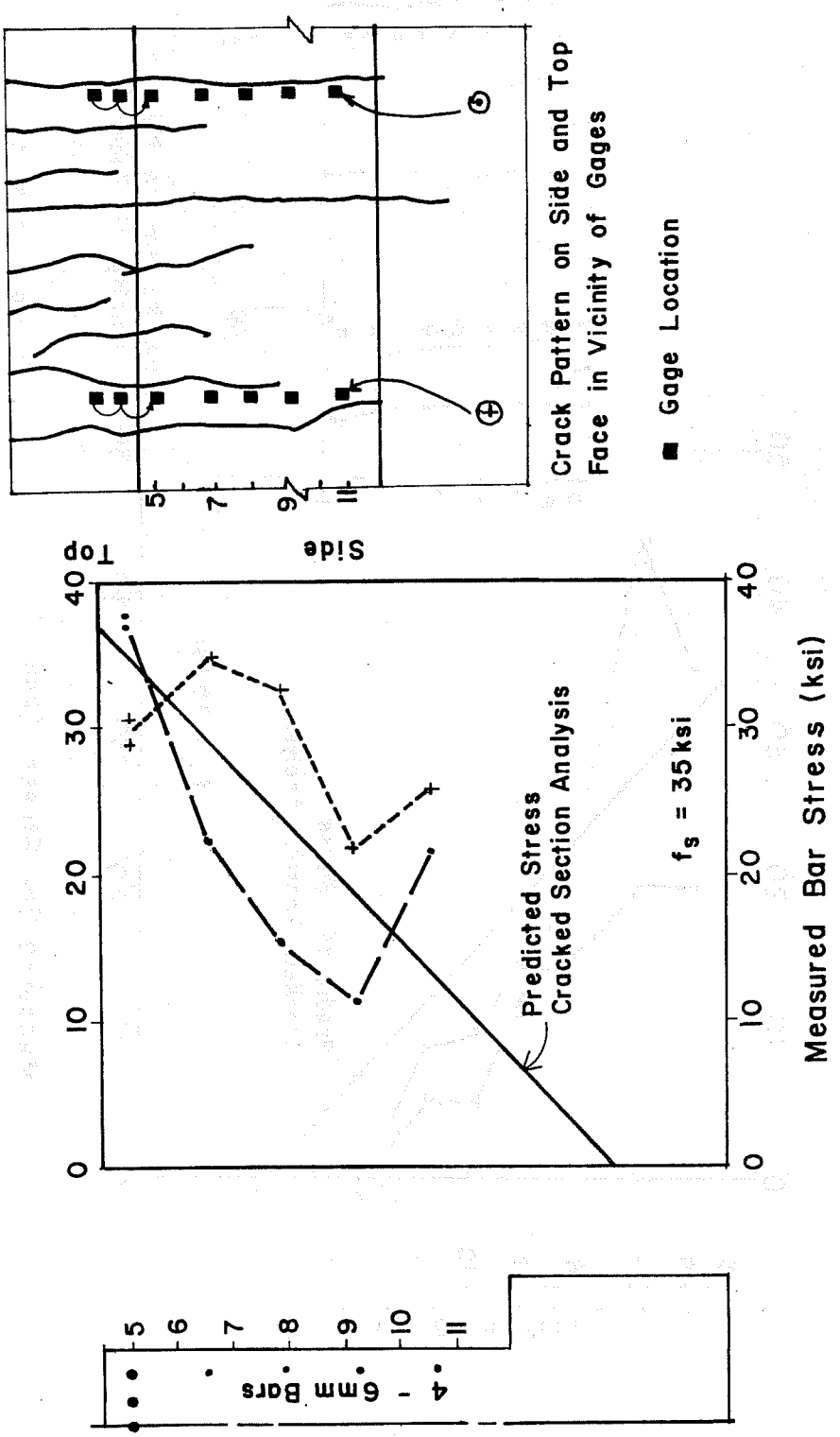

Fig. 6.12 Stresses in reinforcement in Specimen A-7

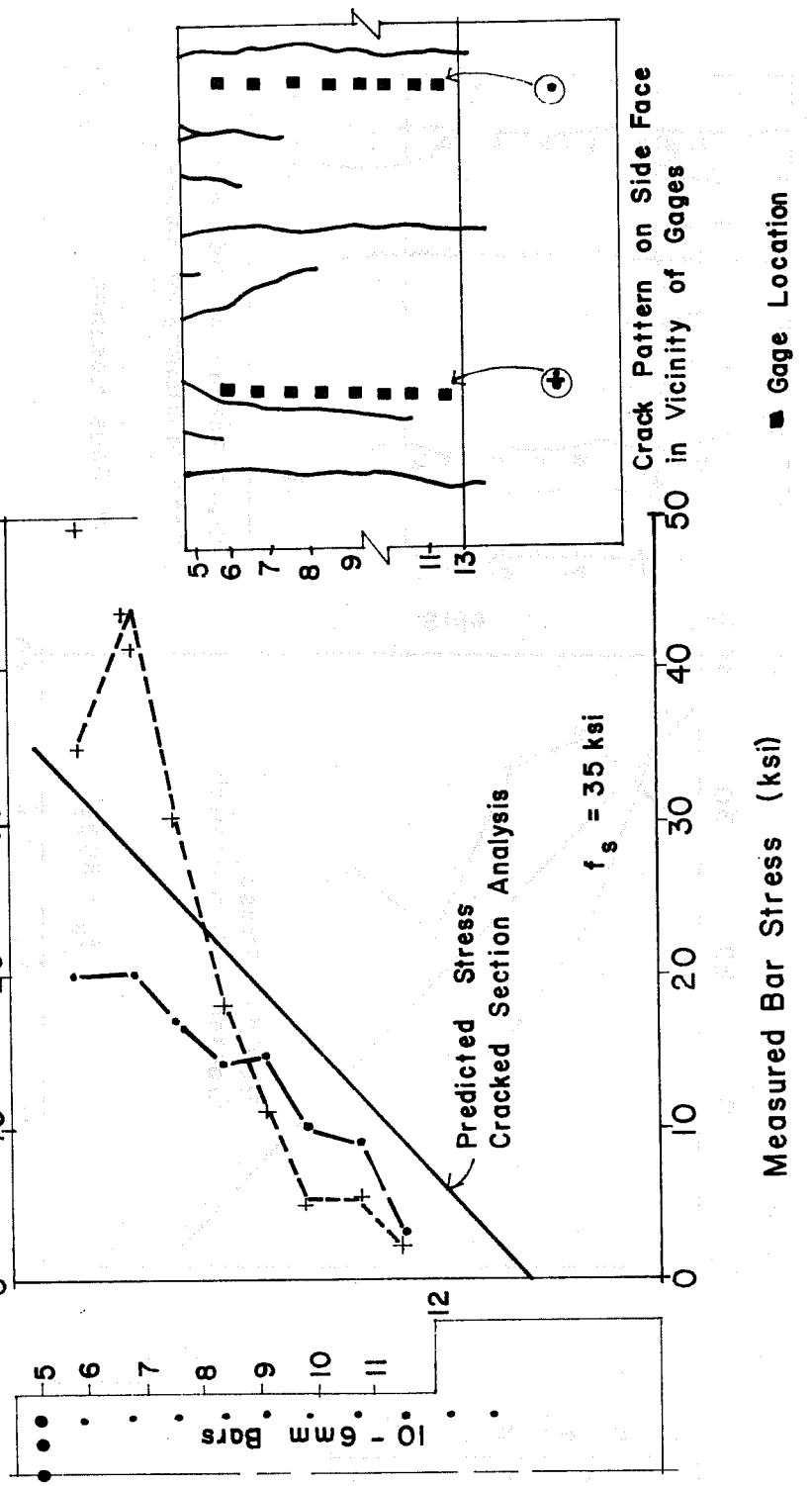

Fig. 6.13 Stresses in reinforcement in Specimen A-4

shown by gages in A-4, with measured stresses exceeding the predicted stresses by up to 59 percent. Notice that none of the gages lie directly across a crack. The stresses in the bars at a crack are probably higher than the values shown here. Data recorded at a crack would be very useful to completely answer this question even if a crack must be forced to form at the gage location.

Figure 6.14 shows the skin reinforcement stresses predicted by the finite element analysis of Chapter 5 for the mathematical model FD-14, which had seven 0.283 in. diameter bars spaced at 2 in. along each side face. The finite element analysis predicts a very large increase in skin reinforcement stresses at a crack. It indicates possible yielding of Grade 60 (minimum 60 ksi yield stress) reinforcement.

The laboratory specimen A-4, which had ten 6 mm bars spaced at 2.375 in. along each side face, is quite similar to the mathematical model FD-14. The measured skin reinforcement stresses from this specimen are also shown in Fig. 6.14. Several of the gages that are closest to cracks indicate stresses well above the stress predicted by a cracked section analysis. As previously noted, none of these strain gages were directly across a crack where the bar stress would be expected to be greatest. The finite element analysis stresses are higher than those measured in the laboratory specimen, but the general pattern is in agreement. Both the finite element and the laboratory results indicate that stress in the skin reinforcement can be higher than the stress which would be predicted from a cracked section analysis assuming a linear strain profile across the full depth of the section.

6.4 Beam Web Width Series

Series W examined the effect of web width on the side face cracking. Except for the variation in web width and distribution of main reinforcement, all section dimensions were the same in each

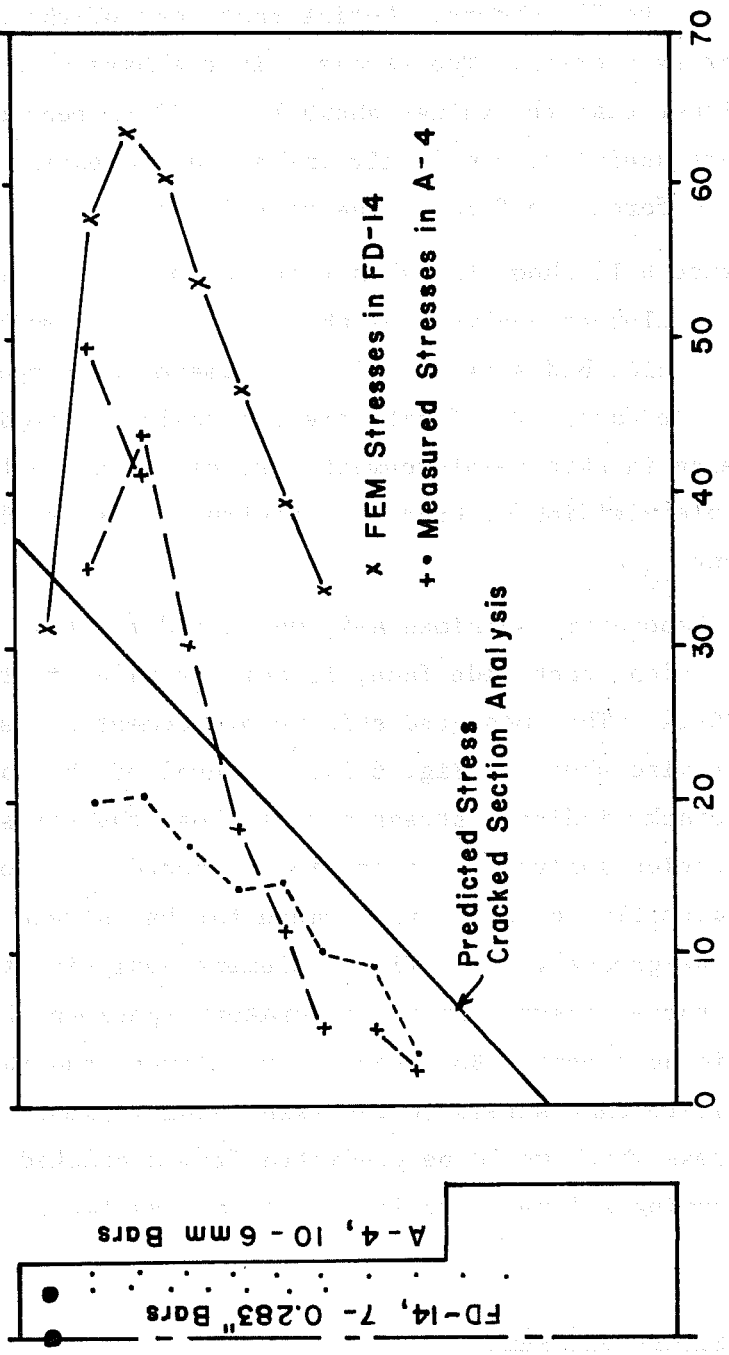

Fig. 6.14 Stresses in reinforcement in finite element specimen--FD-14

specimen. The web width was 7.75, 11.25, or 17 in. Main tension reinforcement was approximately 2.2 sq. in. and was distributed so as to produce the same width crack at the main reinforcement level (as calculated by the Gergely-Lutz[19] equation). One set of three specimens (W-1-0, A-2-0, and W-3-0) had no skin reinforcement, and a second set of three specimens (W-2, A-8, and W-4) had identical amounts of skin reinforcement, eight #3 bars at 4.125 in.

As the web width increases there is a greater area of concrete to help carry the tension force. This means that for any applied moment the average main reinforcement stress, $f_{s,av}$, as measured by surface strain, will vary inversely with the web width. Beeby's[11] cracking equations are based on the average steel strain (or stress). Beeby[50] suggested a method to determine the average steel stress ($f_{s,av}$) based on the section properties and the steel stress calculated by a cracked section analysis (f_s). This method predicts that $f_{s,av}$ will be less than f_s by 13, 19, and 29 ksi in the 7.75, 11.25, and 17 in. webs, respectively. These differences appear to be approximately the change in the reinforcement stress between the uncracked and cracked concrete states. Figure 6.15 shows a comparison between $f_{s,av}$ and f_s (the calculated main reinforcement stress inside the specimen) for several specimens that are identical except for web width. For specimens without skin reinforcement, $f_{s,av}$ does decrease as the web width increases, but not nearly as much as predicted above. As the applied load increases, the results of the three specimens indicate that $f_{s,av}$ approaches f_s (since the concrete is becoming more cracked and less effective in tension). For specimens with skin reinforcement, there seems to be no detectable effect of web width. Because these specimens have more total tension reinforcement, the percentage of the total tension force carried by the concrete in these specimens is less than in specimens with no skin reinforcement.

The specimens in Series W will be compared at equal applied moments or equal f_s. Kaar and Mattock[10] also compared their specimens,

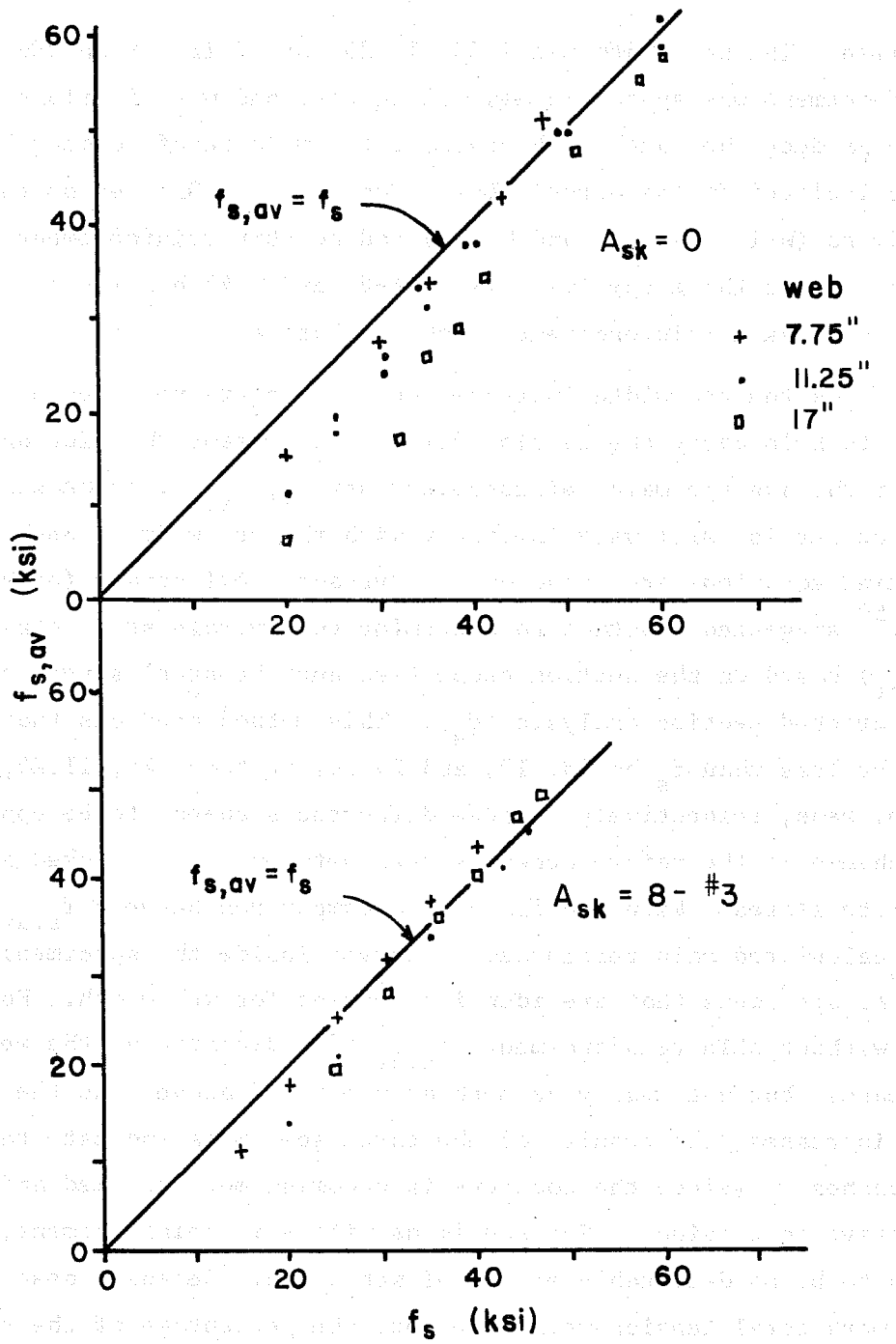

Fig. 6.15 Average steel stress vs cracked section steel stress--various web widths

which had varying web widths at equal applied moments. Figure 6.16 presents the crack profiles for specimens without skin reinforcement at main reinforcement stresses of 30 and 35 ksi. The profile of the specimen with a 17 in. web is less than those of the 7.75 and 11.25 in. webs which are virtually identical. Figure 6.17a shows how the web crack width varied throughout the entire load range. Again, there is a slight difference in the 17 in. web, but virtually no difference between the 7.75 and 11.25 in. webs. Comparison of the crack patterns (Appendix A) for these specimens indicates the web width does not significantly influence the crack pattern. In each case only a few cracks penetrate to middepth.

Figures 6.18 and 6.17b show similar data for the specimens with skin reinforcement. With the addition of skin reinforcement there seems to be no detectable effect of web width on the side face cracking. The crack profiles (Fig. 6.18) are all very similar, both in general shape and in the largest crack width on the side face. Figure 6.17b shows the variation of web crack width with main reinforcement stress, and again the difference in web width seems to have no effect. The crack patterns (Appendix A) are also very similar and show that the specimens with skin reinforcement have a significantly greater number of cracks extending to web middepth than do the companion specimens without skin reinforcement.

The lack of correlation between the web width and the web crack width, especially in specimens with skin reinforcement, is emphasized in Fig. 6.19. The same trend exists at other stress levels. Without any skin reinforcement the web crack width varies from 0.0078 to 0.0098 in. in the three web widths. However, with skin reinforcement the web crack width is apparently unaffected by the web width and is about 0.0038 in. in each specimen. The skin reinforcement seems to affect only narrow strips of concrete along the side faces. Skin reinforcement along one of the side faces does not significantly affect the crack widths on the opposite side face. Although the maximum web

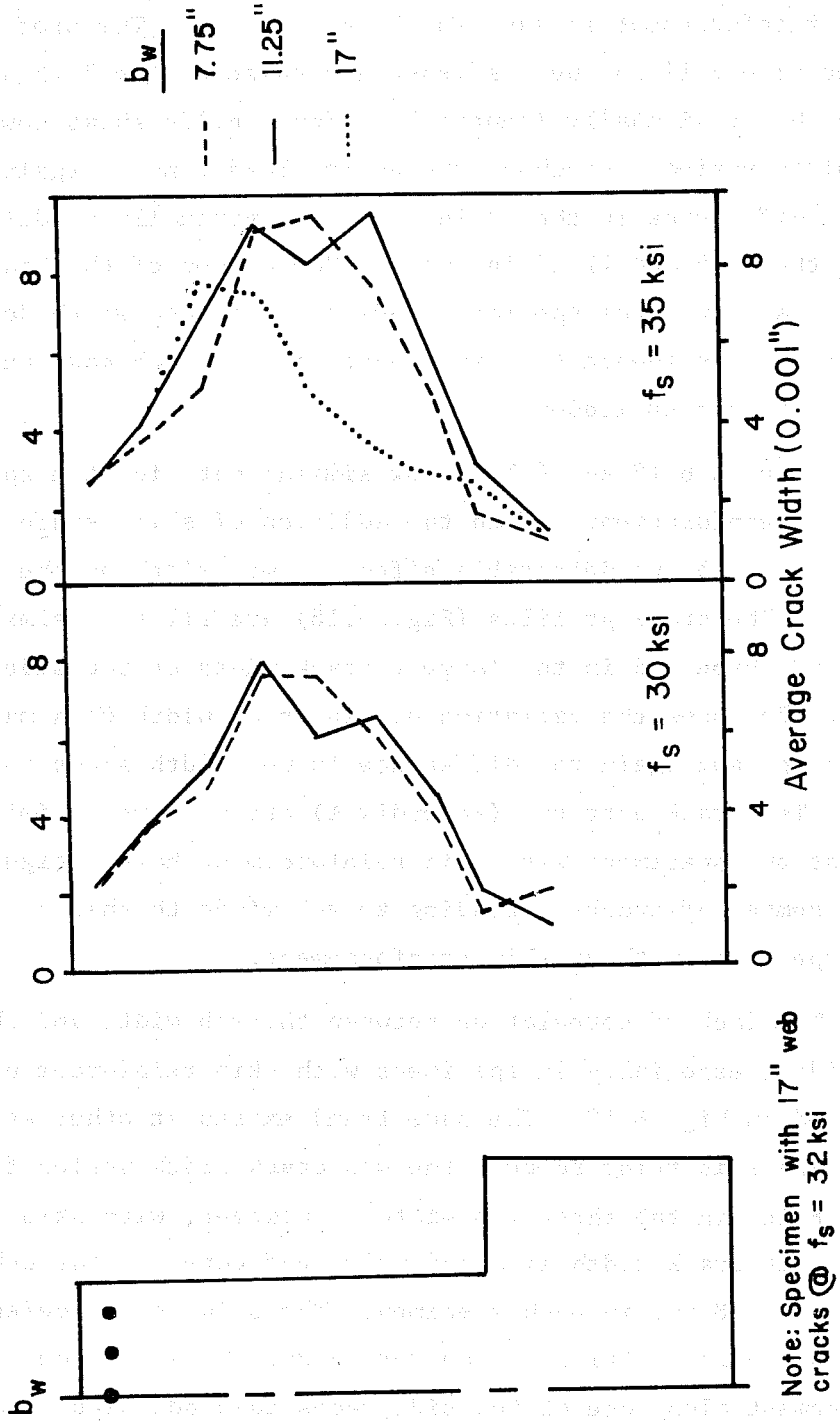

Fig. 6.16 Crack profiles--various web widths, A_{sk} = 0

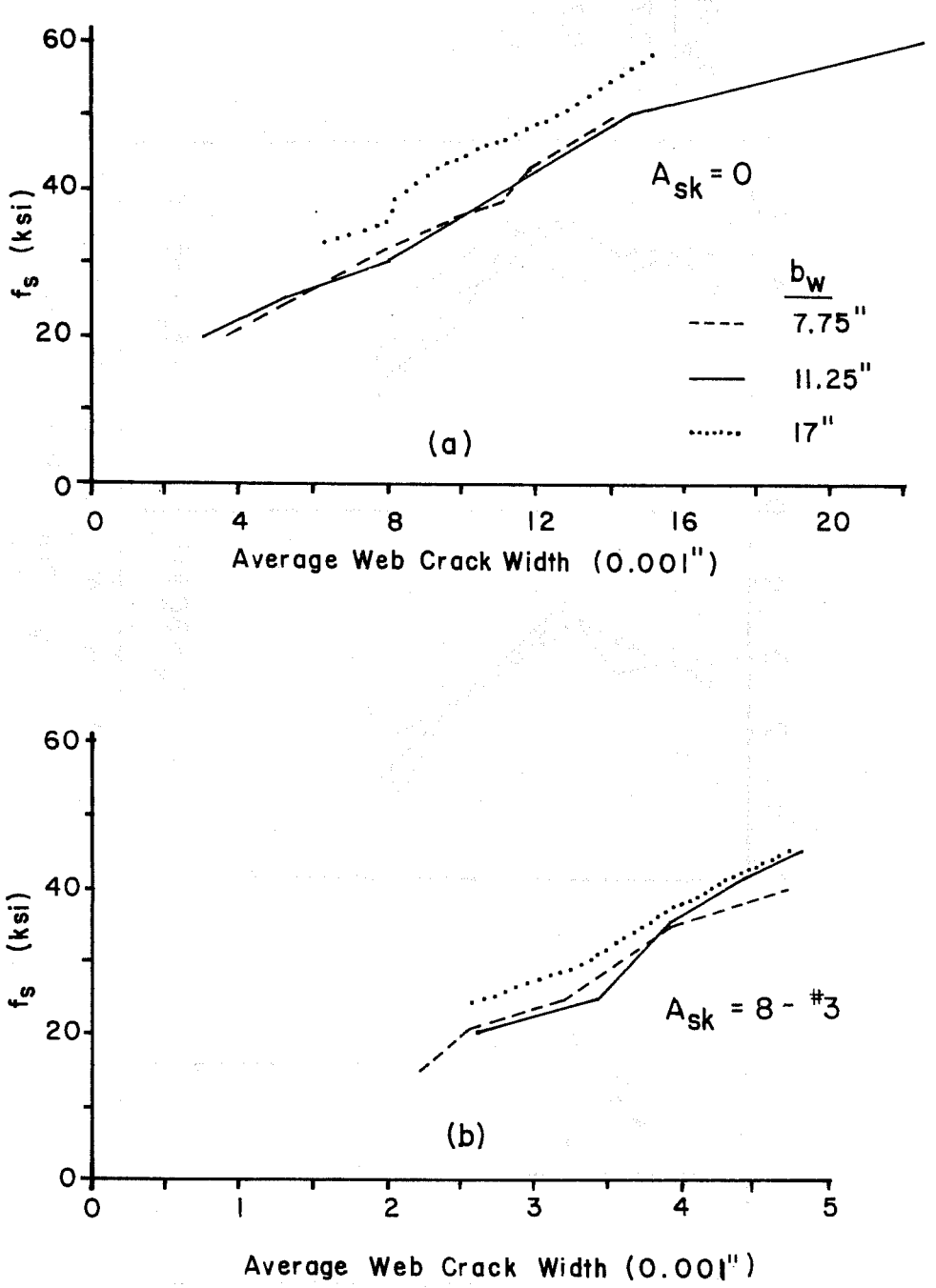

Fig. 6.17 Variation of web crack width with steel stress--various web widths

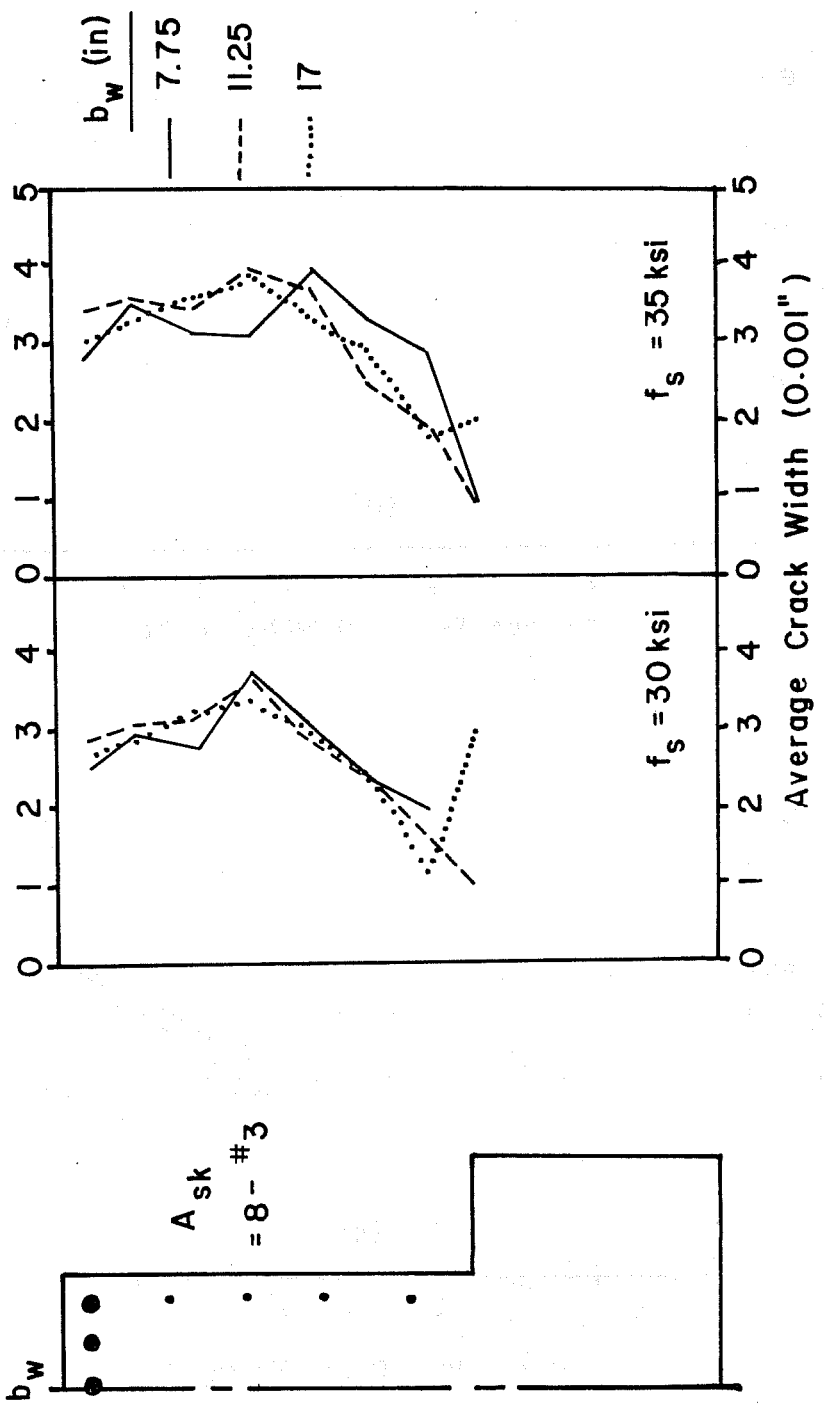

Fig. 6.18 Crack profiles--various web widths, A_{sk} = eight #3

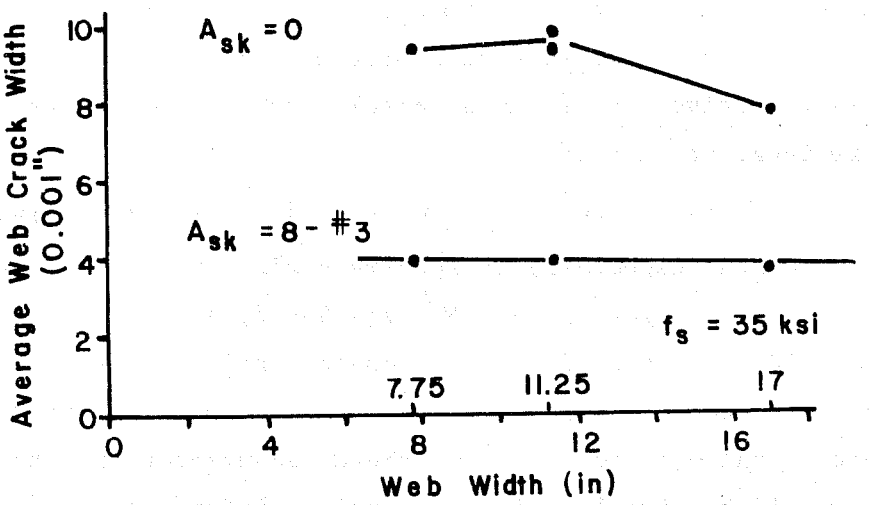

Fig. 6.19 Effect of web width on web crack width

width tested in this model series was 17 in., there is no indication in these test results that the same trend would not apply to wider specimens.

Kaar and Mattock[10] reported on tests of I, T, and rectangular beams with web widths of 3-1/2, 4, and 8 in. Their data indicated that the web width did not significantly affect the average flexural crack width in the web in specimens with or without skin reinforcement (Fig. 6.20a). However, they did conclude that skin reinforcement was less effective in controlling diagonal crack widths in the rectangular section than in the I or T sections (Fig. 6.20b). Sorretz and Colanna-Ceccaldi[12] reported that skin reinforcement controlled diagonal crack widths as effectively as flexural crack widths in their tests, using only a rectangular section.

The conclusion that the web width does not affect the side face crack width, especially in specimens with skin reinforcement, is significant in light of the CEB[9] and Soretz and Colanna-Ceccaldi recommendations for side face crack control reinforcement. Both of these say the required amount of skin reinforcement is linearly dependent on the web width. Using these recommendations, the 17 in. specimen would require 1.5 times the skin reinforcement area of the 11.25 in. specimen and 2.2 times the skin reinforcement area of the 7.75 in. specimen. This study indicates the same amount is just as effective in all three specimens. The tests by Soretz used only one cross section 11.8 in. wide.

Crack widths on the side face and at the bar surface are controlled by the skin reinforcement. However, as the crack extends through the web thickness past the skin reinforcement, the influence of the reinforcement probably decreases and the crack width increases. This result can be inferred from crack width measurements on slabs, reported by Beeby.[50] He reported that on the tension face of slabs the crack widths were smallest directly over the bars and widest

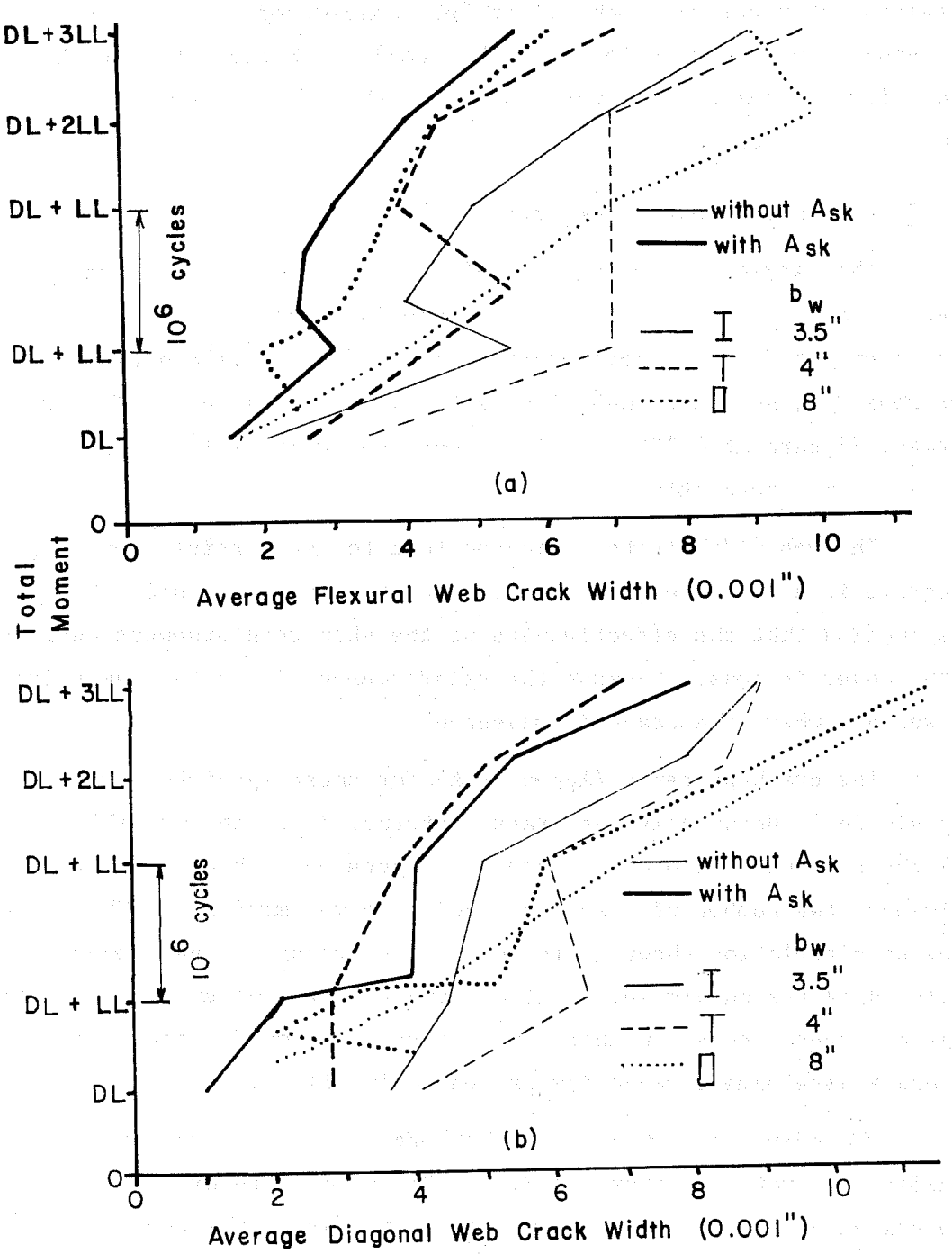

Fig. 6.20 Effect of web width--Kaar and Mattock (Ref. 10)

between the bars (Fig. 6.21). If a longitudinal section of a beam containing skin reinforcement is crudely considered to be a slab, then his results suggest that for a crack extending through the web the crack width decreases from the surface to the bar and then increases from the bar to the center of the web.

6.5 Skin Reinforcement Cover Series

This series of tests examined the effect of skin reinforcement cover on the side face cracking. All specimens had the same cross section except for skin reinforcement cover (Table 4.1 and Fig. 4.1). Specimens C-1, A-8, C-2, C-3, C-4, and C-5 all had skin reinforcement of eight #3 bars at 4.125 in. with a cover of 0.75, 1.125, 1.5, 2, 3, and 3-1/2 in., respectively.

The web width tests indicated that the skin reinforcement is effective in a narrow edge strip of concrete along each side face. This implies that the effectiveness of the skin reinforcement decreases as the cover increases because the reinforcement is further away from the surface where the crack is measured.

The crack patterns (Appendix A) for these specimens are all very similar. Using only the crack patterns, it is not possible to rank the specimens in order of cover. Figure 6.22 shows how cover influenced the number of cracks extending to web middepth. There seems to be no correlation shown in the data; the average values describe all the data reasonably well. It appears that the cover, at least the range of covers tested in this study, does not significantly affect the crack development mechanism presented in Fig. 6.6.

The effect of cover on the web crack width and the crack magnification ratio is shown in Fig. 6.23 for main reinforcement stresses of 30 and 35 ksi. As the cover increases, the web crack width and crack magnification ratio both increase. This trend is shown at each stress level of Fig. 6.23. This results supports the

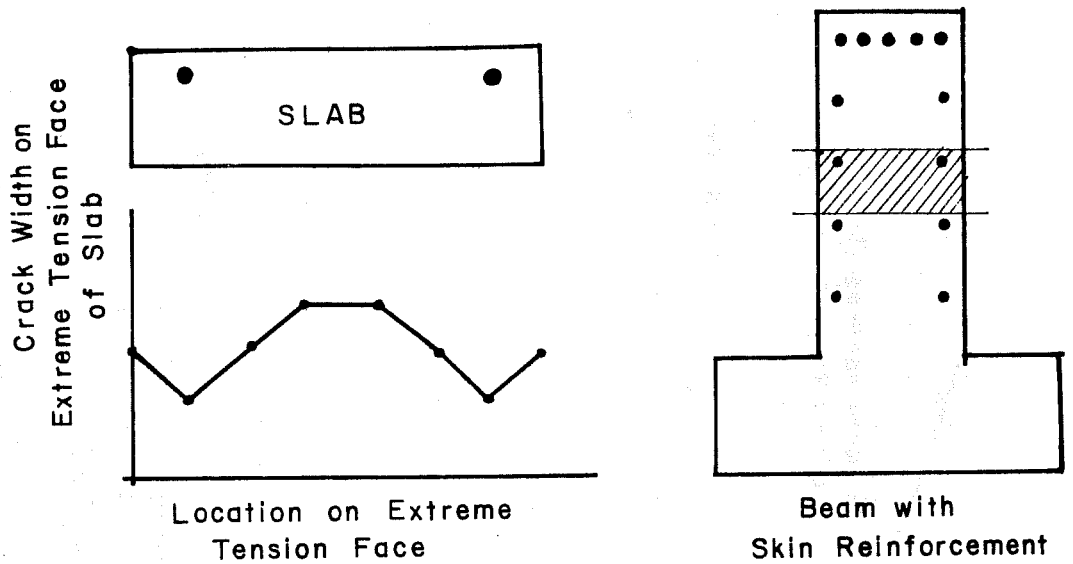

Fig. 6.21 Suggested crack profile inside web

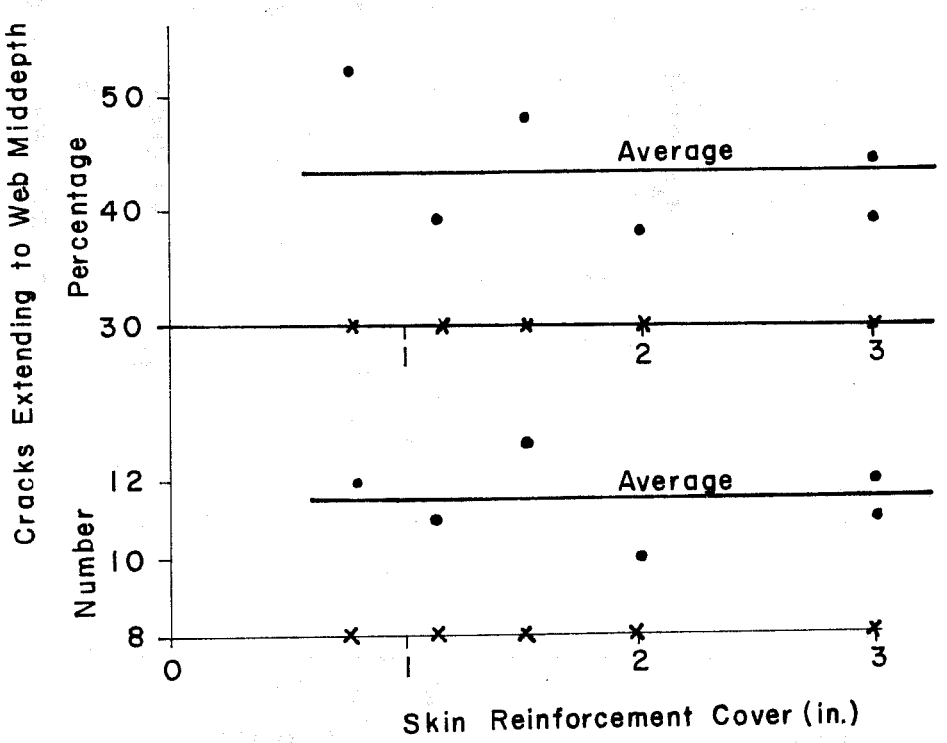

Fig. 6.22 Number of cracks penetrating web--cover series

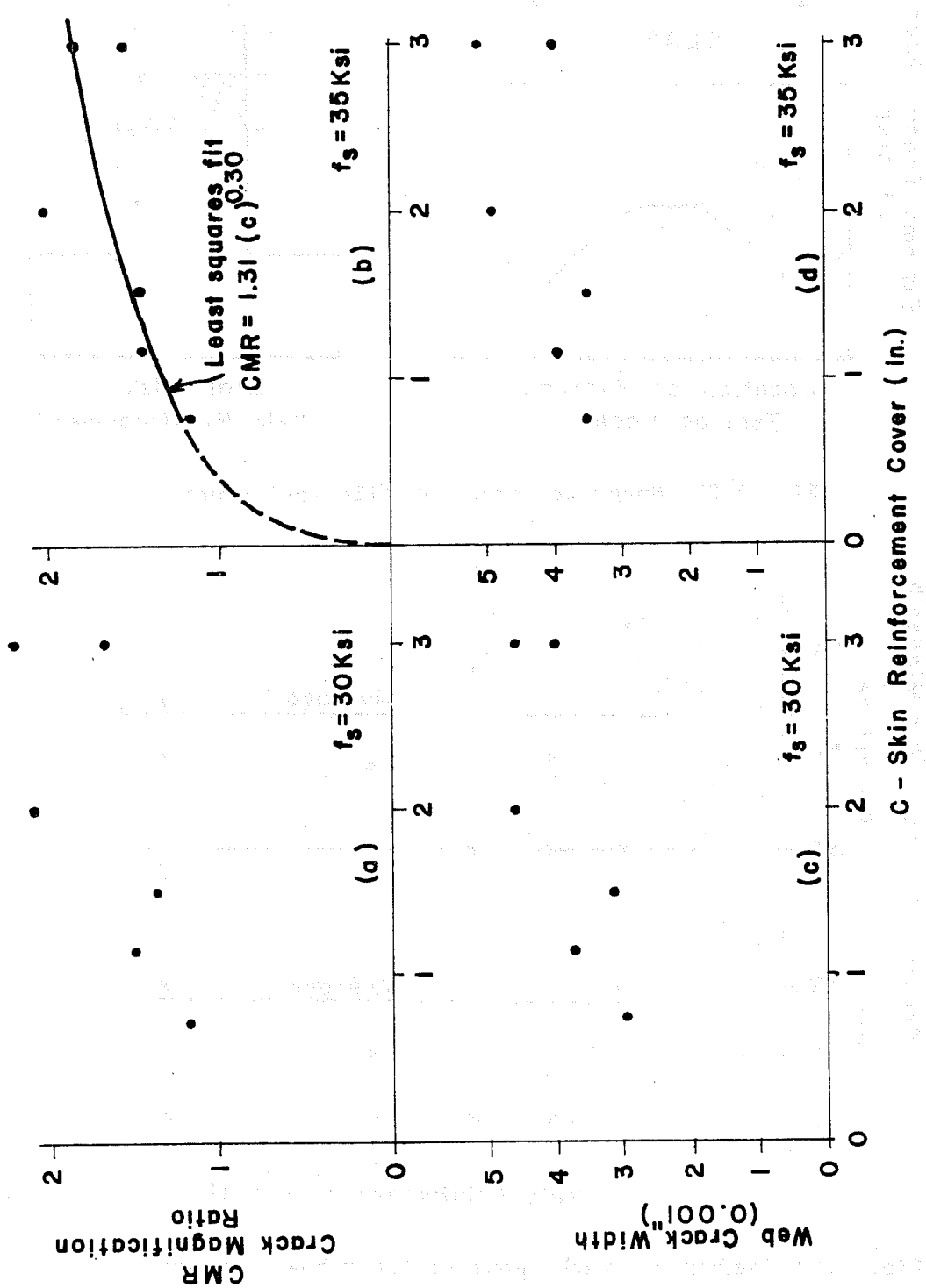

Fig. 6.23 Effect of cover on web crack width and crack magnification ratio

idea that as the distance between the bar and the point of crack measurement increases, the crack width increases. Notice that the crack width and CMR are not directly proportional to the cover. A least squares analysis using the average crack magnification ratio in the stress range of 30 to 40 ksi yielded the following relationship between the average CMR and the skin reinforcement cover, c:

$$CMR = 1.31(c)^{0.30}$$

This equation is plotted in Fig. 6.23b. It describes the data fairly well. The region of the curve at low values of CMR is shown as a dashed line because no tests were done in this region to confirm this section. However, as will be discussed later, the region of practical interest lies between a CMR of about 1.2 and 1.6.

The web width series indicates that the web width apparently does not affect the side face crack widths. This cover series shows that as the skin reinforcement cover increases, the effectiveness of the skin reinforcement in controlling the side face crack widths decreases. This suggests that it may be possible to rate the effectiveness of skin reinforcement on the basis of the area of skin reinforcement in relation to the area of an edge strip of concrete along each side face that is primarily affected by the skin reinforcement. Figure 6.24 shows that this edge strip is assumed to be symmetrical about the skin reinforcement along each side face. This edge strip concept is in agreement with the results from the web width series (variation of web width does not affect side face crack widths) and the results from the skin reinforcement cover series (as skin reinforcement cover increases, the side face crack width increases). Section 6.9 provides further support for this edge strip concept.

Figure 6.25a shows the case where the web width is greater than twice the width of the edge strip. As demonstrated by the Series W specimens, the skin reinforcement along one side face does not affect the crack widths on the other side face in such members (the 7.75 in.

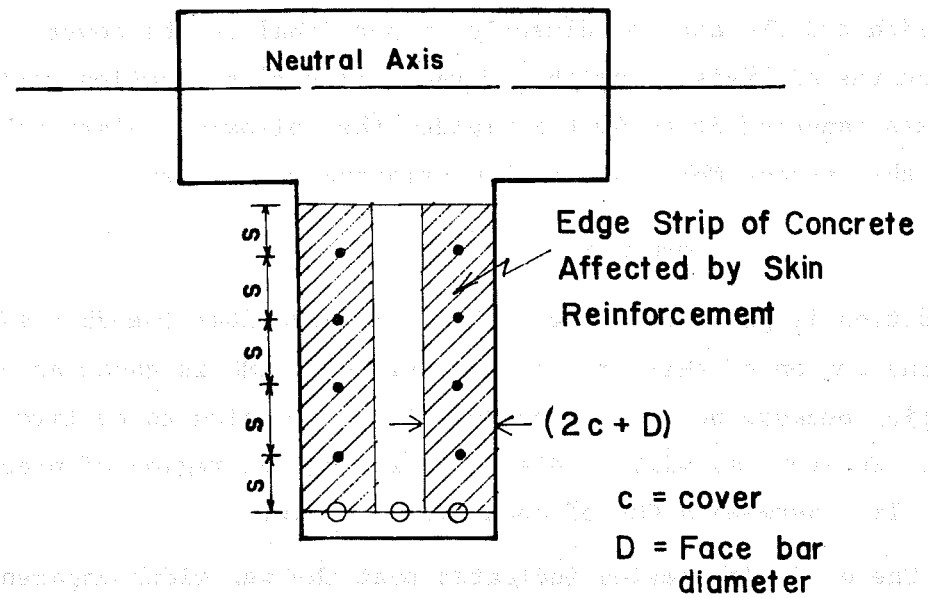

Fig. 6.24 Edge strip of concrete affected by skin reinforcement

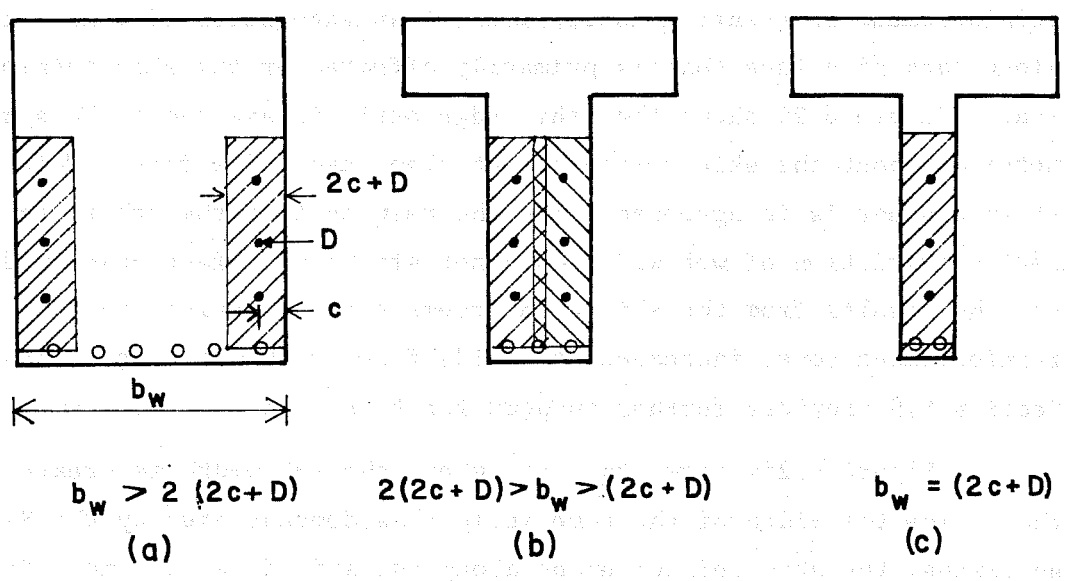

Fig. 6.25 Edge strips in various web widths

web width had an edge strip width of 2.625 in. compared to one-half the web width of 3.875 in.). Figure 6.25c shows the extreme condition of a thin web with skin reinforcement placed in the middle of the web. In this instance the edge strip width is clearly the entire web width. The case shown in Fig. 6.25b is an intermediate condition between these two extremes. For such a case it is difficult to say how much the skin reinforcement along one side face aids in crack control on the other side face, because there were no specimens designed to examine this effect. A reasonable transition from the case of Fig. 6.25a to that of Fig. 6.25c is to specify that the width of the edge strip of concrete affected by the skin reinforcement is equal to twice the cover plus the bar diameter, but not more than half the web width.

Placing the skin reinforcement in the middle of the web, as in Fig. 6.25c, should be used only in thin webs. If the skin reinforcement is too far from the concrete surface, cracks initiating at the surface of the skin reinforcement may not reach the concrete surface and thus may not properly influence the cracking pattern. A maximum web width of about 7 in. is suggested for this method of placing skin reinforcement because the largest edge strip width in this study was 6.4 in. in Specimens C-4 and C-5.

The three specimens tested by Kaar and Mattock[10] all had the same skin reinforcement and had values of (2c + D) equal to 2.25 in., compared to one-half web widths of 1.75, 2, and 4 in. in the I, T, and rectangular shapes, respectively. Therefore, the I and T shapes were in the transition region of Fig. 6.25b. Although the smallest web crack widths were generally measured in either the I or T sections (Fig. 6.20), indicating some possible interaction between the skin reinforcement on each side face, a definite quantitative conclusion cannot be drawn from these specimens regarding this transition zone.

6.6 Beam Depth Series

This series of specimens examined the effect of beam depth on the side face cracking. Five specimens, D-1-0, A-1-0, A-2-0, D-2-0, and D-3-0, were constructed using no skin reinforcement and with depths of 22.81, 32.75, 32.75, 47.125, and 47.125 in., respectively. Except for the depth and flange height, all section dimensions were the same (Table 4.1 and Fig. 4.1). The web/flange height ratio was held constant. There was some doubt whether the 47 in. deep specimen was too large for the test method to accurately simulate flexural cracking. Therefore, an accurate 2/3-scale model (D-4-0) of the larger specimen was also built and tested. This model had a depth of 31.5 in.

Since the full-size beams all had the same main reinforcement, the average steel stress (measured from surface strains) should decrease as the depth and concrete tensile area increases. Figure 6.26 is a plot of average steel stress, $f_{s,av}$, vs cracked section steel stress, f_s. The predicted difference between the cracked section stress and average stress is 13, 19, and 28 ksi in the 22.8, 32.8, and 47.1 (and 2/3 model) in. depths, respectively. The data show that $f_{s,av}$ is less than f_s but not as much as predicted above.

Beeby's[11] equation can be used to predict the web crack width in each of these specimens without skin reinforcement. The test results are compared with the predicted values in Fig. 6.27. The depth is not a good variable to use for the height effect. A better variable is the tension depth, the distance between the neutral axis and the main reinforcement, because the height of the tension zone (not the overall height) affects the crack width increase (see Fig. 6.4). Figure 6.27a uses average steel stress and Fig. 6.27b uses cracked section steel stress. The 2/3-scale model results, shown by open circles, have been increased by a 3/2 factor to correspond to the full-size specimen. Generally, the test results are close to the

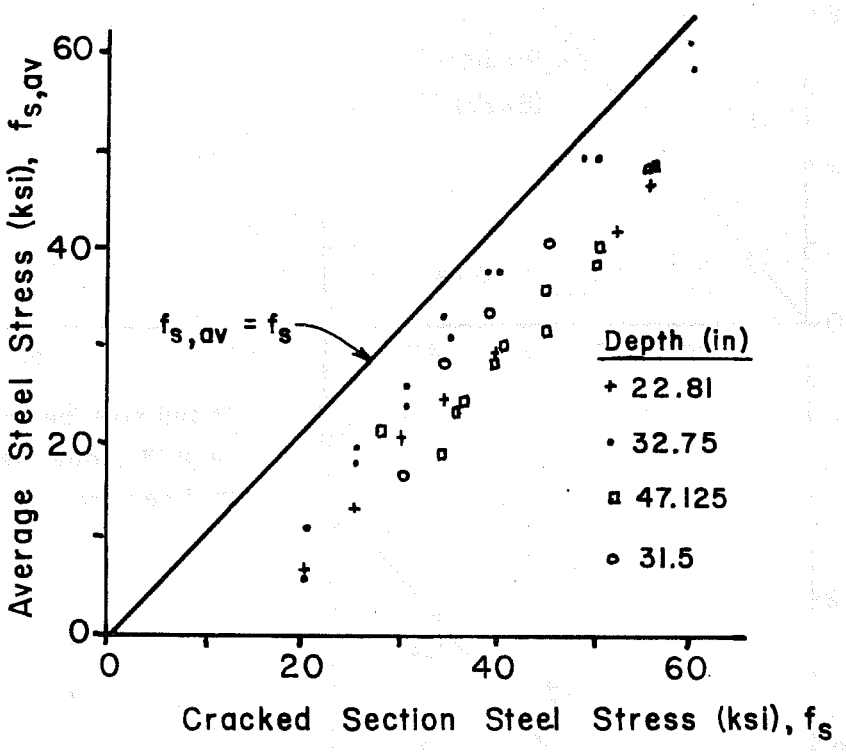

Fig. 6.26 Average steel stress vs cracked section steel stress--variable depths

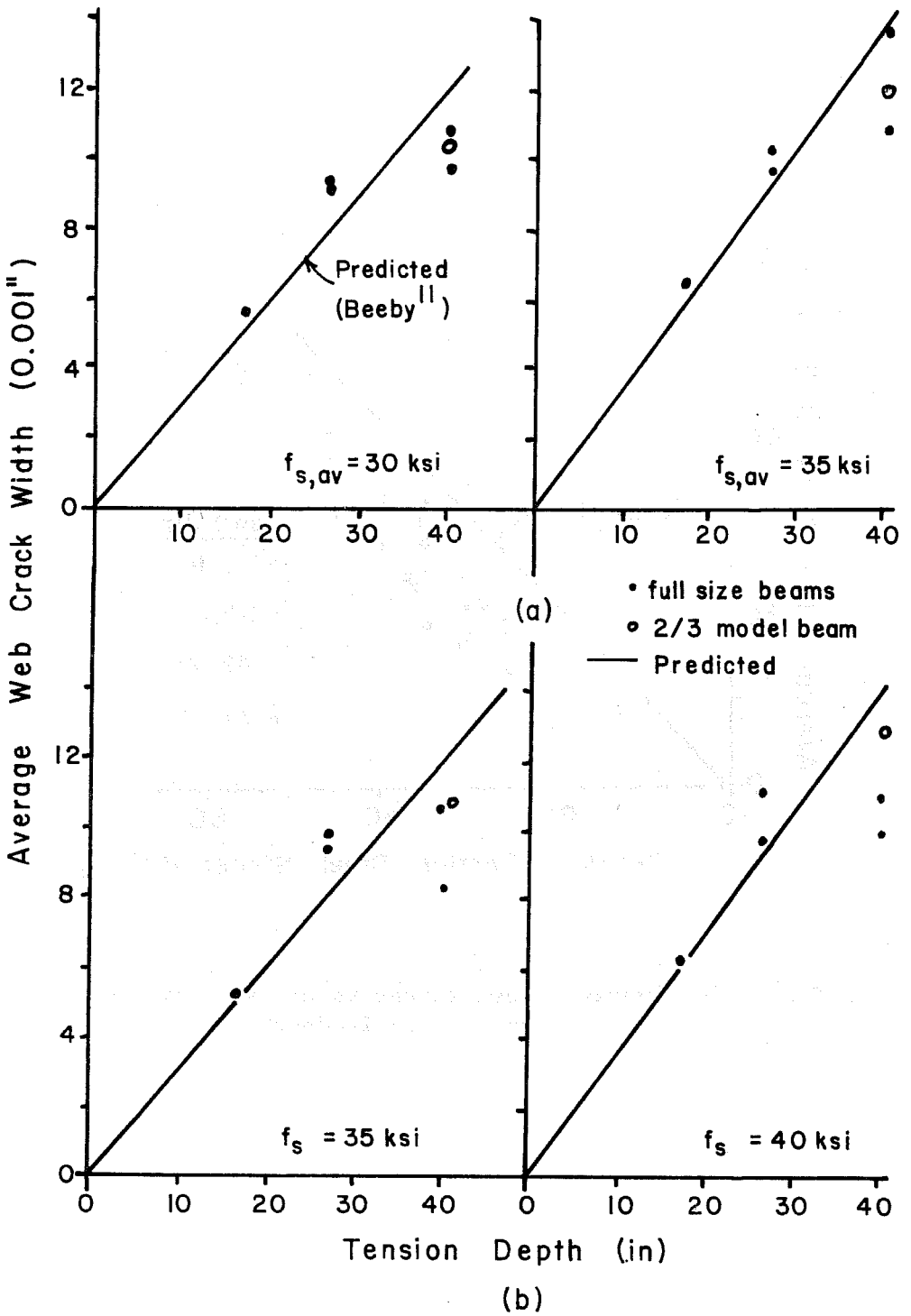

Fig. 6.27 Effect of depth on web crack width, $A_{sk} = 0$

predicted values using either the average or cracked section steel stresses. The predicted and measured crack widths show that as the depth (specifically the tension depth) of a member increases the side face crack width also increases.

As the depth increased, the percentage of cracks extending into the web decreased from 45 percent to 27 percent. Almost one-half of all cracks at the main reinforcement level in the smaller depth specimen (D-1-0) penetrated to web middepth.

Three additional 2/3-scale model specimens, D-5, D-6, and D-7, examined the effect of skin reinforcement in the larger specimens (Table 4.1 and Fig. 4.1). The crack patterns (Appendix A) again show that as the area of skin reinforcement increased the number of long cracks also increased (see Fig. 6.28). The effect of the area of skin reinforcement on the crack magnification ratio and crack width at a steel stress of 35 ksi is shown in Fig. 6.29. The area of skin reinforcement is included in the parameter ρ_{sk}, the skin reinforcement ratio, which is the area of skin reinforcement divided by the edge area of concrete affected by the skin reinforcement (Fig. 6.24). As the percentage of skin reinforcement increased, both the crack magnification ratio and the web crack width decreased. Both curves tend to become horizontal as the percentage of skin reinforcement increased. Figure 6.30 shows how the crack magnification ratio varied with the skin reinforcement percentage. The reason for using $1/\rho_{sk}$ is discussed in Sec. 6.9. The average CMR in the 30 to 40 ksi stress range is shown in Fig. 6.30d along with a "best fit" curve that describes this average CMR data. This same curve is also drawn in Fig. 6.30a, b, and c. In general, there is good agreement between this curve and the measured CMR. The test of D-7 was stopped prior to reaching a main reinforcement stress of 40 ksi. Figure 6.31 shows the effect of the area of skin reinforcement on the average crack width. Best fit curves have been drawn in each part. Figure 6.31d shows all curves together.

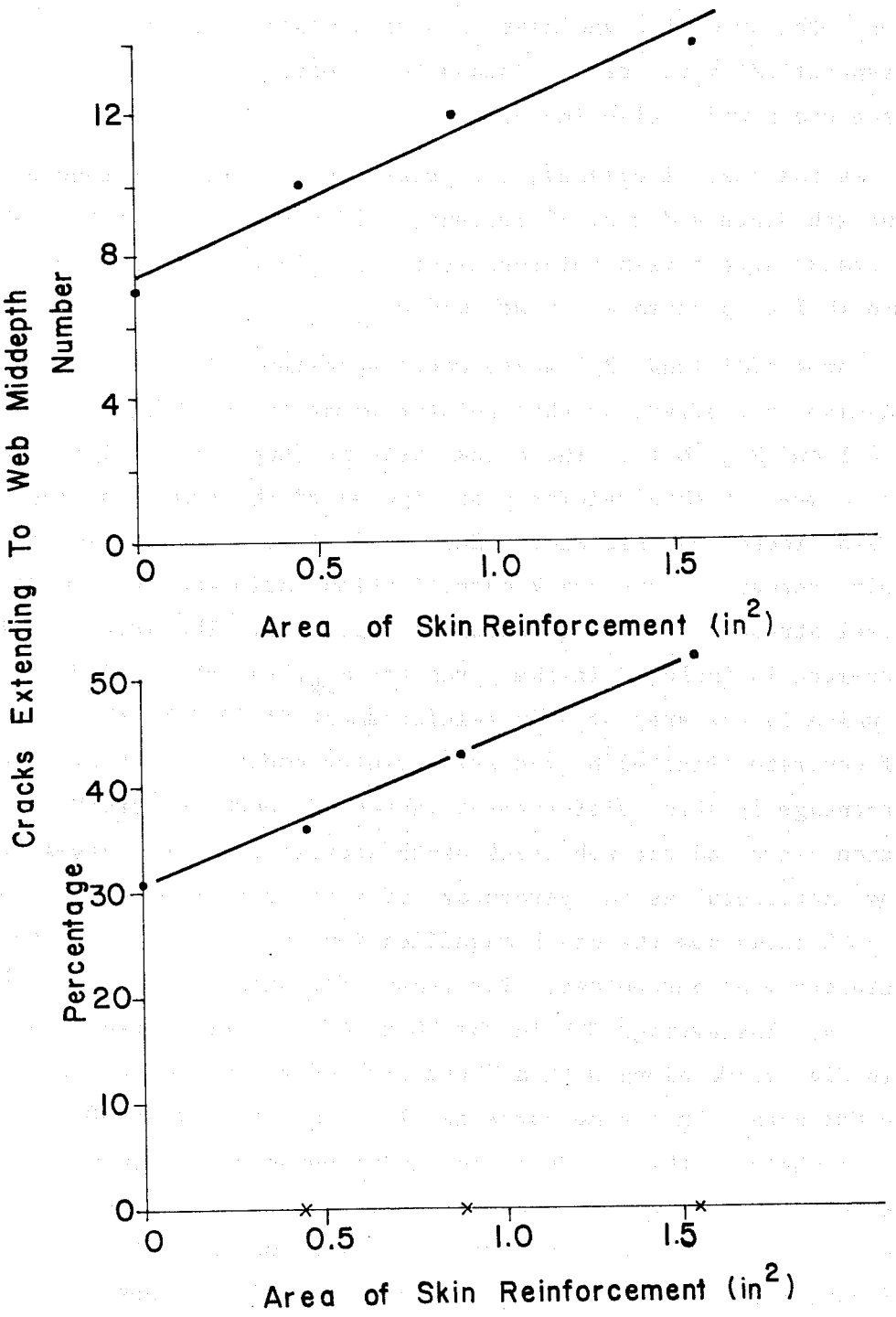

Fig. 6.28 Number of cracks penetrating web--depth series

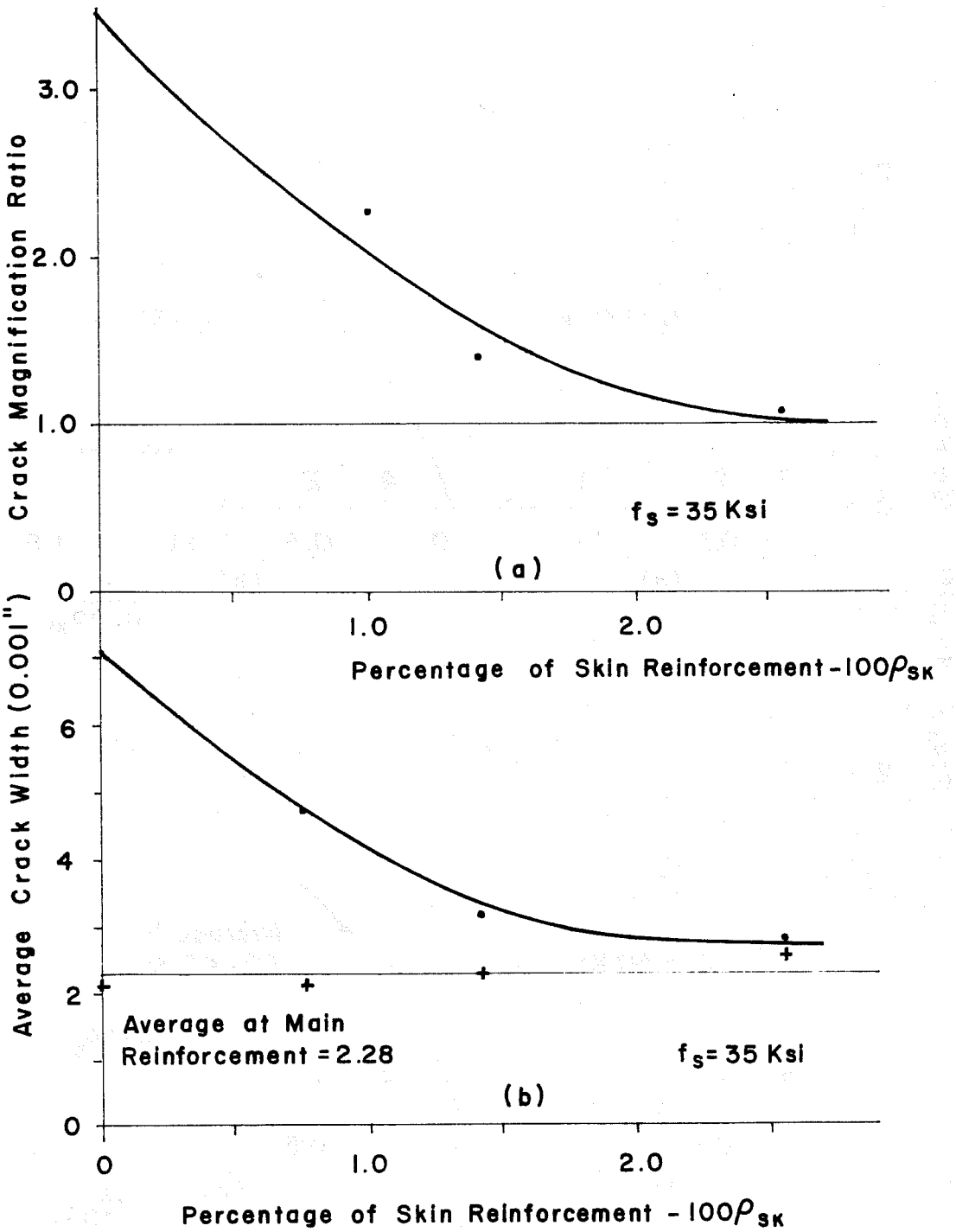

Fig. 6.29 Effect of skin reinforcement--depth series

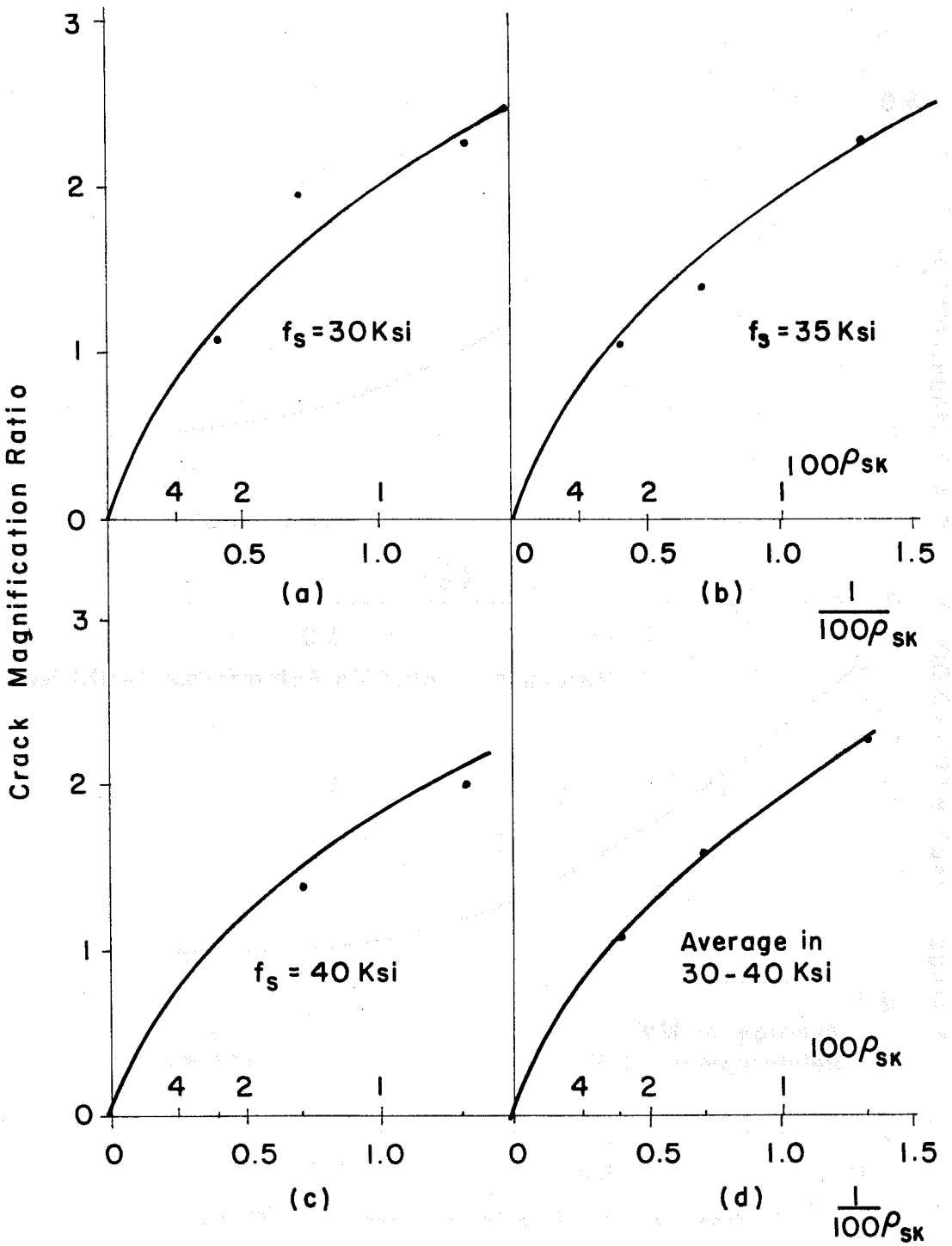

Fig. 6.30 Crack magnification ratios--depth series

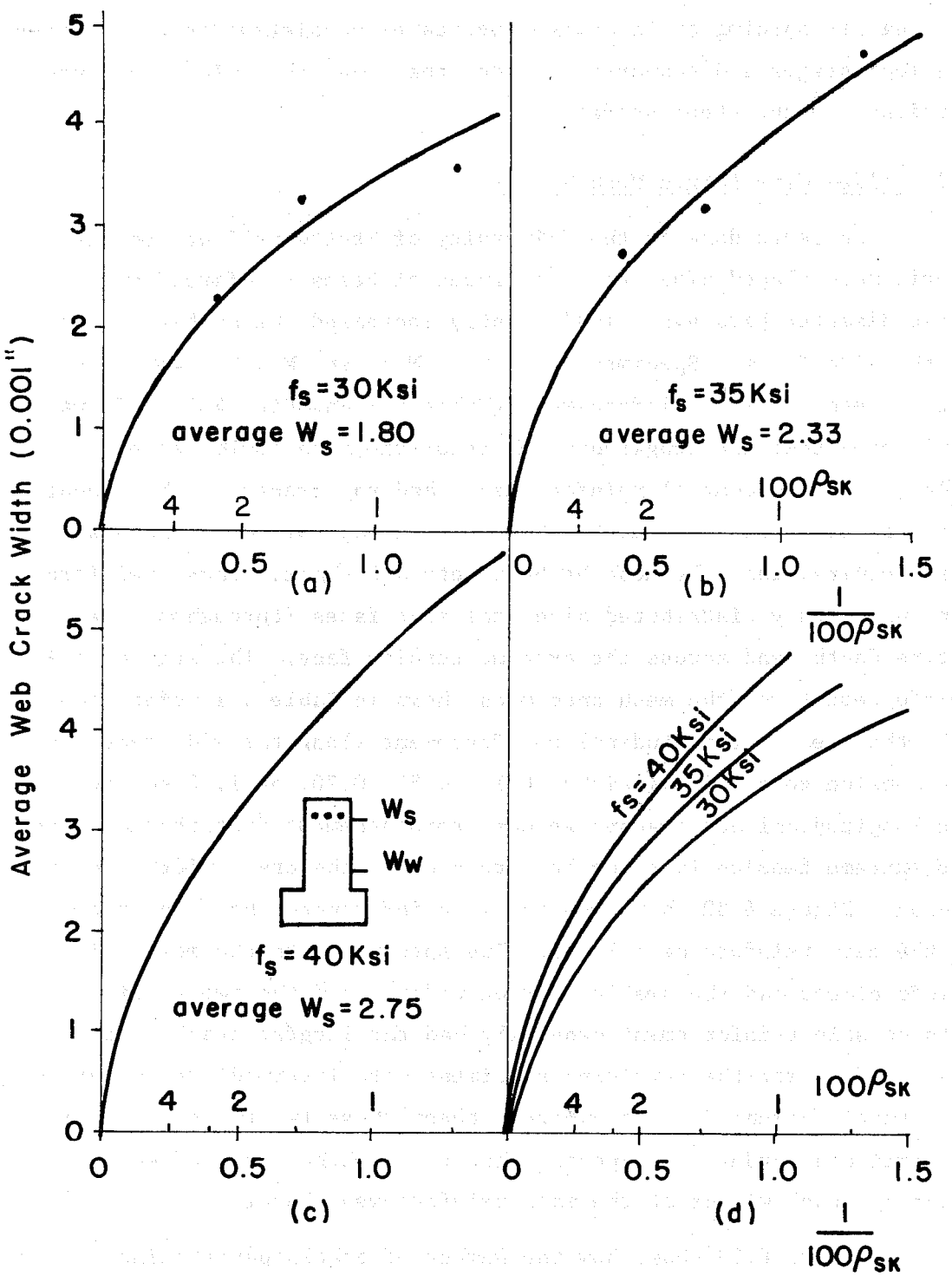

Fig. 6.31 Web crack widths--depth series

The regular spacing of the curves indicates consistent results between the load stages and supports the idea that the crack widths are proportional to the steel stress.

6.7 Welded Wire Fabric Mesh Series

In tests done at the University of Stuttgart[32] welded wire fabric mesh placed along the side faces of beams reinforced with large diameter bars very significantly increased the number of cracks on the side faces. Specimens M-1, M-2, M-3, and M-4 had welded wire fabric mesh as skin reinforcement (Table 4.1 and Fig. 4.1). It was envisioned that the longitudinal bars of the mesh could serve as side face crack control reinforcement, and the transverse bars could serve as shear reinforcement. Proper anchorage of the transverse bars required that the mesh be bent into a U-shape. Thus, reinforcement was evenly distributed along the side faces (throughout the entire depth) and across the extreme tension face. The area of skin reinforcement for the mesh specimens shown in Table 4.1 refers to only the area of longitudinal reinforcement along the side faces in the tension zone and was either 0.17, 0.50, 0.70, or 1.10 sq. in. The longitudinal and transverse mesh reinforcement distributed across the extreme tension face may help to control the crack widths in this region. Figure 6.32 shows how the mesh influenced the crack widths at the main reinforcement level. The specimen with the most skin reinforcement had the smallest crack widths, and the two specimens with no skin reinforcement generally had the largest crack widths. Crack widths for the remaining specimens with intermediate amounts of skin reinforcement fell somewhere between these two extremes but in no particular order. It appears that the mesh had some effect on reducing crack widths at the main reinforcement level.

Figure 6.33 shows how the number of cracks penetrating the web varied with the amount of mesh reinforcement. Although there seems to be a general increase in the number and percentage of long cracks

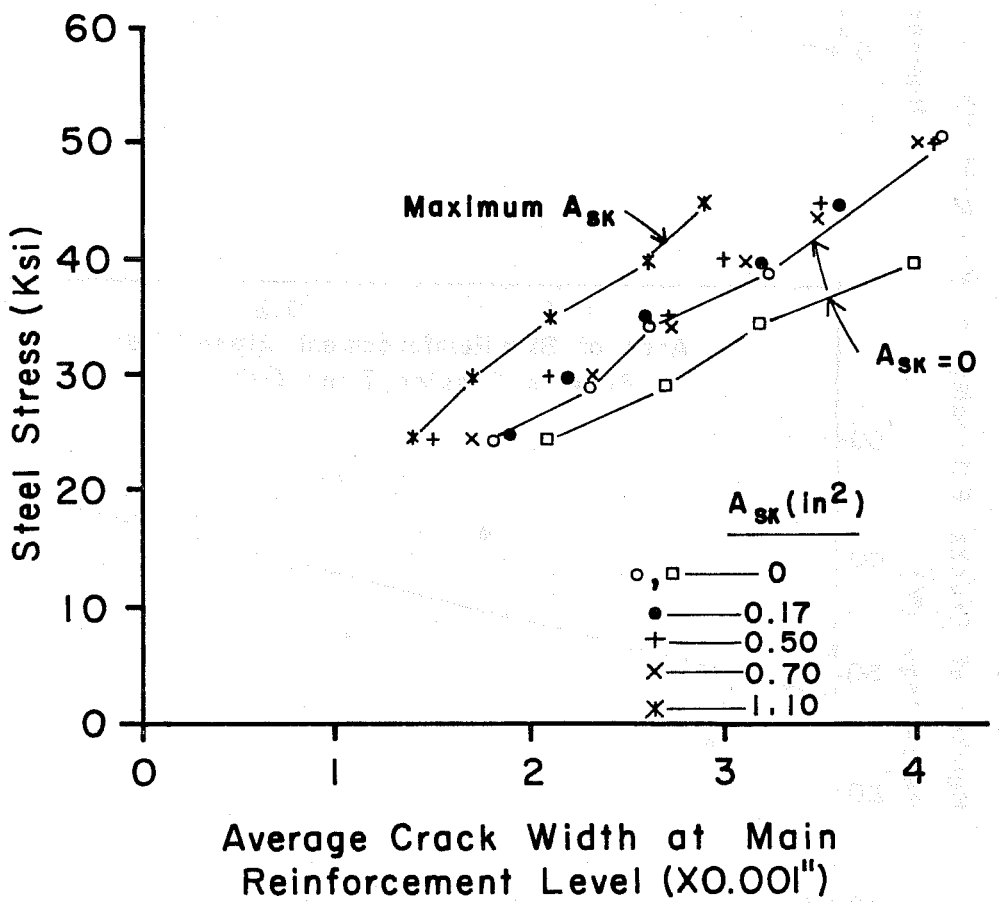

Fig. 6.32 Crack width at the main reinforcement level--mesh series

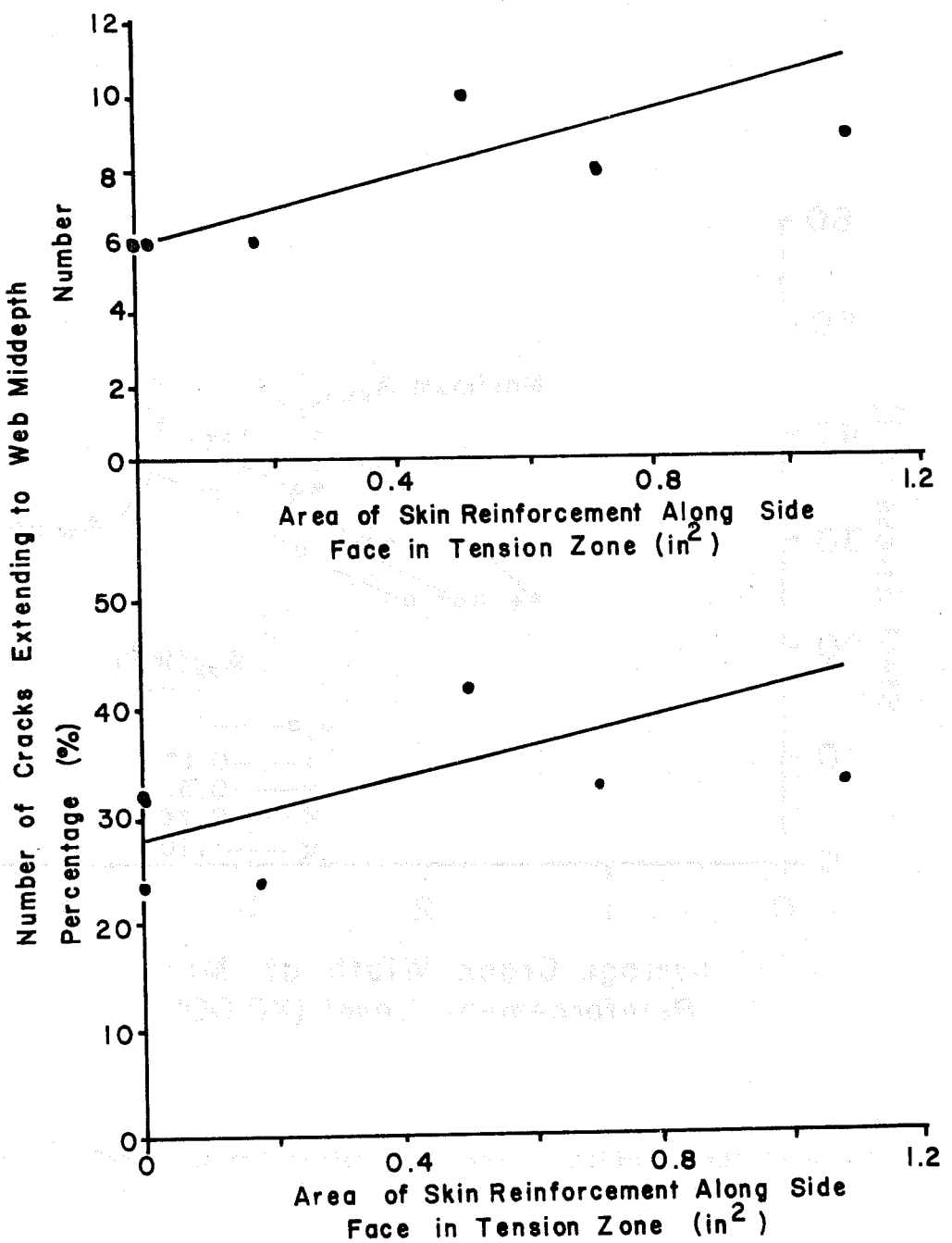

Fig. 6.33 Number of cracks penetrating web--mesh series

as the mesh area increases, the relationship is not as clear as those shown in Figs. 6.7 and 6.28. This may be the result of having the reinforcement distributed throughout the entire tension zone. Probably only about one-half of the skin reinforcement is located close enough to the crack formation zone to really affect the side face crack development (Sec. 6.2.2 and Fig. 6.6). There is not that much difference between the crack patterns of these specimens (especially M-2, M-3, and M-4). However, the tree branch crack pattern predominant in A-1-0 and A-2-0 (no skin reinforcement) does not occur in the mesh specimens.

Beeby[11] suggested that stirrups could act as crack formers and influence the cracking pattern if the predicted crack spacing is close to the stirrup spacing. Figure 6.34 shows the predicted spacing (using the equation in Appendix C, Ref. 54) and the measured average crack spacing on the side face for each specimen with mesh at a steel stress of 35 ksi. The predicted crack spacing at the main reinforcement level is about 3.6 in. All the test results cluster around this value. The 1-1/2 in. transverse wire spacing of M-4 had no effect in reducing the crack spacing further. Betweeen levels 7 and 10, Specimen M-4, which also had the highest amount of longitudinal reinforcement, had a closer spacing than the other specimens. This is the region where the widest crack would occur. Based on these limited data, it would be questionable to try to reach any other conclusions regarding the relationship between crack spacing and transverse wire spacing.

The severity of the side face cracking is shown in Fig. 6.35. Figure 6.35b indicates the web crack width generally decreases with increasing amounts of mesh reinforcement. However, the CMR of M-2, M-3, and M-4 are all approximately the same (Fig. 6.35a). This may be the result of the general decrease in crack width at the main reinforcement level (Fig. 6.32). The effectiveness of welded wire fabric mesh

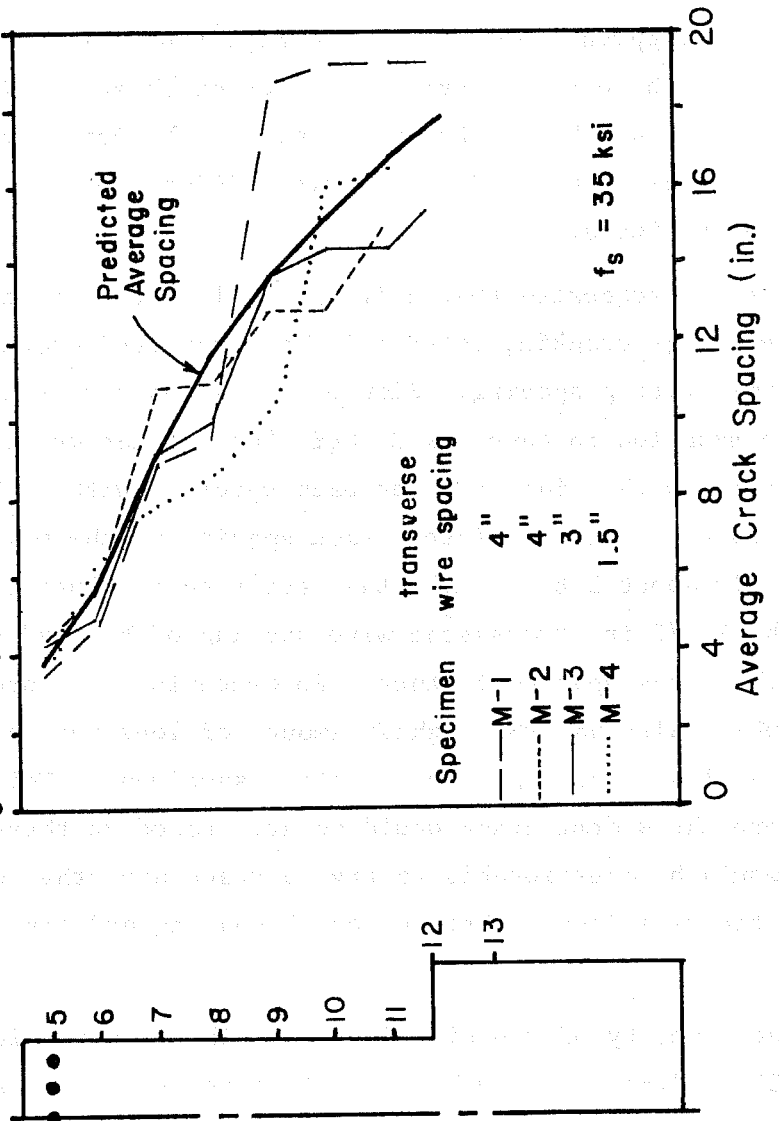

Fig. 6.34 Crack spacing on side face of beams--mesh series (Ref. 45)

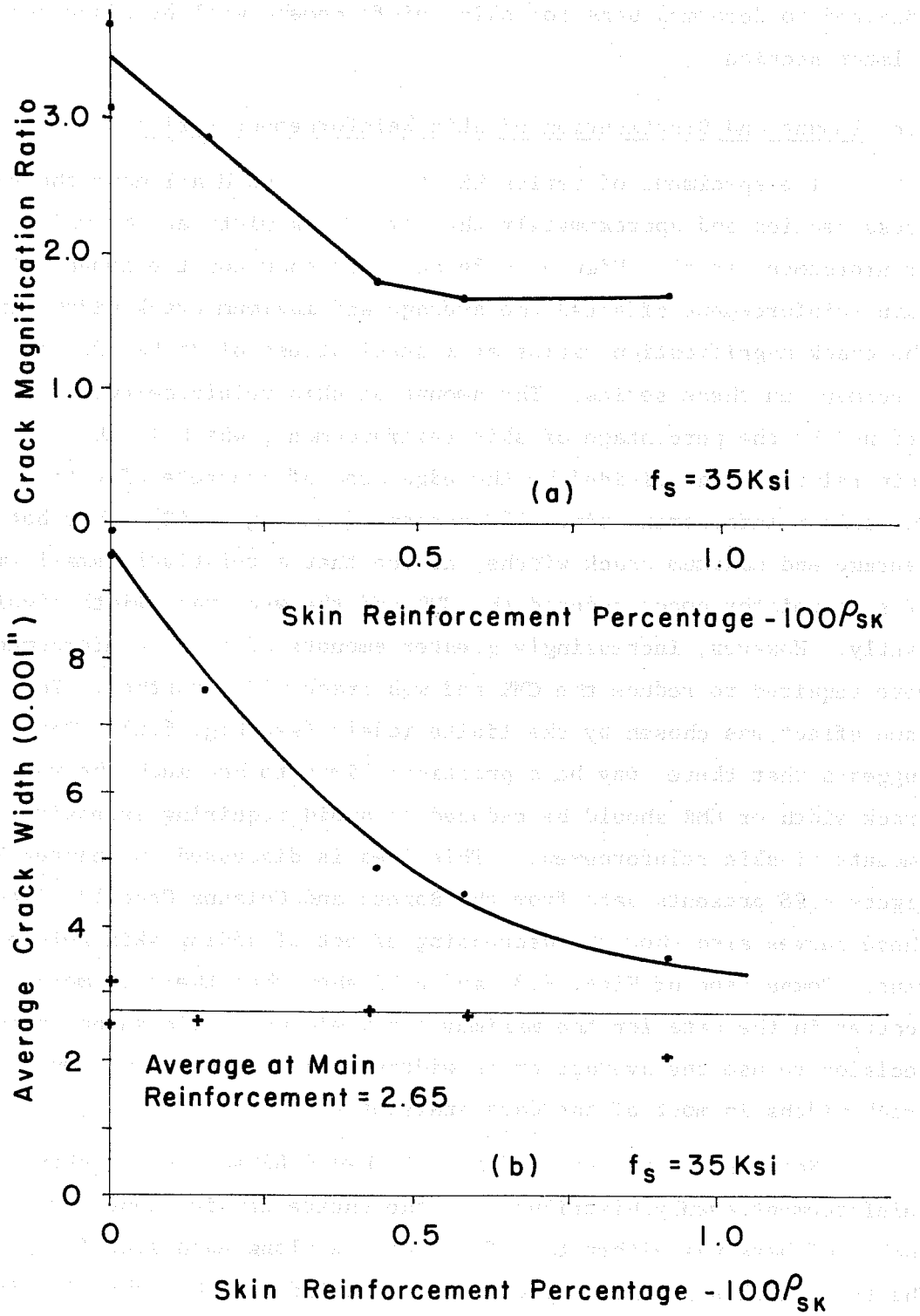

Fig. 6.35 Effect of skin reinforcement--mesh series

compared to deformed bars for skin reinforcement will be discussed in a later section.

6.8 Amount and Distribution of Skin Reinforcement Series

The specimens of Series RS, BC, A, C, and M all have the same cross section and approximately the same crack width at the main reinforcement level. Figures 6.36 and 6.37 show how the amount of skin reinforcement affected the average and maximum crack widths and the crack magnification ratios at a steel stress of 35 ksi for the specimens in these series. The amount of skin reinforcement is defined by the percentage of skin reinforcement, which is the area of skin reinforcement divided by the edge area of concrete affected by the skin reinforcement times 100 percent (see Fig. 6.42). For both average and maximum crack widths, notice that a relatively small amount of skin reinforcement reduced the CMR and the web crack width significantly. However, increasingly greater amounts of skin reinforcement were required to reduce the CMR and web crack width further. This same effect was chosen by the finite models (see Fig. 5.6). This suggests that there may be a practical limit to how much the web crack width or CMR should be reduced to avoid requiring excessive amounts of skin reinforcement. This idea is discussed in Chapter 7. Figure 6.28 presents data from the Soretz and Colanna-Ceccaldi[12] tests. These curves also show the decreasing effect of adding skin reinforcement. Comparison of Figs. 6.36 and 6.37 show that there is more scatter in the data for the maximum crack widths. This supports the decision to use the average crack widths rather than the maximum crack widths in most of the data analyses.

Specimens A-4, A-5, and A-6 all had 0.88 sq. in. of skin reinforcement evenly distributed in the entire tension zone. The number of bars was either ten, four, or one along each side face. The test results of these specimens should indicate how the distribution of skin reinforcement affects the side face cracking.

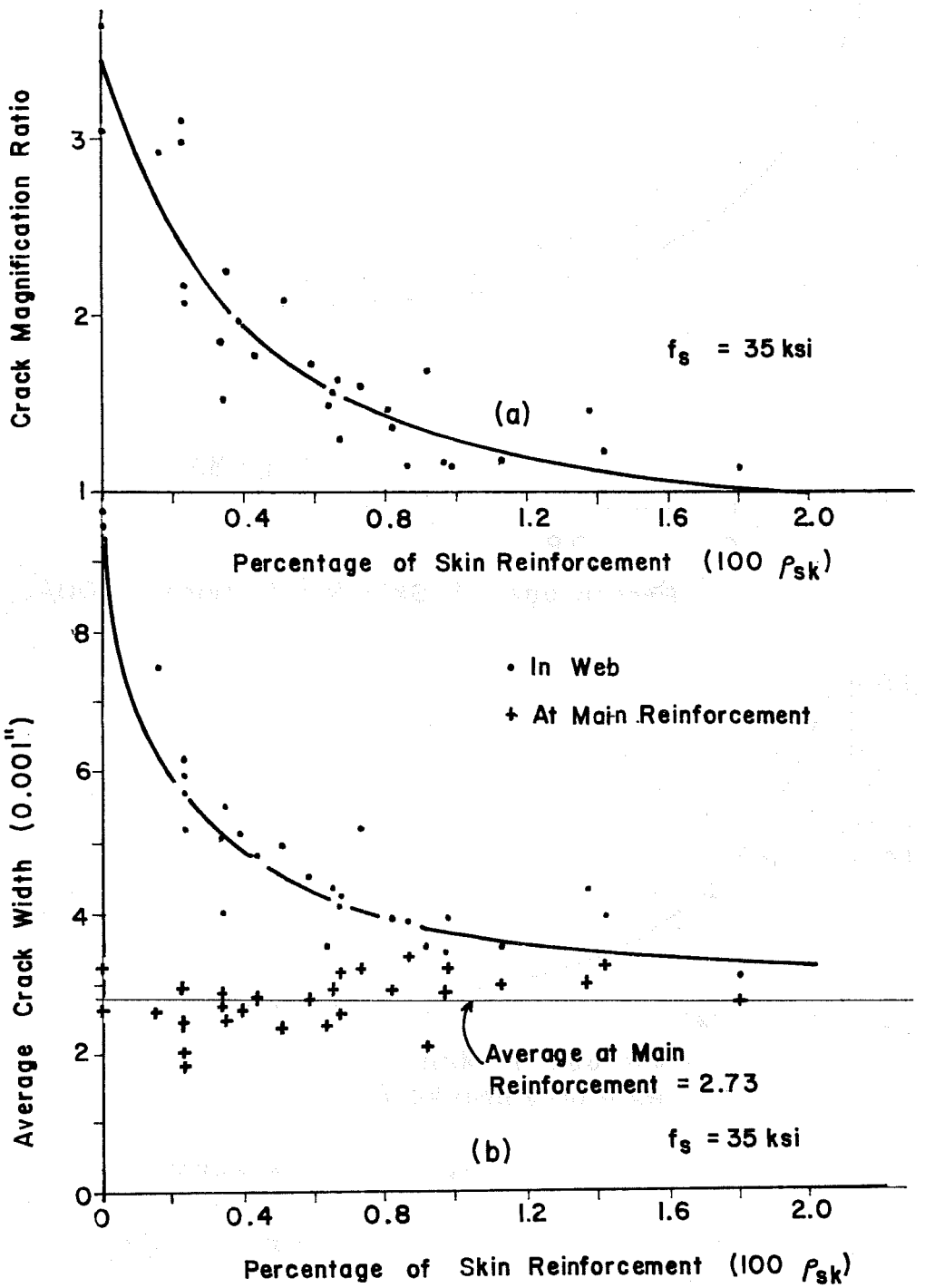

Fig. 6.36 Effect of amount of skin reinforcement on side face cracking--average crack widths

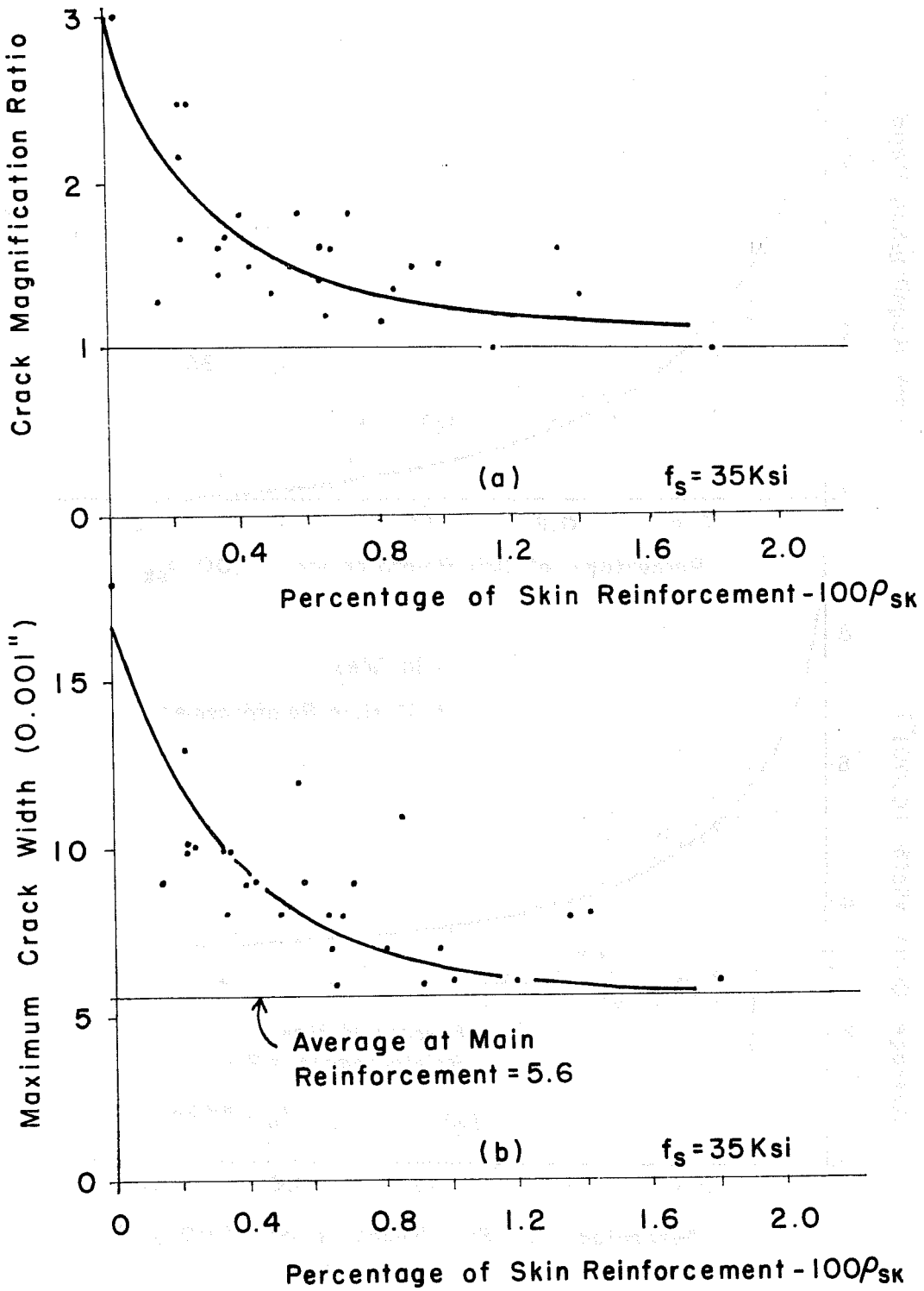

Fig. 6.37 Effect of amount of skin reinforcement on side face cracking--maximum crack widths

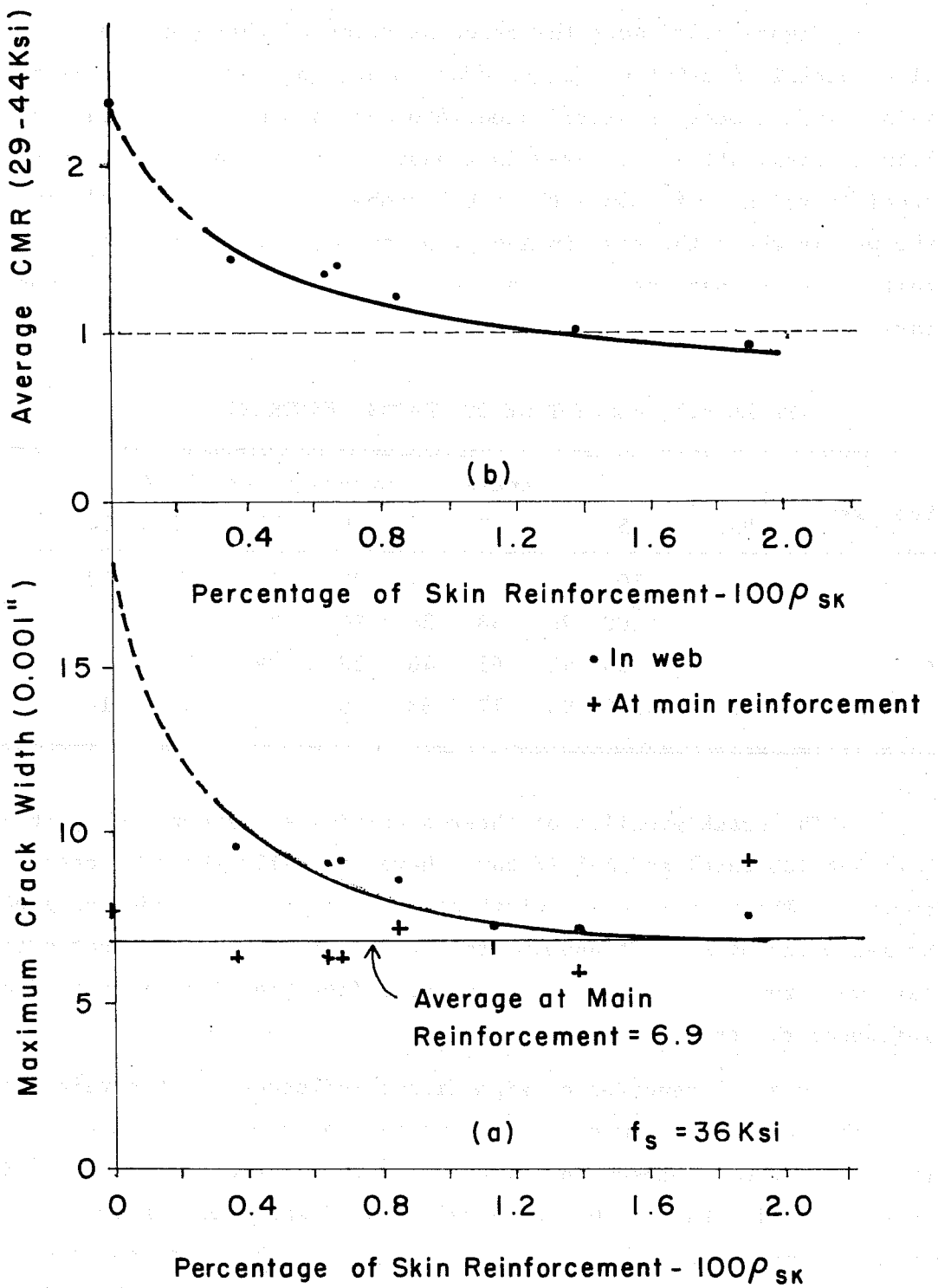

Fig. 6.38 Effect of amount of skin reinforcement on side face cracking--Soretz and Colanna-Ceccaldi (Ref. 12)

Figure 6.39 shows the crack patterns of these specimens and also Specimen A-2-0 (no skin reinforcement) for comparison. As the skin reinforcement is distributed into more and more bars, the tree branch crack pattern of A-2-0 is gradually changed and more cracks remain vertical. Although the total number of cracks at middepth of the web is about the same in A-4, A-5, and A-6, Table 6.1 indicates that a greater percentage of the cracks extend into the web as more bars are used.

TABLE 6.1 PERCENTAGE OF CRACKS PENETRATING WEB

Specimen	No. of Bars	Percentage of Cracks at Level (%)							
		5	6	7	8	9	10	11	12
A-2-0	0	100	77	42	23	23	15	15	12
A-6	2	100	86	38	34	34	34	31	21
A-5	8	100	92	63	46	38	29	25	8
A-4	20	100	95	77	68	45	41	32	18

The crack profiles of these specimens are shown in Fig. 6.40. Both A-4 (20 bars) and A-5 (8 bars) have generally the same crack profile. The maximum crack width of A-6 (2 bars) is almost as great as A-2-0 (no bars). It appears that the bars in A-6 are located too far away from the crack development zone (see Fig. 6.6) to significantly influence the crack formation.

Soretz[12] reported no significant influence of skin reinforcement distribution and recommended that two bars be used and located at one-third of the way between the main reinforcement and the neutral axis. Specimens A-13 and A-15 had an equal area of skin reinforcement (0.88 sq. in.) evenly distributed in about two-thirds of the tension depth using two and eight bars, respectively. Although A-13 and A-15 had different amounts and distributions of main reinforcement, the predicted crack widths at the main reinforcement level were very close

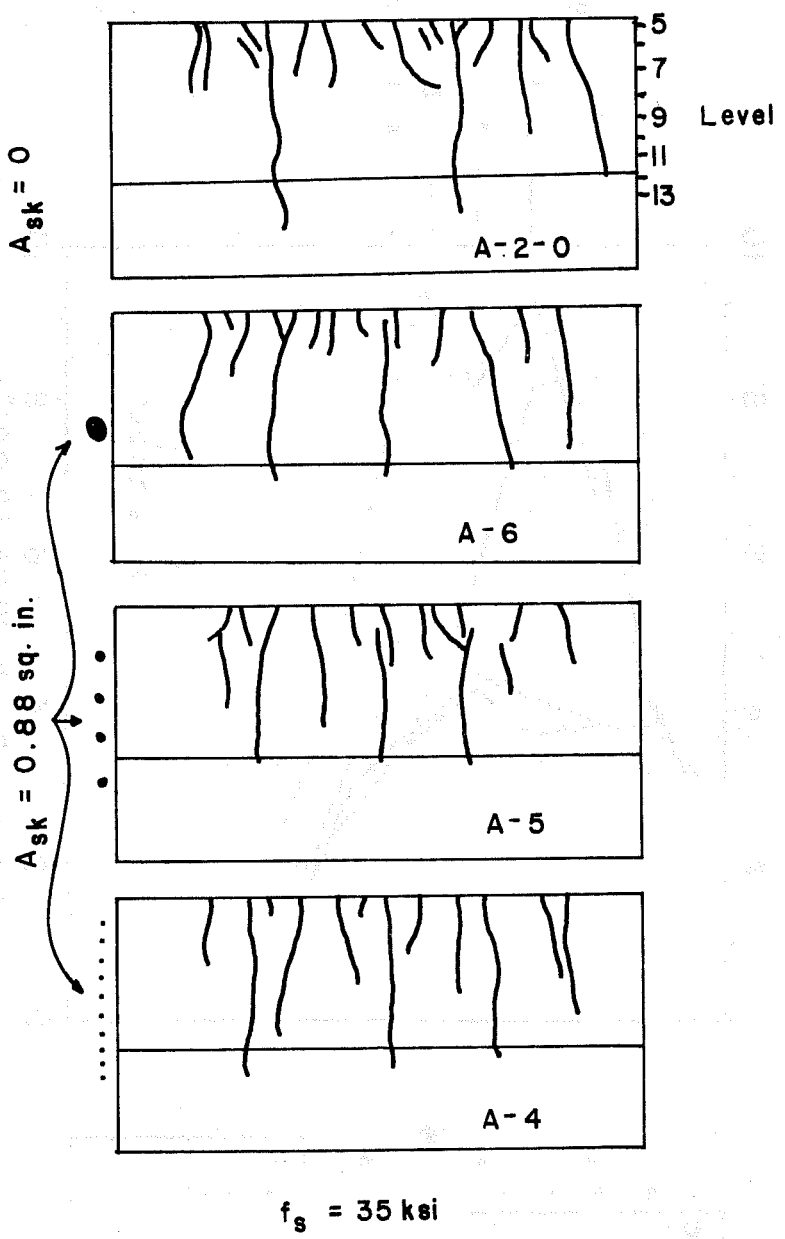

Fig. 6.39 Effect of distribution of skin reinforcement on crack patterns

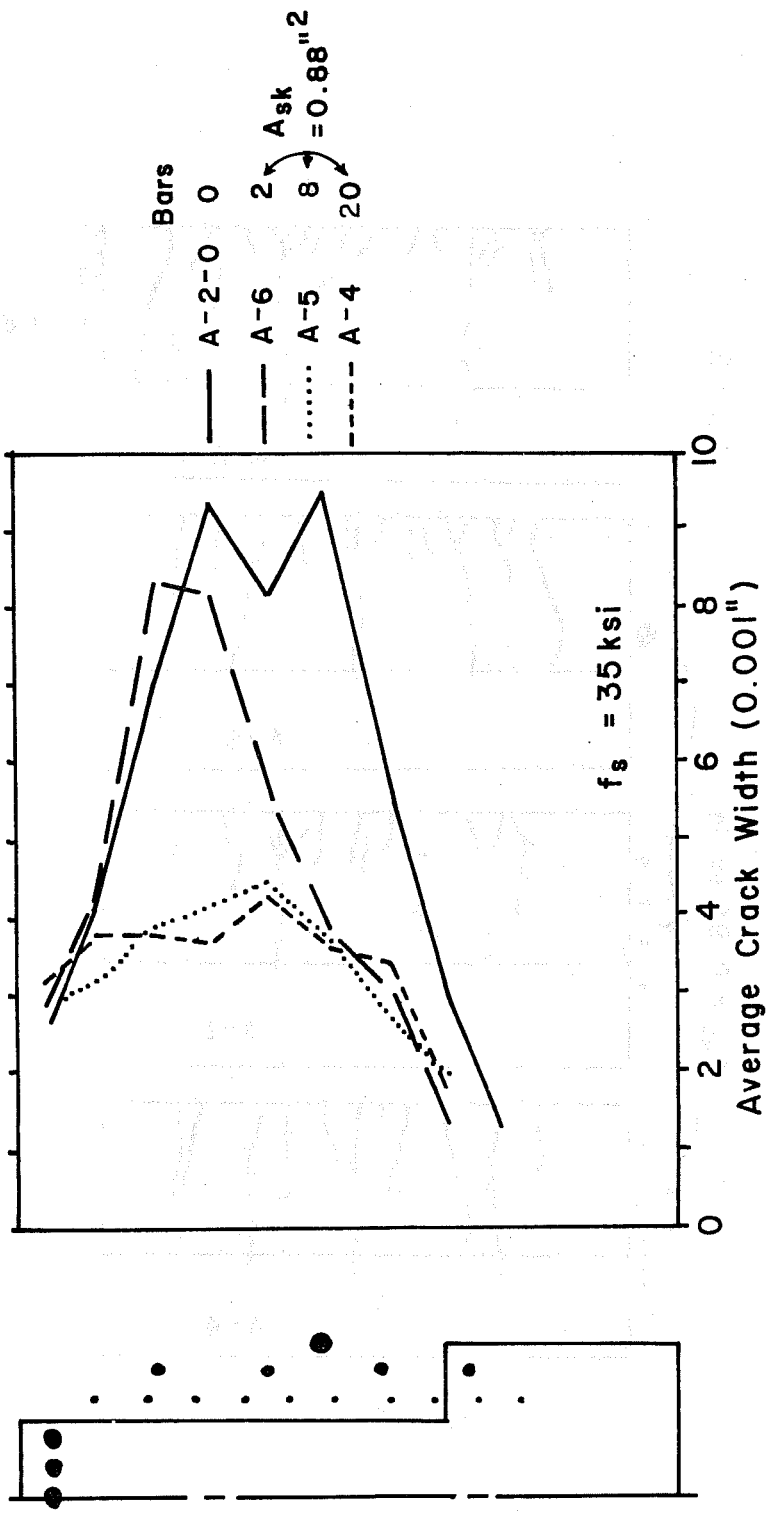

Fig. 6.40 Crack profiles for various skin reinforcement distributions

(0.0056 and 0.0049 in.) and should not noticeably affect the web crack widths. Specimen A-13 (2 bars) had more cracks extending to middepth than A-15, 13 out of 26 and 10 out of 29, respectively. The full length beam, BC-2, was identical to A-15 and had 16 out of 30 cracks in a 6 ft long region extending to middepth (these two specimens are also discussed in Chapter 7). The crack profiles for these three specimens are shown in Fig. 6.41. They are quite close in maximum web crack width, but the 8 bar specimens tend to keep the profile smaller along a greater region of the depth. The finite element model of Chapter 5 evenly distributed in 60 percent of the tension depth an equal area of skin reinforcement (0.88 sq. in.) using two, six, or fourteen bars. The crack profiles (Fig. 5.8) indicated the two bars were significantly less effective than the six or fourteen bars in controlling the crack profile. On the basis of the laboratory tests and finite element model tests the side face cracking is best controlled by evenly distributing three or four bars along each side face within approximately one-half to two-thirds of the tension depth adjacent to the main reinforcement.

6.9 Statistical Analysis of the Data

The variables affecting side face cracking are shown in Fig. 6.42. They are (1) the amount of skin reinforcement, A_{sk}, (2) the distribution of the skin reinforcement (determined by the bar diameter, D, the number of bars, N, the spacing, s, and the amount of the tension zone in which it is located, H_{sk}), (3) the cover, c, (4) the depth of the tension zone, d_t, and (5) the crack width at the main reinforcement level, w_s. In all specimens tested in this study the first skin reinforcement bar was located a full bar spacing, s, from the centroid of the main tension reinforcement. The distance, H_{sk}, which defines the depth of the tension zone in which the skin reinforcement is placed, extends from the centroid of the main reinforcement to one bar spacing beyond the skin reinforcement bar farthest from the main reinforcement. The specimens of Series RS,

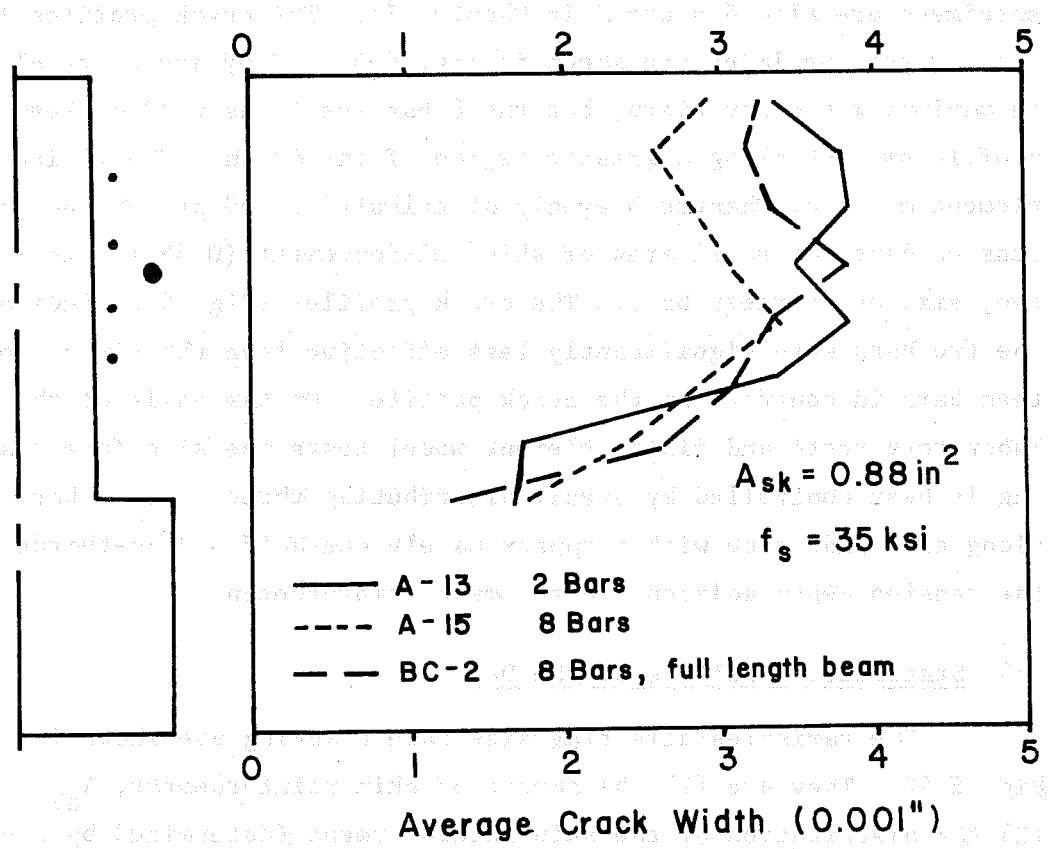

Fig. 6.41 Crack profiles for A-13, A-15, and BC-2

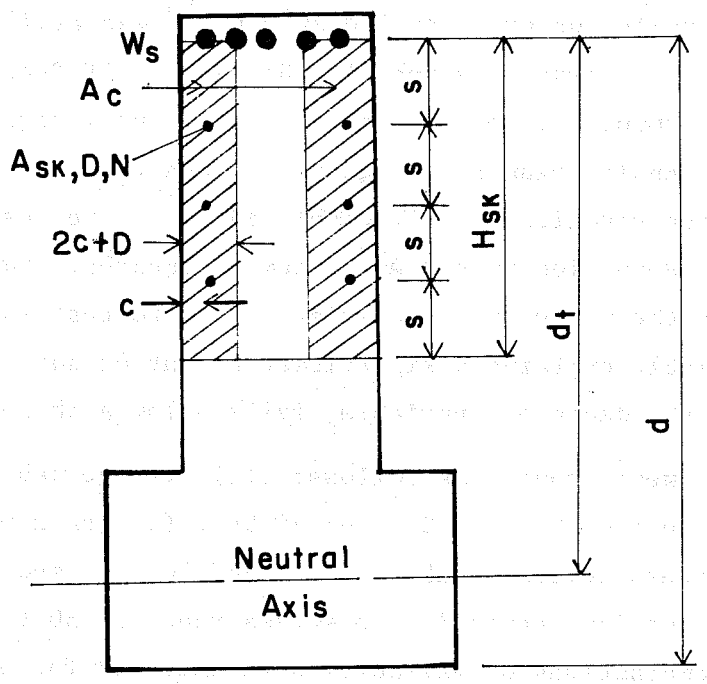

$$A_c = 2(2c+D)(H_{SK})$$

$$\rho_{SK} = \frac{\text{Total } A_{SK}}{\sum(\text{Edge Areas})} = \frac{\text{Total } A_{SK}}{A_c}$$

Fig. 6.42 Variables affecting side face cracking

BC, A, C, and M all have the same cross section and approximately the same crack width at the main reinforcement level. A regression analysis was performed on the data from these specimens to determine what relationship variables (1), (2), and (3) above had on the side face cracking.

A computer program, called STEP-01,[53] was available through the Center for Highway Research, The University of Texas at Austin. The program computes a sequence of multiple linear regression equations in a stepwise manner. At each step one variable is added to the regression equation. The variable added is the one which makes the greatest reduction in the error sum of squares. Variables are removed when their F value, a statistic used to test whether an independent variable explains a significant amount of the variance associated with the dependent variable, falls below a chosen value.

Data were grouped as follows: (1) average web crack widths at stress levels of 25, 30, 35, and 40 ksi; (2) crack magnification ratios at stress levels of 25, 30, 35, and 40 ksi; and (3) average crack magnification ratios in the stress range of 30 to 40 ksi. Many different combinations of variables were examined for each of the data groups. Because of the limited amount of data and the data scatter, it was not possible to find significant correlation between the web cracking (using either web crack width or CMR) and the distribution of skin reinforcement. A rather simple parameter, ρ_{sk}, the skin reinforcement ratio described the data as well as more complicated combinations of variables. The skin reinforcement ratio is defined as the area of skin reinforcement (A_{sk}) divided by the edge area of concrete affected by the skin reinforcement (A_c) (Fig. 6.42). The edge area of concrete is symmetrical with the skin reinforcement along each side face.

The average web crack width data for stress levels of 30, 35, and 40 ksi is presented in Fig. 6.43a, b, and c. The inverse of ρ_{sk} was used as the independent variable so that the regression analysis

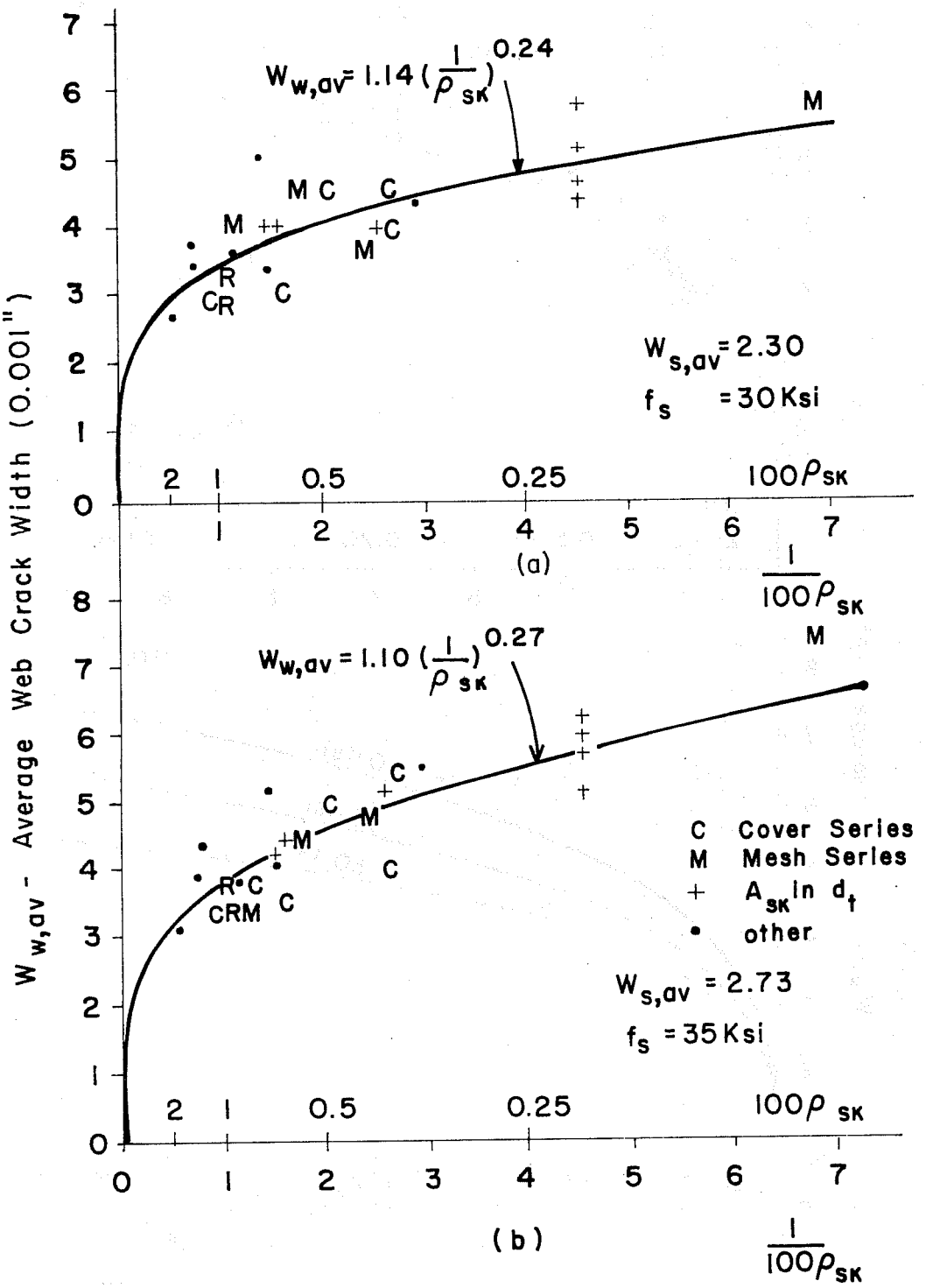

Fig. 6.43 Regression analysis of web crack width data

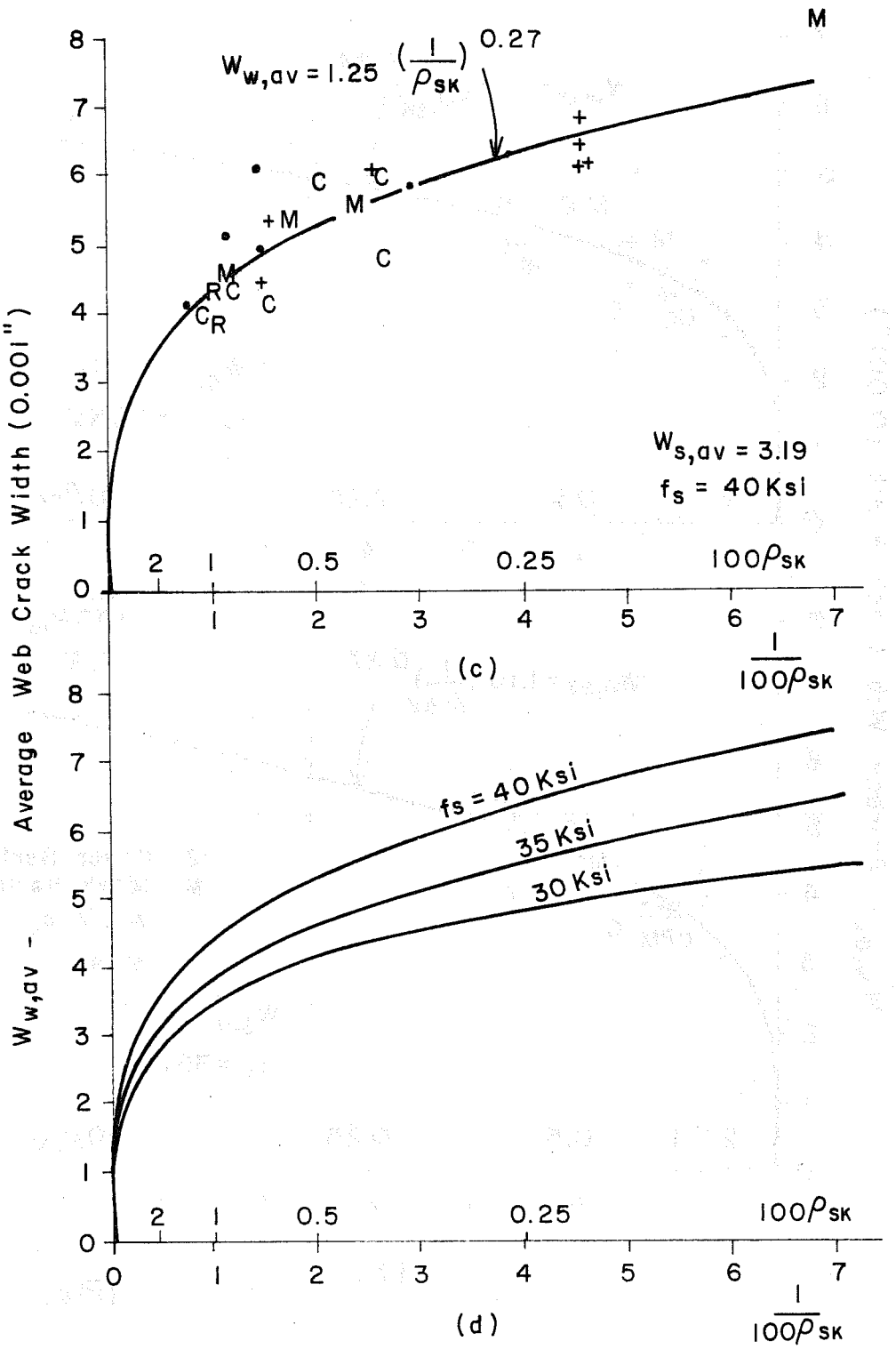

Fig. 6.43 (Continued)

could force fit a zero intercept. It was felt that at the extreme condition of an infinite amount of skin reinforcement the web crack width would be zero. Specimens in the cover or mesh series or with the skin reinforcement distributed throughout the entire tension depth are identified in these plots. The data in each stress level show a distinct trend. The regression equations are as follows:

$$f_s = 30 \text{ ksi} \qquad w_{w,av} = 1.14\ (1/\rho_{sk})^{0.24}$$

$$f_s = 35 \text{ ksi} \qquad w_{w,av} = 1.10\ (1/\rho_{sk})^{0.27}$$

$$f_s = 40 \text{ ksi} \qquad w_{w,av} = 1.25\ (1/\rho_{sk})^{0.27}$$

These equations are plotted separately as Fig. 6.43a, b, and c and all together on Fig. 6.43d. In each case the regression equations describe the data, including the cover and mesh data, quite well. The fairly uniform spacing of the curves in Fig. 6.43d confirms the previously noted result of the web crack width being approximately proportional to the main reinforcement stress. The results of the mesh specimens fit in well with the results of specimens that used deformed bars for skin reinforcement. Therefore, using welded wire fabric mesh is just as effective as using deformed bars for skin reinforcement.

The crack magnification data are similarly shown in Fig. 6.44a-f. The crack magnification ratios show the same trend as the crack width data. The regression equations are as follows:

$$f_s = 30 \text{ ksi} \qquad CMR = 0.283\ (1/\rho_{sk})^{0.35}$$

$$f_s = 35 \text{ ksi} \qquad CMR = 0.209\ (1/\rho_{sk})^{0.40}$$

$$f_s = 40 \text{ ksi} \qquad CMR = 0.211\ (1/\rho_{sk})^{0.39}$$

Average CMR in f_s = 30 - 40 ksi

$$CMR = 0.246\ (1/\rho_{sk})^{0.37}$$

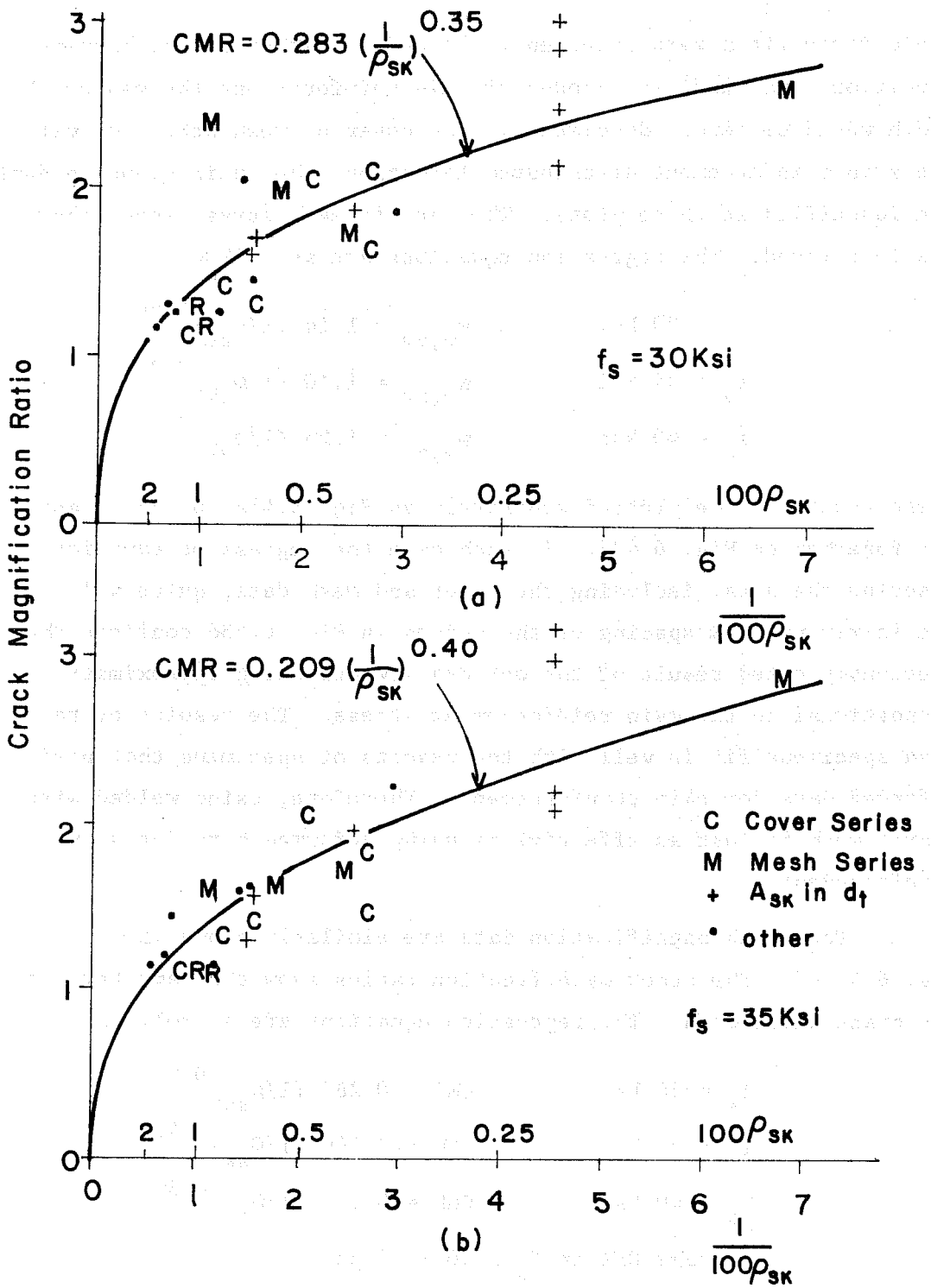

Fig. 6.44 Regression analysis of crack magnification ratio data

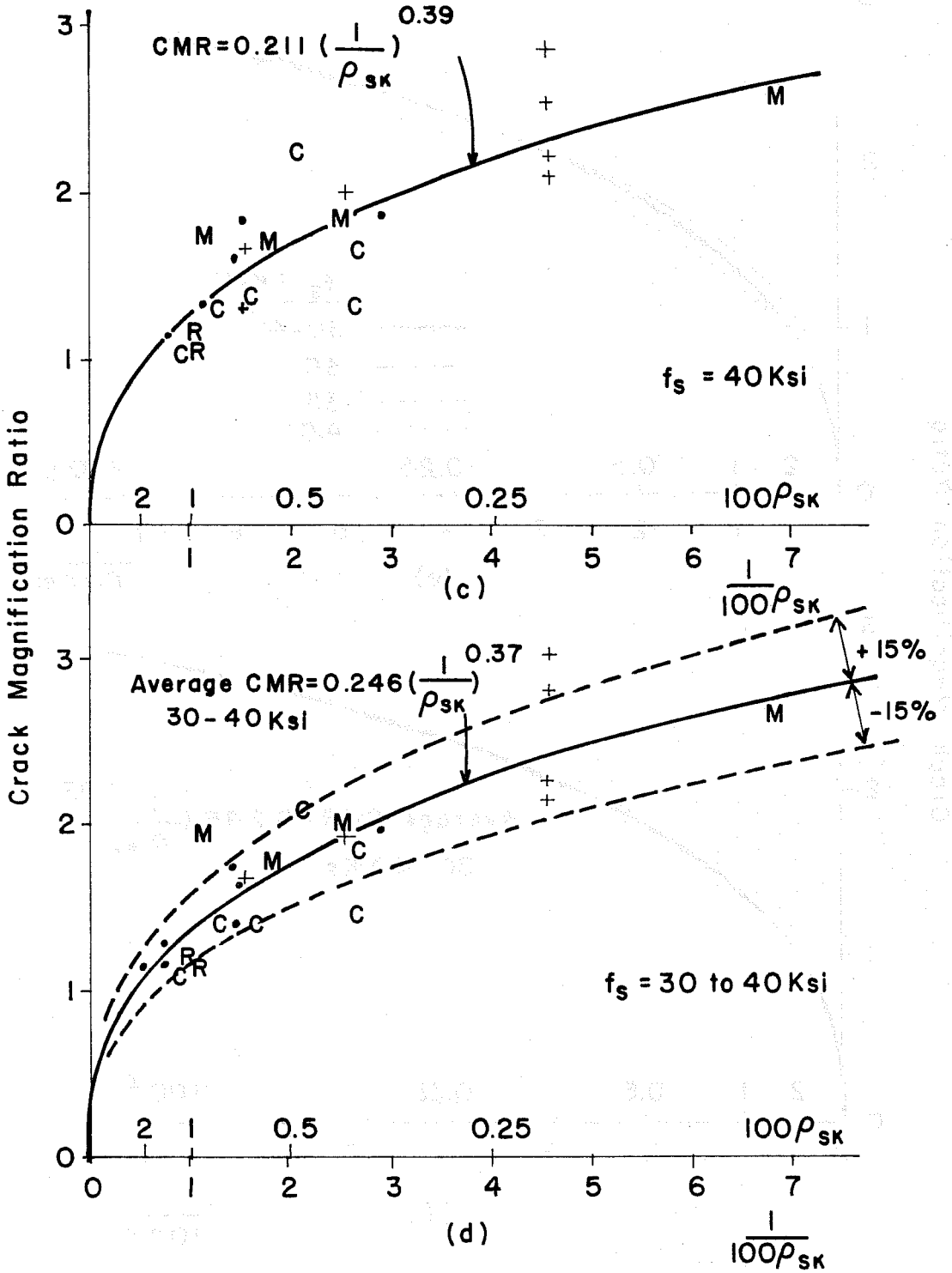

Fig. 6.44 (Continued)

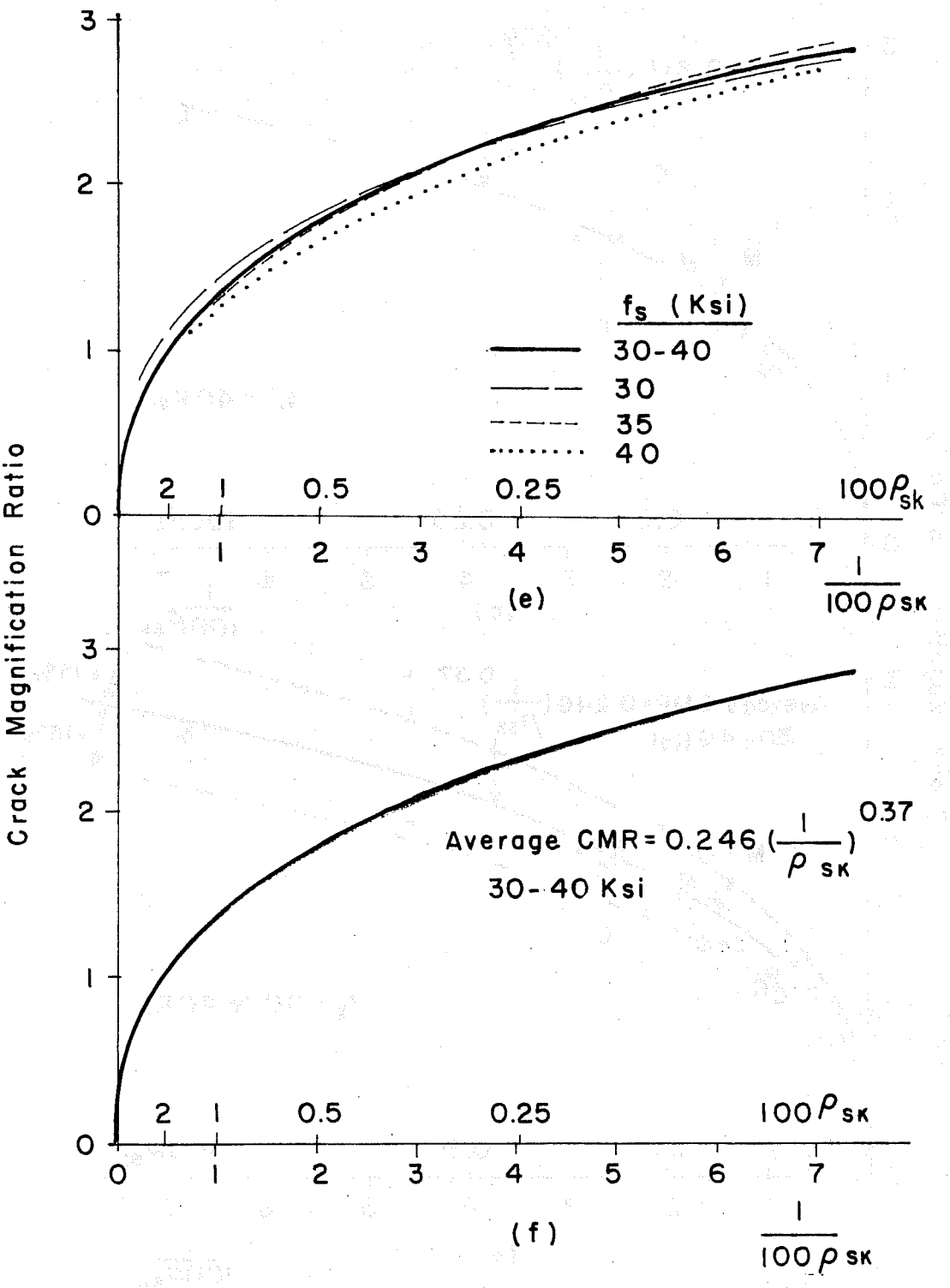

Fig. 6.44 (Continued)

Each equation describes the data generally well. All equations are plotted in Fig. 6.44e. The closeness of all the equations supports the idea of the crack magnification ratio remaining fairly constant in the 30 - 40 ksi stress range. Using the average CMR has the advantage of tending to smooth out any irregularities in the test data at particular load stages. The equation for the average CMR had a measured CMR/predicted CMR ratio for all specimens of 1.01, with a standard deviation of 0.15. This means that 68 percent of all the measured CMR's are within 15 percent of the predicted CMR's and 95 percent are within 29 percent (see Fig. 6.44d). Considering typical crack width data scatter, these results are very good. The data forming the basis of the Gergely-Lutz[19] equation (see Sec. 2.21) for crack widths in the vicinity of the main reinforcement had a scatter such that 67 percent of the measured maximum crack widths were within 25 percent of the predicted value.

The analyses using the web crack widths and the crack magnification ratios are compared by calculating by both methods what ratio of skin reinforcement is required to limit the side face crack to some specified increase in width. For example, for a CMR of 1.4 and using the average CMR equation (Fig. 6.44f), the required ratio of skin reinforcement for Series A specimens with a tension depth of 26.8 in. is

$$1.4 = 0.246\ (1/\rho_{sk})^{0.37} \Rightarrow \rho_{sk} = 0.0091$$

or for the same Series A specimens the desired web crack width of 1.4 times the crack width at the main reinforcement level at a main reinforcement stress of 35 ksi (Fig. 6.43b) yields the required ratio of skin reinforcement to be:

$$1.4 \times 2.73 = 3.83 = 1.10\ (1/\rho_{sk})^{0.27} \Rightarrow \rho_{sk} = 0.0100$$

At stresses of 30, 35, and 40 ksi the predicted ρ_{sk}, using Fig. 6.43, are

at f_s = 30 ksi	ρ_{sk} = 0.0132
at f_s = 35 ksi	ρ_{sk} = 0.0100
at f_s = 40 ksi	ρ_{sk} = 0.0090
Average	ρ_{sk} = 0.0107

The two methods give required skin reinforcement ratios of 0.0091 and 0.0107 and agree well.

Data for beams with a tension depth of 39.8 in. are shown in Figs. 6.30 and 6.31. Similar calculations show that for a CMR of 1.4, the required ratio of skin reinforcement is:

by average CMR ρ_{sk} = 0.0168

by side face crack width:

at f_s = 30 ksi	ρ_{sk} = 0.0190
at f_s = 35 ksi	ρ_{sk} = 0.0151
at f_s = 40 ksi	ρ_{sk} = 0.0140
Average	ρ_{sk} = 0.0160

Again, the two methods agree very well.

Table 6.2 summarizes these comparisons for specimens in Series A (d_t = 26.8 in.) and Series D (d_t = 39.8 in.). There is fairly good agreement between the two methods of calculating the skin reinforcement percentage for Series A specimens at a CMR of 1.5 and 1.4, and poorer agreement at a CMR of 1.3 and 1.2. There is no apparent reason for the poorer correlation at the lower CMR's. The Series D specimens show good agreement at all values of CMR.

Based on the average CMR equation, a skin reinforcement percentage of 0.91 percent was required to limit the CMR to 1.4 for a specimen with a tension depth of 27 in. For a specimen with a tension depth of about 40 in., a skin reinforcement percentage of about 1.7 percent was required for the same CMR of 1.4. Therefore, the required percentage of skin reinforcement is dependent on the tension depth. This result is logical, since as the beam depth is decreased, eventually

TABLE 6.2 COMPARISON OF METHODS OF CALCULATING SKIN REINFORCEMENT PERCENTAGE

Skin Reinforcement Percentage - ρ_{sk}

	Series A (d_t = 26.8 inches)				Series D (d_t = 39.8 inches)			
	1.5	1.4	1.3	1.2	1.5	1.4	1.3	1.2
by average CMR	0.75	0.91	1.11	1.37	1.48	1.68	1.85	2.11
by crack widths								
@ f_s = 30 ksi	0.99	1.32	1.79	2.50	1.68	1.90	2.35	2.50
f_s = 35 ksi	0.77	1.00	1.31	1.76	1.31	1.51	1.70	2.00
f_s = 40 ksi	0.70	0.90	1.18	1.59	1.07	1.40	1.60	1.90
average	0.82	1.07	1.43	1.95	1.35	1.60	1.88	2.13

a depth is reached where 0 percent of skin reinforcement is required. The requirement of how much to reduce the web crack width and what percentage of skin reinforcement to use is discussed in Chapter 7.

6.10 Summary

Analysis of the test results is summarized below:

(1) Skin reinforcement affects principally a narrow strip of concrete along each lateral face of the web (Fig. 6.24). The web width does not otherwise influence the effectiveness of the skin reinforcement in controlling crack widths on the side faces.

(2) Limited test data and scatter in the data did not permit a quantitative conclusion on the best distribution and location of skin reinforcement. However, the test results (both laboratory and finite element models) did indicate it is most effective to place the skin reinforcement as three or four bars evenly distributed along each side face in about one-half to two-thirds of the tension zone adjacent to the main reinforcement (increasing the number of bars increases the effectiveness of the skin reinforcement).

(3) The amount of skin reinforcement can be expressed as a skin reinforcement percentage based on the area of skin reinforcement and the edge strip area of concrete (Fig. 6.42).

(4) As the beam tension depth increases, the side face crack width increases and the required percentage of skin reinforcement also increases.

(5) Using the skin reinforcement percentage and either the side face crack width or the crack magnification ratio, regression equations can be obtained that describe the data reasonably well. Using the average crack magnification ratio, 68 percent of the measured CMR's are within 15 percent of the predicted CMR's.

CHAPTER 7

DEVELOPMENT OF DESIGN METHOD

7.1 Introduction

This section provides an overview of the development of the design procedure. Specific details are presented in subsequent sections.

This study indicated that extremely large amounts of skin reinforcement are required to keep crack magnification ratio (defined as the ratio of maximum crack width on the side face to crack width at the main reinforcement level) values close to 1.0. Fortunately, however, it is not necessary to reduce the crack magnification ratio to 1.0. Section 7.2 presents a method for determining how much crack width increase is acceptable on the side faces of a member.

Test results from specimens with identical amounts and distribution of skin reinforcement but with varying web widths indicated that the web width did not affect the side face crack widths. It is possible to rate the effectiveness of the skin reinforcement by the skin reinforcement ratio, ρ_{sk}, which is the total area of skin reinforcement divided by the area of the edge strips of concrete symmetrical with the skin reinforcement along each side face (see inset in Fig. 7.1).

The effect of skin reinforcement on the side face crack width and the crack magnification ratio was studied using models of different tension depths, d_{t1} and d_{t2}. The resulting experimentally determined curves, as shown in Fig. 7.1a, can be used to predict what skin reinforcement ratio is required to limit the CMR to some specified value in each of the tension depths. For a given CMR, beams with tension depths of d_{t1} and d_{t2} require skin reinforcement ratios of ρ_{sk1} and

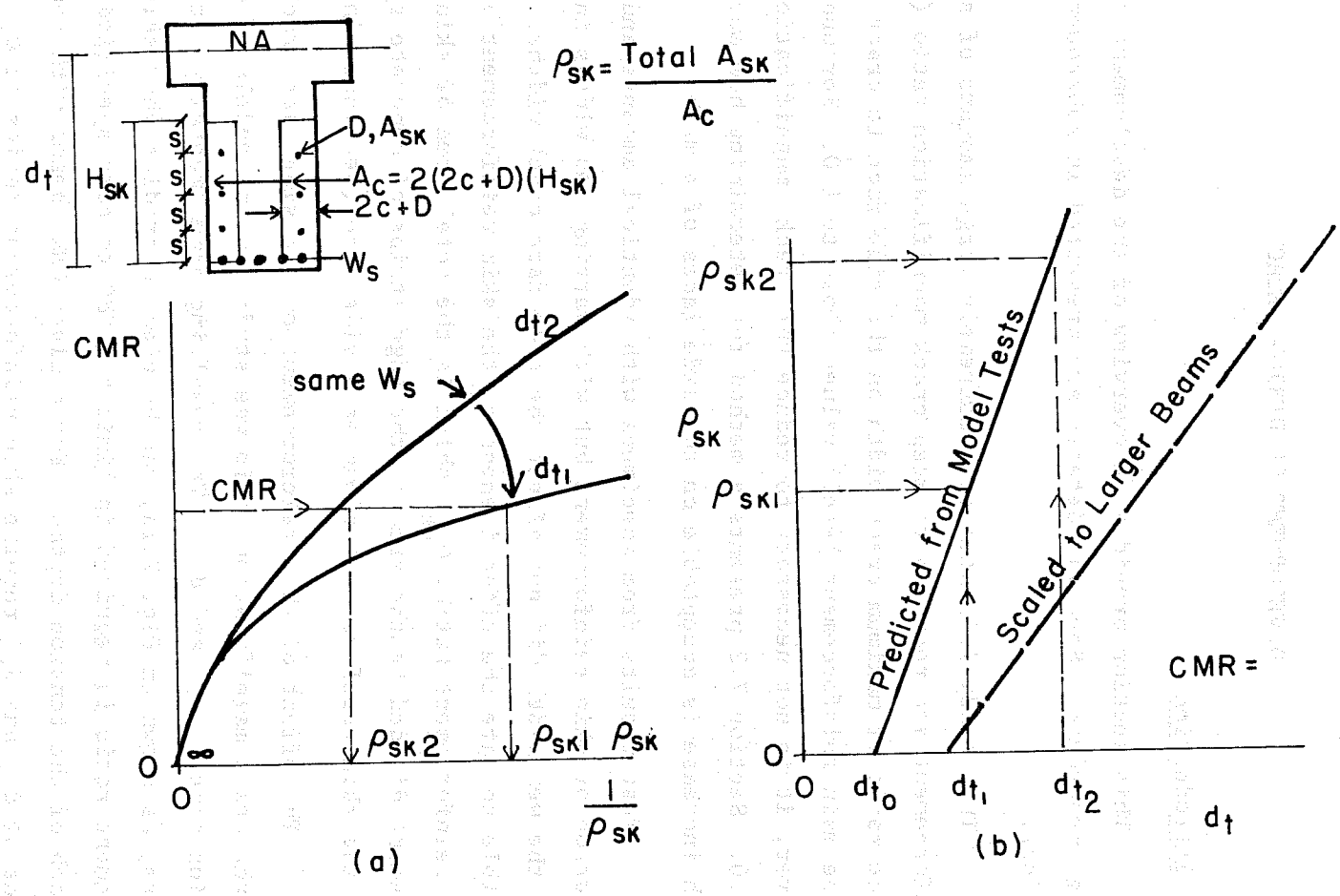

Fig. 7.1 Conceptual development of design method

ρ_{sk2}. Figure 7.1b shows these skin reinforcement ratios plotted with their corresponding tension depths.

Beeby's[11] general crack equation can be used to construct a plot similar to the one shown in Fig. 7.2, which relates the side face crack to the tension depth of beams similar to those used in Fig. 7.1a but with varying depths and no skin reinforcement. For a specified CMR, the side face crack width (w_w) is w_w = CMR w_s, where w_s is the crack width at the main reinforcement level. This particular side face crack width corresponds to a tension depth of d_{t0} (see Fig. 7.2) which is the tension depth of a beam with no skin reinforcement ($\rho_{sk} = 0$) and with the specified CMR. This d_{t0} is plotted in Fig. 7.1b at $\rho_{sk} = 0$.

The solid curve in Fig. 7.1b, therefore, represents the skin reinforcement ratio required to limit the CMR to some specified value for various tension depths in the model specimens. This curve is based on test results of this study and Beeby's crack prediction equations.

The preliminary test of the scale model bent cap (Chapter 3) confirmed that crack widths and crack patterns could be accurately linearly modeled at the scale factor used in this study. Therefore, the predicted curve from the model results (Fig. 7.1b) can be linearly scaled to predict the behavior of larger beams. Figure 7.1b shows such a curve (dashed line) suitable for full size structures. A designer can enter a figure like Fig. 7.1b (dashed line) and predict what skin reinforcement ratio is required for a given tension depth to maintain a certain maximum CMR.

Notice that although the design method has been developed in terms of limiting the crack magnification ratio, it actually limits the maximum crack width on the side face. The curves of Fig. 7.1b refer to beams with a particular crack width at the main reinforcement level (these crack widths in the model and full size specimens are

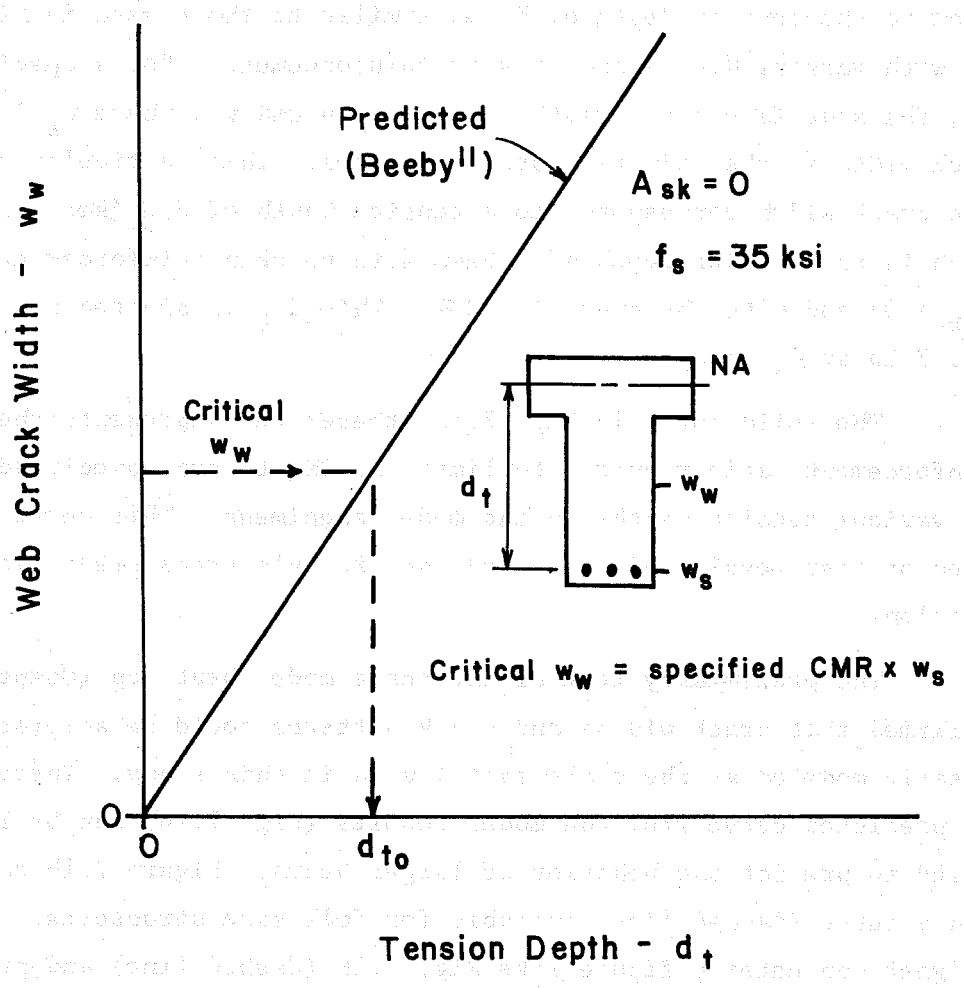

Fig. 7.2 Effect of tension depth on web crack width

related by the scale factor). For the chosen CMR, the maximum side face crack width is, therefore, equal to the CMR times the maximum crack width at the main reinforcement level.

7.2 Acceptable Crack Magnification Ratio and Crack Width

If either a maximum crack magnification ratio or maximum side face crack width criteria is specified, it is possible to determine a required percentage of skin reinforcement for a particular specimen depth (see Sec. 6.9). However, before a generalized design procedure can be developed, it is necessary to decide such a criterion which specifies how much side face crack width increase is acceptable. This criterion must be chosen wisely. Since the test studies indicated that extremely large amounts of skin reinforcement are required to have the crack magnification ratio approach 1.0, such a values does not appear desirable. If the crack magnification ratio is unnecessarily restrictive, excessive amounts of skin reinforcement are required, which increase both material and fabrication costs.

For flexural cracking in the vicinity of the main reinforcement, both the AASHTO Specifications[6] and the ACI Building Code[7] indirectly require that crack widths be limited not at the reinforcement level but on the extreme tension face. As shown in Fig. 6.4, crack widths on the extreme tension face are larger than crack widths at the level of the main reinforcement. The Gergely-Lutz crack width equations (see Sec. 2.2.1) indicate that the ratio of crack widths on the extreme tension face (w_b) to crack widths at the main reinforcement level (w_s) is

$$\frac{w_b}{w_s} = \frac{R}{\frac{1}{1 + t_s/d_t}} = (R)(1 + t_s/d_t)$$

where $R = h_2/d_t$

h_2 = distance from neutral axis to extreme tension face

d_t = distance from neutral axis to main reinforcement level

t_s = distance from center of bar to concrete surface at side

This ratio depends on the depth of the tension zone, the distribution of main reinforcement, and the cover. For specimens in this study, the ratio of w_b/w_s was 1.25, 1.11, and 1.14 for the T series (two #9 bars with 2.5 in. cover), A series (one layer of five #6 bars with 1.125 in. cover), and RS series (two layers of eight #4 plus two #5 bars with 1.125 in. cover), respectively. ACI Committee 224[8] reported that values of R (= h_2/d_t) in T-beam bridges are usually between 1.20 and 1.10. The ACI crack provisions, Article 10.6.4, uses a simplified version of the Gergely-Lutz equation with a value of R equal to 1.20. In general, as the beam depth increases, the value of R decreases. With a clear cover on the main reinforcement of 2 to 2.5 in., the term $(1 + t_s/d_t)$ varies between 1.10 and 1.05 for members with tension zones from 30 to 70 in. deep. This means that the ratio w_b/w_s will probably be in the range of 1.3 (tension depths below 30 in.) to 1.14 (tension depths around 60 in.).

In Chapter 6 the side face crack widths were referenced to the crack widths at the main reinforcement level. The preceding discussion suggests that if the crack magnification ratio is permitted to be about 1.2, cracks on the side face would be approximately the same size as cracks on the extreme tension face. Thus, in general, a reasonable lower limit for the crack magnification ratio is about 1.2.

Setting a reasonable upper limit on the crack magnification ratio is more difficult than setting a lower limit. One estimate of an upper limit can be determined on the basis of limiting the side face crack width (w_w) at some sustained load, say full dead load plus one-half live load (DL + 1/2 LL) to the same maximum value (w_{max}) prescribed for the cracks on the extreme tension face (w_b) at service load, full dead load plus full live load (DL + LL). See Fig. 7.3.

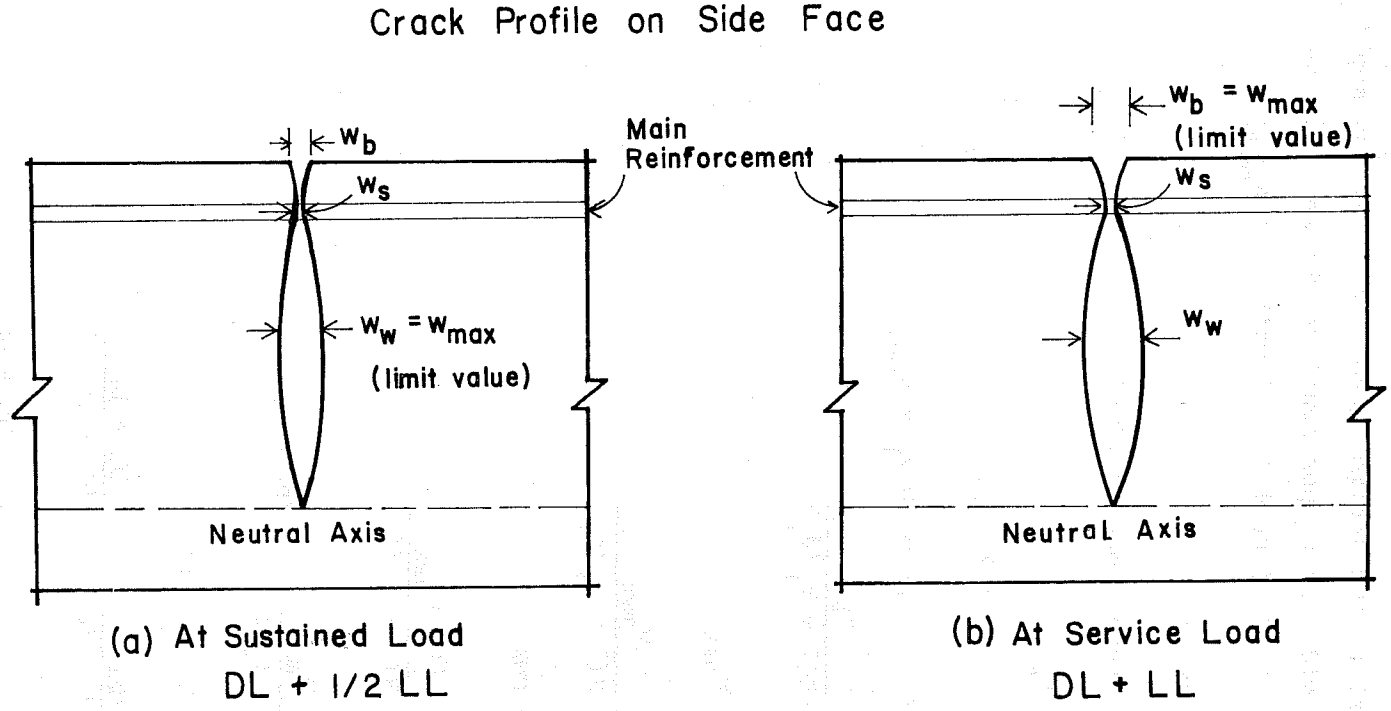

$$\frac{w_b}{w_s} = R\,(1 + t_s/d_t)$$

$$\frac{w_w}{w_s} = CMR$$

Fig. 7.3 Limit condition of crack widths

It was shown that crack widths are proportional to the main reinforcement stress, which is proportional to the applied moment, which is proportional to the applied load. Thus, at any applied load the side face crack width is proportional to the applied load. Therefore, at a sustained load of DL + 1/2 LL with $w_w = w_{max}$,

$$w_w \propto (DL + 1/2\ LL),$$

where "$\propto$" means "is proportional to," since

$$w_w = w_{max}$$

$$w_{max} \propto (DL + 1/2\ LL) \qquad (1)$$

At a service load of DL + LL with $w_b = w_{max}$

$$w_s = \frac{w_b}{R(1 + t_s/d_t)}$$

since $w_b = w_{max}$

$$w_s = \frac{w_{max}}{R(1 + t_s/d_t)}$$

but $w_w = CMR\ w_s$

so $$w_w = \frac{CMR\ w_{max}}{R(1 + t_s/d_t)}$$

and $$\frac{CMR\ w_{max}}{R(1 + t_s/d_t)} \propto (DL + LL) \qquad (2)$$

Dividing Eq. (2) by (1) yields

$$\frac{CMR}{R(1 + t_s/d_t)} = \frac{DL + LL}{DL + 1/2\ LL}$$

so $$CMR = R(1 + t_s/d_t)\ \frac{DL + LL}{DL + 1/2\ LL}$$

or $$CMR = \left[\frac{w_b}{w_s}\right] \left[\frac{1 + \frac{LL}{DL}}{1 + \frac{1}{2}\frac{LL}{DL}}\right]$$

As previously discussed, the first term varies from 1.14 to 1.3. The second term depends on the ratio of live/dead load.

In bridge structures, the dead load is typically greater than the live load. The inverted T-beam bent caps discussed in Chapter 1 were subjected to high dead load. The ratio of live/dead load was 0.31, and the ratio of w_b/w_s was 1.14. Thus, for these structures the minimum CMR is equal to the w_b/w_s ratio, 1.14, which would limit the side face cracks to be no wider than the cracks on the extreme tension face. The maximum CMR, which would limit the side face crack width at sustained load to the maximum allowable crack width is

$$\text{Maximum CMR} = \frac{w_b}{w_s} \frac{1 + \frac{LL}{DL}}{1 + \frac{1}{2}\frac{LL}{DL}}$$

$$= (1.14)\left(\frac{1 + 0.31}{1 + 0.15}\right)$$

$$= 1.30$$

As the live to dead load ratio increases, the maximum CMR indicated by this analysis also increases. In building construction the live/dead load ratio probably varies between 0.5 and 1.0. For a live/dead load ratio of 0.5 and a w_b/w_s ratio varying from 1.14 to 1.3, the maximum CMR varies from 1.37 to 1.56, with an average of about 1.5. For a live/dead load ratio of 1.0 and a w_b/w_s ratio varying from 1.14 to 1.3, the maximum CMR varies from 1.52 to 1.73, with an average of about 1.6. Since every member has its own particular values of w_b/w_s and LL/DL, every member has its own particular maximum CMR which can be calculated.

Protection of the shear reinforcement against corrosion is an important reason for side face crack control. However, the shape of the side face crack profile, especially when significant amounts of well-distributed skin reinforcement are used, indicate only a portion of the side face is subjected to the larger crack widths (see Figs. 5.8 and 6.41). Also, there are fewer cracks on the side face. This suggests that the probability of shear reinforcement corrosion may not be as great as the probability of main reinforcement corrosion. Therefore, the maximum CMR value calculated with the ratios of w_b/w_s and LL/DL can probably be increased slightly. Discussions with engineers from the Texas State Department of Highways and Public Transportation, which had constructed the bent caps previously mentioned, indicated they would consider acceptable a crack magnification ratio in the range of 1.3 to 1.5. A CMR of 1.4 is reasonable for these bent caps, which had a w_b/w_s ratio of 1.14 and a LL/DL ratio of 0.31. A CMR of 1.4 is also a conservative value to use in general, since most structures have $w_b/w_s > 1.14$ and $LL/DL > 0.31$, which means their particular value of $CMR > 1.3$. Of course, if corrosion is not a problem, an even higher value of CMR might be used.

As discussed in Chapter 1, there is considerable disagreement on the importance of cracking in relation to the corrosion of reinforcement. The AASHTO and ACI provisions indirectly consider 0.012 and 0.013 in. as the maximum acceptable crack widths on the extreme tension face for exterior exposure. Since these provisions are generally followed in the United States, the design procedure developed here assumes the maximum allowable crack width on the extreme tension face to be 0.0125 in. (the average of the AASHTO and ACI values).

For beams with tension depths about 4 ft or more, sizes in which the side face cracking can be serious unless controlled, a typical ratio of w_b/w_s is about 1.15. Thus, the crack width at the main reinforcement level is about 0.011 in. With a CMR of 1.4, the maximum side face crack widths should be approximately 0.015 to

0.016 in. Most beams designed to satisfy the AASHTO or ACI cracking provision have crack widths less than the implied maximums at the main reinforcement level. Reducing the crack width at the main reinforcement level also reduces the side face crack widths (see Sec. 6.3.2).

After consideration of all of these factors, a maximum value of CMR of 1.4 was chosen to be the criterion for specific design recommendations.

7.3 Applying Model Test Results to Full Size Structures

The percentage of skin reinforcement can be related to either the crack magnification ratio or the side face crack widths. Using the average crack magnification ratio has the advantage of describing the data through several crack measurement stages. The design procedure was developed using the average crack magnification ratio and specifying the acceptable crack magnification ratio to be 1.4. The results were then compared with results using other ratios.

Based on the test results of this study, Fig. 7.4a shows how the predicted skin reinforcement percentage for a CMR of 1.4 varied with the tension depth. The results of the Series A specimens were used to predict the required skin reinforcement percentage for a CMR of 1.4 and a d_t of 26.8 in. For the Series A specimens (see Fig. 6.44f)

$$\text{CMR} = 0.246\ (1/\rho_{sk})^{0.37}$$

$$1.4 = 0.246\ (1/\rho_{sk})^{0.37}$$

$$\rho_{sk} = 0.0091$$

$$100\% \times \rho_{sk} = 0.91\%$$

This same result can be obtained graphically from Fig. 6.44f (as explained in Sec. 7.1). For the Series D specimens with a d_t of 39.8 in., the predicted skin reinforcement percentage for a CMR of 1.4 is 1.68 percent (see Fig. 6.30d).

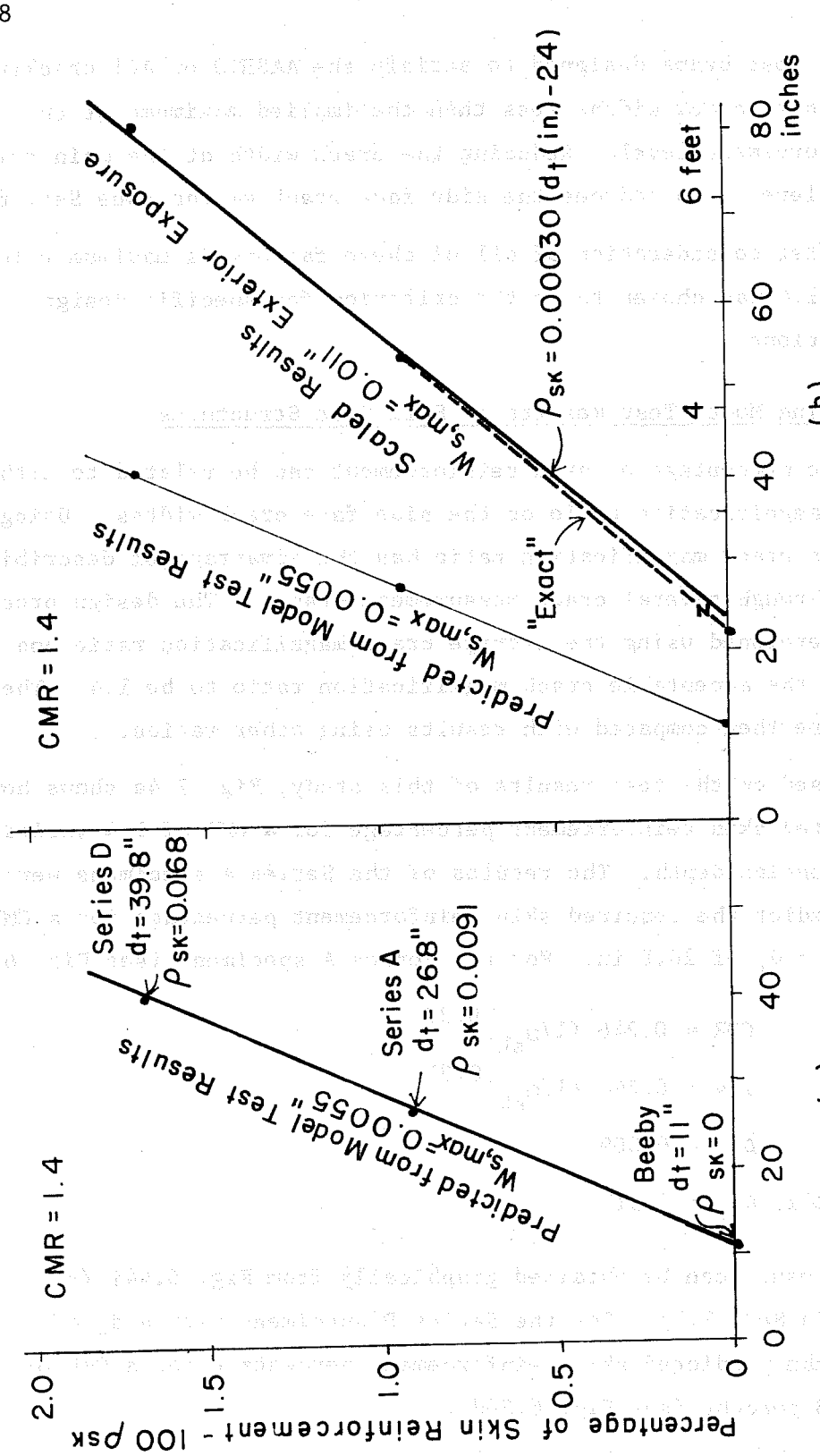

Fig. 7.4 Predicted skin reinforcement percentage for CMR = 1.4

Beeby's cracking equation was used indirectly to predict the tension depth of a member without any skin reinforcement and a CMR of 1.4. Figure 7.5 shows the relationship between the tension depth and the web crack width for specimens similar to those of Series A, but with no skin reinforcement and with varying depths at a stress of 35 ksi. Using Beeby's equations, the average crack width at the main reinforcement was calculated to be 0.0023 in. For a CMR of 1.4, the web crack width was 1.4 x 0.0023 = 0.0032 in. As shown in Fig. 7.5, this critical web crack width indicated that a specimen with a d_t of about 11 in. and with no skin reinforcement would have a CMR of 1.4.

Of course, the exact relationship between the percentage of skin reinforcement and the tension depth could not be determined from these tests. However, based on the results plotted in Fig. 7.4a, it was reasonable to approximate the relationship using a straight line.

The relationship of Fig. 7.4a is correct for specimens with a cover on the main reinforcement of 1.125 in. and a maximum crack width calculated by the Gergely-Lutz equation of 0.0055 in. at the main reinforcement level. The average of the measured maximum crack widths was 0.006 in., very close to the predicted value of 0.0055 in. The test results of Chapter 3 confirmed the similitude of cracking in different size models. Therefore, the model test results shown in Fig. 7.4a can be linearly scaled to predict the behavior of larger specimens with larger cracks at the main reinforcement level.

Figure 7.4b (dashed line) shows the predicted model results scaled up by a factor of 2 to represent specimens with a cover on the main reinforcement of 2.25 in. and a maximum crack width of 0.011 in. at the main reinforcement level. As discussed in Sec. 7.2, members with this size crack width at the main reinforcement level would have crack widths on the extreme tension face approximately equal to those maximum values indirectly prescribed by AASHTO and ACI provisions for structures subjected to exterior exposure. Members with a tension depth exceeding 22 in. require skin reinforcement. This tension depth

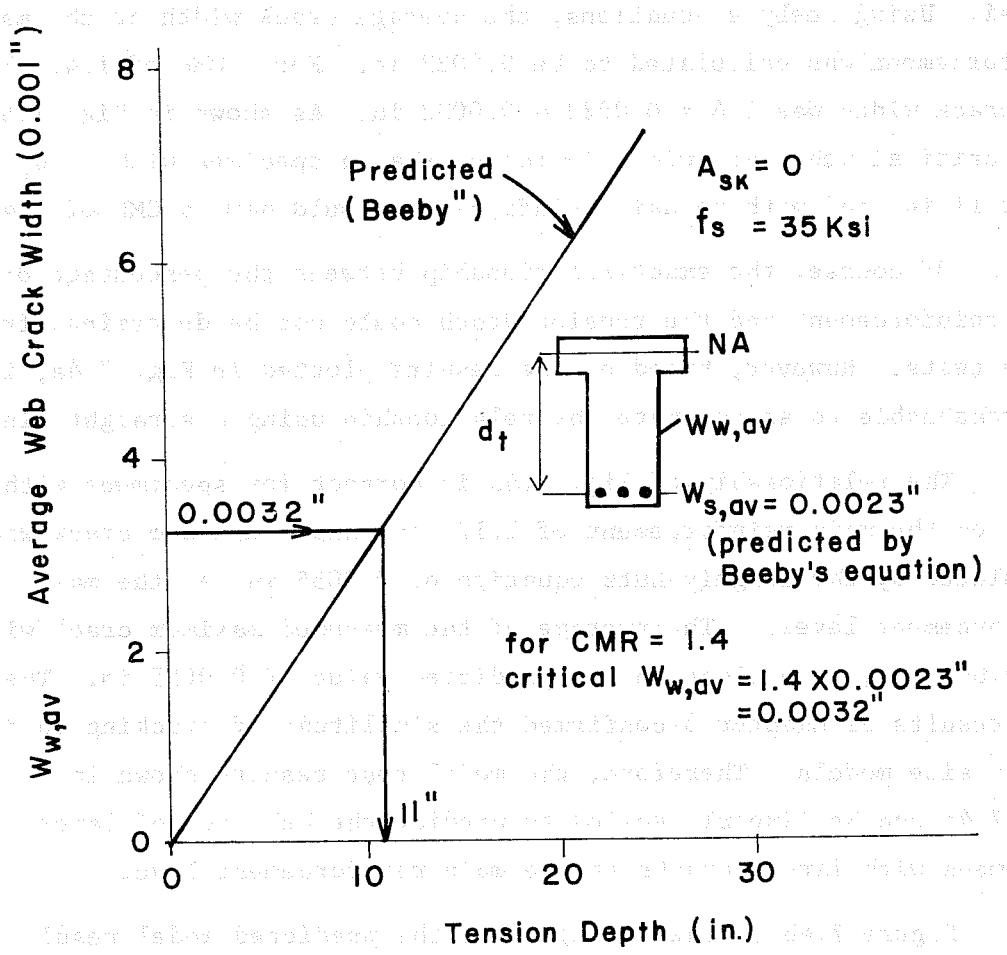

Fig. 7.5 Predicted web crack width vs tension depth (no skin reinforcement)

agrees quite well with the various code provisions concerning the critical section dimension above which skin reinforcement is required: 36 in. web height (ACI Building Code[7]), 24 in. side face height (AASHTO Specifications[6]) and 23 in. web height (CEB Recommendations[9]). The "exact" curve can be described well by the approximate straight line relationship:

$$\rho_{sk} = 0.00030\ (d_t - 24)$$

with d_t expressed in inches.

These full size beams have a maximum crack width at the main reinforcement level of 0.011 in. as calculated by the Gergely-Lutz equation. By limiting the CMR to 1.4, the maximum side face crack width is indirectly limited to 0.0154 in.

Similar procedures were used to derive the curves shown in Figs. 7.6 and 7.7. Table 7.1 lists these results. Although a CMR equal to 1.0 is not desirable, it is listed for comparison purposes. The skin reinforcement percentages for a CMR equal to 1.0 lie slightly outside the range of test results, and, therefore, the validity of these values is not as verifiable as those for other CMR's. Except for a CMR of 1.0, the results can be reasonably represented with a straight line. The equations from the test results can be modified to apply to specimens with crack widths other than 0.0055 in. at the main reinforcement by simply multiplying the slope of the equation by the value of crack width at the main reinforcement level in the new specimens divided by 0.0055 in. The equations for specimens with a crack width of 0.011 in. at the main reinforcement level and a cover of 2.25 in. are listed in Table 7.1 and also plotted in Fig. 7.7. Figure 7.8 shows how a reduction in the allowable CMR from 1.5 to 1.0 increases the required amount of skin reinforcement for a member with a tension depth of 60 in. The area of skin reinforcement is calculated for a 2.25 cover and skin reinforcement of #7 bars evenly distributed in the lower 5/8 of the tension zone. Notice that

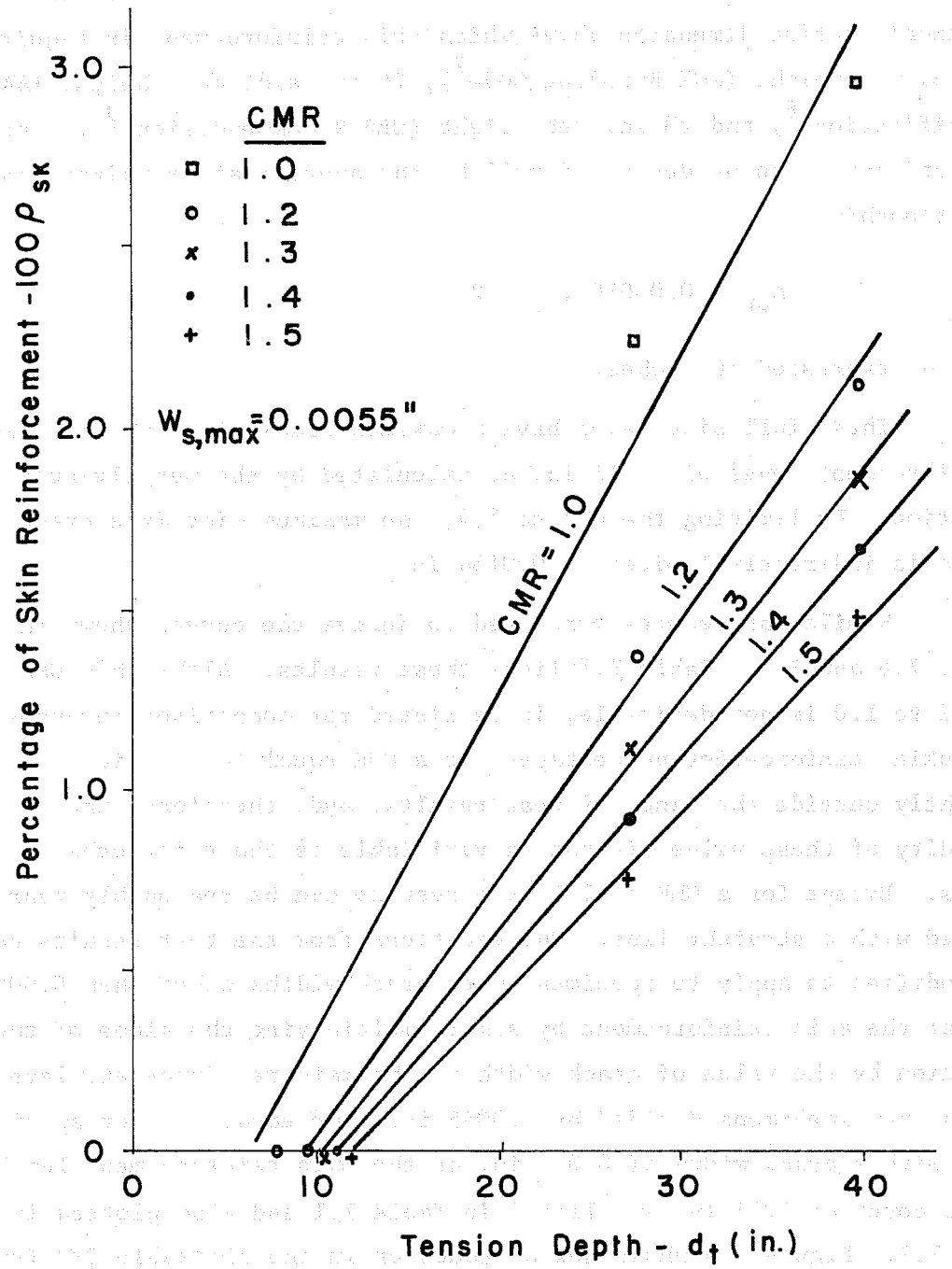

Fig. 7.6 Predicted skin reinforcement percentage for various CMR's--model test results

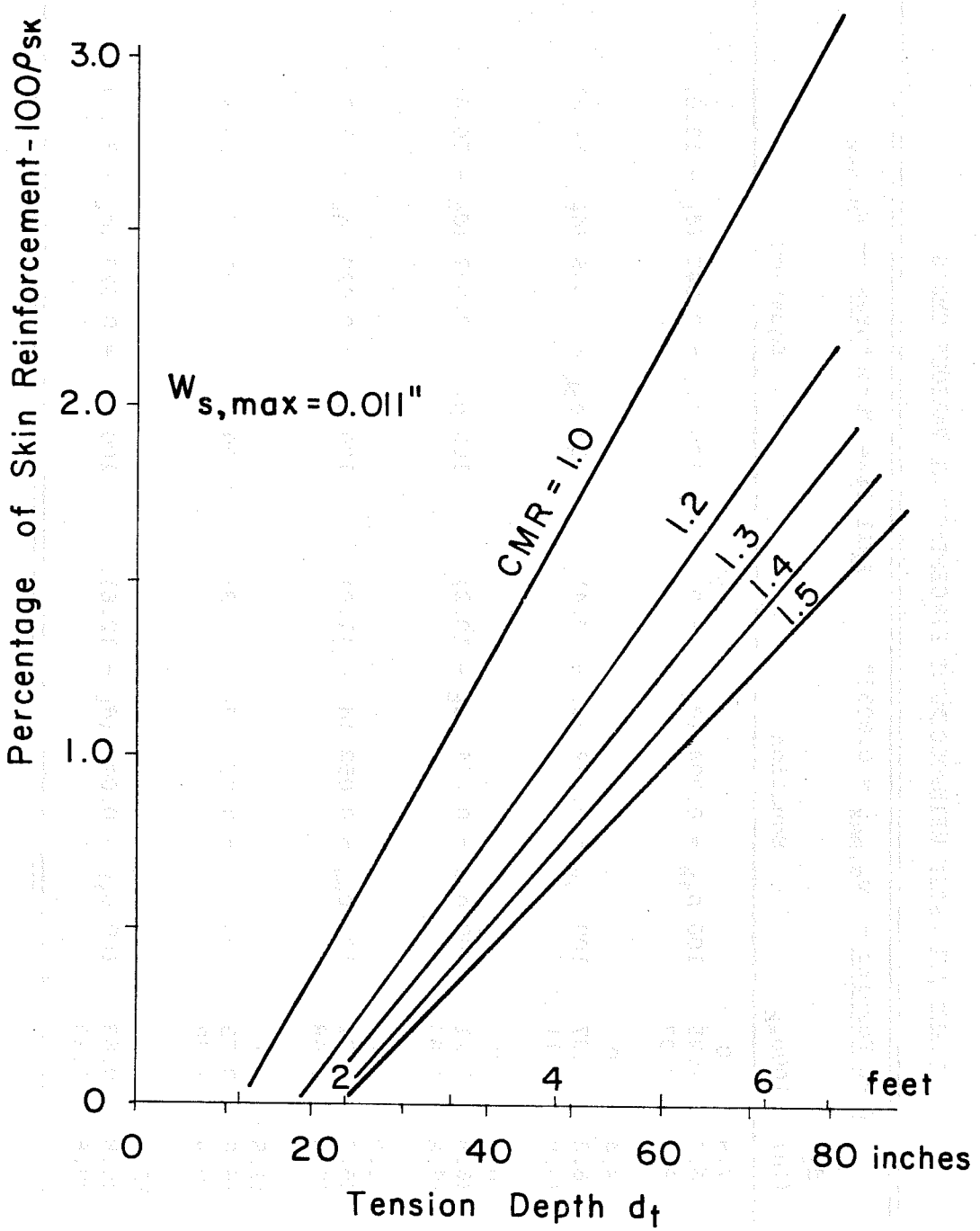

Fig. 7.7 Predicted skin reinforcement percentage for various CMR's--full size structures

TABLE 7.1 SKIN REINFORCEMENT PERCENTAGE AT VARIOUS CMR'S

		Test Results — $w_{s,max}$ = 0.0055"		Full Size Structures — $w_{s,max}$ = 0.011"	
CMR	d_t (in)	$100\rho_{sk}$	Equation	Equation
1.0	7.9	0	$100\ \rho_{sk} = 0.094\ (d_t - 6.0)$	$100\ \rho_{sk} = 0.047\ (d_t - 12.0)$
	26.8	2.25		
	39.8	2.97		
1.2	9.4	0	$100\ \rho_{sk} = 0.072\ (d_t - 9.4)$	$100\ \rho_{sk} = 0.036\ (d_t - 18.8)$
	26.8	1.37		
	39.8	2.11		
1.3	10.2	0	$100\ \rho_{sk} = 0.064\ (d_t - 10.2)$	$100\ \rho_{sk} = 0.032\ (d_t - 20.4)$
	26.8	1.11		
	39.8	1.85		
1.4	11.0	0	$100\ \rho_{sk} = 0.058\ (d_t - 11.0)$	$100\ \rho_{sk} = 0.029\ (d_t - 22.0)$
	26.8	0.91		
	39.8	1.68		
1.5	11.8	0	$100\ \rho_{sk} = 0.052\ (d_t - 11.8)$	$100\ \rho_{sk} = 0.026\ (d_t - 23.6)$
	26.8	0.75		
	39.8	1.48		
1.6	12.6	0	$100\ \rho_{sk} = 0.046\ (d_t - 12.6)$	$100\ \rho_{sk} = 0.023\ (d_t - 25.2)$
	26.8	0.63		
	39.8	1.33		

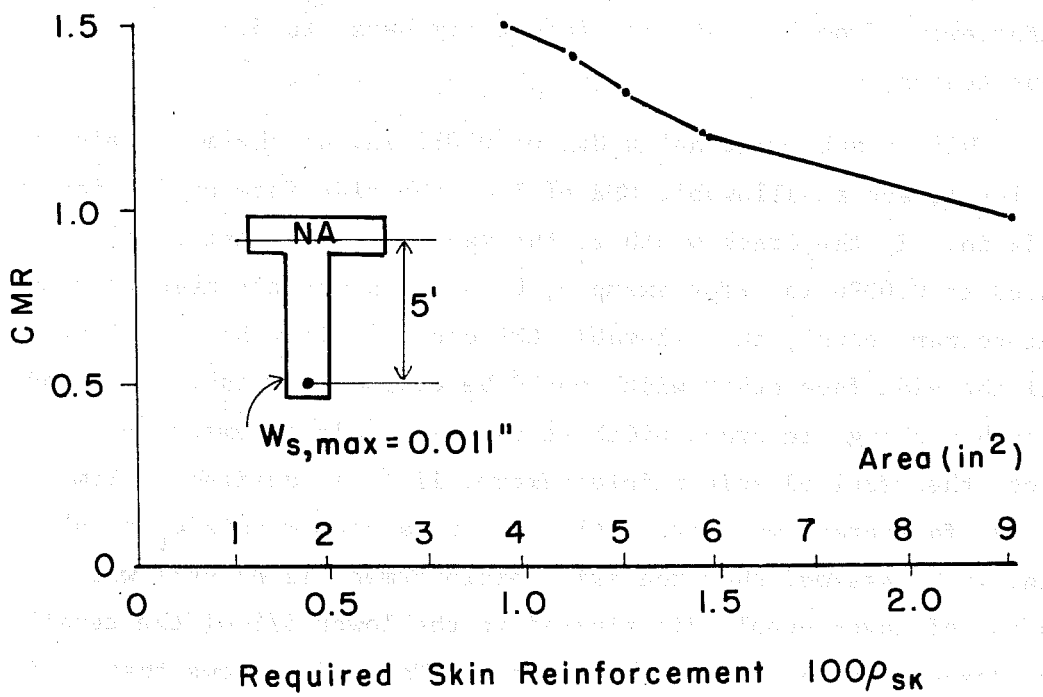

Fig. 7.8 Effect of reducing CMR on required skin reinforcement

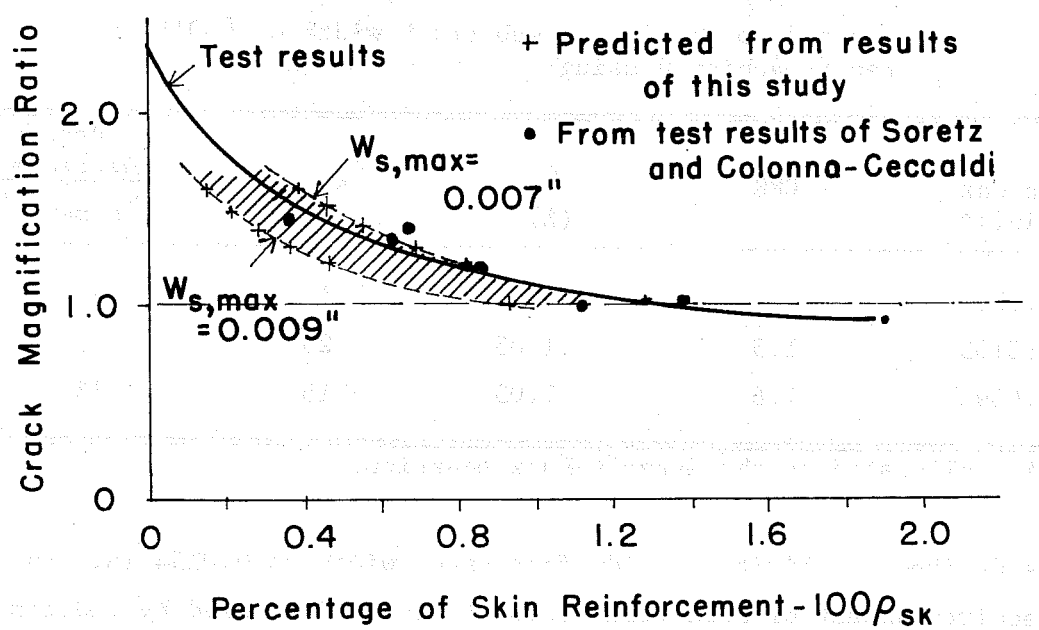

Fig. 7.9 Comparison with test results of Soretz and Colanna-Ceccaldi (Ref. 12)

reducing the CMR from 1.5 to 1.2 increases the required skin reinforcement from 3.79 sq. in. (about six bars) to 5.93 sq. in. (about ten bars).

With a maximum crack width of 0.011 in. at the main reinforcement level, and an allowable CMR of 1.4, the side face crack width is 0.0154 in. If the crack width at the main reinforcement level is reduced to 0.0096 in. (for example, by using a greater number of main reinforcement bars), the allowable CMR could be increased to 1.6, and still the side face crack width would be 0.0154 in. Table 7.2 shows how such a change in crack width at the main reinforcement level affects the required skin reinforcement, if it is desired to limit the side face crack width to 0.0154 in. in a beam with a d_t of 60 in. Again, it is assumed that the skin reinforcement is #7 bars with 2.25 in. of cover evenly distributed in the lower 5/8 of the tension zone adjacent to the main reinforcement. Table 7.2 shows that if it

TABLE 7.2 HOW $w_{s,max}$ AFFECTS THE REQUIRED SKIN REINFORCEMENT PERCENTAGE

For a d_t of 60 in., a web crack width of 0.0154 in. can be achieved using:

$w_{s,max}$ (in.)*	CMR	ρ_{sk} (%)	A_{sk} (in.^{2})	Percent Decrease in $w_{s,max}$	Percent Decrease in A_{sk}
0.0110	1.4	1.11	4.47	--	--
0.0103	1.5	1.05	4.23	7	5
0.0096	1.6	1.03	4.15	13	7

*As calculated by the Gergely-Lutz equation.

is desired to limit the side face crack width to 0.0154 in., the required amount of skin reinforcement can be decreased by reducing the crack width at the main reinforcement level. This confirms the findings of Sec. 6.3.2, which showed that decreasing the crack width

at the main reinforcement level also decreases the side face crack width in specimens without skin reinforcement. However, the reduction in skin reinforcement is not that great, and, as discussed in Sec. 6.3.2, reducing the crack width at the main reinforcement level is neither an efficient nor practical way of controlling the side face crack widths. It is conservative to assume that the crack width at the main reinforcement level is 0.011 in., since this is about the maximum crack width for beams satisfying the ACI or AASHTO provisions for crack control in the vicinity of the main reinforcement.

The results from this study were compared to the results reported by Soretz and Colanna-Ceccaldi.[12] Their specimens had a tension depth of about 26 in. (2.17 ft), a cover of 1.26 in., a crack width calculated by the Gergely-Lutz equation at the main reinforcement level of 0.009 in., and a measured crack width at the main reinforcement level of 0.007 in. The equations of Table 7.1 were modified to correspond to a crack width of 0.009 and 0.007 in. at the main reinforcement level. Recall that the equations of Table 7.1 were derived from specimens with a crack width calculated by the Gergely-Lutz equation of 0.0055 in., which was very close to the measured crack width of 0.006 in. The predicted percentage of skin reinforcement was then calculated for CMR's between 1.6 and 1.0. These predicted values are shown in Fig. 7.9, along with the CMR's obtained using their reported test data. The test results fall within or very close to the band of predicted percentages. In fact, they are very close to the predicted results based on the measured crack width of 0.007 in. It appears that the results from this study adequately explain the results reported by Soretz and Colanna-Ceccaldi.

The model results were linearly scaled to achieve crack width compatibility. Since the model results for development of the equations were based on crack widths at the level of the main reinforcement of 0.0055 in. as calculated by the Gergely-Lutz equation, a scale factor of 2 was used to provide an equivalent crack width of 0.011 in.

at the main reinforcement level in full size structures. Since the largest model tested had a tension zone 40 in. deep, the corresponding full size structure on this basis would have a tension zone 2 x 40 = 80 in. deep. This would correspond roughly to an overall depth of 9 ft. As described in Sec. 7.3 and shown in Fig. 7.4, the relationship between the tension depth and the percentage of skin reinforcement can be closely approximated by a straight line for both the models and the full size structures in these depth ranges.

Several very large structures with serious side face cracking problems were examined. The structures had tension zones up to about 144 in. (12 ft) deep, which were well beyond the 40 in. range of the equation developed from the laboratory results. Using the previously developed equation for these structures resulted in very large and possibly unrealistic required amounts of skin reinforcement. It appeared that it was too conservative to linearly extrapolate the laboratory derived equation to such very large beams ($d > 100$ in.).

Additional studies using the previously described finite element analysis were performed for guidance in extrapolation of the laboratory test results to larger depths. Half-scale mathematical models with tension zones 53 or 79 in. deep were analyzed. The specimens' main reinforcement was designed to result in the same crack width at the main reinforcement as in Specimens FD-6, FA-6a, and FD-6B (described in Chapter 5), which had tension zones 26.5 in. deep. As in these previous specimens, any skin reinforcement was evenly distributed within approximately 60 percent of the tension zone closest to the main reinforcement.

Figure 7.10a shows the effect of the percentage of skin reinforcement on the maximum side face crack width for these three series of specimens. Each series shows similar trends. However, the deeper sections require a larger percentage of skin reinforcement than the shallower section to reduce the side face crack width to the same value.

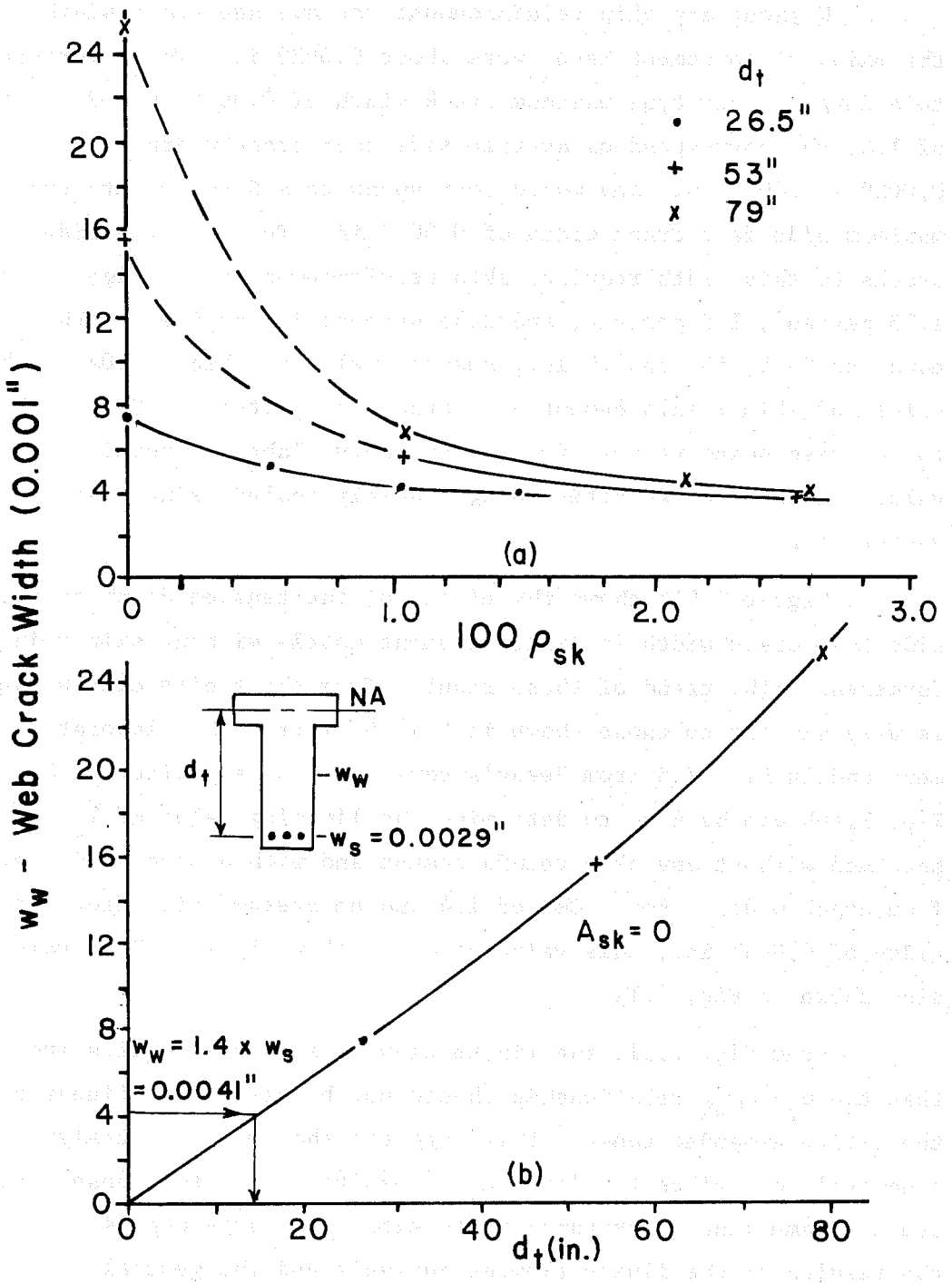

Fig. 7.10 Finite element analysis for effect of d_t

Without any skin reinforcement the average crack widths at the main reinforcement level were about 0.0029 in. These correspond to a Gergely-Lutz type maximum crack width of 0.0055 in. For a CMR of 1.4, the corresponding average side face crack width is 1.4 x 0.0029 = 0.0041 in., and would correspond to a Gergely-Lutz type maximum side face crack width of 0.0077 in. To limit the side face cracks to this width requires skin reinforcement percentages of about 1.15 percent, 1.9 percent, and 2.35 percent in specimens with d_t equal to 26.5, 53, and 79 in., respectively (see Fig. 7.10a). These values of skin reinforcement percentage are plotted in Fig. 7.11 at the corresponding values of d_t on the curve labeled "model". The values are also shown after being linearly scaled using a scale factor of 2.

Figure 7.10b shows the effect of the tension depth on the side face crack width in finite element models without skin reinforcement. The trend of these results from the finite element analysis is very similar to those shown in Fig. 6.27 from the laboratory specimens and in Fig. 7.5 from Beeby's equation. As explained in Sec. 7.3, Fig. 7.10b can be used to determine the limiting value of d_t for a specimen without any skin reinforcement and with a specified side face crack width. For a CMR of 1.4 and an average side face crack width of 0.0041 in., this value of d_t is about 14 in. This value is also shown in Fig. 7.11.

From Fig. 7.11, the finite element analysis results indicate that the d_t - ρ_{sk} relationship should not be assumed as linear over the entire expanded range. This suggests that while a straight line adequately describes the laboratory results, it is too conservative to use the same line to extrapolate to extremely large depths. Based on the results of the finite element analysis and the generally good agreement with the experimental program in the range where both did apply, a bilinear relationship is proposed. For values of d_t within the general range of the scaled up laboratory tests, the previously

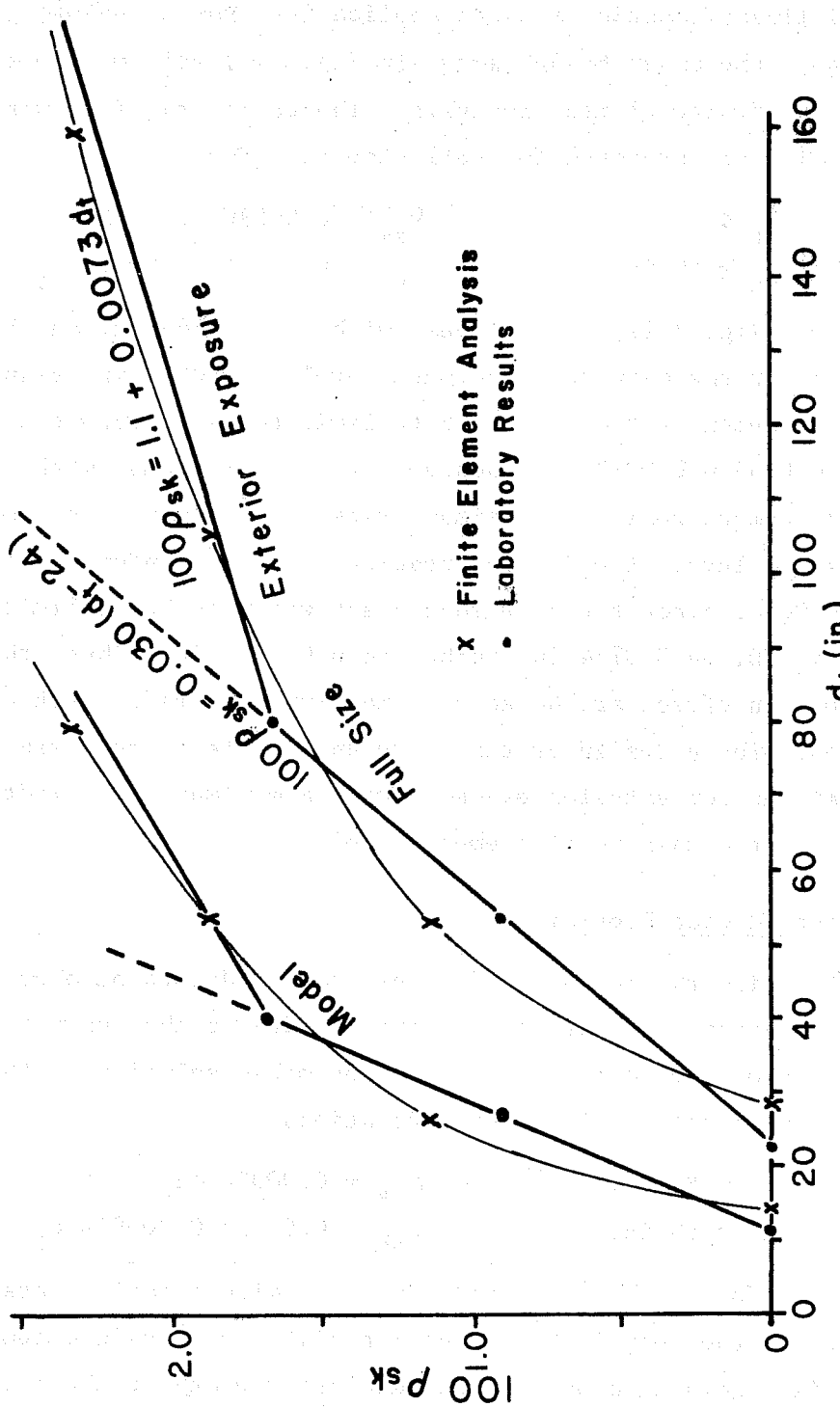

Fig. 7.11 Extrapolation of test results

developed linear equation is most applicable. For d_t values greater than 80 in., the upper branch shown in Fig. 7.11 follows the trend shown by the finite element analysis. Therefore, the following relationships are proposed for full size structures.

For $d_t \leq 80$ in. $\quad \rho_{sk} = 0.00030\ (d_t - 24)$

For $d_t > 80$ in. $\quad \rho_{sk} = 0.011 + 0.000073\ d_t$

From Fig. 7.11, a model beam with a d_t of 40 in. and a maximum crack width at the main reinforcement level of 0.0055 in. requires a skin reinforcement ratio of 0.0168 to limit the side face crack width to 1.4 x 0.0055 = 0.0077 in. However, a full size beam with a d_t of 40 in. and a more realistic maximum crack width limit at the main reinforcement level of 0.011 in. requires a skin reinforcement ratio of only 0.0048, since the side face crack width is being limited to only 1.4 x 0.011 = 0.0154 in. rather than 0.0077 in. Thus, the design expressions in effect are based on a maximum side face crack width limitation. These design criteria are applicable to full size structures designed for exterior exposure with a maximum crack width of 0.011 in. at the main reinforcement level.

7.4 Suggested Code Provision

Limiting the maximum side face crack width to be about 40 percent larger than the maximum crack width at the main reinforcement level should be a practical and economical solution to the side face cracking problem. The design equations

For $d_t \leq 80$ in. $\quad \rho_{sk} = 0.00030\ (d_t - 24)$

For $d_t > 80$ in. $\quad \rho_{sk} = 0.011 + 0.000073\ d_t$

were derived for a CMR of 1.4 and for beams with a maximum crack width calculated by the Gergely-Lutz equation at the main reinforcement level of 0.011 in. This is about the maximum crack width at the main reinforcement level for structures designed to satisfy the AASHTO or ACI provisions for distribution of main reinforcement for exterior

exposure. With a CMR of 1.4, the maximum crack width on the side face should be in the range of 0.015 to 0.016 in. (± about 33 percent, typical crack width data scatter).

This required skin reinforcement ratio requires computation of the value of the tension depth of the beam at service load, which is not otherwise computed in strength design. It requires the engineer to calculate the neutral axis location using elastic theory concepts that have largely been replaced by ultimate strength concepts. However, the tension depth can be related to the overall depth. Using the working stress formula for locating the neutral axis depth (kd),

$$k = \sqrt{(n\rho)^2 + 2(n\rho)} - (n\rho)$$

where $n = E_s/E_c$, modular ratio

$\rho = A_s/bd$, main tension reinforcement ratio

then $$d_t = d - kd$$

The main reinforcement ratio that can be used in a beam is limited from a minimum of $200/f_y$ to a maximum of 0.75 ρ_{bal} (ρ_{bal} refers to the main reinforcement ratio producing a balanced strain condition). For rectangular beams with Grade 60 reinforcement (f_y = 60,000 psi), d_t will vary between 0.80d and 0.45d as the main reinforcement varies between the minimum and maximum allowable amounts (the concrete compressive strength has very little effect on the value of d_t).

From Sec. 7.3, for a CMR of 1.4,

$$\rho_{sk} = 0.00030\ (d_t - 24) \quad \text{for } d_t \leq 80 \text{ in.}$$

$$\rho_{sk} = 0.011 + 0.000073\ d_t \quad \text{for } d_t > 80 \text{ in.}$$

These equations can be expressed in terms of d instead of d_t. For $d_t = 0.8d$,

$$\rho_{sk} = 0.00024\ (d - 30) \quad \text{for } d \leq 100 \text{ in.}$$

$$\rho_{sk} = 0.011 + 0.000058\ d \quad \text{for } d > 100 \text{ in.}$$

Similar expressions can be obtained for other values of d_t/d. Figure 7.12 shows how the choice of d_t/d affects the predicted skin reinforcement percentage. The curve shown for $d_t = 0.64d$ corresponds to a main reinforcement ratio of $\rho = 0.18f'_c/f_y$, which was the "balanced reinforcement ratio" in working stress design concepts. It is shown because reinforcement ratios about equal to this value are found in many beams. Using d_t equal to the maximum value of 0.8d is a conservative approximation, since the required ρ_{sk} increases with increasing d_t. Such an approximation is justifiable, because (1) the scatter in the data used to develop this method and the randomness of cracking in general indicate that great accuracy in crack control computations is not warranted, (2) the side face cracking problem is a "secondary" design problem, and (3) although it is important to control the side face crack widths, the design method should be as simple and easy to use as possible and still be effective. As discussed in Chapter 6, the skin reinforcement is most effective if distributed within about 5/8 of the tension zone adjacent to the main reinforcement. Using $d_t = 0.8d$ means that the skin reinforcement should be evenly distributed within half of the beam depth nearest the main reinforcement. Figure 7.13 shows how the area of skin reinforcement is calculated.

Table 7.3 shows how the total area of skin reinforcement varies with depth using the previous equation with $d_t = 0.8d$. Suitable skin reinforcement bars are also chosen. For comparison, the present ACI and AASHTO required area of skin reinforcement is shown for rectangular beams with a d/b ratio of 3 and a main reinforcement ratio of 0.01. For the smaller depths, the predicted skin reinforcement area from this study is only 1.5 to 2 times as much as the AASHTO and ACI amounts. However, at depths over 84 in. (7 ft depths, where severe side face cracking has been reported) the predicted amount is 3 times or more than these AASHTO and ACI amounts.

The equation for $d \leq 100$ in. was derived from test specimens with tension depths up to 40 in. and a crack width at the main

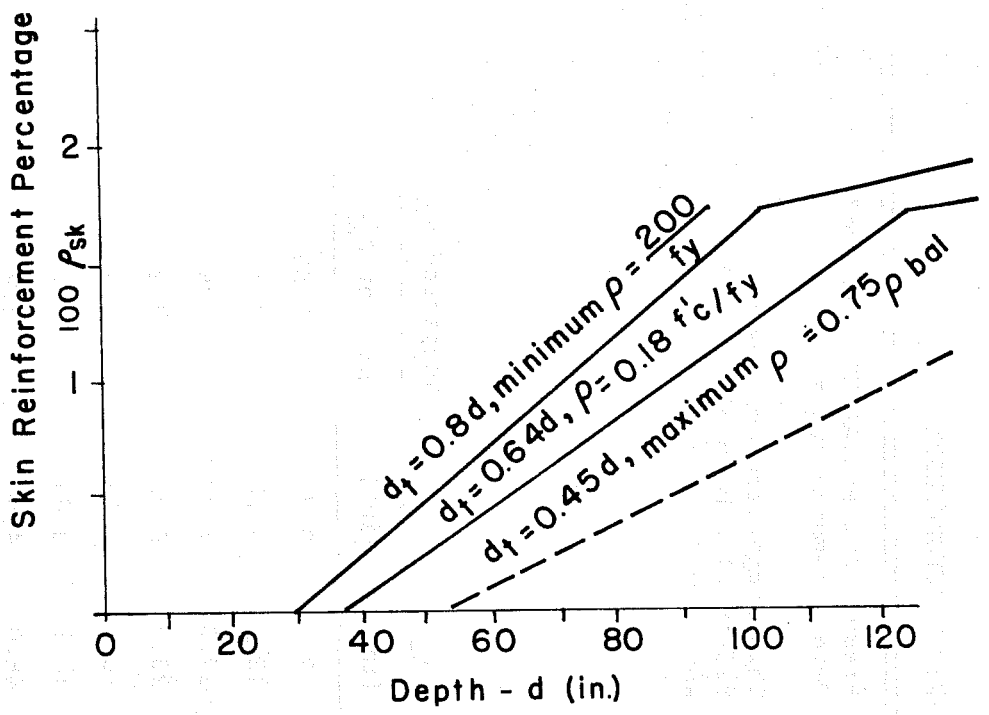

Fig. 7.12 Effect of choice of d_t/d on $100\,\rho_{sk}$

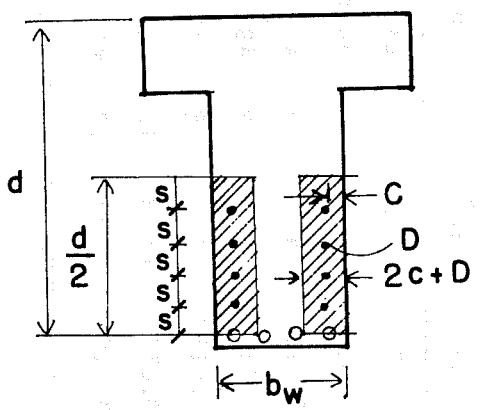

$$\rho_{SK} = \frac{\text{Total } A_{SK}}{(2)(2c+D)(\frac{d}{2})}$$

$$\text{or Total } A_{SK} = \rho_{SK}\,(2c+D)(\frac{d}{2})(2)$$

$$\text{with } (2c+D) \leq \frac{bw}{2}$$

Fig. 7.13 Skin reinforcement ratio as defined for suggested code provision

TABLE 7.3 REQUIRED AREA OF SKIN REINFORCEMENT

$\rho_{sk} = 0.00024\ (d - 30)$ for $d \leq 100$ inches

$\rho_{sk} = 0.011 + 0.000058\ d$ for $d > 100$ inches

$A_{sk} = \rho_{sk}\ (2c + D)\ (d/2)\ (2)$

for $c = 2" + \#5$ stirrup $= 2.625"$

$A_{sk} = \rho_{sk}\ (5.25 + D)\ (d/2)\ (2)$

Present ACI and AASHTO Required Skin Reinforcement: $A_{sk} = 10\%\ A_s$

This comparison assumes a rectangular beam with $b = d/3$ and $A_s = 0.01\ bd$

d (ft)	ρ_{sk}	A_{sk} (in^2)	Bars	A_s (in^2)	A_s (in^2)	suggested A_{sk} / present A_{sk}
4	0.0043	1.19	8 - #4 @ 4.8"	7.7	0.77	1.50
5	0.0072	2.54	8 - #5 @ 6"	12.0	1.20	2.1
6	0.0101	4.45	8 - #7 @ 7.2"	17.3	1.73	2.5
7	0.0130	6.83	8 - #8 @ 8.4"	23.5	2.35	2.9
8	0.0158	9.87	8 - #10 @ 9.6"	30.7	3.07	3.2
9	0.0173	12.16	10 - #10 @ 9"	38.9	3.89	3.1
10	0.0180	14.05	12 - #10 @ 8.5"	48.0	4.80	2.9

reinforcement level of 0.0055 in., as calculated by the Gergely-Lutz equation. These results were then linearly scaled using a scale factor of 2 to apply to larger structures, with a crack width of 0.011 in. at the main reinforcement level. Therefore, using a scale factor of 2, the corresponding tension depth of the full size structure is 2 x 40 in. = 80 in. = 6.7 ft. For beams with small amounts of main reinforcement (d_t = 0.8d), the corresponding depth is 6.7 ft/0.8 = 8.4 ft. For beams with average amounts (d_t = 0.64d) and large amounts (d_t = 0.45d) of main reinforcement, the corresponding depths are 10.5 and 14.9 ft, respectively. This covers a very wide range of flexural members. Using the results of a finite element analysis, a second equation was suggested for depths > 100 in. It should be noted that the equations were derived using conservative assumptions: (1) d_t = 0.8d, (2) crack width at the main reinforcement level = 0.011 in., and (3) CMR = 1.4.

The ratio of the beam depth to the web width varied from 4.2 to 1.9 for specimens in this study. In these specimens, which had a cover on the skin reinforcement of 1.125 in., the web width (varying from 7.75 to 17 in.) did not noticeably affect the side face cracking. This supports the idea that the skin reinforcement can be considered effective in narrow edge strips along the side faces. Each strip is assumed to be symmetrical about the skin reinforcement along each side face. The strip has a height of d/2 and a width of twice the distance from the center of the skin reinforcement bar to the side face (see Fig. 7.13). As the web width decreases, the skin reinforcement along each side face gets closer to the other side face, and there is a possibility that it may help in reducing crack widths on the other side face. To account for this possible interaction it is suggested that the width of the edge strip be limited to not more than one-half of the web width (see Fig. 6.25).

Skin reinforcement cover is included in the definition of the skin reinforcement ratio (by the edge strip width, 2c + D). In this

study the skin reinforcement cover varied from 0.75 to 3 in. The expressions developed in this chapter are to be used within the ordinary ranges of cover set by the various codes.

Both the analytical and experimental studies indicated that the skin reinforcement is most effective if placed as a large number of small bars rather than only a few larger bars. Based on the results of the laboratory tests and the finite element analysis, placing a minimum of four bars per side in the lower half of the depth should be adequate. Since the first bar was located one bar spacing from the centroid of main reinforcement and the farthest bar was located one bar spacing from middepth, the maximum bar spacing is $(d/2)/5 = d/10$. To ensure that the spacing does not become excessive in very large beams, it is also suggested that the maximum spacing be limited to 12 in.

The equation $\rho_{sk} = 0.00024\ (d - 30)$ implies that skin reinforcement is required in beams exceeding 30 in. (2.5 ft) deep. This equation is based on the conservative assumption that the crack width at the main reinforcement level is 0.011 in. and is intended to limit the side face crack widths to a maximum value of about 0.015 to 0.016 in. It also assumes that the ratio of w_b/w_s is 1.14. As discussed in Sec. 7.2, the ratio of w_b/w_s is probably closer to 1.3 for beams with d_t values around 30 in. (or d values around 36 in.). For such beams the crack width at the main reinforcement level is more likely to be 0.009 to 0.010 in. when the crack width on the extreme tension face is 0.012 to 0.013 in., the implied maximum allowable values in the AASHTO and ACI provisions. Figure 6.9 shows the effect of depth on the maximum side face crack width in specimens without skin reinforcement and with various values of crack width at the main reinforcement level. For a maximum side face crack width of 0.015 to 0.016 in. and a maximum crack width at the main reinforcement level of 0.009 to 0.010 in., Fig. 6.9 indicates that the critical value of d_t is in the range of 26.5 to 28.5 in., which corresponds to a depth range of

33.5 to 35.6 in. (assuming $d_t = 0.8d$). Beams with depths below these values would have side face crack widths less than 0.015 to 0.016 in. For this reason it is suggested that beams with depths less than 36 in. (3 ft) be excluded from the requirement of providing skin reinforcement.

Based on this study, it is recommended that AASHTO and ACI adopt the following side face crack control reinforcement provision:

> Distribution of Skin Reinforcement. If the depth d exceeds 36 in., longitudinal skin reinforcement shall be uniformly distributed along the side faces of the member over the one-half of the depth nearest the principal reinforcement. The proportion of such reinforcement, ρ_{sk}, is the ratio of the total area of skin reinforcement to the sum of the areas of strips along each side face, each strip having a height of d/2 and a width of twice the distance from the center of the skin reinforcement to the side face but not more than one-half the web width. For d between 36 and 100 in., $\rho_{sk} \geq 0.00024\ (d - 30)$, and for d greater than 100 in., $\rho_{sk} \geq 0.011 + 0.000058d$, with d expressed in inches. The maximum spacing of the skin reinforcement shall be the smaller of d/10 or 12 in.
>
> Such reinforcement may be included in strength computations if a strain compatibility analysis is made to determine the stresses in the individual bars or wires.

Great precision should not be attached to any cracking data or crack prediction formulas. The objective of this provision is to reduce the objectionable very wide side face cracking observed in large structures. For example, design utilizing this provision would reduce the side face crack width magnification in the inverted T-beam bent caps of Chapter 1 from 2.5 to 1.4. Use of the last paragraph in the provision removes any severe economic penalty due to the increase in the required skin reinforcement.

Although this provision has been developed in terms of limiting the crack magnification ratio to 1.4, it actually limits the maximum crack widths on the side face. As previously discussed, the maximum crack width at the main reinforcement level considered acceptable by the present ACI and AASHTO provisions is approximately

0.011 in. This maximum crack width at the main reinforcement level increased by the CMR of 1.4 results in a maximum crack width on the side face of 0.0154 in. While a beam with a smaller crack width at the level of the main reinforcement may have a greater CMR, the product which is the side face crack width should not exceed this limit of 0.0154 in.

7.5 Illustration of Design Procedure

Design of beams with skin reinforcement can be separated into two cases. In the first case, the beam dimensions and the main tension reinforcement area are calculated neglecting the flexural strength contribution of the skin reinforcement. The required skin reinforcement ratio, ρ_{sk}, is calculated by

$$\rho_{sk} \geq 0.00024\ (d - 30) \quad \text{for } d \leq 100 \text{ in.}$$

$$\rho_{sk} \geq 0.011 + 0.000058\ d \quad \text{for } d > 100 \text{ in.}$$

This ratio of skin reinforcement is a geometric ratio with respect to areas along each side face symmetrical with the longitudinal skin reinforcement (see Fig. 7.13). Knowing the cover on the skin reinforcement, c, and choosing a bar diameter, D, the required total area of skin reinforcement is

$$A_{sk} = \rho_{sk} \times (\text{edge areas symmetrical with } A_{sk})$$

$$= \rho_{sk} \times (2c + D)\ (d/2)\ (2)$$

Half of this A_{sk} is evenly distributed along each side face in the lower half of the depth.

In the second case, the flexural capacity of the skin reinforcement is included in the design. A trial section and area of skin reinforcement are determined using the previous procedure. With this amount of skin reinforcement, the required area of main reinforcement is recalculated to satisfy the design moment.

Both of these cases are illustrated by redesigning the inverted T-beam bent cap discussed in Chapter 1, so that the CMR would be reduced from the original 2.5 to 1.4 in the redesigned bent cap. The cross section of the original bent cap is shown in Fig. 7.14. In the first case, the flexural strength contribution of the skin reinforcement is ignored and the cross section is the same as shown in Fig. 7.14. For this d of 87.8 in. (7.32 ft) the required skin reinforcement ratio is

$$\rho_{sk} = 0.00024(d - 30)$$
$$= 0.00024(87.8 - 30)$$
$$\rho_{sk} = 0.0139$$

Using the #8 bars for skin reinforcement with 2.875 in. clear cover over the skin reinforcement evenly distributed in one-half of the depth, this ρ_{sk} requires a skin reinforcement area of

$$A_{sk} = \rho_{sk} \times (2c + D)(d/2)(2)$$
$$= (0.0139(2 \times 2.875 + 1.0) \times (87.8/2)(2)$$
$$= 8.24 \text{ sq. in.}$$
$$= 10.4 - \#8 \text{ bars}$$
$$\text{Use } 10 - \#8 \text{ bars}$$

Half of this A_{sk} is evenly distributed along each side face over half of the depth nearest the principal reinforcement. The bars are distributed so that the first bar is located a spacing, s, away from the centroid of the principal reinforcement and the farthest bar is one spacing from middepth (see Fig. 7.11). Therefore, using a spacing of

$$s = (d/2)/6$$
$$= (87.8/2)/6 = 7.3$$
$$\text{Use } 7.25 \text{ in.}$$

This area of skin reinforcement is about 4.2 times the skin reinforcement area originally provided (six #5 bars). Since the area of skin reinforcement is so large (about 50 percent of the main reinforcement

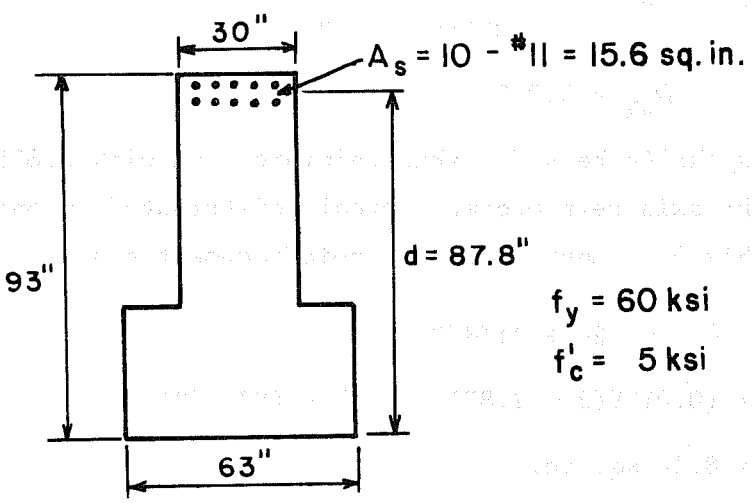

Fig. 7.14 Original bent cap section (only main flexural reinforcement shown)

area), it would be more economical to include the flexural strength of the skin reinforcement in the design, as done in the following case.

In the second case the flexural strength contribution of the skin reinforcement is included in the design. It is assumed that the original bent cap is the trial section; that is, d = 87.8 in. and the main reinforcement area is 15.6 sq. in. Proceeding as in the first case, the required ρ_{sk} is 0.0139, indicating a required skin reinforcement of ten #8 bars spaced at 7.25 in. The original bent cap had a calculated nominal moment capacity of 6700 kip-ft, assuming f_y = 60 ksi, f'_c = 5 ksi, and neglecting the six #5 bars (as in the original design). The new bent cap was designed for the same nominal capacity.

Approximate calculations assuming A_s = 15.6 sq. in. and A_{sk} = 0 (see Fig. 7.15) indicated that at ultimate moment capacity of the bent cap the skin reinforcement would be yielded. Complete design calculations are shown in Fig. 7.16, beginning with the chosen depth of 87.8 in. To satisfy the required nominal moment capacity, a main reinforcement area of 9.71 sq. in. is required. The reinforcement chosen was ten #9 bars to keep the distribution of main reinforcement the same in each bent cap (ten bars).

If the skin reinforcement is placed as required in the suggested provision, Grade 40 skin reinforcement will always be yielded at ultimate capacity of the member and in almost all cases (except for cases with ρ near ρ_{max}) Grade 60 skin reinforcement will also be yielded at ultimate.

Table 7.4 includes a summary of the original and redesigned bent cap designs. Although the redesigned bent cap has substantially more skin reinforcement than the original bent cap, the total reinforcement area is essentially the same in each if the bent cap is designed to include the flexural strength contributed by the skin reinforcement. Both have the same nominal moment capacity, using a yield stress of 60 ksi. In this case it is simply a matter of

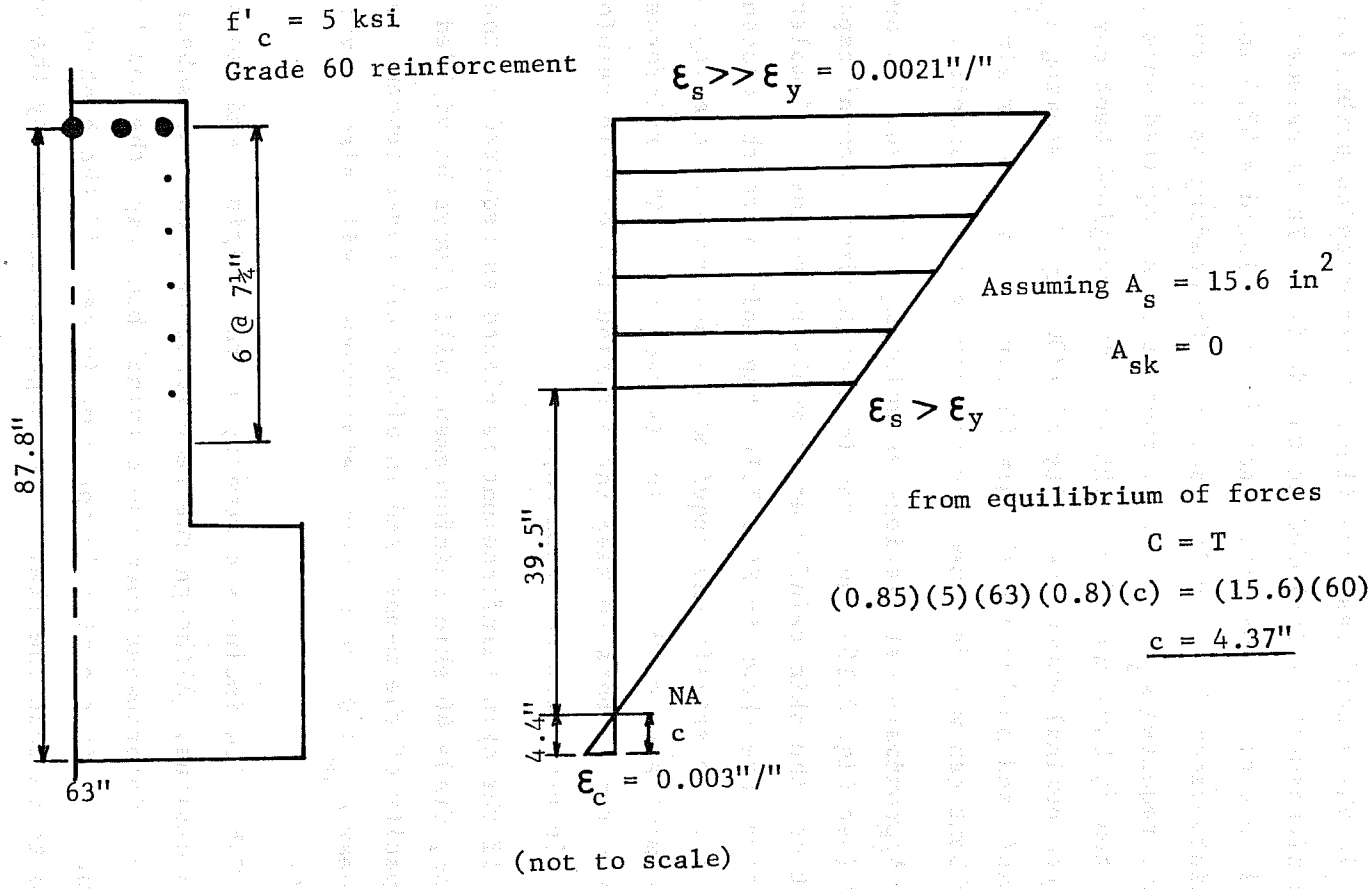

Fig. 7.15 Approximate calculations to check skin reinforcement stress

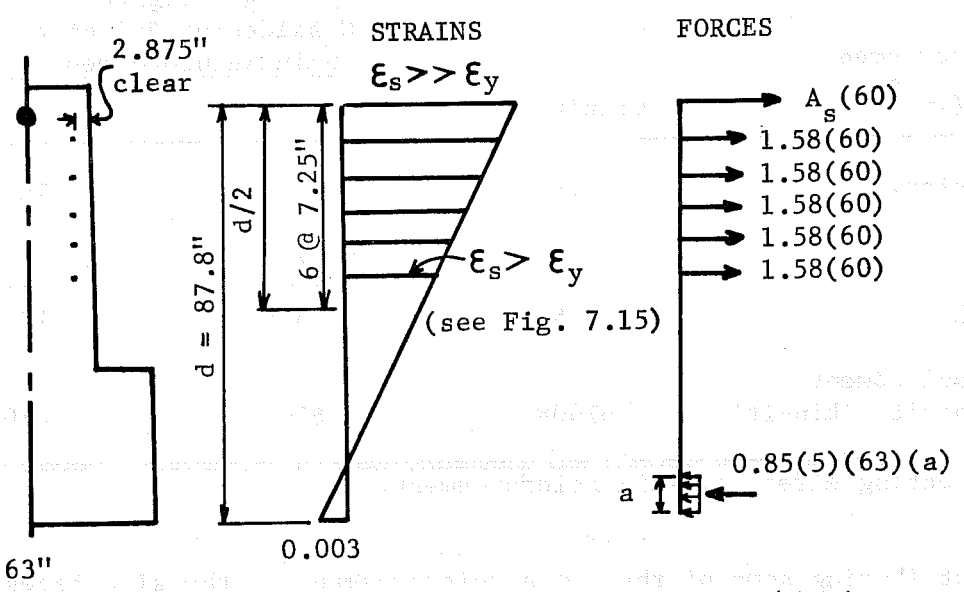

A_{sk}: $\rho_{sk} = 0.00024(d-30)$
$= 0.00024(87.8-30)$
$= 0.0139$

$A_{sk} = \rho_{sk}(2c + D)(d/2)(2)$
$= 0.0139(2x2.875+1.0)(\frac{87.8}{2})(2)$
$= 8.24$ sq. in. $= 10.4$ - #8
use 10 - #8 @ (d/2)/6 = 7.25 in.

$\Sigma F = 0$: $C = T$

$(0.85)(5)(63)(a) = (A_s + 7.9)(60)$

$267.8a = 60A_s + 474$

$a = 0.224A_s + 1.77$ ①

$\Sigma M = 0$ $M_n = 6700$ kip-ft $= 80400$ kip-in

ΣM about resultant of concrete compression force

$80400 = A_s(60)(87.8 - a/2) + 1.58(60)(5)(87.8 - 3(7.25) - a/2)$

$80400 = 5268A_s - 30A_s a + 31310 - 237a$

$A_s = \frac{49090 + 237a}{5268 - 30a}$ ②

solve ① and ② by trial and error

$a = 3.94$ in., $A_s = 9.71$ sq. in., use 10 - #9 Bars

Fig. 7.16 Redesign of bent cap

TABLE 7.4 COMPARISON OF ORIGINAL AND REDESIGNED BENT CAPS

Reinforcement ($in.^2$)	Original	Redesigned Considering Effect of Skin Reinforcement	
		No	Yes
Principal	15.6	15.6	10.0
Skin	1.9	7.9	7.9
Total	17.5	23.5	17.9
Nominal Moment Capacity (kip-ft)	6700*	6700*	6700

*Neglecting effect of skin reinforcement.

redistributing some of the main reinforcement to the side faces where it is also effective in side face crack control. By including the strength of the skin reinforcement in the design, the redesigned bent cap would cost no more than the original bent cap, but would have greatly reduced side face crack widths. Also, the distribution of a portion of the principal reinforcement along the side faces would lessen congestion and might make concrete placement easier leading to further economies.

7.6 Verification of Design Method

7.6.1 Specimen Design. To verify the design method it was felt necessary to redesign the original bent cap and test a 3/8-scale model. The design equations suggested in this study were formulated for structures with a crack width at the main reinforcement level of 0.011 in. at a stress of 35 ksi as calculated by the Gergely-Lutz equation. However, the full size bent cap had a calculated crack width of about 0.0125 in. at this stress level. To maintain accuracy in the 3/8 models (both in the original and in the redesigned bent caps) the larger crack width was used. The design equation can be modified for

this larger crack width by linearly scaling the equation as follows (see Sec. 7.3):

$$\rho_{sk} = 0.00024(d - 30)$$

for $w_s = 0.011$ in.

To change from $w_s = 0.011$ in. to $w_s = 0.0125$ in., use a scale factor of $0.0125/0.011 = 1.14$, so

$$\rho_{sk} = 0.00021(d - 34.2)$$

for $d = 87.8$ in.

$$\rho_{sk} = 0.0113 \text{ or } A_{sk} = 6.7 \text{ sq. in.}$$

A_{sk} = 8.5 - #8 bars

Use 8 - #8 bars at $(87.8/2)/5 = 8.75$ in.

With this amount of skin reinforcement, the required main tension reinforcement is 10.95 sq. in.

For a 3/8-scale model bent cap, these amounts reduce to $A_s = 1.54$ sq. in. and A_{sk} = eight #3 bars at 3.28 in. The main reinforcement chosen was five #4 plus five #3 bars to keep the distribution of main reinforcement the same in the original and redesigned bent caps (ten bars). The skin reinforcement spacing actually used was 3.5 in. rather than 3.28 in., because the specimen was constructed and tested before the design procedure suggested here was completely formalized. However, the difference is small and should not affect the results. Using this redesigned cross section, a reduced segment specimen (A-15) and a full length bent cap specimen (BC-2) were constructed and tested.

Table 7.5 includes a summary of the original and redesigned bent cap designs. Both have the same nominal moment capacity. By including the flexural strength contributed by the skin reinforcement, the redesigned bent cap has essentially the same total reinforcement area as the original bent cap. The redesigned bent cap would cost no more than the original bent cap.

TABLE 7.5 COMPARISON OF ORIGINAL AND REDESIGNED MODEL BENT CAPS

	Original	Redesign
CMR		
Desired	---	1.4
Measured	2.5	1.2
Reinforcement ($in.^2$)		
Principal	2.22	1.55
Skin	0.26	0.88
Total	2.48	2.43
Moment Capacity (kip-ft)		
Nominal (f_y = 60 ksi)	353*	351
(with A_{sk} and actual f_y)	432	406
Measured Ultimate	473	443
Measured/Predicted	1.09	1.09

*Neglecting effect of skin reinforcement.

7.6.2 Test Results. The crack patterns for the redesigned reduced segment specimen A-15 and the full length bent cap specimen BC-2 (Appendix A) were very similar and had significantly more cracks extending down the side face than the original specimens (for example, RS-3 and BC-1). The average crack profiles of these four specimens are compared in Fig. 7.17. Figure 7.17a and Fig. 7.17b compare the profiles at equal main reinforcement stresses of 30 and 40 ksi. The profiles of the segments are generally in good agreement with the companion full length specimens. Since both the original and redesigned specimens have the same distribution of main reinforcement (ten bars), the maximum crack width as the main reinforcement level at f_s = 35 ksi is predicted by the Gergely-Lutz equation to be approximately 0.0048 in. in each. Although the redesigned bent cap, BC-2, has the

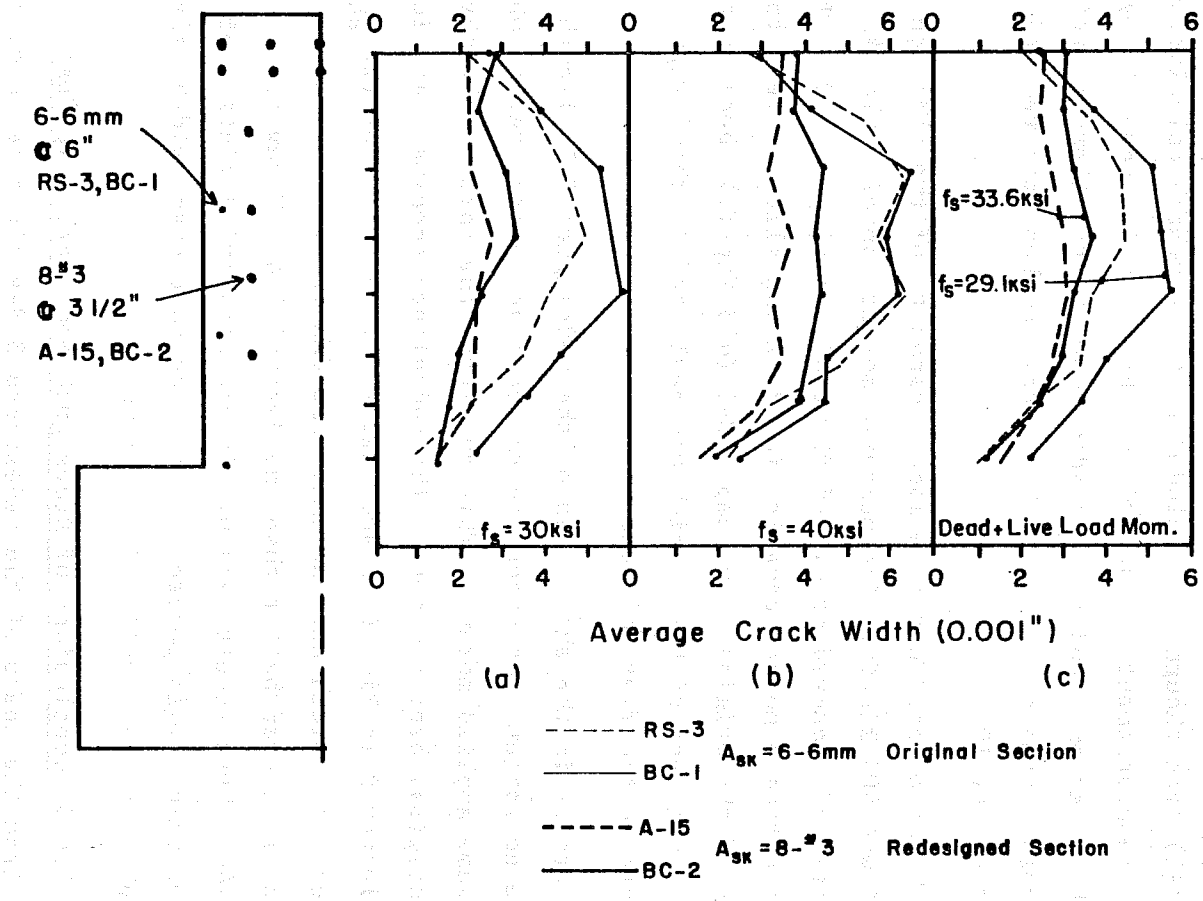

Fig. 7.17 Crack profiles--original and redesigned model bent caps

highest crack width at the main reinforcement level for f_s = 40 ksi, it is still within the accuracy of the equation (±33 percent). In Fig. 7.17c the specimens are compared at the same applied moment of full dead plus full live load moment. The main reinforcement stress in the redesigned specimens is higher than in the original specimens because (1) even though not included in the strength calculations, the skin reinforcement of the original bent cap increased the yield moment by 4 percent, and (2) spreading more of the flexural reinforcement across a greater depth in the redesigned bent cap reduced the yield moment by 10 percent.

The predicted ultimate moment capacity of the redesigned bent cap BC-2 was 406 kip-ft. The measured moment capacity was 443 kip-ft for a ratio of measured/predicted flexural capacity of 1.09. The measured ultimate moment capacity for BC-2 was slightly less than the capacity of the original bent cap, BC-1 (473 kip-ft), because the side face reinforcement of BC-1, which was neglected in the design, did contribute to the flexural capacity.

Cracks in the shear span of the redesigned full length bent cap were no larger than cracks in the constant moment region observed at the same applied moment. This confirmed the same result observed in the original bent cap test. The redesigned specimens are identified by the letter R in Fig. 6.43 and Fig. 6.44, the plots of $(1/\rho_{sk})$ vs the side face crack width and the CMR. The CMR of both redesigned specimens was about 1.2, even better than the desired 1.4. However, as shown in Fig. 6.44d, these results are within one standard deviation of the predicted values (±15 percent). The side face crack widths also agree quite well with the predicted values in Fig. 6.43.

7.6.3 Conclusions of Redesigned Model Bent Cap Test. The results from the tests of the redesigned 3/8-scale model specimens, A-15 and BC-2, support the following conclusions:

(1) In this test, cracks in the shear span were not significantly larger than cracks in the constant moment region.

(2) There was no apparent decrease in flexure or shear capacity in the redesigned structure.

(3) The skin reinforcement percentage used in the redesigned structure was the same as calculated by the suggested design procedure.

(4) The measured crack magnification ratio in both redesigned specimens was 1.2, even better than the desired 1.4.

7.7 Summary

This chapter used the experimental and analytical results of this study to develop a design method to reduce the wide crack widths that can develop on the side faces of large reinforced concrete beams. A method was presented for determining how much crack width increase is acceptable for cracks extending down the side faces of a flexural member, and a permissible crack magnification ratio of 1.4 was suggested. The model test results were reduced to a series of equations relating the tension depth of the specimen to the predicted skin reinforcement ratio for various CMR's. These model results were then linearly scaled to predict the behavior of larger structures. It was shown that the results of this study adequately explain the side face crack width results from a series of tests reported by Soretz and Colanna-Ceccaldi. The equations were then modified to relate the beam depth rather than the tension depth to the required skin reinforcement. A detailed code provision was suggested for limiting the maximum side face crack widths to about 0.015 to 0.016 in. (a CMR of about 1.4) in full size structures subjected to exterior exposure. The design method was verified by redesigning the 3/8-scale model bent cap of Chapter 3 so that the crack magnification ratio would be reduced from the original 2.5 to about 1.4 Tests of a redesigned 3/8-scale model full length bent

cap specimen and a companion reduced segment specimen yielded measured CMR's of about 1.2, even better than the desired 1.4. This improved performance was achieved without any increase in the cost of the structure.

CHAPTER 8

CONCLUSIONS AND RECOMMENDATIONS

8.1 General

A number of large reinforced concrete highway bent caps, designed according to AASHTO and ACI provisions, had cracks near mid-depth on the side faces that were up to three times as wide as cracks at the main reinforcement level. Wide side face cracking is not only unsightly, but it also indicates potential corrosion and durability problems. The overall objective of this study was to develop a simple and effective design method to reduce the wide crack widths that can develop on the side faces of large reinforced concrete beams.

Preliminary tests indicated that the side face cracking problem could be studied using laboratory size specimens. In the experimental study a series of 44 specimens examined the variables that affect side face cracking: amount and distribution of side face reinforcement, cover, web width, and beam depth. The results of a two-dimensional finite element analysis were in general agreement with the laboratory results. A new design procedure was developed and simplified for code use. It was verified by redesigning and testing the original model bent cap specimen that had the serious side face cracking problem.

This study has the following limitations:

(1) All loading was short term and one cycle.
(2) The beam depth/web width ratio varied from 1.9 to 4.2.
(3) The effect of high shear forces was not studied.
(4) Model beams with tension zones up to 40 in. deep were studied.

Using a very conservative scale factor of 8/3, the test results are applicable to full size beams with tension zones up to 108 in. deep or overall depths up to approximately 144 in. or 12 ft.

8.2 Conclusions

The major conclusions from this study are summarized below.

(1) Specimens with the prescribed AASHTO and ACI amounts of side face crack control reinforcement had side face cracks that near middepth were well over twice as wide as cracks at the main reinforcement level (see Secs. 1.2 and 3.2.4).

(2) Providing a relatively small amount of side face (or skin) reinforcement significantly reduced the side face crack widths and the crack magnification ratio. As the provided area of skin reinforcement increased, the side face crack width decreased, but at a decreasing rate (see Secs. 5.2.3, 6.6, 6.7, and 6.8).

(3) Very large amounts of skin reinforcement were required as the crack magnification ratio approached 1.0. However, accepting maximum side face crack widths about 40 percent larger than the maximum crack widths at the main reinforcement level is a reasonable solution to the side face cracking problem because of economy and the decreased probability of corrosion of the shear reinforcement (see Sec. 7.2).

(4) Skin reinforcement affected only a narrow strip of concrete along each side face of the web. The effectiveness of the skin reinforcement in controlling crack widths on the side faces was independent of web width in series of otherwise identical specimens (see Sec. 6.4).

(5) A detailed design recommendation was developed (see Sec. 7.4).

Other important conclusions from this study are summarized below.

(1) The laboratory models very accurately reproduced both the crack pattern and crack widths of the prototype at 3/8 scale, using the direct modeling technique which employed deformed bars and reduced maximum size aggregate (see Sec. 3.2.4).

(2) The reduced segment specimen accurately reproduced the crack pattern, the crack widths, and the deformation of a region of a full length beam under constant moment (see Sec. 3.3.3.4).

(3) The wide side face cracking problem can exist under conditions of pure moment as well as with shear present (see Sec. 3.2.4).

(4) Side face cracks in the shear span were not noticeably larger than cracks in the constant moment region at the same applied moment (see Secs. 3.2.4 and 7.6.2).

(5) The moment capacities of the test specimens were not affected by wide side face cracks (see Sec. 3.2.4).

(6) A series of three reduced segment specimens, identical except for concrete compressive strength, had very similar crack patterns and side face crack width profiles, indicating good reproducibility of results (see Sec. 3.3.3.4).

(7) A variation in the concrete compressive strength from 2944 psi to 4290 psi did not noticeably affect the crack pattern development or the side face crack widths in three otherwise identical specimens (see Secs. 3.3.3.4 and 6.3.1).

(8) The crack magnification ratio (the ratio of maximum crack width on the side face to crack width at the main reinforcement level) stayed fairly constant as the applied load varied from first cracking to yield (see Sec. 6.1.2).

(9) Without any skin reinforcement a "tree branch" crack pattern developed where several of the cracks originating on the extreme tension face curved and joined together to form one wide crack extending into the web. As the area of skin reinforcement increased, this crack pattern gradually changed to one where more cracks remained vertical and extended further down into the web, resulting in smaller crack widths near middepth. Modification of the crack pattern is one of the principal benefits from using skin reinforcement (see Sec. 6.2.2).

(10) The amount of skin reinforcement can be expressed as a skin reinforcement ratio based on the area of skin reinforcement divided by the edge strip area of concrete affected by the skin reinforcement. These edge strips are symmetrical about the skin reinforcement along each side face with a width defined as twice the distance from the center of the skin reinforcement to the side face and a height defined as the distance from the centroid of the main reinforcement to one bar spacing beyond the skin reinforcement bar farthest from the main reinforcement (see Secs. 6.5 and 6.9).

(11) A simple two-dimensional finite element model idealizing the side face cracking problem indicated very similar results when compared to the physical models tested in the laboratory (see Sec. 6.8).

(12) Both the laboratory tests and the finite element analysis indicated it was most effective to place the skin reinforcement as many distributed small bars rather than as a few large bars. Generally, bars evenly distributed along each side face in about one-half to two-thirds of the tension zone closest to the main reinforcement were adequate. To ensure effective distribution, the maximum spacing of these bars should be the smaller of d/10 or 12 in. (see Secs. 5.2.3, 6.8, and 7.4).

(13) Welded wire fabric mesh was as effective as deformed bars for skin reinforcement (see Secs. 6.7 and 6.9).

(14) Using the skin reinforcement ratio and either the side face crack widths or the crack magnification ratios, regression equations were derived that described the data well. Using the average crack magnification ratio, 68 percent of the measured crack magnification ratios were within 15 percent of the predicted values, which is very acceptable scatter in cracking studies (see Sec. 6.9).

(15) As the beam tension depth increased, the side face crack width increased, and the ratio of skin reinforcement required to maintain a maximum side face crack width also increased (see Secs. 6.7 and 6.9).

8.3 Recommendations

On the basis of the laboratory tests and the finite element analysis, it is suggested that ACI and AASHTO adopt the following skin reinforcement design provision (as developed in Chapter 7):

> Distribution of Skin Reinforcement. If the depth, d, exceeds 36 in., longitudinal skin reinforcement shall be uniformly distributed along the side faces of the member over the one-half of the depth nearest the principal reinforcement. The proportion of such reinforcement, ρ_{sk}, is the ratio of the total area of skin reinforcement to the sum of the area of strips along each side face, each strip having a height of d/2 and a width of twice the distance from the center of the skin reinforcement to the side face but not more than one-half the web width. For d between 36 and 100 in., $\rho_{sk} \geq 0.00024(d - 30)$, and for d greater than 100 in., $\rho_{sk} \geq 0.011 + 0.000058d$, with d expressed in inches. The maximum spacing of the skin reinforcement shall be the smaller of d/10 or 12 in.
>
> Such reinforcement may be included in strength computations if a strain compatibility analysis is made to determine the stresses in the individual bars or wires.

A finite element analysis provided the basis for extrapolating the results to beams with tension zones exceeding 80 in. deep (see Sec. 7.3). This suggested design procedure was proven by redesigning and testing the original model bent cap specimen that had the serious side face cracking problem (see Sec. 7.6). The test was successful. Although the new design procedure requires substantially more skin reinforcement for large beams than the present provisions do, it appears that the side face cracking problem can be controlled at little or no additional cost by including the flexural strength contribution of the skin reinforcement (see Secs. 7.5 and 7.6).

REFERENCES

1. Kliethermes, J. C., "Repair of Spalling Bridge Decks," Highway Research Record, No. 400, 1972, pp. 83-92.

2. Depuy, G. W., and Dikeou, J. T., "Development of Polymer-Impregnated Concrete as a Construction Material for Engineering Projects," ACI Publication, SP-40, Detroit, 1973, pp. 33-56.

3. ACI Committee 201, "Durability of Concrete in Service," Journal of the American Concrete Institute, Vol. 59, December 1962, pp. 1772-1820.

4. "Corrosion of Steel in Concrete," RILEM Symposium on Bond and Crack Formation in Reinforced Concrete, Stockholm, Vol. III, 1957, pp. 239-247.

5. Husain, S. I., and Ferguson, P. M., "Flexural Crack Width at Bars in Reinforced Concrete Beams," Research Report 102-1F, Center for Highway Research, The University of Texas at Austin, June 1968.

6. Interim Specifications - Bridges, 1976, American Association of State Highway and Transportation Officials, Washington, D.C., 1976.

7. ACI Committee 318, Building Code Requirements for Reinforced Concrete (ACI 318-77), American Concrete Institute, Detroit, 1977.

8. ACI Committee 224, "Control of Cracking in Concrete Structures," Journal of the American Concrete Institute, No. 12, Vol. 69, December 1972.

9. Recommendation International CEB-FIP, 1970, Comite Europeen du Beton - Federation Internationale de la Precontrainte, Paris, 1970.

10. Kaar, P. H., and Mattock, A. H., "High Strength Bars as Concrete Reinforcement, Part 4 - Control of Cracking," Journal of the PCA Research and Development Laboratories, Vol. 5, No. 1, January 1963, pp. 15-38.

11. Beeby, A. W., "An Investigation of Cracking on the Side Faces of Beams," Technical Report 42.466, Cement and Concrete Association, London, December 1971.

12. Soretz, S., and Colonna-Ceccaldi, J., "Large Reinforced Concrete Beams with a Main Reinforcement Consisting of Two Thick Bars," Betonstahl in Entwicklung, Vol. 46, published by TOR-ISTEG Steel Corporation, Luxembourg, March 1972.

13. Filho, F. M. G., "A Simplified Test Method for Determination of Reinforced Concrete Side Face Crack Profiles," unpublished M.S. thesis, The University of Texas at Austin, May 1977.

14. Hognestad, E., "High Strength Bars as Concrete Reinforcement, Part 2 - Control of Flexural Cracking," Journal of the PCA Research and Development Laboratories, Vol. 5, No. 1, January 1962, pp. 46-63.

15. Brice, L. P., "Relation Entre 1'Ouverture des Fissures, la Constrainte des Aciers et les Diverses Caracteristiques d'Une Piece en Beton Arme," RILEM Symposium on Bond and Crack Formation in Reinforced Concrete, Stockholm, Vol. I, 1957, pp. 39-48.

16. Odman, S. T. A., "Slip between Reinforcement and Concrete," RILEM Symposium on Bond and Crack Formation in Reinforced Concrete, Stockholm, Vol. II, pp. 407-420.

17. Bulletin d'Information, No. 12, Comite Europeen du Beton, translated by Cement and Concrete Association, London, February 1959.

18. Watstein, D., and Mathey, R. G., "Width of Cracks in Concrete at the Surface of Reinforcing Steel Evaluated by Means of Tensile Bond Specimens," Journal of the American Concrete Institute, Proc. Vol. 56, July 1959, pp. 47-56.

19. Gergely, P., and Lutz, L., "Maximum Crack Width in Reinforced Concrete Beams," Causes, Mechanisms, and Control of Cracking in Concrete, SP-20, American Concrete Institute, Detroit, 1968, pp. 87-117.

20. Base, G. D., Read, J. B., Beeby, A. W., and Taylor, H. P. J., "An Investigation of the Crack Control Characteristics of Various Types of Bar in Reinforced Concrete Beams," London, Research Report No. 18, Part I and Part II, Cement and Concrete Association, London, December 1966.

21. Ferry-Borges, J., "Cracking and Deformability of Reinforced Concrete Beams," Bulletin d'Information, No. 61, Comite Europeen du Beton, June 1967, pp. 33-77.

22. Albandar, F., and Mills, G. M., "The Prediction of Crack Widths in Reinforced Concrete Beams," Magazine of Concrete Research, Vol. 26, No. 88, September 1974.

23. Bulletin d'Information, No. 61, Comite Europeen du Beton, June 1967, pp. 22-23.

24. Chow, L., Conway, H., and Winter, G., "Stresses in Deep Beams," Transactions, American Society of Civil Engineers, Vol. 118, 1953, pp. 686-708.

25. Ros, M., "Fortschritt, Erfolgung die zukunftige Gestaltung des Stahlbetons in der Schweiz," Zement und Beton, No. 11, February 1958.

26. Lazard, A., "Essay jusqu'a rupture de poutres armees 1'une en acier TOR 40, 1'autre en ronds ordinaires," Preliminary Publication, Fifth Congress, International Association for Bridge and Structural Engineering, Lisbon, 1956, pp. 753-762.

27. Lazard, A., "Essais jusqu'a rupture de poutres armees d'acier TOR 60 et 80," International Association for Bridge and Structural Engineering, Publications Vol. 16, Zurich, 1956, pp. 333-344.

28. Gaston, J., and Hognestad, E., "Precast Concrete Girders Reinforced with High Strength Deformed Bars," Journal of the American Concrete Institute, Vol. 30, No. 4, October 1958, pp. 469-484.

29. Gaston, J., and Hognestad, E., "High Strength Bars as Concrete Reinforcement, Part 3 - Tests of Full-Scale Roof Girders," Journal of the PCA Research and Development Laboratories, Vol. 4, No. 2, May 1962, pp. 10-23.

30. Beeby, A. W., "An Investigation of Cracking in Slabs Spanning One Way," Technical Report TRA 443, Cement and Concrete Association, London, April 1970.

31. Beeby, A. W., "A Study of Cracking in Reinforced Concrete Members Subjected to Pure Tension," Technical Report 42.468, Cement and Concrete Association, London, June 1972.

32. From personal correspondence with B. Neubert and G. Rehm, Department of Structural Engineering, University of Stuttgart, Stuttgart, Germany, May 1976.

33. ASCE-ACI Task Committee 426, "The Shear Strength of Reinforced Concrete Members, Journal of the Structural Division, ASCE, Vol. 99, No. ST6, June 1973.

34. "Design of Deep Beams," Concrete Information, No. ST66, Structures Bureau, Portland Cement Association, Skokie, Illinois, 1944.

35. Preece, B. W., and Davies, J. D., Models for Structural Concrete, CR Limited, The Adelphi, John Adam Street, London, WC2, 1964.

36. Ferry-Borges, J., and Lima, J. A., "Crack and Deformation Similitude in Reinforced Concrete," RILEM Bulletin No. 7, Paris, June 1960, pp. 79-90.

37. Janney, J. R., "Microconcrete Models--Comparison of Failure Loads and Behavior with Prototype Test Members," Protective Structures Development Center, Department of the Army, Washington, D.C., May 1967.

38. Alami, Z., "Accuracy of Models Used in Research on Reinforced Concrete," Ph.D. dissertation, The University of Texas at Austin, June 1962.

39. Swamy, R. N., and Shamsuddin, A. Q., "Cracking and Deformational Similitude in Reinforced T Beams under Bending and Shear," Part I, Journal of the American Concrete Institute, Vol. 68, March 1971, pp. 187-195. (Part II available from ACI Headquarters.)

40. Kaar, P. H., "An Approach to the Control of Cracking in Reinforced Concrete," Causes, Mechanisms, and Control of Cracking in Concrete, SP-20, American Concrete Institute, Detroit, 1968, pp. 141-157.

41. Clark, L. A., "Crack Similitude in 1:3.7 Scale Models of Slabs Spanning One Way," Technical Report 42.455, Cement and Concrete Association, London, 1971.

42. Kani, G. N. J., "The Riddle of Shear Failure and Its Solution," Journal of the American Concrete Institute, Proc. V. 61, April 1964, p. 441.

43. Kemp, E. L., and Wilhelm, W. J., "An Investigation of the Parameters Influencing Bond Behavior with a View Towards Establishing Design Criteria," Interim Research Report WVDOH 46-1, Department of Civil Engineering, West Virginia University, Morgantown, August 1974.

44. Herrin, T. R., "Welded Wire Fabric for Control of Side Face Cracking in Reinforced Concrete Beams," unpublished M.S. report, The University of Texas at Austin, August 1977.

45. Nilson, A. H., "Nonlinear Analysis of Reinforced Concrete by the Finite Element Method," Journal of the American Concrete Institute, Vol. 65, September 1968, p. 757.

46. Nixon, O. D., Manuel, R. F., and Bowes, W. H., "Finite Element Analysis of Diagonal Cracking Behavior in Reinforced Concrete," Engineering Journal, Montreal, Vol. 56, No. 7-8, July-August 1973, p. i-v.

47. Nam, C., and Salmon, C., "Finite Element Analysis of Concrete Beams," Journal of the Structural Division, ASCE, Vol. 100, ST12, December 1974, pp. 2419-2432.

48. Rostam, S., and Byskov, E., "Fracture Mechanics Approach to Determine Crack Lengths in Concrete Structures Utilizing the Finite Element Method," Bulletin d'Information, No. 89, Comite Europeen du Beton, March 1973.

49. Faulkner, H., "Manual on Cracking," Bulletin d'Information, No. 89, Comite Europeen du Beton, March 1973.

50. Beeby, A. W., "Suggested Modifications to the Crack Prediction Formula in the 1970 CEB Recommendations," Bulletin d'Information, No. 89, Comite Europeen du Beton, March 1973.

51. Dunham, R. S., and Becker, E. B., "TEXGAP--The Texas Grain Analysis Program," TICOM Report 73-1, The Texas Institute for Computational Mechanics, The University of Texas at Austin, August 1973.

52. Williams, D., An Introduction to the Theory of Aircraft Structures, Edward Arnold LTD, London, 1960.

53. Dixon, W. J. (Ed.), BMD - Biomedical Computer Programs, Health Sciences Computing Facility, Department of Biomathematics, School of Medicine, University of California, Los Angeles, University of California Press, January 1973.

54. Frantz, G. C., "Control of Cracking on the Side Faces of Large Reinforced Concrete Beams," unpublished Ph.D. dissertation, The University of Texas at Austin, August 1978.

A P P E N D I X A

CRACK PATTERNS AT 35 KSI

CRACK WIDTH DATA

NUMBER OF CRACKS ON SIDE FACE

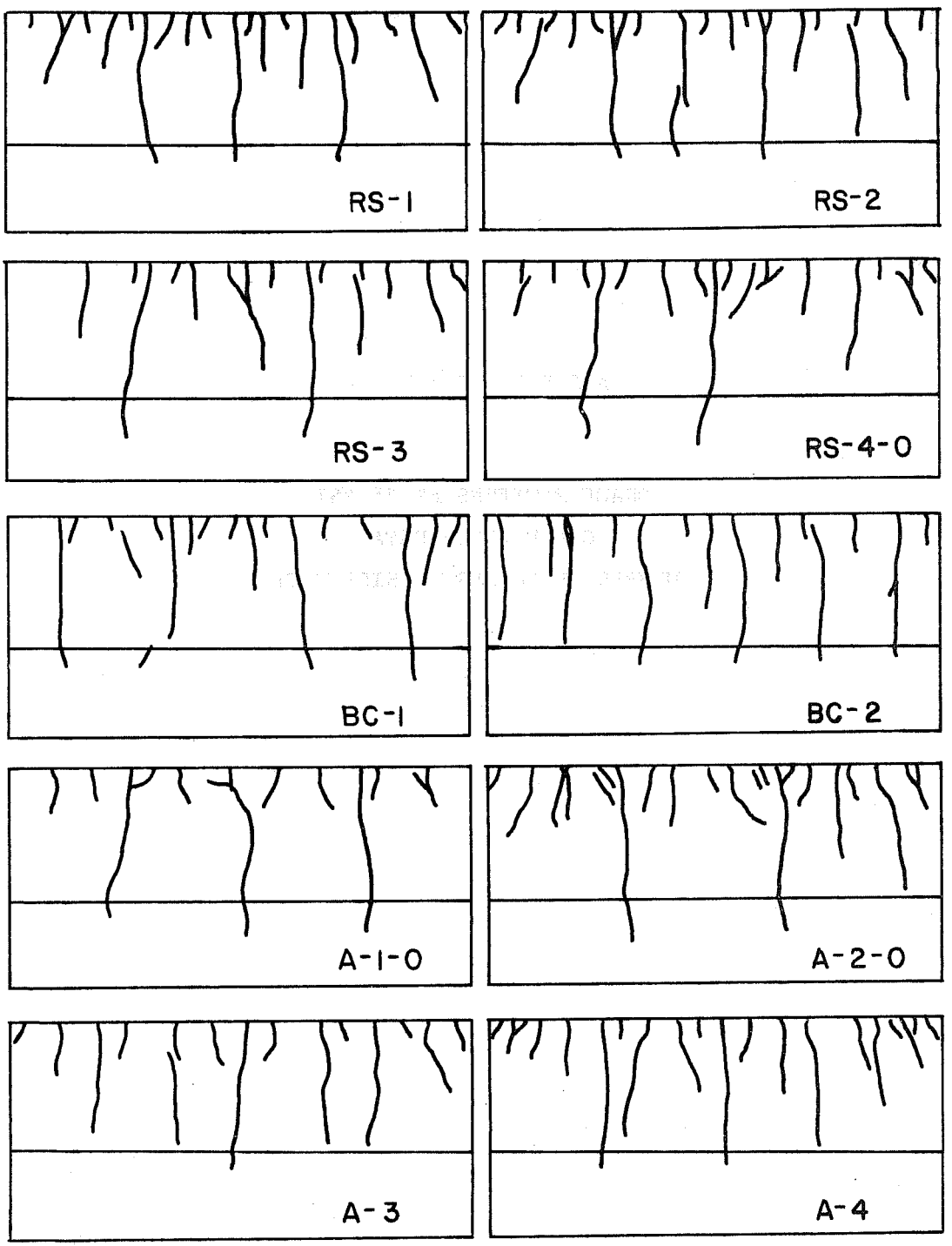
RS-1
RS-2
RS-3
RS-4-0
BC-1
BC-2
A-1-0
A-2-0
A-3
A-4

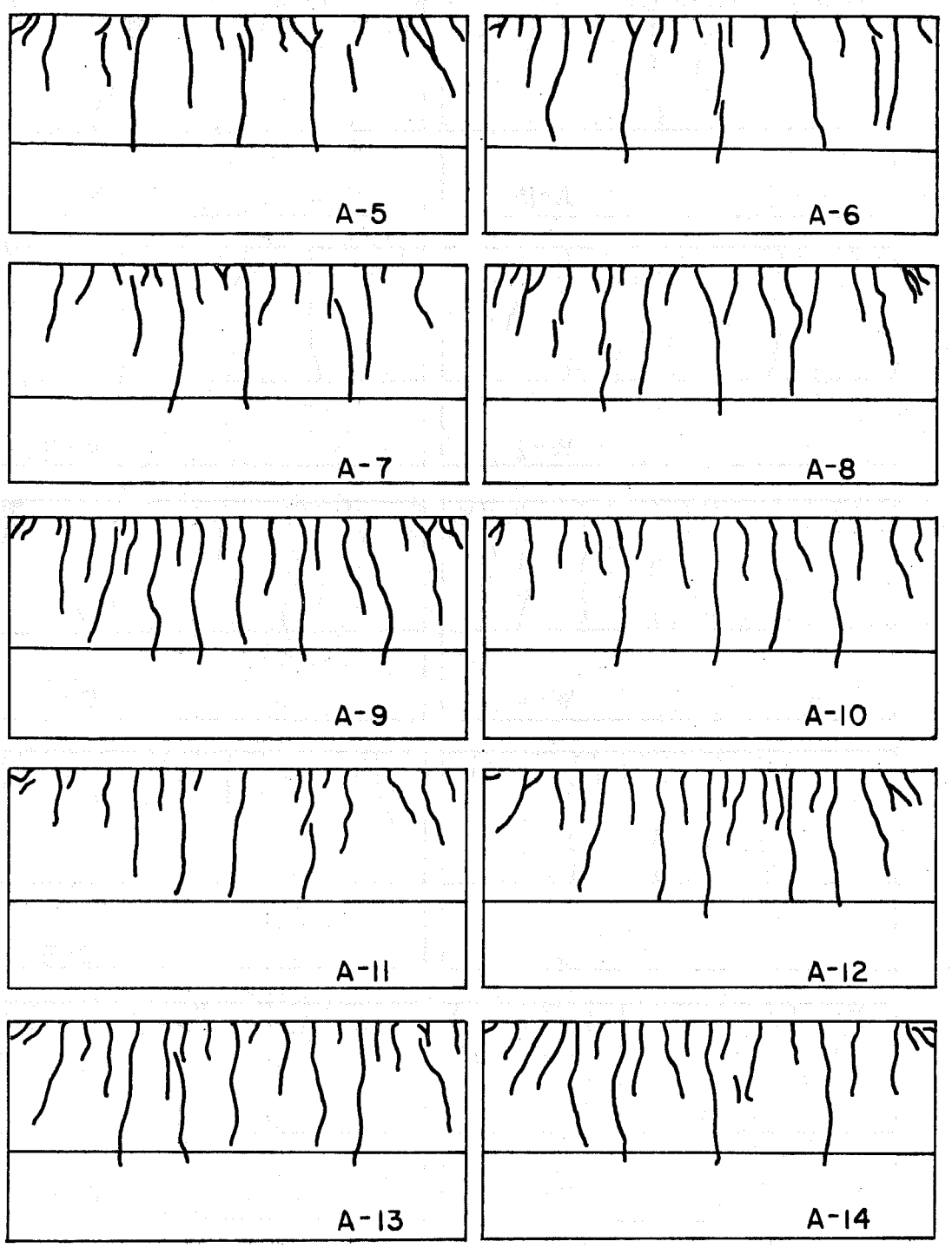
A-5
A-6
A-7
A-8
A-9
A-10
A-11
A-12
A-13
A-14

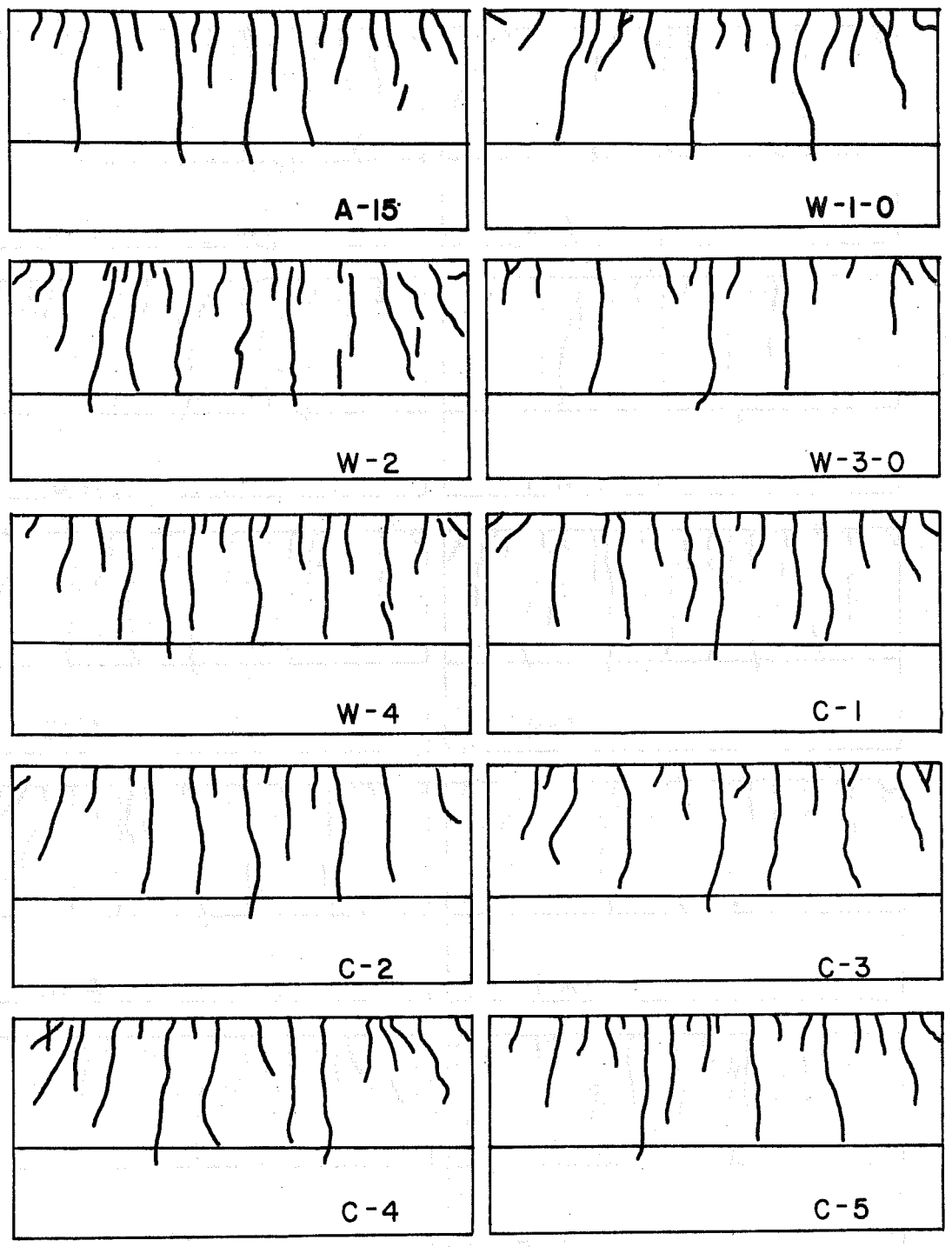
A-15
W-1-0
W-2
W-3-0
W-4
C-1
C-2
C-3
C-4
C-5

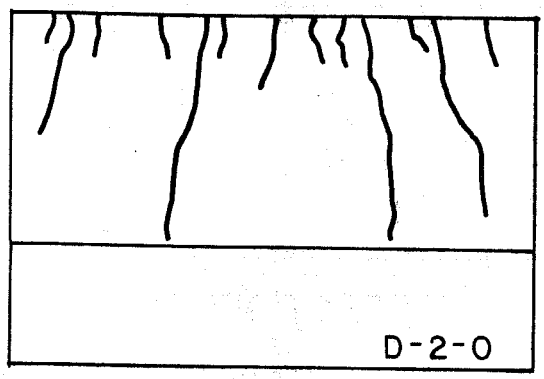
D-2-0

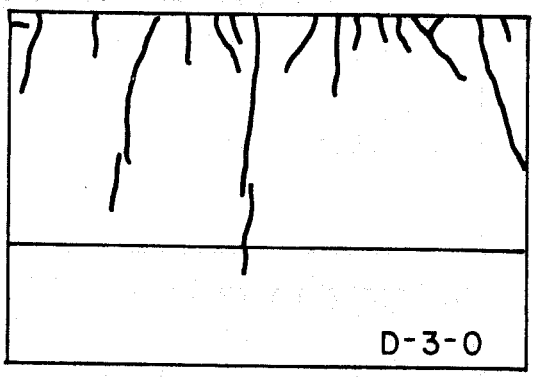
D-3-0

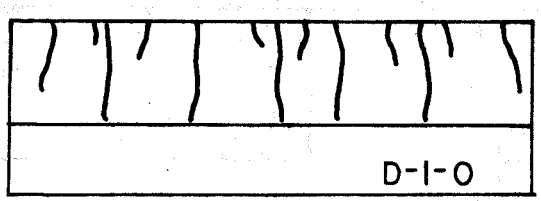
D-1-0

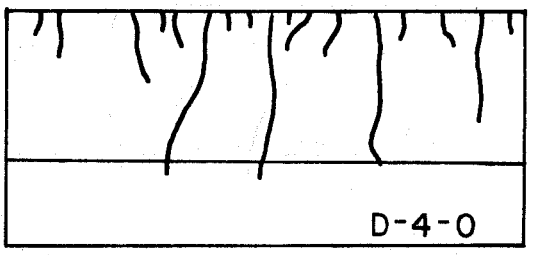
D-4-0

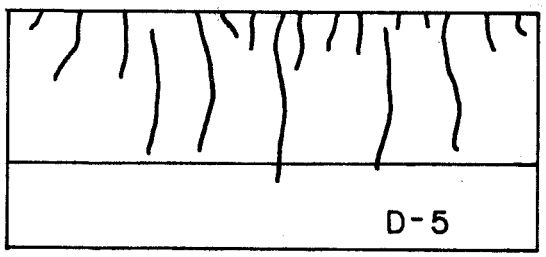
D-5

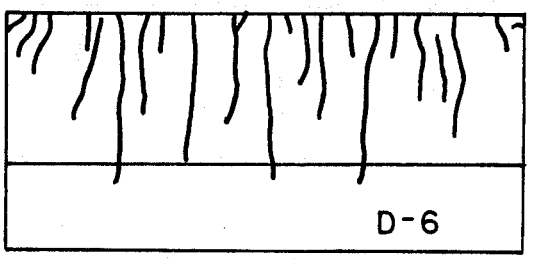
D-6

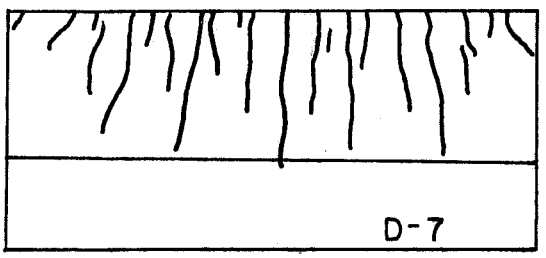
D-7

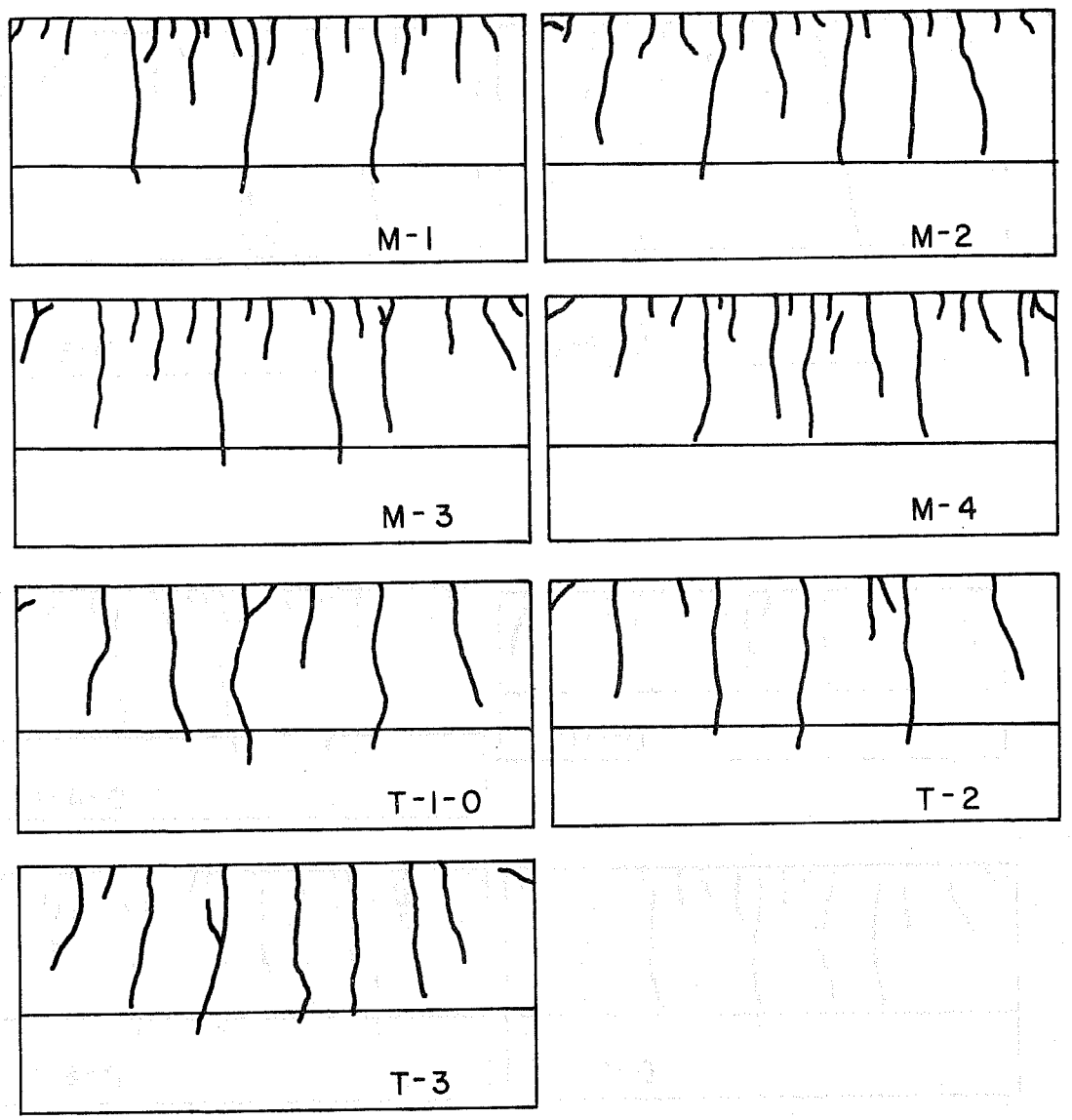
M-1
M-2
M-3
M-4
T-1-0
T-2
T-3

Specimen	Crack Width (0.001") (Average / Maximum) @ ___ Ksi: At Main Steel Level				In Web				Number of Cracks (at Main Steel Level / at Web Middepth) @ ___ Ksi			
	25	30	35	40	25	30	35	40	25	30	35	40
RS-1	1.6 3	1.8 3	2.0 4	2.4 5	4.6 8	5.1 9	5.9 10	6.2 14	19 6	-	29 7	31 9
RS-2	1.3 3	1.6 3	1.8 4	2.4 5	3.6 6	4.7 8	5.7 10	6.8 12	19 6	-	28 8	29 8
RS-3	1.7 3	2.1 4	2.4 6	2.8 8	4.3 5	4.5 8	5.1 10	6.2 12	16 5	-	25 8	28 8
RS-4-0	2.0 4	2.8 5	3.5 6	4.0 7	5.2 8	8.1 14	10.9 20	12.2 22	17 6	-	23 6	28 6
BC-1	2.0 4	2.5 6	2.9 6	3.0 7	4.8 11	5.8 11	6.2 13	6.4 15	23 10	24 10	-	31 10
BC-2	2.0 3	2.7 4	3.4 6	3.8 7	2.0 3	3.2 6	3.9 7	4.5 8	-	27 16	30 16	37 18
A-1-0	2.1 4	2.7 5	3.2 6	4.0 8	7.2 10	8.7 15	9.8 18	9.7 20	18 6	18 6	19 6	21 6
A-2-0	1.8 3	2.3 4	2.6 5	3.2 6	5.2 8	8.0 14	9.5 15	11.2 17	19 6	23 6	26 6	27 6
A-3	2.0 4	2.1 4	2.6 5	3.0 6	3.6 8	3.9 7	5.2 9	6.0 10	14 4	20 9	22 10	-
A-4	2.2 3	2.5 4	3.2 5	3.4 6	4.6 6	4.0 7	4.2 8	4.4 9	19 6	21 10	22 10	24 12
A-5	2.0 4	2.4 4	2.9 5	3.2 6	3.9 6	4.0 7	4.4 8	5.3 10	20 8	20 8	24 9	27 11
A-6	2.2 5	2.9 6	2.9 8	4.1 10	6.2 9	7.9 10	8.3 12	10.4 14	25 9	27 9	29 9	30 10
A-7	2.1 4	2.3 5	2.5 6	3.2 9	3.3 6	4.3 8	5.5 10	5.8 14	16 7	22 9	28 9	28 10
A-8	1.9 3	2.5 4	2.8 6	3.4 7	3.4 5	3.7 6	3.9 7	4.4 8	23 9	23 10	28 10	28 11
A-9	2.2 4	2.8 6	3.2 6	-	3.4 5	3.8 7	3.9 8	-	25 13	26 15	28 16	-
A-10	2.0 4	2.4 5	3.3 5	3.8 6	4.6 6	5.0 8	5.2 9	6.1 10	19 6	27 8	27 9	27 9
A-11	1.8 3	2.3 4	2.6 5	2.7 6	2.7 4	3.4 5	4.1 6	4.9 7	13 6	18 8	22 9	26 10
A-12	1.7 3	2.3 4	2.8 5	-	2.2 4	2.7 5	3.2 5	-	21 10	24 12	28 13	-
A-13	2.2 5	2.8 7	3.4 8	3.9 10	3.2 6	3.6 9	3.8 11	5.1 10	25 12	25 13	26 18	28 13
A-14	2.0 3	2.7 5	3.0 5	3.6	2.8 5	3.4 7	4.3 8	4.1	26 9	29 11	30 14	31 14
A-15	1.6 2	2.1 4	2.9 4	3.5 5	2.5 4	2.8 5	3.4 6	3.8 7	16 4	28 8	29 10	30 13
C-1	1.8 5	2.5 5	3.0 6	3.8 8	2.9 4	2.9 5	3.5 6	3.9 6	19 7	22 11	22 12	23 12

Specimen	Crack Width (0.001") (Average / Maximum) @ ___ Ksi: At Main Steel Level				In Web				Number of Cracks (at Main Steel Level / at Web Middepth) @ ___ Ksi			
	25	30	35	40	25	30	35	40	25	30	35	40
C-2	1.8 3	2.3 5	2.4 5	3.0 6	2.3 4	3.1 5	3.5 7	4.1 9	19 7	22 10	25 13	27 13
C-3	1.9 4	2.2 4	2.4 6	2.6 5	3.3 5	4.6 7	4.9 8	5.8 10	15 6	17 8	22 8	26 10
C-4	1.6 3	2.4 5	2.6 5	3.5 7	3.5 6	4.0 7	4.0 8	4.8 10	17 6	24 10	26 10	28 11
C-5	1.9 5	2.1 5	2.8 7	3.6 9	3.7 7	4.6 8	5.1 10	5.9 11	21 8	26 9	27 11	27 12
D-1-0	2.1 4	2.6 4	3.5 6	3.7 8	3.0 5	4.1 6	5.1 7	6.2 9	16 10	22 10	22 10	22 10
D-2-0	-	-	3.3 7	4.1 8	-	-	8.6 14	10.1 18	-	-	21 6	21 6
D-3-0	-	-	3.5 9	4.2 10	-	-	10.7 21	11.0 23	-	-	24 5	24 5
D-4-0	-	2.0 3	2.1 4	2.6 5	-	5.5 8	7.2 12	8.6 14	-	14 4	23 7	26 8
D-5	1.7 2	1.6 3	2.1 4	2.7 5	3.8 6	3.6 7	4.8 10	5.4 11	13 4	26 7	28 10	29 10
D-6	1.5 2	1.7 3	2.3 4	2.8 5	2.6 5	3.3 6	3.2 6	3.9 7	17 7	23 8	28 12	28 15
D-7	1.6 3	2.1 3	2.6 4	-	1.8 3	2.3 4	2.8 5	-	22 11	27 14	27 14	-
M-1	1.9 3	2.2 4	2.6 7	3.2 8	4.3 6	5.8 8	7.5 9	8.3 12	19 6	23 6	26 6	27 7
M-2	1.5 3	2.1 5	2.7 6	3.0 7	3.1 5	3.7 8	4.8 9	5.6 11	20 7	24 9	24 10	26 11
M-3	1.7 3	2.3 4	2.7 5	3.1 5	4.0 7	4.6 7	4.5 9	5.3 9	21 7	25 7	25 8	26 10
M-4	1.4 2	1.7 3	2.1 4	2.6 4	2.7 5	4.1 5	3.5 6	4.5 7	22 7	27 7	28 9	29 10
T-1-0	4.6 8	6.2 11	7.7 12	8.5 12	4.6 7	7.2 12	8.5 13	9.2 14	9 7	11 9	14 10	15 10
T-2	4.3 6	6.1 10	9.0 14	7.0 15	4.8 6	6.7 10	8.9 13	9.5 14	7 6	8 6	8 6	14 6
T-3	4.5 7	5.8 10	7.9 12	8.9 14	4.2 7	5.5 9	6.5 10	8.0 12	12 10	13 10	13 11	14 11
W-1-0	1.8 3	2.1 4	2.7 5	3.3 6	5.6 8	7.7 11	9.5 15	11.7 17	-	22 6	26 6	27 6
W-2	2.2 5	2.9 5	3.5 6	4.2 7	3.2 5	3.6 7	3.9 8	4.7 9	24 14	24 16	25 16	27 16
W-3-0	-	-	2.7 5	3.3 6	-	-	7.8 12	8.6 16	-	-	20 6	21 6
W-4	2.0 4	2.6 5	3.0 6	3.6 6	2.6 5	3.4 5	3.7 7	4.2 8	14 10	19 11	25 15	26 15